LECTURE NOTES

Contents

Notation page

In this page, we write down the common conventions we are going to use throghout the lecture notes.

0.1 Mathematical notation

We denote vectors with bold symbols, i.e. $\boldsymbol{u}$, $\boldsymbol{v}$. We should use

```
\boldsymbol{}
```

as much as possible, since it preserves the inclination of the symbols, whereas

```
\mathbf{}
```

does not.

Partial derivatives are denoted as $\frac{\partial}{\partial t}$, with variable **not** indexed. Whereas one could use ∂_t when the situation is suitable.

In the integrals, the differentials are always in the end, namely

$$\int f(x)dx, \qquad \int \boldsymbol{u}(\boldsymbol{x})d\boldsymbol{x} \tag{1}$$

We denote the Laplacian as Δ (instead of ∇^2).

We use a compactified notation for the Dirac delta function in which all variables in the upper index are summed and all those in the lower index are subtracted. For example,

$$\delta^{\boldsymbol{k}}_{\boldsymbol{k}_1\boldsymbol{k}_2} = \delta(\boldsymbol{k} - \boldsymbol{k}_1 - \boldsymbol{k}_2) \tag{2}$$ not:delta

$$\delta^{\boldsymbol{k}\boldsymbol{k}_1}_{\boldsymbol{k}_2\boldsymbol{k}_3} = \delta(\boldsymbol{k} + \boldsymbol{k}_1 - \boldsymbol{k}_2 - \boldsymbol{k}_3). \tag{3}$$

We use bold symbols with a chapeau $\hat{\boldsymbol{x}}$ to denote a unit vector.

0.2 Other notation

Here we can list any other notational convenience we are going to use.

We denote relative vorticity or simply vorticity by ζ, the potential vorticty (PV) by Q, the height of a free surface by η.

We denote the non-dimensional parameters Rossby number by Ro and Brunt Vaisala frequency by N.

We should agree on itemize or lists we are using (for the moment it seems ok though)

Chapter 1

Wave Turbulence: a theoretical physics perspective

MD: I will use the colour blue to write down comments/discussions that are not on the slides.

1.1 Introduction

intro to the lecture notes

1.2 Phenomenology of turbulence and cascade phenomena

intro to the Lecture 1

1.2.1 Hydrodynamic turbulence

To introduce the main mechanisms observed in a turbulent phenomenon, we first review the classical theory of *hydrodynamic turbulence*. Consider a 3D incompressible fluid flow satisfying the Navier-Stokes equations in $\mathbb{R}^3$ (or $\mathbb{T}^3$), namely

$$\rho\left(\frac{\partial \boldsymbol{v}}{\partial t}+(\boldsymbol{v}\cdot\nabla)\,\boldsymbol{v}\right)=-\nabla p+\nu\Delta\boldsymbol{v}+\boldsymbol{f},\qquad \boldsymbol{x}\in\mathbb{R}^3,\,t\geq 0 \tag{1.1}$$ eq:momNS

$$\nabla\cdot\boldsymbol{v}=0, \tag{1.2}$$ eq:div

where $\boldsymbol{v}(\boldsymbol{x},t)$ is the velocity field, $p(\boldsymbol{x},t)$ is the pressure, $\boldsymbol{f}(\boldsymbol{x},t)$ is an external forcing and ρ,ν are constants corresponding respectively to the density and the kinematic viscosity.

A first key consequence of the divergence-free condition (1.2), is that multiplying (1.1) by $\boldsymbol{v}$ and integrating in space we get

$$\int(\boldsymbol{v}\cdot(\boldsymbol{v}\cdot\nabla)\boldsymbol{v}+\boldsymbol{v}\cdot\nabla p)\,(\boldsymbol{x},t)d\boldsymbol{x}=-\int\left(\frac{1}{2}|\boldsymbol{v}|^2+p\right)(\boldsymbol{x},t)\nabla\cdot\boldsymbol{v}(\boldsymbol{x},t)d\boldsymbol{x}=0, \tag{1.3}$$

where in the first identity above we have simply integrated by parts. As a consequence, we obtain

$$E(t) = \frac{1}{2}\int \rho|\boldsymbol{v}(\boldsymbol{x},t)|^2 d\boldsymbol{x} = E(0) - \nu \iint |\nabla \boldsymbol{v}(\boldsymbol{x},t)|^2 d\boldsymbol{x}dt + \iint (\boldsymbol{f}\cdot\boldsymbol{v})(\boldsymbol{x},t)d\boldsymbol{x}dt. \quad (1.4)$$ eq:consE

Thus, when $\nu = \boldsymbol{f} = 0$ we get that the energy is conserved. In the sequel, for the sake of convenience we will assume $\rho = 1$.

To investigate the influence of the viscosity parameter on the dynamics, it is important to non-dimensionalise the equations. In particular, let V, L be the characteristic velocity and length scales. [1] The characteristic time scale is then $T = L/V$. With a slight abuse of notation, we pass to non-dimensional quantities as

$$\boldsymbol{v} \to V\boldsymbol{v}, \quad \boldsymbol{x} \to L\boldsymbol{x}, \quad t \to \frac{L}{V}t, \quad p \to V^2 p, \quad \boldsymbol{f} \to \frac{L}{V^2}\boldsymbol{f}. \quad (1.5)$$ scaling

With this rescaling, (1.1) become

$$\left(\frac{\partial \boldsymbol{v}}{\partial t} + (\boldsymbol{v}\cdot\nabla)\,\boldsymbol{v}\right) = -\nabla p + \frac{1}{R}\Delta\boldsymbol{v} + \boldsymbol{f} \quad (1.6)$$ eq:NS

where the *Reynolds number* is defined as

$$R = \frac{LV}{\nu}. \quad (1.7)$$

This parameter has a crucial influence on the dynamics of a fluid flow. Indeed, as observed by O. Reynolds [39] in his famous pipe-flow experiment, a laminar fluid flow remains laminar for small values of R. On the other hand, for $R \gg 1$ (obtained by increasing the velocity of the background laminar flow), Reynolds observed the transition to a turbulent regime, i.e. the flow become spatially and temporally disordered. Add maybe picture of Reynolds experiment?.

A first heuristic explanation of this phenomena goes as follows: the forcing term supply energy to the flow at large spatial scales. However, when $R \gg 1$ viscosity is effective only at small scales. Therefore, the separation of scales between forcing and dissipation requires a transfer of energy across scales via the inertial term, i.e. $\boldsymbol{v}\cdot\nabla\boldsymbol{v}$. See Figure 1.1 for a schematic picture of this cascade mechanism.

1.2.1.1 Statistical theory of turbulence

The experimental evidences suggests that turbulent flows are chaotic, namely, $\boldsymbol{v}$ is not predictable. However, the *statistical properties* of $\boldsymbol{v}$ are predictable - for example *moments* of $\boldsymbol{v}$. Some important examples are

$$E = \langle \frac{1}{2}|\boldsymbol{v}|^2\rangle, \qquad \text{mean energy}$$
$$\Omega = \langle \frac{1}{2}|\nabla\times\boldsymbol{v}|^2\rangle, \qquad \text{mean enstrophy},$$

where $\langle\cdot\rangle$ denotes "some" average.

[1] For instance, considering a fluid flow in a pipe, V is the mean velocity of the fluid and L is the length of the pipe.

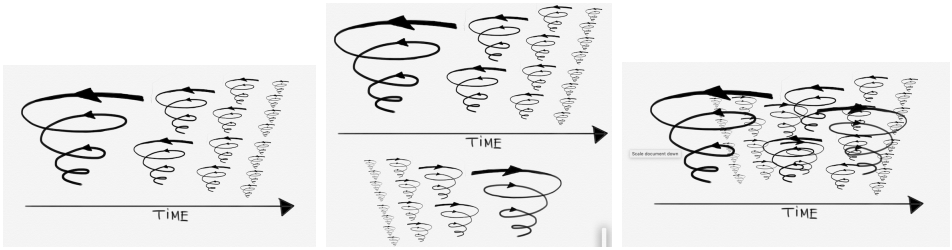

Figure 1.1: Large scale structures are split into smaller ones, with the total energy being conserved at each scale. However, also the inverse process can happen, called *backscatter*. The observed energy transfer from large scales to small ones should be considered *on average*, but fluctuations can be strong. This mechanism is also known as *Richardson cascade*. Pictures to be properly made

Richardson

Remark 1. *In the rest of these notes we will be a bit loose in the use of averages, but usually we can distinguish two main point of views: 1) mathematically,* $\langle\cdot\rangle$ *denotes an ensemble average with respect to realisations of the initial condition. 2) Experimentally,* $\langle\cdot\rangle$ *usually denotes a spatial or time average.*

In absence of boundaries, for a turbulent fluid flow we assume that a statistically steady state is eventually reached in which forcing and dissipation balance on average. In addition, it is believed that at small scales, symmetries of the Navier-Stokes equations are restored in a statistical sense [22]. We will then assume that moments of $\boldsymbol{v}$ have the following properties:

- **Stationarity:** $\langle v_i(\boldsymbol{x},t)\, v_j(\boldsymbol{x}',t')\rangle = f_{ij}(\boldsymbol{x},\boldsymbol{x}',t-t')$.
- **Homogeneity:** $\langle v_i(\boldsymbol{x},t)\, v_j(\boldsymbol{x}',t')\rangle = f_{ij}(\boldsymbol{x}-\boldsymbol{x}',t,t')$.
- **Isotropy:** $\langle v_i(\boldsymbol{x},t)\, v_j(\boldsymbol{x}',t')\rangle = \boldsymbol{f}(|\boldsymbol{x}-\boldsymbol{x}'|,t,t')$.

We now investigate some of the fundamental properties that one can deduce from the above mentioned hypothesis.

Consider $\langle\cdot\rangle$ to be the spatial average, ignoring the forcing term in (1.4), we can define the *mean rate of energy dissipation* as

$$\varepsilon(\nu) = -\frac{1}{2}\partial_t\langle \boldsymbol{v}^2\rangle = \nu\langle|\nabla \boldsymbol{v}|^2\rangle. \tag{1.8}$$

eq:meanendiss

In a turbulent regime, it is often observed *anomalous dissipation*, which can be quantified as follows.

p:dissanom

Hypothesis 1 (Dissipative anomaly)**.** *The mean rate of energy dissipation remains finite (and positive) in the limit* $\nu \to 0$*. More precisely, there exists a constant* ϵ *such that*

$$\lim_{\nu\to 0}\varepsilon(\nu) = \epsilon > 0. \tag{1.9}$$

This feature may seem unusual at a first glance. However, a basic example where this can be computed explicitly is the viscous forced Burgers equation

$$\partial_t u + u\partial_x u = \nu\partial_{xx}u + f. \tag{1.10}$$

This equation can be solved through the so-called Cole-Hopf transformation and, for some initial data, one observes this anomalous dissipation. This is strongly related with the formation of shocks when $\nu = 0$, that will dissipate energy even in absence of viscosity. We refer to [46] for more details and for other toy models where anomalous dissipation can be explicitly characterized. Add also reference to the example of Drivas et al in passive transport

To progress beyond the global energy budget, we need to look at the solution to (1.1) in the Fourier space. We define the Fourier transform as to check definition of Fourier transform with other lectures

$$\boldsymbol{v}(\boldsymbol{x},t) = \int \hat{\boldsymbol{v}}(\boldsymbol{k},t)\, e^{i\boldsymbol{k}\cdot\boldsymbol{x}} d\boldsymbol{k} \quad \hat{\boldsymbol{v}}(\boldsymbol{k},t) = \frac{1}{(2\pi)^d}\int \boldsymbol{v}(\boldsymbol{x},t)\, e^{-i\boldsymbol{k}\cdot\boldsymbol{x}} d\boldsymbol{x}. \tag{1.11}$$

From the divergence-free condition (1.2), we readily get

$$\boldsymbol{k}\cdot\hat{\boldsymbol{v}} = 0, \tag{1.12}$$

so that $\hat{\boldsymbol{v}}$ must be orthogonal to $\boldsymbol{k}$. We can directly project $\hat{\boldsymbol{v}}$ on this hyperplane on the Fouries space thanks to Leray-projection operator given by

$$\hat{\mathbb{P}}(\boldsymbol{k}) = Id - \frac{\boldsymbol{k}\otimes\boldsymbol{k}}{|\boldsymbol{k}|^2}. \tag{1.13}$$ def:Leray

Notice that $\mathbb{P}(\nabla g) = 0$ for any function g. Thus, taking the Fourier transform of (1.6) with $\boldsymbol{f} = 0$ and applying the operator $\mathbb{P}$ we obtain

$$(\partial_t + \nu k^2)\,\hat{\boldsymbol{v}}_i(\boldsymbol{k}) = \int T_{ijm}(\boldsymbol{k},\boldsymbol{p},\boldsymbol{q})\,\hat{\boldsymbol{v}}_j(\boldsymbol{p})\,\hat{\boldsymbol{v}}_m(\boldsymbol{q}) d\boldsymbol{p}\, d\boldsymbol{q} \tag{1.14}$$ eq:FNS

where the summation convention on repeated indices is implied and we define

$$T_{ijm}(\boldsymbol{k},\boldsymbol{p},\boldsymbol{q}) \;= -ik_j\left(\delta_{im} - \frac{k_i k_m}{|\boldsymbol{k}|^2}\right)\delta^{\boldsymbol{k}}_{\boldsymbol{p},\boldsymbol{q}}, \tag{1.15}$$

where we recall the notation add REF to notation delta function. Notice that the term in the righ-hand side of (1.14) is nothing more than the Fourier transform of $\mathbb{P}(\boldsymbol{v}\cdot\nabla\boldsymbol{v})$. Let us now present some classical result that can be obtained combining the Fourier representation of the velocity field and the hypothesis we made on it. These results are named after Kolmogorov REF and some historical discussion?

◇ **The Kolmogorov spectrum.** Thanks to the isotropy hypothesis, we can thus define the *spectral energy density*. In order to do so, ignoring the time-dependence for the sake of simplicity, first observe that from the Parseval's identity we have

$$E = \frac{1}{2}\int |\boldsymbol{v}(\boldsymbol{x})|^2 d\boldsymbol{x} = \frac{1}{2}\int |\hat{\boldsymbol{v}}(\boldsymbol{k})|^2\, d\boldsymbol{k}.$$

Then, assuming isotropy on $\hat{\boldsymbol{v}}$, namely $\hat{\boldsymbol{v}} = \hat{\boldsymbol{v}}(|\boldsymbol{k}|) := \hat{\boldsymbol{v}}(k)$ one has

$$E = \frac{2}{3}\pi\int |\hat{\boldsymbol{v}}(k)|^2\, dk := \int E(k) dk. \tag{1.16}$$ def:ENSsp

$E(k)$ is the aforementioned spectral energy density, which describes how energy is distributed across scales of motion.

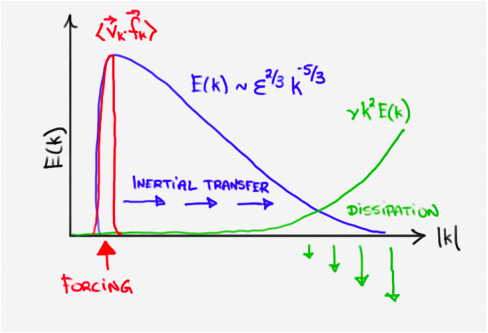

fig:K41

Figure 1.2: Schematic picture of the power-law behaviour of the energy spectrum when forcing at large scales. Make the picture in tikz

In the long-time limit, we assume that we reached a (statistically) stationary state, so that $\partial_t E(t) = 0$. Then, taking the time derivative of (1.4) we infer

$$\langle \boldsymbol{f} \cdot \boldsymbol{v} \rangle = \nu \langle |\nabla \boldsymbol{v}|^2 \rangle. \tag{1.17}$$

If the forcing injects energy at a constant mean rate, namely

$$\langle \mathbf{f} \cdot \boldsymbol{v} \rangle = \epsilon > 0, \tag{1.18}$$

we must also have that the mean rate of energy dissipation satisfy $\nu \langle |\nabla \boldsymbol{v}|^2 \rangle = \epsilon$. Compare this with the Hypothesis **??** of dissipative anomaly. At this point, it is important to distinguish different length scales. From a dimensional argument, first observe that

$$[\epsilon] = L^2 T^{-3}, \qquad [\nu] = L^2 T^{-1}. \tag{1.19}$$

Hence, the only length scale that can depend on ν, ϵ is

$$L_\nu = C \epsilon^{-\frac{1}{4}} \nu^{\frac{3}{4}}, \qquad \text{(viscous length scale)} \tag{1.20}$$

eq:viscousL

Notice that $L_\nu \to 0$ as $\nu \to 0$. This length scale quantify the small-scales where dissipation becomes effective. On the other hand, we assume that the forcing $\boldsymbol{f}$ acts on a fixed large length scale L_f. The regime we are interested in is

$$L_\nu \ll |\boldsymbol{x}| \ll L_f, \qquad \text{inertial range.} \tag{1.21}$$

One of the main hypothesis in hydrodynamic turbulence is the following add REF:

Hypothesis 2 (Kolmogorov 1941)**.** *When $\nu \to 0$, in the inertial range, $E(k)$ depends only on ϵ and k.*

We can now deduce the famous Kolmogorov 5/3 law by a simple dimensional argument to verify the assertion above. Indeed, we know that the quantity of interest have the following dimension

$$[k] = L^{-1}, \qquad [E(k)] = L^3 T^{-2}, \tag{1.22}$$

which imply that the only possible scaling law is

$$E(k) = C\, \epsilon^{\frac{2}{3}}\, k^{-\frac{5}{3}}. \tag{1.23}$$

eq:K53

Add comments about the power spectrum (1.23) and its experimental and numerical verification?

◇ **The Kolmogorov's 4/5-law.** Notation slightly changed wrt slides Proceeding with the analysis in the Fourier space, we can split the velocity into low and high frequencies, depending on a fixed frequency scale K, as

$$\hat{\boldsymbol{v}}(\boldsymbol{k},t) = (\hat{\boldsymbol{v}})_{\leq K}(\boldsymbol{k},t) + (\hat{\boldsymbol{v}})_{>K}(\boldsymbol{k},t), \tag{1.24}$$ eq:lowhigh

where

$$(\hat{\boldsymbol{v}})_{\leq K}(\boldsymbol{k},t) = \hat{\boldsymbol{v}}(\boldsymbol{k},t)\chi_{|\boldsymbol{k}|\leq K}, \qquad (\hat{\boldsymbol{v}})_{>K}(\boldsymbol{k},t) = \hat{\boldsymbol{v}}(\boldsymbol{k},t)\chi_{|\boldsymbol{k}|>K} \tag{1.25}$$

and χ it is just a frequency cut-off.

Remark 2. *In the physical space, the low-high frequency splitting* (1.24) *correspond to a large-small scale splitting of* $\boldsymbol{v}$ *at a fixed length scale* $l = K^{-1}$*. More precisely,*

$$\boldsymbol{v}(\boldsymbol{x},t) = (\boldsymbol{v})_{\leq K}(\boldsymbol{x},t) + \boldsymbol{v}_{>K}(\boldsymbol{x},t), \tag{1.26}$$

where

$$(\boldsymbol{v})_{\leq K}(\boldsymbol{x},t) = \int_{|\boldsymbol{k}|\leq K} \hat{\boldsymbol{v}}(\boldsymbol{k},t)\, e^{i\boldsymbol{k}\cdot\boldsymbol{x}} d\boldsymbol{k}, \qquad (\boldsymbol{v})_{>K}(\boldsymbol{x},t) = \int_{|\boldsymbol{k}|>K} \hat{\boldsymbol{v}}(\boldsymbol{k},t)\, e^{i\boldsymbol{k}\cdot\boldsymbol{x}} d\boldsymbol{k}. \tag{1.27}$$

In addition, for any function f, g *one has*

$$\langle f_{\leq K} g_{>K} \rangle = 0. \tag{1.28}$$ eq:ort

The low frequency part of the solution carry on the cumulative mean energy between wave-numbers 0 and K, given by

$$E^{(K)} = \frac{1}{2}\langle |\boldsymbol{v}_{\leq K}|^2 \rangle = \int_{k\leq K} E(k)\, dk. \tag{1.29}$$

To compute the time derivative of $E^{(K)}$, it is more convenient to directly work with the equations in the physical space (1.1). Multiply the equation (1.1) by $\boldsymbol{v}_{\leq K}$, integrate in space and use Parseval's identity to get the *scale resolved energy budget*

$$\frac{\partial E^{(K)}}{\partial t} + \Pi^{(K)} = -2\nu\Omega^{(K)} + F^{(K)}, \tag{1.30}$$ eq:enbud

where we define:

$$\Omega^{(K)} = \frac{1}{2}\langle |\nabla \boldsymbol{v}_{\leq K}|^2 \rangle = \frac{1}{2}\langle |\nabla \times \boldsymbol{v}_{\leq K}|^2 \rangle = \int_{k<K} k^2\, E(k)\, dk \qquad \text{(cumulative enstrophy)}.$$

This term simply comes from the dissipation. Notice that we also used the identity $|\boldsymbol{k} \times \widehat{\boldsymbol{v}}(\boldsymbol{k},t)| = |\boldsymbol{k}||\widehat{\boldsymbol{v}}(\boldsymbol{k},t)|$ which holds since $\boldsymbol{v}$ is divergence-free (hence orthogonal to $\boldsymbol{k}$). In addition, the divergence-free condition removed also the pressure term.

Then we have

$$F^{(K)} = \langle \mathbf{f} \cdot \boldsymbol{v}_{\leq K} \rangle = \int_{|\boldsymbol{k}|<K} \hat{\mathbf{f}}(\boldsymbol{k}) \cdot \hat{\mathbf{v}}(\boldsymbol{k})\, d\boldsymbol{k} \qquad \text{(cumulative energy input)}.$$

Finally, we have

$$\Pi^{(K)} = \langle (\boldsymbol{v} \cdot \nabla \boldsymbol{v}) \cdot \boldsymbol{v}_{\leq K} \rangle \qquad \text{(energy transfer)}.$$

The term above does not cancels as if we were multiplying by $\boldsymbol{v}$. However, this term still enjoys some cancellations. More precisely, since $\boldsymbol{v} = \boldsymbol{v}_{\leq K} + \boldsymbol{v}_{>K}$ and

$$\langle (\boldsymbol{v}_{\leq K} \cdot \nabla \boldsymbol{v}_{\leq K}) \cdot \boldsymbol{v}_{\leq K} \rangle = -\frac{1}{2} \langle |\boldsymbol{v}_{\leq K}|^2 \nabla \cdot \boldsymbol{v}_{\leq K} \rangle = 0, \tag{1.31}$$

$$\langle (\boldsymbol{v}_{>K} \cdot \nabla \boldsymbol{v}_{\leq K}) \cdot \boldsymbol{v}_{\leq K} \rangle = \frac{1}{2} \langle \boldsymbol{v}_{>K} \cdot \nabla |\boldsymbol{v}_{\leq K}|^2 \rangle = 0, \tag{1.32}$$

where the last identity follows by (1.28). Therefore

$$\Pi^{(K)} = \langle (\boldsymbol{v}_{\leq K} \cdot \nabla \boldsymbol{v}_{>K}) \cdot \boldsymbol{v}_{\leq K} \rangle + \langle (\boldsymbol{v}_{>K} \cdot \nabla \boldsymbol{v}_{>K}) \cdot \boldsymbol{v}_{\leq K} \rangle.$$

Differentiating (1.30) with respect to K gives a local equation for the spectral energy density, $E(k)$:

$$\frac{\partial E(k)}{\partial t} + \frac{\partial \Pi^{(k)}}{\partial k} = -\nu k^2 E(k) + \frac{\partial F^{(k)}}{\partial k}. \tag{1.33}$$

The scale resolved energy budget equations express the physically reasonable fact that in the inertial range, where forcing and dissipation are negligible, the rate of change of energy at a given scale is equal to the flux of energy through that scale due to the energy-conserving nonlinear interactions.

Assume now that we reach a stationary state, namely $\partial_t E^{(K)} = 0$, with a finite mean energy $E = \langle |\boldsymbol{v}|^2 \rangle < +\infty$. Since $\boldsymbol{f}$ acts only on small frequencies, let K be large enough so that it is outside the forcing range. If this is the case, the cumulative energy input becomes the total energy input, namely $F^{(K)} = \langle \boldsymbol{f} \cdot \boldsymbol{v} \rangle = \epsilon$. Under these hypothesis, the scale resolved energy budget relation becomes

$$\Pi^{(K)} = -2\nu\Omega^{(K)} + \epsilon. \tag{1.34}$$

We are now interested in taking the limit $\nu \to 0$. For a fixed frequency scale K, we claim that

$$\lim_{\nu \to 0} \nu \Omega^{(K)} = 0,$$

which means that a dissipative anomalous behaviour can only be observed at large frequencies. To prove this fact, notice that

$$2\nu\Omega^{(K)} = \nu \langle |\nabla \boldsymbol{v}_{\leq K}|^2 \rangle \leq \nu K^2 \langle |v|^2 \rangle = \nu K^2 E,$$

which goes to zero as $\nu \to 0$ since E and K are fixed and finite. Under the assumptions made above, the energy transfer is now constant (as a function of K) and equal to ϵ:

$$\Pi^{(K)} = \epsilon. \tag{1.35}$$ const-flux

This relationship is exact for stationary, homogeneous, isotropic turbulence.

It is also possible (not obvious though, see [22, Sec. 6]) to show that $\Pi^{(K)}$ can be written in terms of velocity increments in physical space, defined as:

$$\delta \boldsymbol{v}(\boldsymbol{r},t) = \boldsymbol{v}(\boldsymbol{x}+\boldsymbol{r},t) - \boldsymbol{v}(\boldsymbol{x},t)$$
$$\delta \boldsymbol{v}_{\parallel}(\boldsymbol{r},t) = [\boldsymbol{v}(\boldsymbol{x}+\boldsymbol{r},t) - \boldsymbol{v}(\boldsymbol{x},t)] \cdot \frac{\boldsymbol{r}}{|\boldsymbol{r}|}.$$

In particular, $\Pi^{(K)}$ is a Fourier sine transform of a 3rd order correlation function of velocity increments add computations here?:

$$\begin{aligned}\Pi^{(K)} &= -\frac{1}{8\pi^2}\int \frac{\sin(Kr)}{r}\nabla_{\boldsymbol{r}}\cdot\left(\frac{\boldsymbol{r}}{r^2}\nabla_{\boldsymbol{r}}\cdot\langle|\delta\boldsymbol{v}(\boldsymbol{r})|^2\,\delta\boldsymbol{v}(\boldsymbol{r})\rangle\right)d\boldsymbol{r}\\ &= -\frac{1}{6\pi}\int_0^\infty \frac{\sin(Kr)}{r}(1+r\partial_r)(3+r\partial_r)(5+r\partial_r)\frac{\langle\delta\boldsymbol{v}_{\parallel}(r)^3\rangle}{r}dr.\end{aligned}$$

The first identity above holds only under the homogeneity hypothesis, where the second one crucially requires the isotropy. Letting $x = Kr$, the relation $\Pi^{(K)} = \epsilon$ becomes

$$\frac{1}{6\pi}\int_0^\infty \frac{\sin x}{x}F\left(\frac{x}{K}\right)dx = -\epsilon \tag{1.36}$$ eq:Pik

where

$$F(r) = (1+r\partial_r)(3+r\partial_r)(5+r\partial_r)\frac{S_3(r)}{r}, \qquad S_3(r) = \langle\delta\boldsymbol{v}_{\parallel}(r)^3\rangle \tag{1.37}$$

Now assume that $F(r)$ must become constant for small r, say $F(r) = c$ when $r \ll 1$. Noting that

$$\int_0^\infty \frac{\sin x}{x}dx = \frac{\pi}{2}, \tag{1.38}$$

sending $K \to \infty$ in (1.36), we deduce

$$F(r) = -12\epsilon, \qquad r \ll 1.$$

Thus in the inertial range limit $K \to \infty$, $S_r(r)$ satisfies an ODE:

$$(1+r\partial_r)(3+r\partial_r)(5+r\partial_r)\frac{S_3(r)}{r} = -12\epsilon \tag{1.39}$$

The general solution of this ODE is

$$S_3(r) = c_1 r^{-4} + c_2 r^{-2} + c_3 - \frac{4}{5}\epsilon r, \tag{1.40}$$

but the only solution vanishing as $r \to 0$ is

$$S_3(r) = -\frac{4}{5}\epsilon r. \tag{1.41}$$ eq:K45

This is the celebrated Kolmogorov's $\frac{4}{5}$-law.

This paragraph was not on the slides

◇ **Onsanger's conjecture and Dissipative anomaly** MD: Is it worth it to say something about Onsanger's conjecture? Namely from K45 law, one deduce that $\langle\delta\boldsymbol{v}^3\rangle \sim r$

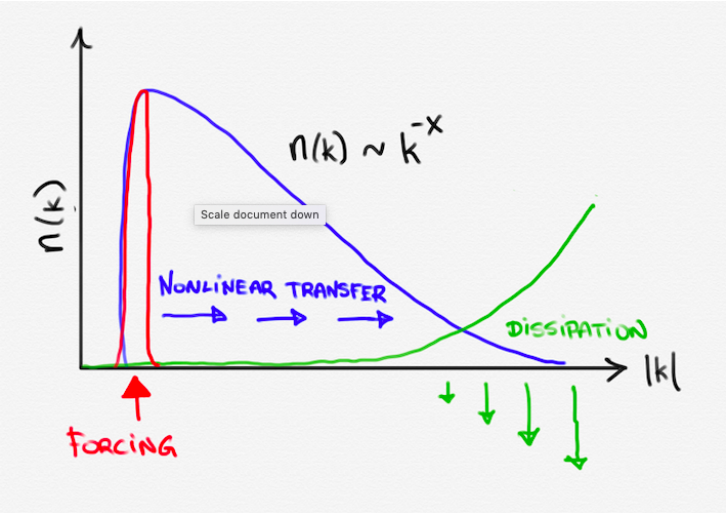

Figure 1.3: Schematic picture of the power-law behavior of the wave spectrum when forcing at large scales.

which imply $|\boldsymbol{v}(\boldsymbol{x}+r,t)-\boldsymbol{v}(\boldsymbol{x},t)| \sim (\epsilon r)^{1/3}$. If the velocity field is more regular, then the energy must be conserved (Constantin et. al.). If the velocity field is less regular, then non-uniqueness via convex integration (De Lellis- Szekelihydi up to Isett). Exponent 1/3 is open

One can also show that the 4/5-law is consistent with the dissipative anomaly assumption. Indeed, recalling that our considerations hold in the inertial range, so that $r \gg L_\nu$, we deduce

$$\nu\langle|\nabla \boldsymbol{v}|^2\rangle \approx \nu \lim_{r\to L_\nu} \frac{1}{r^2}\langle|\boldsymbol{v}(\cdot+\boldsymbol{r})-\boldsymbol{v}(\cdot)|^2\rangle \approx \nu\epsilon^{\frac{2}{3}}(L_\nu)^{-\frac{4}{3}} \approx \epsilon, \tag{1.42}$$

where in the last line we used (1.20).

1.2.2 Wave turbulence and cascade phenomena

Now, we move on to other turbulent phenomena. In many other non-linear PDEs, we have conserved quantities, and we expect similar cascades to the hydrodynamic case when these PDEs are subjected to forcing and dissipation that are separated in scale. In general, wave turbulence is the theory of cascade phenomena in nonlinear dispersive wave equations taking the form

$$\frac{\partial \Psi}{\partial t} = \mathcal{L}(\Psi) + \mathcal{N}(\Psi) + \Gamma, \tag{1.43}$$

where $\mathcal{L}$ is our linear term, $\mathcal{N}$ is our nonlinear term (which is analogous to advection in the Navier-Stokes case), and Γ represents both the forcing and dissipation on our PDE.

We represent the wave spectrum by

$$\mathbf{n_k} = \langle|\hat{\Psi}_\mathbf{k}|^2\rangle, \tag{1.44}$$

which is analogous to our spectral energy density $E(k)$ in the hydrodynamic case. In fact, we can keep the same picture in mind, replacing the energy spectrum with the wave spectrum.

There are several examples of such PDEs in which we may find one (or even two) conserved quantities:

1. **Nonlinear Schrodinger Equation (NLS)**: Some physical situations which can be modelled using this PDE include Bose-Einstein condensates modelling the dynamical formation of cold atoms, nonlinear optics, and modulation of monochromatic dispersive wave trains in surface gravity waves. Here, we write the Hamiltonian Equation for the complex field $\Psi(\mathbf{x}, t)$ as

$$i\frac{\partial \psi}{\partial t} = -\Delta\psi + V(\boldsymbol{x})\psi + g\left|\psi\right|^2\psi \tag{1.45}$$

$$= \frac{\delta \mathcal{H}}{\delta \psi^*}, \tag{1.46}$$

where $\mathcal{H} = \int d\mathbf{x}[|\nabla\Psi|^2 + \frac{g}{2}|\Psi|^4]$ represents our energy when our confining potential $V(x) = 0$. This is the first of our conserved quantities. In fact, for the NLS, we also have a second conserved quantity, the wave action $\mathcal{N} = \int |\Psi|^2 d\mathbf{x}$. This is in contrast to the 3D Navier-Stokes example, and here each conserved quantity will experience its own cascade.

2. **Water Wave Equations** This models the motion of a free fluid surface subject to gravity and surface tension. There are two limiting regimes, the capillary limit where there are short waves that feel the surface tension the most due to the curvature, and the gravity limit in which long waves experience negligible surface tension but gravity is dominant. For our mathematical model, we take an incompressible, irrotational fluid with free surface $z = \eta(x, y)$ and the bottom of the fluid $z = -h(x, y)$, and g, σ, and ρ representing gravity, surface tension, and density respectively. The equations are given by

$$\begin{aligned}
\Delta\phi &= 0 && \text{on } -h(x,y) < z < \eta(x,y,t)\\
\frac{\partial\phi}{\partial z} + \nabla\phi\cdot\nabla h &= 0 && \text{on } z = -h(x,y)\\
\frac{\partial\eta}{\partial t} + \nabla\phi\cdot\nabla\eta &= \frac{\partial\eta}{\partial z} && \text{on } z = \eta(x,y,t)\\
\frac{\partial\phi}{\partial t} + \frac{1}{2}\left|\nabla\phi\right|^2 + g\eta &= \frac{\sigma}{\rho}\nabla\cdot\left(\frac{\nabla\eta}{\sqrt{1+|\nabla\eta|^2}}\right) && \text{on } z = \eta(x,y,t)
\end{aligned}$$

The first equation here represents our incompressibility condition, the second that our system is closed from below and has no transverse velocity, the third represents the velocity on the surface, and the last is the Bernoulli equation giving the energy balance across our free surface. Note that the last two equations are the more significant ones here. For the third equation, the shape of the free surface is time dependent and must be determined as part of solving the equation. Zakharov showed that this is a 2-dimensional Hamiltonian system with conserved quantity $H = \int \mathcal{H}\, dxdy$ for

$$\mathcal{H} = \int_{-h(x,y)}^{\eta(x,y,t)} \frac{1}{2}\left|\nabla\phi\right|^2 dz + \frac{1}{2}\eta^2 + \frac{\sigma}{\rho}\left(\sqrt{1+|\nabla\eta|^2}-1\right)$$

3. **Barotropic Potential Vorticity Equation** Here, as seen in Peter's lectures, the singular quasi geostrophic equation models the large scale dynamics of Rossby

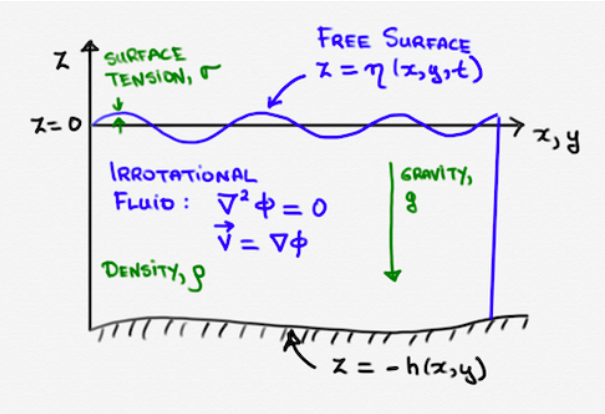

Figure 1.4: Water Waves

Waves:

$$\frac{\partial}{\partial t}(\nabla^2\psi - F\psi) + \beta\frac{\partial\psi}{\partial x} + \frac{\partial\psi}{\partial x}\frac{\partial\nabla^2\psi}{\partial y} - \frac{\partial\psi}{\partial y}\frac{\partial\nabla^2\psi}{\partial x} = 0\,.$$

with F being the Rossby deformation radius, and we use the quantity $\boldsymbol{v} = \nabla \times \psi(x,y,t)\,\hat{\mathbf{z}}$ to represent the velocity of geostrophic wind. Like in the case of the NLS, we have two conserved quantities, E the energy and Q the potential enstrophy:

$$E = \frac{1}{2}\int d\boldsymbol{x}\left[|\nabla\psi|^2 + F\psi^2\right],$$
$$Q = \frac{1}{2}\int d\boldsymbol{x}\left[\nabla^2\psi - F\psi\right]^2.$$

4. **Föppl-von Kármán equation** This is used to represent the turbulence of waves on a thin elastic plate. The equation describes the evolution of the surface displacement ζ and the 2-dimensional stress χ as

$$\rho\frac{\partial^2\zeta}{\partial t^2} = -\frac{D}{h}\nabla^4\zeta + \mathcal{N}[\chi,\zeta] \tag{1.47}$$
fvk1

$$\nabla^4\chi = -\frac{E}{2}\mathcal{N}[\zeta,\zeta]\,, \tag{1.48}$$

where ρ, h, D, and E represent the denisty, thickness, bending stiffness, and Young's modulus of the plate respectively. Here, the nonlinear term $\mathcal{N}$ is given by

$$\mathcal{N}[f,g] = \frac{\partial^2 f}{\partial x^2}\frac{\partial^2 g}{\partial y^2} - 2\frac{\partial^2 f}{\partial x\partial y}\frac{\partial^2 g}{\partial x\partial y} + \frac{\partial^2 f}{\partial y^2}\frac{\partial^2 g}{\partial x^2}. \tag{1.49}$$
fvk2

Miquel et. al. 2013 paper picture and description: experiment vs. simulation

Just as with the Navier-Stokes Equation example, we want to talk about exchange between various scales in these examples, and to do this we will once again look at these equations in Fourier Space. To simplify matters, we will choose appropriate choice of complex variables $a_{\boldsymbol{k}}$ in which all of these equations can be written roughly (here the equalities are not necessarily strict) in one of the following two ways, one for a 3-wave interaction and the second for a 4-wave interaction:

$$\partial_t a_{\boldsymbol{k}} + i\omega_{\boldsymbol{k}} a_{\boldsymbol{k}} = \int d\boldsymbol{k}_1 d\boldsymbol{k}_2 T^{\boldsymbol{k}}_{\boldsymbol{k}_1\boldsymbol{k}_2}\, a_{\boldsymbol{k}_1} a_{\boldsymbol{k}_2}\, \delta^{\boldsymbol{k}}_{\boldsymbol{k}_1\boldsymbol{k}_2} \tag{1.50}$$

$$\partial_t a_{\boldsymbol{k}} + i\omega_{\boldsymbol{k}} a_{\boldsymbol{k}} = \int d\boldsymbol{k}_1 d\boldsymbol{k}_2 d\boldsymbol{k}_3 T^{\boldsymbol{k}\boldsymbol{k}_1}_{\boldsymbol{k}_2\boldsymbol{k}_3}\, \overline{a}_{\boldsymbol{k}_1} a_{\boldsymbol{k}_2} a_{\boldsymbol{k}_3}\, \delta^{\boldsymbol{k}\boldsymbol{k}_1}_{\boldsymbol{k}_2\boldsymbol{k}_3}. \tag{1.51}$$

In each of these, $\omega_{\boldsymbol{k}}$ represents the dispersion relation depending on the linear part of the equation of motion, and the right hand side is a convolution with some nonlinear interaction coefficient $T^{\boldsymbol{k}}_{\boldsymbol{k}_1\boldsymbol{k}_2}$ or $T^{\boldsymbol{k}\boldsymbol{k}_1}_{\boldsymbol{k}_2\boldsymbol{k}_3}$. Note that we had a very similar looking equation for the Navier-Stokes equation 1.14.

With this setup, let us look at two of our four examples: First for the NLS, we can write it in the 4-wave interaction equation with

$$a_{\boldsymbol{k}} = \hat{\psi}_{\boldsymbol{k}} \tag{1.52}$$
$$\omega_{\boldsymbol{k}} = k^2 \tag{1.53}$$
$$T^{\boldsymbol{k}\boldsymbol{k}_1}_{\boldsymbol{k}_2\boldsymbol{k}_3} = -i\,g \tag{1.54}$$

Here, we have a 4-wave interaction as we are dealing with cubic nonlinearity. On the other hand, for our third example of the Barotropic Potential Vorticity Equation, we have a 3-wave interaction due to the quadratic nonlinearity. Therefore, in the notation of our 3-wave interaction equation, we have

$$a_{\boldsymbol{k}} = \frac{k^2 + F}{\sqrt{|k_x|}}\,\hat{\psi}_{\boldsymbol{k}} \tag{1.55}$$ def:aBPV
$$\omega_{\boldsymbol{k}} = -\frac{k_x}{k^2 + F} \tag{1.56}$$ def:omBPV
$$W^{\boldsymbol{p}}_{\boldsymbol{q}\,\boldsymbol{r}} = -\frac{1}{2}\sqrt{\frac{|q_x|\,|r_x|}{|p_x|}}\,\frac{(\boldsymbol{q}\times\boldsymbol{r})_z\,(q^2 - r^2)}{(q^2+F)\,(r^2+F)}. \tag{1.57}$$ def:WBPV

I'm not sure why it was switched into W notation on the slides, but I changed it here. MD: It is W because is the one he uses afterwards. Maybe explain here this change of notation?

Note that in the Barotropic Potential Vorticity example, the complex variable $a_{\boldsymbol{k}}$ is more complicated than simply $\hat{\psi}_{\boldsymbol{k}}$. The reason for this is that we want the $a_{\boldsymbol{k}}$ to have specific properties. Namely,

1. We want the quadratic part of the spectral energy density to take the form

$$E_{\boldsymbol{k}} = |\omega_{\boldsymbol{k}}|\; n_{\boldsymbol{k}}.$$

2. We want the lowest order "non-resonant" terms to be removed from the equations of motion. For example, an equation that looks quadratic may not actually have any nonlinear resonances at the quadratic level. For water waves equations in the gravity wave limit, we have

$$a_{\boldsymbol{k}} = \frac{1}{\sqrt{2\lambda_{\boldsymbol{k}}}}\eta_{\boldsymbol{k}} + i\sqrt{\frac{\lambda_{\boldsymbol{k}}}{2}}\varphi_{\boldsymbol{k}},$$

where $\eta_{\boldsymbol{k}}$ and $\varphi_{\boldsymbol{k}}$ are the 2-dimensional Fourier transforms of $\eta(x,y,t)$ and $\phi(x,y,z=\eta(x,y,t),t)$ respectively and

$$\lambda_{\boldsymbol{k}} = \frac{\omega_{\boldsymbol{k}}}{g + \sigma k^2/\rho}$$
$$\omega_{\boldsymbol{k}} = \sqrt{k(g + \sigma k^2/\rho)\tanh(kh)}.$$

acascade

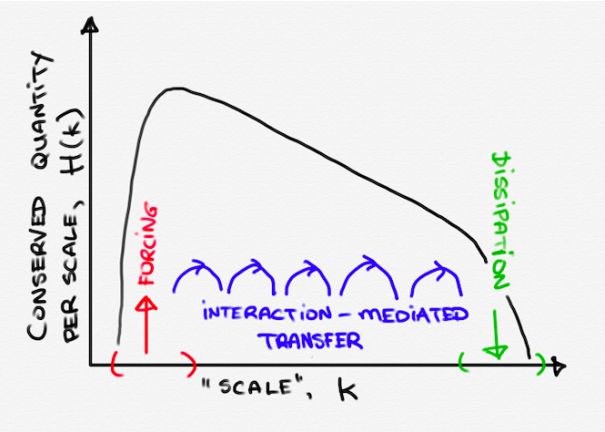

Figure 1.5: An Abstract Cascade Phenomena

The change of variables allows us to remove the lowest-order non-resonant term, and get a diagonal Hamiltonian. This phenomenon is also present for the Föppl-von Kármán Equation, and the expressions for the wave interaction coefficients for each can be seen in [55]. Include some of that? Calculations?

From now on, we will assume that the $a_{\boldsymbol{k}}$ are given and use the general 3-wave and 4-wave interaction formulas. Hydrodynamics is just one of a large class of driven-dissipative systems that exhibit some sort of cascade phenomena. In contrast to wave turbulence, condensed matter and soft matter experience cascade in mass space rather than frequency space. There are also models related to self-organized criticality in which cascade phenomena are present. In all of these, we have a conserved quantity, H which is preserved by nonlinear interactions in the inertial range between forcing and dissipation and a source and sink of H that are strongly separated. For each of these, Figure ?? gives a general picture of the cascade phenomena for each of these systems.

For each of these systems, we also distinguish between direct and inverse cascades depending on the direction of the transfer. For direct cascades, forcing is large scale and dissipation is small scale and vice versa for inverse cascades, as seen in Figure 1.2.2 in frequency space. Note that inverse cascade is separate from the phenomena of backscatter. For systems that involve more than one conserved quantity we often see both sorts of cascades happening simultaneously. For example in the NLS, the energy exhibits a direct cascade, while the wave action exhibits an inverse cascade. On the other hand, ror the BVP, the energy exhibits an inverse cascade, the potential enstrophy exhibits a direct cascade. This is why for a mathematical analysis it is important how limits are taken. If direct cascade scaling is being examined, it is important to take limits in such a way that forcing is on a large scale relative to the frequencies being looked at.

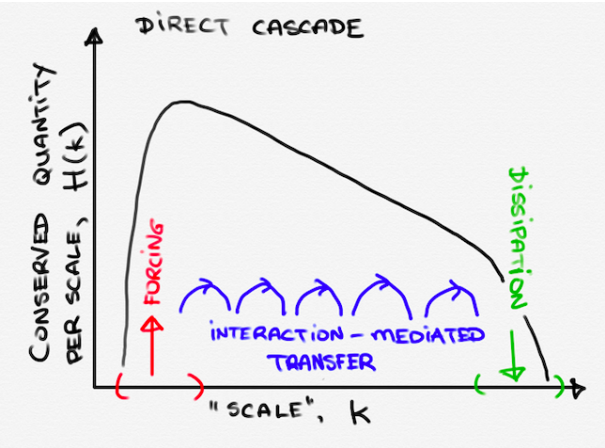

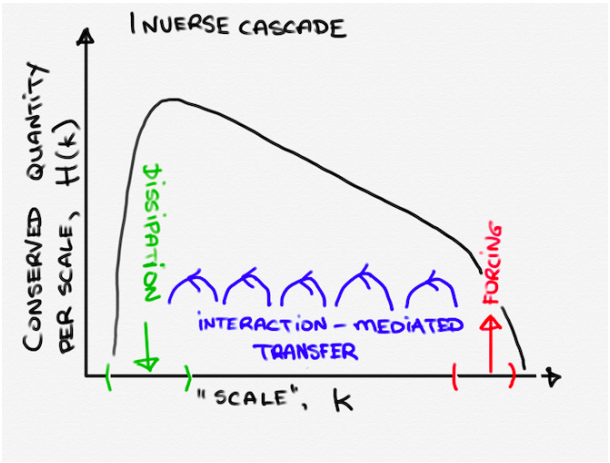

1.2.2.1 Dimensional analysis and phenomenology of wave turbulence

Schematically, the equations of motion in Fourier Space are

$$\frac{\partial a_{\boldsymbol{k}}}{\partial t} \sim -i\,\omega_{\boldsymbol{k}}\,a_{\boldsymbol{k}} + \int (d\boldsymbol{k})^{n-1}\,W_{\boldsymbol{k}}^{(n)}(a_{\boldsymbol{k}})^{n-1}\,\delta(\boldsymbol{k}). \tag{1.58}$$ eq-EoMk

The important parts of this equation are that we have a time derivative of a Fourier variable, our dispersion relation term, and a convolution of fields in the nonlinear term. The $W_{\boldsymbol{k}}$ now represents our nonlinear interaction coefficient. The $\delta_{\boldsymbol{k}}$ term encodes spatial homogeneity and reflects the conservation of momentum how?. Here, n is the number of waves participating in the interaction, for example 4 for the NLS and 3 for BPV. Most of the systems we are interested in here are scale invariant, and as such we may write

$$\omega_{\boldsymbol{k}} = c\,k^{\alpha}$$
$$W^{(n)}_{\boldsymbol{k}\,\boldsymbol{k}_1\ldots\boldsymbol{k}_{n-1}} = g\,k^{\gamma_n}\,f_{\boldsymbol{k}\,\boldsymbol{k}_1\ldots\boldsymbol{k}_{n-1}}.$$

In these, α and γ_n are scaling exponents and c and g are dimensional constants. For example for the NLS $\alpha = 2$, and for capillary waves $\alpha = 3/2$, and for gravity waves $\alpha = 1/2$. Note that these assumptions on $\omega_{\boldsymbol{k}}$ and $W^{(n)}_{\boldsymbol{k}\,\boldsymbol{k}_1\ldots\boldsymbol{k}_{n-1}}$ do not hold for Rossby waves as the system is not isotropic. In contrast to the Navier-Stokes case, we have two dimensional constants rather than one.

Based on our choice of $a_{\boldsymbol{k}}$, we have for the spectral energy density in the isotropic case:

$$E = \int |\omega_{\boldsymbol{k}}|\; n_{\boldsymbol{k}} d\boldsymbol{k}$$
$$= \int E_{\boldsymbol{k}}\,d\boldsymbol{k} = \int_0^{\infty} E_k\,dk.$$

Just as for Navier-Stokes we want a scale-by-scale energy budget in the inertial range which is given as

$$\frac{\partial E_k}{\partial t} = -\frac{\partial J_k}{\partial k}.$$

So, we have a spectral conservation law: that the rate of change of energy at scale k is the divergence of a current or flux.

We can also perform similar dimensional analysis to the Navier-Stokes case to get some enlightening results in the inertial range. These allow us to orient ourselves before getting involved in more detailed computations. using dimensional analysis, we get that

$$[k] = L^{-1} \quad [d\boldsymbol{k}] = L^{-d} \quad [\delta(\boldsymbol{k})] = L^{d} \quad [\omega_{\boldsymbol{k}}] = T^{-1}.$$

For some explanation of where these come from, note that as $\boldsymbol{k}$ is a wave vector, it should correspond to L^{-1} and $\omega_{\boldsymbol{k}}$ is a frequency, so it should correspond to T^{-1}. For $d\boldsymbol{k}$ and $\delta(\boldsymbol{k})$, we are using the schematic equations of motion. From here, since $E = \int \omega_{\boldsymbol{k}} a_{\boldsymbol{k}} \bar{a}_{\boldsymbol{k}} d\boldsymbol{k}$:

$$[a_{\boldsymbol{k}}] = E^{\frac{1}{2}} T^{\frac{1}{2}} L^{\frac{d}{2}},$$

leaving E as a unit as in different scenarios it could have different units. We will use this dimensional analysis to infer the units of of our constants c and g to get

$$\begin{aligned}[c] &= L^{\alpha} T^{-1} \\ [g] &= E^{\frac{2-n}{2}} T^{-\frac{n}{2}} L^{\left(\frac{n-2}{2}\right)d+\gamma_n}.\end{aligned}$$

I actually can't figure out how g was obtained. Using that the spectrum $\langle a_{\boldsymbol{k}} \bar{a}_{\boldsymbol{k}'} \rangle = n(\boldsymbol{k})\, \delta(\boldsymbol{k} - \boldsymbol{k}')$,

$$[n_{\boldsymbol{k}}] = ET.$$

Finally, for the energy dissipation per unit volume, J

$$[J] = ET^{-1} L^{-d}.$$

Now, we can copy Kolmogorov's argument and assume that in the inertial range, $n_{\boldsymbol{k}}$ depends on c, g, J and k only:

$$n_{\boldsymbol{k}} = c^{u}\, g^{v}\, J^{w}\, k^{-x}$$

Using our dimensional analysis above,

$$ET = \left(L^{\alpha} T^{-1}\right)^{u} \left(E^{\frac{2-n}{2}} T^{-\frac{n}{2}} L^{\left(\frac{n-2}{2}\right)d+\gamma_n}\right)^{v} \left(ET^{-1} L^{-d}\right)^{w} L^{x}$$

This gives undetermined system of 3 equations for 4 unknowns:

$$\begin{aligned} \left(\frac{2-n}{2}\right) v + w &= 1 \\ -u - \frac{n}{2} v - w &= 1 \\ \alpha\, u + \left(\left(\frac{n-2}{2}\right) d + \gamma_n\right) v - d\, w &= -x. \end{aligned}$$

So, unlike for Navier-Stokes, where we used a Kolmagorov argument and got a $\frac{5}{3}$ value for x, we cannot do that here without additional constraints. One such constraint may be that c (the dispersive part) and g (the nonlinear part) may be dependent physically depending on the system. An example of this would be gravity waves where gravity controls both c and g. However, in the NLS they are independent and this cannot be done (c comes from dispersion and g from the scattering length).

A priori, we have no way of knowing the exponent x. So, we may fix an x to get equations for u, v, and w:

$$\begin{aligned} u &= \frac{2\gamma_n + (n-1)d - (n-1)x}{(n-1)\alpha - \gamma_n} \\ v &= -\frac{2\alpha + d - x}{(n-1)\alpha - \gamma_n} \\ w &= \frac{(n-2)x + 2\alpha - 2\gamma_n - (n-2)d}{2((n-1)\alpha - \gamma_n)}. \end{aligned}$$

There are two choices for x that are special spectra that appear as limiting cases, namely

1. If we assume the wave spectrum dimension has no dependence on c, namely $u = 0$. Then we get that

$$x = \frac{2\gamma_n}{n-1} + d.$$

   This is called the **Kolmogorov-Zakharov spectrum**.

2. If we assume the wave spectrum dimension has no dependence on J, the dissipation rate, namely $w = 0$. Then, we get that

$$x = \frac{2\gamma_n - 2\alpha}{n-2} + d.$$

   This is called the **Generalized Phillips/Critical Balance spectrum**. Although it does not appear in the solution of any known equation, it is known and studied by oceanographers in the case of gravity waves in the open ocean as it is believed to be relevant.

Referring back to Equation 1.58, we can investigate the two time scales involved in the problem using the fact that if $n_{\boldsymbol{k}} \sim k^{-x}$ then $a_{\boldsymbol{k}} \sim k^{-\frac{x+d}{2}}$ (Why?). There is one timescale that results from the linear term of Equation 1.58 and one resulting from the nonlinear term. For the former, we compare $\partial_t a_{\boldsymbol{k}}$ to $\omega_{\boldsymbol{k}} a_{\boldsymbol{k}}$ and see that the linear time scale is on the order of $\tau_{\mathrm{L}} \sim k^{-\alpha}$. For the latter, we compare $\partial_t a_{\boldsymbol{k}}$ to the nonlinear interaction term and see the nonlinear time scale is on the order of $\tau_{\mathrm{NL}} \sim k^{-\gamma_n + \left(\frac{n}{2}-1\right)(x-d)}$. Then, if we assume $\tau_{\mathrm{L}} \ll \tau_{\mathrm{NL}}$ as $k \to \infty$, the nonlinear evolution becomes slow going into the inertial range and we have

$$\frac{\tau_{\mathrm{L}}}{\tau_{\mathrm{NL}}} \sim k^{-\alpha + \gamma_n - \frac{n-2}{2}(x-d)} \ll 1.$$

This is equivalent to assuming the nonlinearity is weak.

We can check if this condition is satisfied on the two spectrum above. For the Kolmogorov-Zakharov spectrum, we have $x = \frac{2\gamma_n}{n-1} + d$, and thus

$$\frac{\tau_{\mathrm{L}}}{\tau_{\mathrm{NL}}} \sim k^{\frac{\gamma_n}{n-1} - \alpha} \ll 1$$

as $k \to \infty$ except in the case that $\gamma_n - (n-1)\alpha > 0$, the breakdown criterion. If the breakdown criterion holds, the Kolmogorov-Zakharov spectrum is inconsistent with weak nonlinearity. Note that larger γ_n corresponds to stonger nonlinearity. For more details

outlining the breakdown criterion, see [34]. For the Generalised Phillips' Spectrum, we have $x = \frac{2\gamma_n - 2\alpha}{n-2} + d$, so $\frac{\tau_L}{\tau_{NL}} \sim 1$. This explains the other name for this spectrum, the critical balance spectrum. Although this spectrum is inconsistent with weak nonlinearity, it is believed to be relevant for strong wave turbulence.

Next, we will restrict ourselves to the Kalmogorov-Zakharov Spectrum. In this case, if forcing supplies energy at a constant rate, $E \sim Jt$, then we can write the energy of the system as an integral from the forcing scale k_F to the dissipation scale k_D:

$$\begin{aligned} E &\sim \int_{k_F}^{k_D} \omega_k n_k k^{d-1} dk \\ &\sim \int_{k_F}^{k_D} k^{\alpha} k^{-\frac{2\gamma_n}{n-1} - d} k^{d-1} dk \\ &\sim \int_{k_F}^{k_D} k^{(\alpha - \frac{2\gamma_n}{n-1}) - 1} dk \\ &\sim k_D^{\alpha - \frac{2\gamma_n}{n-1}} \end{aligned}$$

If the exponent of k is positive ($\alpha - \frac{2\gamma_n}{n-1} > 0$), we say the system has **infinite capacity** since taking the turbulent limit where the dissipation scale goes to infinity results in the system accommodating an infinite amount of energy. On the other hand, the more interesting case is when $\alpha - \frac{2\gamma_n}{n-1} < 0$ in which we say the system has **finite capacity**. Then, the integral of of spectral energy density is finite as we send the $k_d \to \infty$. Therefore, if energy is growing linearly with respect to time, at some point there must be dissipation. Therefore, the spectrum must have extended to infinity and in that sense we have "filled" the Kalmogorov-Zakharov spectrum. Note that in order for us to have finite capacity, γ_n must be sufficiently large and thus the cascade process to large k happens faster with stronger nonlinearity and can reach infinity in finite time.

1.3 Equations for Correlation Functions

Just as we have Kolmogorov's $\frac{4}{5}$ law in the case of Navier-Stokes, we want something similar in general, and it turns out this is possible and we will develop that in this section. To simplify our assumptions, we will always assume our system is stationary, isotropic, and statistically homogeneous. This last assumption means that the moments of the wave field depend only on relative geometry, so for taking averages of a field a, it does not depend on the base coordinate $\boldsymbol{x}$. For example:

$$\begin{aligned} \langle a(\boldsymbol{x})\, a(\boldsymbol{x}+\boldsymbol{r})\rangle &= M_2^{++}(\boldsymbol{r}) \\ \langle a(\boldsymbol{x})\, \overline{a}(\boldsymbol{x}+\boldsymbol{r}_1)\, \overline{a}(\boldsymbol{x}+\boldsymbol{r}_2)\rangle &= M_3^{+--}(\boldsymbol{r}_1, \boldsymbol{r}_2), \end{aligned}$$

Note that the subscript $+$ and $-$ only denote if it's the field or its conjugate in the average. Looking at our field via its Fourier transform shows that the Fourier space moments are proportional to delta functions, evidence of spatial homogeneity. For the ones above,

$$\begin{aligned} \langle a(\boldsymbol{k})\, a(\boldsymbol{k}')\rangle &= \hat{M}_2^{++}(\boldsymbol{k}, \boldsymbol{k}')\, \delta(\boldsymbol{k} + \boldsymbol{k}') \\ \langle a(\boldsymbol{k})\, \overline{a}(\boldsymbol{k}')\, \overline{a}(\boldsymbol{k}'')\rangle &= \hat{M}_3^{+--}(\boldsymbol{k}, \boldsymbol{k}', \boldsymbol{k}'')\, \delta(\boldsymbol{k} - \boldsymbol{k}' - \boldsymbol{k}''). \end{aligned}$$

The moment of most relevance to us is the second moment, which gives us the wave spectrum:

$$\langle \overline{a}(\boldsymbol{k})\, a(\boldsymbol{k}')\rangle = n(\boldsymbol{k})\,\delta(\boldsymbol{k}-\boldsymbol{k}'). \tag{1.59}$$ def:wavespe

Moments, which summarize the properties of probability distributions, are in one to one correspondence with cumulants, an alternative to moments. In our case, where fields have mean $0(\langle a_{\boldsymbol{k}}\rangle = 0)$, we have the following correspondence between moments and cumulants, where $s_i = \pm 1$:

$$\begin{aligned}
\langle a^{s_1}(\boldsymbol{k}_1)\, a^{s_2}(\boldsymbol{k}_2)\rangle &= Q_2^{s_1 s_2}(\boldsymbol{k}_1)\,\delta(s_1\boldsymbol{k}_1 + s_2\boldsymbol{k}_2),\\
\langle a^{s_1}(\boldsymbol{k}_1)\, a^{s_2}(\boldsymbol{k}_2)\, a^{s_3}(\boldsymbol{k}_3)\rangle &= Q_3^{s_1 s_2 s_3}(\boldsymbol{k}_1,\boldsymbol{k}_2)\,\delta(s_1\boldsymbol{k}_1 + s_2\boldsymbol{k}_2 + s_3\boldsymbol{k}_3),\\
\langle a^{s_1}(\boldsymbol{k}_1)\, a^{s_2}(\boldsymbol{k}_2)\, a^{s_3}(\boldsymbol{k}_3)\, a^{s_4}(\boldsymbol{k}_4)\rangle &= Q_4^{s_1 s_2 s_3 s_3}(\boldsymbol{k}_1,\boldsymbol{k}_2,\boldsymbol{k}_3)\,\delta(s_1\boldsymbol{k}_1 + s_2\boldsymbol{k}_2 + s_3\boldsymbol{k}_3 + s_4\boldsymbol{k}_4),\\
&\quad + Q_2^{s_1 s_2}(\boldsymbol{k}_1)\, Q_2^{s_3 s_4}(\boldsymbol{k}_3)\,\delta(s_1\boldsymbol{k}_1 + s_2\boldsymbol{k}_2)\delta(s_3\boldsymbol{k}_3 + s_4\boldsymbol{k}_4)\\
&\quad + Q_2^{s_1 s_3}(\boldsymbol{k}_1)\, Q_2^{s_2 s_4}(\boldsymbol{k}_2)\,\delta(s_1\boldsymbol{k}_1 + s_3\boldsymbol{k}_3)\delta(s_2\boldsymbol{k}_2 + s_4\boldsymbol{k}_4)\\
&\quad + Q_2^{s_1 s_4}(\boldsymbol{k}_1)\, Q_2^{s_2 s_3}(\boldsymbol{k}_2)\,\delta(s_1\boldsymbol{k}_1 + s_4\boldsymbol{k}_4)\delta(s_2\boldsymbol{k}_2 + s_3\boldsymbol{k}_3).
\end{aligned}$$

Here, we've written out to the fourth moment to see that you must go this far to distinguish between moments and cumulants. The cumulants themselves measure deviations from Gaussianity. For a Gaussian field, all cumulants of order larger than 2 are zero. In the equation for the fourth moment, notice that we have our fourth order cumulant summed with all possible pairings of our wave vectors. So, the fourth order cumulant is essentially measuring how different the fourth order moment is from if we assumed we had a Gaussian field. (On some level, this correspondence between moments and cumulants relates to Feynman diagrams seen in the below Chapter).

As many of our example systems are Hamiltonian, we will consider a 3-wave Hamiltonian system of the form $H = Q + U = \int \mathcal{H}_{\boldsymbol{k}}\, d\boldsymbol{k}$ where $\mathcal{H}_{\boldsymbol{k}}$ is the Hamiltonian density written in phase space with a quadratic part $\mathcal{Q}_{\boldsymbol{k}}$ and interaction part $\mathcal{U}_{\boldsymbol{k}}$ as

$$\mathcal{H}_{\boldsymbol{k}} = \omega_{\boldsymbol{k}} a_{\boldsymbol{k}} a^*_{\boldsymbol{k}} + \int d\boldsymbol{k}_1 d\boldsymbol{k}_2 W^{\boldsymbol{k}}_{\boldsymbol{k}_1\boldsymbol{k}_2}\left(a^*_{\boldsymbol{k}} a_{\boldsymbol{k}_1} a_{\boldsymbol{k}_2} + a_{\boldsymbol{k}} a^*_{\boldsymbol{k}_1} a^*_{\boldsymbol{k}_2}\right)\delta^{\boldsymbol{k}}_{\boldsymbol{k}_1\boldsymbol{k}_2}. \tag{1.60}$$ eq-3waveH

Therefore, Hamilton's equations are

$$\dot{a}_{\boldsymbol{k}} = i\frac{\delta H}{\delta a^*_{\boldsymbol{k}}} = i\omega_{\boldsymbol{k}} a_{\boldsymbol{k}} + i\frac{\delta U}{\delta a^*_{\boldsymbol{k}}} \tag{1.61}$$ eq-3W1

$$= i\omega_{\boldsymbol{k}} a_{\boldsymbol{k}} + i\int d\boldsymbol{k}_1 d\boldsymbol{k}_2 \left(W^{\boldsymbol{k}}_{\boldsymbol{k}_1\boldsymbol{k}_2}\, a_{\boldsymbol{k}_1} a_{\boldsymbol{k}_2}\,\delta^{\boldsymbol{k}}_{\boldsymbol{k}_1\boldsymbol{k}_2} + 2W^{\boldsymbol{k}_1}_{\boldsymbol{k}\boldsymbol{k}_2}\, a_{\boldsymbol{k}_1} a^*_{\boldsymbol{k}_2}\,\delta^{\boldsymbol{k}_1}_{\boldsymbol{k}\boldsymbol{k}_2}\right). \tag{1.62}$$ eq-3W2

A generic issue whenever you replace a detailed description of a nonlinear equation with a statistical description is that you have a closure problem. For example, when you write an equation for the second moment, it will depend on the third moment:

$$\begin{aligned}
\partial_t\langle a_{\boldsymbol{k}} a^*_{\boldsymbol{k}'}\rangle &= i\int d\boldsymbol{k}_1 d\boldsymbol{k}_2 \left(W^{\boldsymbol{k}}_{\boldsymbol{k}_1\boldsymbol{k}_2}\langle a^*_{\boldsymbol{k}'} a_{\boldsymbol{k}_1} a_{\boldsymbol{k}_2}\rangle\,\delta^{\boldsymbol{k}}_{\boldsymbol{k}_1\boldsymbol{k}_2} + 2W^{\boldsymbol{k}_1}_{\boldsymbol{k}\boldsymbol{k}_2}\langle a^*_{\boldsymbol{k}'} a_{\boldsymbol{k}_1} a^*_{\boldsymbol{k}_2}\rangle\,\delta^{\boldsymbol{k}_1}_{\boldsymbol{k}\boldsymbol{k}_2}\right)\\
&\quad - i\int d\boldsymbol{k}_1 d\boldsymbol{k}_2 \left(W^{\boldsymbol{k}'}_{\boldsymbol{k}_1\boldsymbol{k}_2}\langle a_{\boldsymbol{k}} a^*_{\boldsymbol{k}_1} a^*_{\boldsymbol{k}_2}\rangle\,\delta^{\boldsymbol{k}'}_{\boldsymbol{k}_1\boldsymbol{k}_2} + 2W^{\boldsymbol{k}_1}_{\boldsymbol{k}'\boldsymbol{k}_2}\langle a_{\boldsymbol{k}} a^*_{\boldsymbol{k}_1} a_{\boldsymbol{k}_2}\rangle\,\delta^{\boldsymbol{k}_1}_{\boldsymbol{k}'\boldsymbol{k}_2}\right).
\end{aligned}$$

Similarly, writing an equation for the third moment with will similarly involve the fourth moment. If we try to write equations for cumulants rather than moments, we run into the same issue. In hydrodynamic turbulence, this problem is often addressed at the level

of modelling, where some assumptions are imposed on the moments. For example, they may assume the fourth moment is a function of the second and third. Lots of literature on what these functions are and how they work. This is less true for Wave turbulence rather than hydrodynamic turbulence.

For the Navier-Stokes equation, we had a constant flux relation expressed in equation (1.35) that measured the transfer of energy through a given wave number $\boldsymbol{k}$ in the inertial range in the limit of low viscosity and large time. We would like a parallel relation here. However here, the quadratic part of the energy is not conserved but rather the entire Hamiltonian. So, we may write an analogue of the scale resolved energy balance equation (1.30):

$$\begin{aligned}\partial_t\langle \mathcal{H}_{\boldsymbol{k}}\rangle + \nabla_{\boldsymbol{k}}\cdot\langle J^{(\mathcal{H})}_{\boldsymbol{k}}\rangle &= \mathcal{F}_{\boldsymbol{k}} - \mathcal{D}_{\boldsymbol{k}}\\ &= 0 \quad \text{(in the inertial range)}.\end{aligned}$$

In the steady-state, we further have a divergence free condition on the current of our Hamiltonian density:

$$\nabla_{\boldsymbol{k}}\cdot\langle J^{(\mathcal{H})}_{\boldsymbol{k}}\rangle = 0.$$

So, if we have a turbulent statistically stationary state, using equation (1.61) we have the constraints:

$$\begin{aligned}0 &= -\nabla_{\boldsymbol{k}}\cdot\langle J^{(\mathcal{H})}_{\boldsymbol{k}}\rangle = \langle \dot{\mathcal{H}}_{\boldsymbol{k}}\rangle\\ 0 &= \omega_{\boldsymbol{k}}\langle \dot{a}_{\boldsymbol{k}}a^*_{\boldsymbol{k}}\rangle + \omega_{\boldsymbol{k}}\langle a_{\boldsymbol{k}}\dot{a}^*_{\boldsymbol{k}}\rangle + \langle \dot{u}_{\boldsymbol{k}}\rangle\\ 0 &= \langle \dot{u}_{\boldsymbol{k}} - \dot{a}_{\boldsymbol{k}}\frac{\delta U}{\delta a_{\boldsymbol{k}}} - \dot{a}^*_{\boldsymbol{k}}\frac{\delta U}{\delta a^*_{\boldsymbol{k}}}\rangle.\end{aligned}$$

More calculations?: Here, we want to deduce something about correlation functions by expressing our current in terms of $a_{\boldsymbol{k}}$. Using these constraints, you can deduce conservation of energy in the inertial range expressed in terms of correlation functions of the wave field:

$$0 = 2\int d\boldsymbol{k}_1 d\boldsymbol{k}_2 \left[W^{\boldsymbol{k}}_{\boldsymbol{k}_1\boldsymbol{k}_2}\,\mathrm{Re}\langle a^*_{\boldsymbol{k}}\dot{a}_{\boldsymbol{k}_1}a_{\boldsymbol{k}_2}\rangle\,\delta^{\boldsymbol{k}}_{\boldsymbol{k}_1\boldsymbol{k}_2} - W^{\boldsymbol{k}_1}_{\boldsymbol{k}\boldsymbol{k}_2}\,\mathrm{Re}\langle a^*_{\boldsymbol{k}_1}\dot{a}_{\boldsymbol{k}}a_{\boldsymbol{k}_2}\rangle\,\delta^{\boldsymbol{k}_1}_{\boldsymbol{k}\boldsymbol{k}_2}\right]. \tag{1.63}$$

Note that although we have lots of cancellations, we still have a time derivative on $a_{\boldsymbol{k}_1}$. This gives the following correlation function (assuming isotropy and using angle averaging):

$$C^{(\mathcal{H})}(k,k_1,k_2) = \int d\Omega_1 d\Omega_2 \mathrm{Re}\langle a^*_{\boldsymbol{k}}\dot{a}_{\boldsymbol{k}_1}a_{\boldsymbol{k}_2}\rangle\,\delta^{\boldsymbol{k}}_{\boldsymbol{k}_1\boldsymbol{k}_2}.$$

We then have the following integral equation over scalar modulus of wave vectors:

$$\int dk_1 dk_2 (k_1k_2)^{d-1}\left[W^{\boldsymbol{k}}_{\boldsymbol{k}_1\boldsymbol{k}_2}C^{(\mathcal{H})}(k,k_1,k_2) - W^{\boldsymbol{k}_1}_{\boldsymbol{k}\boldsymbol{k}_2}C^{(\mathcal{H})}(k_1,k,k_2)\right] = 0. \tag{1.64}$$ int-mod

This is a desirable way to see the flux as it is a term expressing the amount going into a particular wave number minus a term expressing the amount leaving a particular wave number.

Now, assuming scale invariance, we have scaling properties on our correlation function:

$$\begin{aligned}W^{h\boldsymbol{k}}_{h\boldsymbol{k}_1\,h\boldsymbol{k}_2} &= h^{\gamma}W^{\boldsymbol{k}}_{\boldsymbol{k}_1\boldsymbol{k}_2}\\ C^{(\mathcal{H})}(hk,hk_1,hk_2) &= h^{-y}C^{(\mathcal{H})}(k,k_1,k_2).\end{aligned}$$

Using this, we may modify the equation (1.64) using a Zakharov-Kraichnan change of variables to map the second term onto the first:

$$k_1 = \frac{k^2}{k_1'}, \qquad k_2 = \frac{kk_2'}{k_1'},$$

giving

$$\int dk_1 dk_2 (k_1 k_2)^{d-1} W^{\boldsymbol{k}}_{\boldsymbol{k}_1\boldsymbol{k}_2} C^{(\mathcal{H})}(k, k_1, k_2) \left[1 - \frac{k}{k_1}^{\gamma+3d-y}\right] = 0.$$

Therefore, looking at the term in brackets, we must have $y = \gamma + 3d$.

Using this analysis, we can see why there is no Wave Turbulence analogue of the Kalmogorov's 4/5 law. We derived that $\gamma + 3d$ scaling is exact without any assumptions of weak nonlinearity or closure. However, we expressed everything in phase space and have no local $\boldsymbol{x}$ representation. Also, our Hamiltonian density $\mathcal{H}_{\boldsymbol{k}}$ is not quadratic.

However, we may look at one particular example and get an analogue of the Kalmogorov's 4/5 law. For the Föppl-von Kármán equations (1.47 - 1.49), the Hamiltonian is quadratic and the field equations are local in $\boldsymbol{x}$-space. It turns out, we have the Düring and Krstulovic 1-law here, as seen in [18]. In particular, they showed that in the inertial range,

$$\langle \mathcal{J}[\delta\chi, \delta\zeta]\, \delta\dot{\zeta} \rangle \cdot \hat{\boldsymbol{r}} = -\epsilon\, r, \tag{1.65}$$

where $\delta\zeta = \zeta(\boldsymbol{x} + \boldsymbol{r}) - \zeta(\boldsymbol{x})$. Note that you can show

$$\mathcal{N}[f, g] = -\nabla \cdot \mathcal{J}[f, g]$$

with

$$\mathcal{J}[f, g] = \begin{pmatrix} f_y g_{yx} - f_x g_{yy} \\ f_x g_{xy} - f_y g_{xx} \end{pmatrix}.$$

So, $\mathcal{J}$ is cubic in the fields, and 1-law correlation function is quartic in the amplitude variables. This is consistent with the leading interaction being 4-wave. This is only result like this for strong wave turbulence.

1.4 Wave Kinetic Equations via Multiple Scale Analysis

The aim of this section is to derive the wave-kinetic equation (WKE) via a multiple scale analysis. In particular, the WKE is an effective equation to describe the evolution of the wave-spectrum, valid on a certain time-scale. Recall that the wave spectrum $n(\boldsymbol{k})$, defined in (1.59), relates to the second moment. Our main goal is to (formally) justify the following

Claim: *when the nonlinearity is weak, the long time behaviour of $n_{\boldsymbol{k}}(t)$ is determined by the wave kinetic equation:*

$$\begin{aligned}
\frac{\partial n_{\boldsymbol{k}_1}}{\partial t} = \pi \int & \left|W^{\boldsymbol{k}_1}_{\boldsymbol{k}_2\boldsymbol{k}_3}\right|^2 (n_{\boldsymbol{k}_2} n_{\boldsymbol{k}_3} - n_{\boldsymbol{k}_1} n_{\boldsymbol{k}_2} - n_{\boldsymbol{k}_1} n_{\boldsymbol{k}_3}) \delta^{\omega_{\boldsymbol{k}_1}}_{\omega_{\boldsymbol{k}_2},\omega_{\boldsymbol{k}_3}} \delta^{\boldsymbol{k}_1}_{\boldsymbol{k}_2,\boldsymbol{k}_3}\, d\boldsymbol{k}_2 d\boldsymbol{k}_3 \\
+ \pi \int & \left|W^{\boldsymbol{k}_2}_{\boldsymbol{k}_1\boldsymbol{k}_3}\right|^2 (n_{\boldsymbol{k}_2} n_{\boldsymbol{k}_3} + n_{\boldsymbol{k}_1} n_{\boldsymbol{k}_2} - n_{\boldsymbol{k}_1} n_{\boldsymbol{k}_3}) \delta^{\omega_{\boldsymbol{k}_2}}_{\omega_{\boldsymbol{k}_3},\omega_{\boldsymbol{k}_1}} \delta^{\boldsymbol{k}_2}_{\boldsymbol{k}_3,\boldsymbol{k}_1}\, d\boldsymbol{k}_2 d\boldsymbol{k}_3 \\
+ \pi \int & \left|W^{\boldsymbol{k}_3}_{\boldsymbol{k}_1\boldsymbol{k}_2}\right|^2 (n_{\boldsymbol{k}_2} n_{\boldsymbol{k}_3} - n_{\boldsymbol{k}_1} n_{\boldsymbol{k}_2} + n_{\boldsymbol{k}_1} n_{\boldsymbol{k}_3}) \delta^{\omega_{\boldsymbol{k}_3}}_{\omega_{\boldsymbol{k}_1},\omega_{\boldsymbol{k}_2}} \delta^{\boldsymbol{k}_3}_{\boldsymbol{k}_1,\boldsymbol{k}_2}\, d\boldsymbol{k}_2 d\boldsymbol{k}_3,
\end{aligned} \tag{1.66}$$

eq:3WKE

where we recall the notation introduced in (2) for the δ.

We will only sketch the derivation for the BPV equation since it is (slightly) less messy. Recalling (1.55)-(1.57), the equation we consider is

$$\frac{\partial a_{\boldsymbol{k}}}{\partial t} + i\,\omega_{\boldsymbol{k}}\,a_{\boldsymbol{k}} = \int W^{\boldsymbol{k}}_{\boldsymbol{k}_1\,\boldsymbol{k}_2}\,a_{\boldsymbol{k}_1}\,a_{\boldsymbol{k}_2}\,\delta^{\boldsymbol{k}}_{\boldsymbol{k}_1\,\boldsymbol{k}_2}\,d\boldsymbol{k}_1 d\boldsymbol{k}_2. \tag{1.67}$$ eq-CHMk

It is convenient to introduce *interaction* variables that incorporate the linear dynamics and a formal small parameter ϵ:

$$\epsilon\, b_{\boldsymbol{k}} = a_{\boldsymbol{k}}\,\mathrm{e}^{i\,\omega_{\boldsymbol{k}}\,t}, \tag{1.68}$$ eq-interactionRepresentation

in which the equation (1.67) takes the form

$$\frac{\partial b_{\boldsymbol{k}}}{\partial t} = \epsilon \int W^{\boldsymbol{k}}_{\boldsymbol{k}_1\,\boldsymbol{k}_2}\,b_{\boldsymbol{k}_1}\,b_{\boldsymbol{k}_2}\,\delta^{\boldsymbol{k}}_{\boldsymbol{k}_1\,\boldsymbol{k}_2}\,\mathrm{e}^{i\,\Omega^{\boldsymbol{k}}_{\boldsymbol{k}_1\,\boldsymbol{k}_2}\,t}\,d\boldsymbol{k}_1 d\boldsymbol{k}_2, \tag{1.69}$$ eq-CHMk3

where we defined the shorthand notation

$$\Omega^{\boldsymbol{p}}_{\boldsymbol{q}\,\boldsymbol{r}} = \omega_{\boldsymbol{p}} - \omega_{\boldsymbol{q}} - \omega_{\boldsymbol{r}}. \tag{1.70}$$ def:Omres

1.4.1 Asymptotic expansions and approximations

Defining the interaction variables $b_{\boldsymbol{k}}$ with a parameter ϵ is equivalent to assume a weak nonlinearity regime. In order to exploit this assumption, we aim at solving (1.69) perturbatively, namely

$$b_{\boldsymbol{k}}(t) = b^{(0)}_{\boldsymbol{k}}(t) + \epsilon\, b^{(1)}_{\boldsymbol{k}}(t) + \epsilon^2\, b^{(2)}_{\boldsymbol{k}}(t) + \dots \tag{1.71}$$

Usually, in perturbation theory, a first non-trivial answer can be already obtained to first order in ϵ, however in this case it turns out to be necessary to go to second order in ϵ. This issue is the main source of the algebraic complexity of the computations we are going to sketch below.

The first few terms in the expansion can be computed explicitly (Add some computation?) and are

$$b^{(0)}_{\boldsymbol{k}}(t) = B_{\boldsymbol{k}} \tag{1.72}$$ eq-order0

$$b^{(1)}_{\boldsymbol{k}}(t) = \int W^{\boldsymbol{k}}_{\boldsymbol{k}_1\,\boldsymbol{k}_2}\,B_{\boldsymbol{k}_1}\,B_{\boldsymbol{k}_2}\,\delta^{\boldsymbol{k}}_{\boldsymbol{k}_1\,\boldsymbol{k}_2}\,\Delta(\Omega^{\boldsymbol{k}}_{\boldsymbol{k}_1\,\boldsymbol{k}_2}, t)\,d\boldsymbol{k}_1 d\boldsymbol{k}_2 \tag{1.73}$$ eq-order1

$$b^{(2)}_{\boldsymbol{k}}(t) = -2\int W^{\boldsymbol{k}}_{\boldsymbol{k}_1\,\boldsymbol{k}_2}\,W^{\boldsymbol{k}_1}_{\boldsymbol{k}_3\,\boldsymbol{k}_4}B_{\boldsymbol{k}_2}\,B_{\boldsymbol{k}_3}\;B_{\boldsymbol{k}_4}\;\delta^{\boldsymbol{k}}_{\boldsymbol{k}_1\,\boldsymbol{k}_2}\,\delta^{\boldsymbol{k}_1}_{\boldsymbol{k}_3\,\boldsymbol{k}_4}\,E(\Omega^{\boldsymbol{k}_2\,\boldsymbol{k}_3\,\boldsymbol{k}_4}_{\boldsymbol{k}}, \Omega^{\boldsymbol{k}_1\,\boldsymbol{k}_2}_{\boldsymbol{k}}, t)\,d\boldsymbol{k}_1 d\boldsymbol{k}_2 d\boldsymbol{k}_3 d\boldsymbol{k}_4 \tag{1.74}$$ eq-order2

check for typos in the equations above where the $B_{\boldsymbol{k}}$ are constants and

$$\Delta(x,t) = \int_0^t \mathrm{e}^{i\,x\,\tau}\,d\tau = \frac{\mathrm{e}^{i\,x\,t} - 1}{i\,x} \tag{1.75}$$ eq-DeltaIntegral

$$E(x,y,t) = \int_0^t \Delta(x-y,\tau)\,\mathrm{e}^{i\,y\,\tau} d\tau. \tag{1.76}$$ eq-EIntegral

Notice that all the time-dependence is in the integrals.

We are interested in studying the limiting case $t = +\infty$, however, the integrals above are not well defined in this scenario. To overcome this problem, we consider

$$\Delta^{\varepsilon}(x,t) = \int_0^t \mathrm{e}^{i\,x\,\tau-\varepsilon\tau}\,d\tau = \frac{e^{ixt-\varepsilon t}-1}{ix-\varepsilon} = i\frac{1-e^{ixt-\varepsilon t}}{x+i\varepsilon}. \tag{1.77}$$ eq-DeltaInt

Clearly, $\Delta^{\varepsilon}(x,t) \xrightarrow[\varepsilon\to 0]{} \Delta(x,t)$, but notice that

$$\lim_{t\to+\infty} \Delta^{\varepsilon}(x,t) = i\frac{1}{x+i\varepsilon} \tag{1.78}$$

Thus, taking the limits in the correct order and interpreting them in the distributional sense, from the Sokhotski–Plemelj Theorem add at least the heuristic proof in appendix? we get

$$\lim_{t\to+\infty} \Delta(x,t) := \lim_{\varepsilon\to 0}\lim_{t\to+\infty} \Delta^{\varepsilon}(x,t) = \pi\delta(x) + i\mathcal{P}\left(\frac{1}{x}\right), \tag{1.79}$$ eq:SokPlem

where $\mathcal{P}$ is the Cauchy principal value distribution add definition in appendix?.

At this point we begin to see why *resonant* interactions, i.e. when $x = 0$, play such a central role in weak wave turbulence. For instance, the term $b_{\boldsymbol{k}}^{(1)}(t)$, see (1.73), in the long-time limit concentrates on the resonant sets:

$$\omega_{\boldsymbol{k}} = \omega_{\boldsymbol{k}_1} + \omega_{\boldsymbol{k}_2}. \tag{1.80}$$

In addition, the other δ function impose that $\boldsymbol{k} = \boldsymbol{k}_1 + \boldsymbol{k}_2$. Likewise for $b_{\boldsymbol{k}}^{(2)}(t)$, one can show that

$$\lim_{t\to+\infty} E(x,y,t) = \left(\pi\delta(x) + i\mathcal{P}\left(\frac{1}{x}\right)\right)\left(\pi\delta(y) + i\mathcal{P}\left(\frac{1}{y}\right)\right) \tag{1.81}$$

Shall we comment more about this limit? The product of two distributions does not make sense, what do we mean here? Can we deduce a more precise version as above?

1.4.1.1 Averaging

Combining (1.72)-(1.74) with the definition of the wave spectrum (1.59), to order ϵ^2 we find that some more computation here?

$$\begin{aligned} n_{\boldsymbol{p}}(t)\,\delta^{\boldsymbol{p}}_{\boldsymbol{p}'} =& \langle B_{\boldsymbol{p}}\,\overline{B}_{\boldsymbol{p}'}\rangle \\ &+ \epsilon \int W^{\boldsymbol{p}'}_{\boldsymbol{k}_1\,\boldsymbol{k}_2}\,\langle B_{\boldsymbol{p}}\overline{B}_{\boldsymbol{k}_1}\,\overline{B}_{\boldsymbol{k}_2}\rangle\,\delta^{\boldsymbol{p}'}_{\boldsymbol{k}_1\,\boldsymbol{k}_2}\,\Delta(\Omega^{\boldsymbol{k}_1\,\boldsymbol{k}_2}_{\boldsymbol{p}'},t)d\boldsymbol{k}_1 d\boldsymbol{k}_2 \\ &+ \epsilon \int W^{\boldsymbol{p}}_{\boldsymbol{k}_1\,\boldsymbol{k}_2}\,\langle \overline{B}_{\boldsymbol{p}'}B_{\boldsymbol{k}_1}\,B_{\boldsymbol{k}_2}\rangle\,\delta^{\boldsymbol{p}}_{\boldsymbol{k}_1\,\boldsymbol{k}_2}\,\Delta(\Omega^{\boldsymbol{p}}_{\boldsymbol{k}_1\,\boldsymbol{k}_2},t)d\boldsymbol{k}_1 d\boldsymbol{k}_2 \\ &- 4\,\epsilon^2 \int W^{\boldsymbol{p}}_{\boldsymbol{k}_1\,\boldsymbol{k}_2}\,W^{\boldsymbol{k}_1}_{\boldsymbol{k}_3\,\boldsymbol{k}_4}\mathrm{Re}\left[\langle\overline{B}_{\boldsymbol{p}'}\,B_{\boldsymbol{k}_2}\,B_{\boldsymbol{k}_3}\,B_{\boldsymbol{k}_4}\rangle\right] \\ &\qquad \delta^{\boldsymbol{p}}_{\boldsymbol{k}_1\,\boldsymbol{k}_2}\,\delta^{\boldsymbol{k}_1}_{\boldsymbol{k}_3\,\boldsymbol{k}_4}\,E(\Omega^{\boldsymbol{k}_2\,\boldsymbol{k}_3\,\boldsymbol{k}_4}_{\boldsymbol{p}},\Omega^{\boldsymbol{k}_1\,\boldsymbol{k}_2}_{\boldsymbol{p}},t)d\boldsymbol{k}_1 d\boldsymbol{k}_2 d\boldsymbol{k}_3 d\boldsymbol{k}_4 \\ &+ \epsilon^2 \int W^{\boldsymbol{p}}_{\boldsymbol{k}_1\,\boldsymbol{k}_2}\,W^{\boldsymbol{p}'}_{\boldsymbol{k}_3\,\boldsymbol{k}_4}\langle B_{\boldsymbol{k}_1}\,B_{\boldsymbol{k}_2}\,\overline{B}_{\boldsymbol{k}_3}\,\overline{B}_{\boldsymbol{k}_4}\rangle \\ &\qquad \delta^{\boldsymbol{p}}_{\boldsymbol{k}_1\,\boldsymbol{k}_2}\,\delta^{\boldsymbol{p}'}_{\boldsymbol{k}_3\,\boldsymbol{k}_4}\,\Delta(\Omega^{\boldsymbol{p}}_{\boldsymbol{k}_1\,\boldsymbol{k}_2},t)\,\Delta(\Omega^{\boldsymbol{k}_3\,\boldsymbol{k}_4}_{\boldsymbol{p}'},t)d\boldsymbol{k}_1 d\boldsymbol{k}_2 d\boldsymbol{k}_3 d\boldsymbol{k}_4. \end{aligned} \tag{1.82}$$ eq-perturba

Taking into account that $\langle B_{\boldsymbol{k}}\rangle = 0$, using the fact that $\overline{b}_{\boldsymbol{k}} = b_{-\boldsymbol{k}}$ and taking $s_i = \pm 1$, one can write a general third or fourth order correlation function as:

$$\langle B_{s_1\boldsymbol{k}_1} B_{s_2\boldsymbol{k}_2} B_{s_3\boldsymbol{k}_3}\rangle = Q^{(3)}_{s_1\boldsymbol{k}_1\, s_2\boldsymbol{k}_2\, s_3\boldsymbol{k}_3} \tag{1.83}$$ eq-M3

$$\langle B_{s_1\boldsymbol{k}_1} B_{s_2\boldsymbol{k}_2} B_{s_3\boldsymbol{k}_3} B_{s_4\boldsymbol{k}_4}\rangle = n_{\boldsymbol{k}_1}\, n_{\boldsymbol{k}_2}\, \delta^{s_1\boldsymbol{k}_1}_{s_3\boldsymbol{k}_3}\delta^{s_2\boldsymbol{k}_2}_{s_4\boldsymbol{k}_4} + n_{\boldsymbol{k}_1}\, n_{\boldsymbol{k}_3}\, \delta^{s_1\boldsymbol{k}_1}_{s_2\boldsymbol{k}_2}\delta^{s_3\boldsymbol{k}_3}_{s_4\boldsymbol{k}_4} \tag{1.84}$$ eq-M4

$$+ n_{\boldsymbol{k}_1}\, n_{\boldsymbol{k}_2}\, \delta^{s_1\boldsymbol{k}_1}_{s_4\boldsymbol{k}_4}\delta^{s_2\boldsymbol{k}_2}_{s_3\boldsymbol{k}_3} + Q^{(4)}_{s_1\boldsymbol{k}_1\, s_2\boldsymbol{k}_2\, s_3\boldsymbol{k}_3\; s_4\boldsymbol{k}_4} \tag{1.85}$$

where $Q^{(3)}$ and $Q^{(4)}$ are the appropriate third and fourth order cumulants of the field $B_{\boldsymbol{k}}$.

We now have to introduce a the so called Random phase "approximation" or Wick closure, namely we neglect $Q^{(3)}_{s_1\boldsymbol{k}_1\, s_2\boldsymbol{k}_2\, s_3\boldsymbol{k}_3}$ and $Q^{(4)}_{s_1\boldsymbol{k}_1\, s_2\boldsymbol{k}_2\, s_3\boldsymbol{k}_3\; s_4\boldsymbol{k}_4}$.

Remark 3. *The Wick closure cannot be really considered as an approximation since it is not clear even at a formal level why one should be able to neglect those terms. In fact, there is no guess of what should be the correction to this approximation.*

Are we somehow implicitly assuming that if we start with a random Gaussian initial data it will remain Gaussian also at later times?

Thanks to the Wick closure, we can compute the averages in (1.82). Denoting $\langle B_{\boldsymbol{p}}\overline{B}_{\boldsymbol{p}'}\rangle = n^{(0)}_{\boldsymbol{p}}$ and integrating out the two delta functions coming from (1.84), we get

$$\begin{aligned} n_{\boldsymbol{p}}(t)\,\delta^{\boldsymbol{p}}_{\boldsymbol{p}'} &= n^{(0)}_{\boldsymbol{p}}\,\delta^{\boldsymbol{p}}_{\boldsymbol{p}'} \\ &+ 2\,\epsilon^2 \int W^{\boldsymbol{p}}_{\boldsymbol{k}_1\,\boldsymbol{k}_2} W^{\boldsymbol{p}}_{\boldsymbol{k}_1\,\boldsymbol{k}_2}\, \delta^{\boldsymbol{p}}_{\boldsymbol{k}_1\,\boldsymbol{k}_2}\, n_{\boldsymbol{k}_1}\, n_{\boldsymbol{k}_2}\; \Delta(\Omega^{\boldsymbol{p}}_{\boldsymbol{k}_1\,\boldsymbol{k}_2}, t)\, \Delta(\Omega^{\boldsymbol{k}_1\,\boldsymbol{k}_2}_{\boldsymbol{p}}, t)\; \delta^{\boldsymbol{p}}_{\boldsymbol{p}'} d\boldsymbol{k}_1 d\boldsymbol{k}_2 \\ &- 8\,\epsilon^2 \int W^{\boldsymbol{p}}_{\boldsymbol{k}_1\,\boldsymbol{k}_2} W^{\boldsymbol{k}_1}_{\boldsymbol{p}\,\boldsymbol{k}_2}\, \delta^{\boldsymbol{p}}_{\boldsymbol{k}_1\,\boldsymbol{k}_2}\, n_{\boldsymbol{p}}\, n_{\boldsymbol{k}_2}\; \mathrm{Re}\left[E(0, \Omega^{\boldsymbol{p}}_{\boldsymbol{k}_1\,\boldsymbol{k}_2}; t)\right]\; \delta^{\boldsymbol{p}}_{\boldsymbol{p}'} d\boldsymbol{k}_1 d\boldsymbol{k}_2, \end{aligned} \tag{1.86}$$ eq-perturbativenk2

where we have also used the symmetries of $W^{\boldsymbol{p}}_{\boldsymbol{k}_1\,\boldsymbol{k}_2}$ to group similar terms together. Add some computation here?

1.4.1.2 The wave kinetic equation for the BPV

Notice that the averaging procedure introduced some singular integrals that diverge as $t \to \infty$. For large time, they behave as add REF [Newell, 1968]:

$$\Delta(x;t)\,\Delta(-x;t) \sim 2\,\pi\, t\delta(x) + 2\,\mathcal{P}\left(\frac{1}{x}\right)\frac{\partial}{\partial x}$$

$$E(0,x;t) \sim \left[\pi\,\delta(x) + i\,\mathcal{P}\left(\frac{1}{x}\right)\right]\, t - i\,\left[\pi\delta(x) + i\,\mathcal{P}\left(\frac{1}{x}\right)\frac{\partial}{\partial x}\right],$$

It seems to me that the computation of this limit may be analogous to the limit of E. See if it is worth trying to make some more explicit computation.

We now see that our expansion breaks down at $t \sim \epsilon^{-2}$:

$$n_{\boldsymbol{p}}(t) = n^{(0)}_{\boldsymbol{p}} - (\epsilon^2\, t)\, S\left[n^0_{\boldsymbol{k}}\right] + \epsilon^2\,[\text{terms bounded in } t], \tag{1.87}$$ eq-perturbativenk3

where the divergent (secular) part is

$$\begin{aligned} S\left[n^0_{\boldsymbol{k}}\right] &= 4\pi \int W^{\boldsymbol{p}}_{\boldsymbol{k}_1\,\boldsymbol{k}_2} W^{\boldsymbol{p}}_{\boldsymbol{k}_1\,\boldsymbol{k}_2}\, \delta^{\boldsymbol{p}}_{\boldsymbol{k}_1\,\boldsymbol{k}_2}\, n_{\boldsymbol{k}_1}\, n_{\boldsymbol{k}_2}\; \delta(\Omega^{\boldsymbol{p}}_{\boldsymbol{k}_1\,\boldsymbol{k}_2}) d\boldsymbol{k}_1 d\boldsymbol{k}_2 \\ &- 8\pi \int W^{\boldsymbol{p}}_{\boldsymbol{k}_1\,\boldsymbol{k}_2} W^{\boldsymbol{k}_1}_{\boldsymbol{p}\,\boldsymbol{k}_2}\, \delta^{\boldsymbol{p}}_{\boldsymbol{k}_1\,\boldsymbol{k}_2}\, n_{\boldsymbol{p}}\, n_{\boldsymbol{k}_2}\; \delta(\Omega^{\boldsymbol{p}}_{\boldsymbol{k}_1\,\boldsymbol{k}_2}) d\boldsymbol{k}_1 d\boldsymbol{k}_2. \end{aligned}$$

Remark 4. *The divernces concentrate on the resonant curves.*

The term $(\epsilon^2 t)S[n_{\boldsymbol{k}}^0]$ may give rise to a *secular growth*, but this mechanism it is not believed to persist for long times. One possibility to overcome this problem is to take a step back and assume that $n_{\boldsymbol{p}}^{(0)}$ varies slowly on the nonlinear timescale $T_2 = \epsilon^2 t$. We then treat T_2 as an additional independent variable so that we have $n_{\boldsymbol{p}}^{(0)}(t, T_2)$. In our case, we assume that $n_{\boldsymbol{p}}^{(0)}$ is constant with respect t so we get:

$$\frac{dn_{\boldsymbol{p}}^{(0)}}{dt} = \frac{\partial n_{\boldsymbol{p}}^{(0)}}{\partial t} + \frac{\partial n_{\boldsymbol{p}}^{(0)}}{\partial T_2}\frac{dT_2}{dt} = \epsilon^2 \frac{\partial n_{\boldsymbol{p}}^{(0)}}{\partial T_2} \tag{1.88}$$

Differentiating the equation (1.87) with respect to t, we have

$$\frac{dn_{\boldsymbol{p}}}{dt} = \epsilon^2 \frac{\partial n_{\boldsymbol{p}}^{(0)}}{\partial T_2} - \epsilon^2\, S\left[n_{\boldsymbol{k}}^0\right] + \epsilon^2 \frac{d}{dt}[\text{terms bounded in } t]. \tag{1.89}$$

Therefore, we conclude that the expansion is consistent to times $\sim \epsilon^4 t$ if

$$\frac{\partial n_{\boldsymbol{p}}^{(0)}}{\partial T_2} = S\left[n_{\boldsymbol{k}}^0\right] \qquad \text{(3-wave kinetic equation)} \tag{1.90}$$

eq-consiste

Is it actually what we had at the claim at the beginning of this section?

Remark 5. *The kinetic equation can be seen as a consistency condition that must be satisfied by the second moment to account for the effect of resonant interactions on the timescale of $\epsilon^2 t$.*

The procedure to derive the WKE presented here is fundamentally non-perturbative. In particular, solution of the kinetic equation adds up an infinite number of terms in the original regular perturbation expansion but we do not which are the relevant terms to consider do someone know?.

We also point out that, in principle, the method of multiple scales can be extended to higher orders to describe behaviour on longer timescales, $\epsilon^4 t$ etc. However, it is not even guaranteed that the *solution* of the kinetic equation is consistent with the assumption of weak nonlinearity/separation of timescales used in this derivation.

1.4.1.3 Nonlinear frequency correction

We focused thus far on the the correlation function $\langle \overline{a}(\boldsymbol{k})\, a(\boldsymbol{k}')\rangle$. What about the expansion of $\langle a(\boldsymbol{k})\, a(\boldsymbol{k}')\rangle$? In this case, the $i\omega_{\boldsymbol{k}} a_{\boldsymbol{k}}$ terms do not disappear at leading order so a "fast" time dependence remains. We could carry on computations analogous to the one in previous subsection (with more or less the same level of algebraic complexity) and find secular terms on the ϵt timescale in the expansion. However, the consistency condition for the removal of these secular terms is less complex and can be solved explicitly by correcting the frequency as

$$\omega_{\boldsymbol{k}} \to \omega_{\boldsymbol{k}} + \Omega_\epsilon[n_{\boldsymbol{k}}]. \tag{1.91}$$

in the notes there wasn't the ϵ dependence on Ω. I have included it because in general it depends on ϵ.

$$\Omega_\epsilon[n_{\boldsymbol{k}}] \sim \epsilon^q \int \left|W_{\boldsymbol{k}_1\boldsymbol{k}_2}^{\boldsymbol{k}}\right|^2 n_{\boldsymbol{k}_1} \delta_{\boldsymbol{k}_1\boldsymbol{k}_2}^{\boldsymbol{k}} \delta(\Omega_{\boldsymbol{k}_1\boldsymbol{k}_2}^{\boldsymbol{k}}) d\boldsymbol{k}_1 d\boldsymbol{k}_2 \tag{1.92}$$

and q can be explicitly computed. This nonlinear frequency correction should have some relation with the removal of "trivial" resonances done in Bianchini's lecture. Check this and add maybe some reference to that chapter.

1.4.2 The asymptotic closure argument of Newell

In deriving the kinetic equation we *assumed* the Wick closure. The asymptotic closure argument shows that the Wick closure arises naturally from the dynamics for long times is this the argument of Newell or do we mean that the previous approximation is natural?. In REF Newell? it was proposed the following procedure to avoid the formal random phase approximation:

- Go back to equation (1.86) but *do not* neglect $Q^{(3)}_{s_1\boldsymbol{k}_1\, s_2\boldsymbol{k}_2\, s_3\boldsymbol{k}_3}$ and $Q^{(4)}_{s_1\boldsymbol{k}_1\, s_2\boldsymbol{k}_2\, s_3\boldsymbol{k}_3\ s_4\boldsymbol{k}_4}$.
- Write perturbative expansions for $Q^{(3)}_{s_1\boldsymbol{k}_1\, s_2\boldsymbol{k}_2\, s_3\boldsymbol{k}_3}(t)$ and $Q^{(4)}_{s_1\boldsymbol{k}_1\, s_2\boldsymbol{k}_2\, s_3\boldsymbol{k}_3\ s_4\boldsymbol{k}_4}(t)$ and identify any additional secular terms that should be included in the consistency condition (1.90).
- No *new* secular terms appear that are not already accounted for in the consistency conditions for $\langle \overline{a}(\boldsymbol{k})\, a(\boldsymbol{k}')\rangle$ (kinetic equation) and $\langle a(\boldsymbol{k})\, a(\boldsymbol{k}')\rangle$ (nonlinear frequency correction).

Remark 6. *We claim that this finding is general. More precisely, the dynamics generates correlations in such a way that the secular (divergent) terms appearing in the higher order cumulants are functions of lower order cumulants only.*

This does not say that there is no closure problem. Rather, the asymptotic consistency conditions for the removal of divergences from perturbation theory (for all cumulants) are closed. However, it may provide useful insights for mathematical treatments of wave kinetics. We stress again that accounting for the nonlinear frequency correction is essential to asymptotic closure.

The derivation of the WKE related to the NLS has been achieved by Deng and Hani in [16] *and we mention also the previous contributions* [3, 6]. *For a multi-d KdV type equation we refer to the work of Staffilani and Tran* [47].

1.5 Stationary Solutions of the Wave Kinetic Equation

In the previous section we derived the 3-wave kinetic equation for the BPV. The general symmetric form a 3-wave kinetic equation is

$$\partial_t n_{\boldsymbol{k}_1} = S[n_{\boldsymbol{k}_1}] = \int_{\mathbf{R}^{2d}} \left(R_{\boldsymbol{k}_1\boldsymbol{k}_2\boldsymbol{k}_3} - R_{\boldsymbol{k}_2\boldsymbol{k}_3\boldsymbol{k}_1} - R_{\boldsymbol{k}_3\boldsymbol{k}_1\boldsymbol{k}_2}\right) d\boldsymbol{k}_2 d\boldsymbol{k}_2 \tag{1.93}$$ eq-S

where

$$R_{\boldsymbol{k}_1\boldsymbol{k}_2\boldsymbol{k}_3} = 4\pi \left|W^{\boldsymbol{k}_1}_{\boldsymbol{k}_2\boldsymbol{k}_3}\right|^2 (n_{\boldsymbol{k}_2} n_{\boldsymbol{k}_3} - n_{\boldsymbol{k}_1} n_{\boldsymbol{k}_3} - n_{\boldsymbol{k}_1} n_{\boldsymbol{k}_2}) \delta^{\omega_{\boldsymbol{k}_1}}_{\omega_{\boldsymbol{k}_2},\omega_{\boldsymbol{k}_3}}\, \delta^{\boldsymbol{k}_1}_{\boldsymbol{k}_2\boldsymbol{k}_3}. \tag{1.94}$$ def:Rk

In this section, we aim at investing the stationary solutions of (1.93). First observe that the (quadratic) energy and wave action, defined respictively as

$$E = \int \omega_{\boldsymbol{k}} n_{\boldsymbol{k}} d\boldsymbol{k} \quad \text{and} \quad N = \int n_{\boldsymbol{k}} d\boldsymbol{k}, \tag{1.95}$$

are (formally) conserved quantities of (1.93). In fact, this a direct consequence of the conservation of energy and momentum at the microscopic level which is enconded in the two delta functions appearing in (1.94).

Remark 7. *E is a conserved quantity for the 3-WKE but not necessarily for the original dynamical equation.*

To actually find explicit stationary solutions, we will only consider *isotropic systems* for which

$$\omega_{\boldsymbol{k}} = ck^{\alpha}.$$

some REF to justify that isotropic systems are also physically relevant in some cases?. Under the isotropy assumption, it is clearly more convenient to average with respect the angular variables. Denoting $\Omega^{(d)}$ as the integration of the solid angle, i.e. the surface area of the d-dimensional sphere, we rewrite N as

$$\begin{aligned} N &= \Omega^{(d)} \int_0^{\infty} n_k k^{d-1} \frac{dk}{d\omega} d\omega = \frac{\Omega^{(d)}}{\alpha}\, c^{-\frac{\alpha}{d}} \int_0^{\infty} n_\omega\, \omega^{\frac{d-\alpha}{\alpha}}\, d\omega \\ &:= \int_0^{\infty} N_\omega\, d\omega. \end{aligned} \tag{1.96}$$

def:Nav

We call N_ω the *angle-averaged frequency spectrum*. This can be seen as the analogue of the spectral energy density (1.16) introduced in the isotropic hydrodynamical turbulence framework.

Arguing analogously for the energy, we find that

$$E = \int_0^{\infty} \omega N_\omega d\omega. \tag{1.97}$$

def:Eav

Remark 8. *In terms of N_ω, the integrals in the kinetic equation become one-dimensional integrals of ω's rather than d-dimensional integrals over $\boldsymbol{k}$'s.*

Integrating (1.93) in the angular variables, we find the following kinetic equation in the frequency space

$$\frac{\partial N_{\omega_1}}{\partial t} = S_1[N_{\omega_1}] + S_2[N_{\omega_1}] + S_3[N_{\omega_1}] \tag{1.98}$$

eq-3WKEB

where

$$\begin{aligned} S_1[N_{\omega_1}] = &\int K_1(\omega_2, \omega_3)\, N_{\omega_2} N_{\omega_3} \delta^{\omega_1}_{\omega_2,\omega_3}\, d\omega_2 d\omega_3 \\ &- \int K_1(\omega_3, \omega_1)\, N_{\omega_1} N_{\omega_3} \delta^{\omega_2}_{\omega_1,\omega_3}\, d\omega_2 d\omega_3 \\ &- \int K_1(\omega_1, \omega_2)\, N_{\omega_1} N_{\omega_2} \delta^{\omega_3}_{\omega_1,\omega_2}\, d\omega_2 d\omega_3, \end{aligned} \tag{1.99}$$

eq-S1

and $K_1(\omega_1, \omega_2)$ is a homogeneous function of degree

$$\lambda = \frac{2\gamma - \alpha}{\alpha}. \tag{1.100}$$

def:lambda

The second term is defined as

$$\begin{aligned} S_2[N_{\omega_1}] = &- \int K_2(\omega_2, \omega_3)\, N_{\omega_1} N_{\omega_2} \delta^{\omega_1}_{\omega_2,\omega_3}\, d\omega_2 d\omega_3 \\ &+ \int K_2(\omega_3, \omega_1)\, N_{\omega_2} N_{\omega_3} \delta^{\omega_2}_{\omega_1,\omega_3}\, d\omega_2 d\omega_3 \\ &+ \int K_2(\omega_1, \omega_2)\, N_{\omega_1} N_{\omega_3} \delta^{\omega_3}_{\omega_1,\omega_2}\, d\omega_2 d\omega_3 \end{aligned} \tag{1.101}$$

eq-S2

with

$$K_2(\omega_1,\omega_2) = K_1(\omega_1,\omega_2)\left(\frac{\omega_1+\omega_2}{\omega_2}\right)^{\frac{\alpha-d}{\alpha}}. \tag{1.102}$$

Finally we have

$$\begin{aligned} S_3[N_{\omega_1}] = &-\int K_3(\omega_2,\omega_3)\, N_{\omega_1} N_{\omega_3} \delta^{\omega_1}_{\omega_2,\omega_3}\, d\omega_2 d\omega_3 \\ &+\int K_3(\omega_3,\omega_1)\, N_{\omega_1} N_{\omega_2} \delta^{\omega_2}_{\omega_1,\omega_3}\, d\omega_2 d\omega_3 \\ &+\int K_3(\omega_1,\omega_2)\, N_{\omega_2} N_{\omega_3} \delta^{\omega_3}_{\omega_1,\omega_2}\, d\omega_2 d\omega_3, \end{aligned} \tag{1.103}$$

eq-S3

with

$$K_3(\omega_1,\omega_2) = K_1(\omega_1,\omega_2)\left(\frac{\omega_1+\omega_2}{\omega_1}\right)^{\frac{\alpha-d}{\alpha}}. \tag{1.104}$$

Is it there a more symmetric way to write S_1, S_2, S_3 and write down just one single term S_i?

There are some advantages in this long-form representation of the collision integral in (1.98). Firstly, we have only a single scaling parameter, λ, instead of 3 (γ, α and d). Secondly, S_1, S_2 and S_3 have natural physical interpretations:

- $S_1[N_{\omega_1}]$ represents a forward transfer mechanism. Indeed, the term with a positive sign in (1.99) requires that $\omega_1 = \omega_2 + \omega_3$, meaning that we generate a higher frequency level ω_1 from two lower frequency ones ω_2, ω_3. The terms with a negative sign in (1.99) accounts for the natural backscatter involved in the process. In particular, we can loose some portion of ω_1 to create other particles. See figure (1.6)

- $S_2[N_{\omega_1}]$, $S_3[N_{\omega_1}]$ instead accounts for the backscatter mechanism. The first term with a negative sign in (1.101)-(1.103) is telling us that we loose an entire ω_1 to generate ω_2, ω_3. Analogously as before, also here we have the natural counterpart of the forward transfer mechanism associated to the backscatter. See figure (1.6).

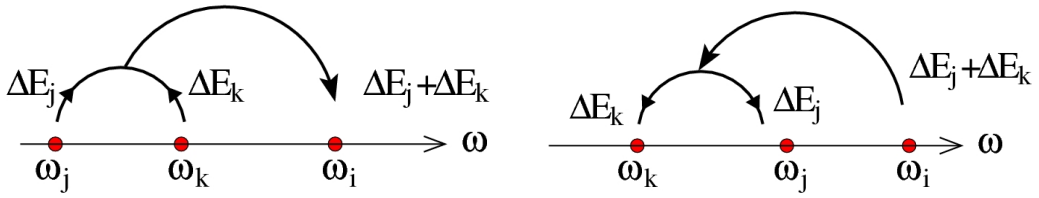

Figure 1.6: Forward transfer and bakcscatter processmaybe the figure should be redone with $\omega_1, \omega_2, \omega_3$

fig:fortran

sligthly reorganized w.r.t. slides for clearness of discussion.

The parameter λ is related to a *phase transition* phenomenon (a sort of or exactly?), where we distinguish the following cases:

- Infinite capacity: $\lambda < 1$. Finite capacity: $\lambda > 1$.

- Breakdown at small scales: $\lambda > 3$. Breakdown at large scales: $\lambda < 3$.

1.5.1 The Kolmogorov-Zakharov spectra

From the scaling laws dictated by (1.100) (and properties of the kernels and the delta function), one can deduce the following **exact** solutions to (1.98):

- Kolmogorov–Zakharov: $N_\omega = c_{\mathrm{KZ}}\sqrt{J}\,\omega^{-\frac{\lambda+3}{2}}$.
- Generalised Phillips (critical balance): $N_\omega = c_P\omega^{-\lambda}$.
- Thermodynamic: $N_\omega \sim \omega^{-2+\frac{d}{\alpha}}$.

In analogy with the terminology in hydrodynamic turbulence, the equilibrium states above are also called **spectra**. Supposing that $K_1(\omega_i,\omega_j)$ has asymptotics $K_1(\omega_i,\omega_j)\sim\omega_i^\mu\omega_j^\nu$ with $\mu+\nu=\lambda$ for $\omega_1\gg\omega_2$, the KZ spectrum is called **local** if

- $\mu<\nu+3$ and $x_{KZ}>x_T$ is this inequality asking that $(\lambda+3)/2<2-d/\alpha$? Maybe better stating like this because we never defined x_{KZ}, x_T before.

Proving that the exact solutions given above are indeed stationary states it is not always straightforward. Hence, we outline how to obtain the KZ-spectra as an example.

First consider the $S_1[N_\omega]$ term only. We seek a stationary solution $N_\omega = c_{\mathrm{KZ}}\,\omega^{-x}$ such that $S_1[N_\omega]=0$:

$$\begin{aligned} 0 = c_{\mathrm{KZ}}^2 &\int K_1(\omega_2,\omega_3)\,(\omega_2\omega_3)^{-x}\delta^{\omega_1}_{\omega_2,\omega_3}\,d\omega_2 d\omega_3 \\ &- c_{\mathrm{KZ}}^2\int K_1(\omega_3,\omega_1)\,(\omega_1\omega_3)^{-x}\delta^{\omega_2}_{\omega_1,\omega_3}\,d\omega_2 d\omega_3 \\ &- c_{\mathrm{KZ}}^2\int K_1(\omega_1,\omega_2)\,(\omega_1\omega_2)^{-x}\delta^{\omega_3}_{\omega_1,\omega_2}\,d\omega_2 d\omega_3. \end{aligned} \tag{1.105}$$

eq-S1C

We now apply the *nonlinear* changes of variables to the second and third integrals, also known as *Zakharov-Kraichanan transformations*:

$$(\omega_2,\omega_3)\to\left(\frac{\omega_1^2}{\omega_2'},\frac{\omega_1\omega_3'}{\omega_2'}\right),\qquad (\omega_2,\omega_3)\to\left(\frac{\omega_1\omega_2}{\omega_3},\frac{\omega_1^2}{\omega_3}\right). \tag{1.106}$$

eq-ZT1

These change of variables are exploiting the fact that the system is invariant under translation, rotation and dilation. Make REF to Laure's lectures where it is explained better how to guess the change of variables from these properties. See Figure **??** for a graphical representation of the ZK-transformations. The Jacobians of the change of variables in (1.106) are

$$\left(\frac{\omega_1}{\omega_2}\right)^3,\qquad \left(\frac{\omega_1}{\omega_3}\right)^3$$

respectively. Exploiting the scaling properties of K_1, notice that, under the change of variables, we have

$$K_1(\omega_1,\omega_3)\to K_1\left(\omega_1,\frac{\omega_1\omega_3'}{\omega_2'}\right)=\left(\frac{\omega_1}{\omega_2'}\right)^\lambda K(\omega_2',\omega_3').$$

fig:ZKtran

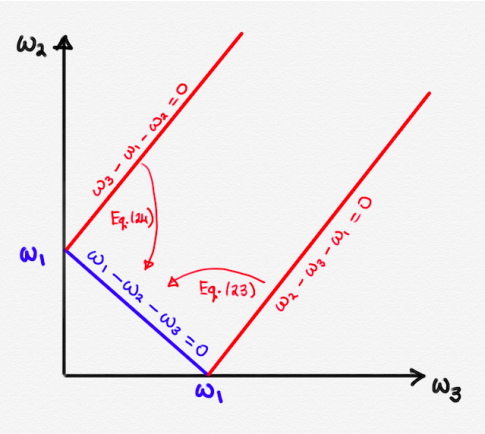

Figure 1.7: Graphical representation of Zakharov-Kraichnan transformations. picture to make on tikz

Arguing analogously for the $\delta^{\omega_2}_{\omega_1,\omega_3}$, one can show that the supports end concentrated on $\delta^{\omega_1}_{\omega_2,\omega_3}$. add computation of this. The result is then a single integral,

$$0 = c_{\mathrm{KZ}}^2 \int K_1(\omega_2,\omega_3)\,(\omega_2\omega_3)^{-x}\delta^{\omega_1}_{\omega_2,\omega_3}\omega_1^{\lambda+2-2x}\left[\omega_1^{2x-\lambda-2} - \omega_2^{2x-\lambda-2} - \omega_3^{2x-\lambda-2}\right] d\omega_2 d\omega_3. \tag{1.107}$$

eq-S1AfterZT

It is now easy to see that the right hand side vanishes when $2x-\lambda-2 = 1$ (or $2x-\lambda-2 = 0$). This yields the KZ exponent (for the flux of energy when we equate to 1, flux of particles when we equate to 0):

$$x = \frac{\lambda+3}{2}. \tag{1.108}$$

Identical analysis applies to S_2 and S_3 and we omit the computations.

The equilibrium exponent $x = \frac{\alpha-d}{\alpha}+1$ appears only in the sum $S_1+S_2+S_3$ (detailed balance) I don't understant this comment

It is also of interest to compute the Zakharov constant c_{KZ}. In order to do so, we first define the the energy flux J_ω at frequency ω as

$$\partial_t\left(\omega N_\omega\right) = \sum_{i=1}^{3} \omega\, S_i[N_\omega] := -\partial_\omega J_\omega. \tag{1.109}$$

eq-energyConservation

Remark 9. *The KZ exponent can be deduced also by imposing that J_ω is scale invariant if it has to be constant. If it is of interest, I could add a little computation of that. It may be nice since you can guess the KZ exponent by a physical argument rather than a "magical" transformation.*

Arguing as done to obtain (1.107), on power law spectrum $N_\omega = c\omega^{-x}$, we have

$$\partial_\omega J_\omega = -c^2\,\omega^{\lambda-2\boldsymbol{x}+2}\,I(x), \tag{1.110}$$

eq:fluxen

where we define

$$I(x) = \int_0^1 \Big[K_1(u,1-u)\,(u(1-u))^{-x} - K_2(u,1-u)\,u^{-x} - K_3(u,1-u)\,(1-u)^{-x}\Big] \Big[1-(1-u)^{2x-\lambda-2} - u^{2x-\lambda-2}\Big]\,du. \tag{1.111}$$

Integrating once (1.110) gives

$$J_\omega = -\omega^{\lambda-2x+3}\frac{c^2 I(x)}{\lambda-2x+3}. \tag{1.112}$$

Since the KZ-spectra is a stationary solution, if we send $x \to x_{KZ} = \frac{\lambda+3}{2}$ we expect that $J_\omega \to J$ with J being constant. The latter is then computed as

$$J = \lim_{x\to_{KZ}} -\omega^{\lambda-2x+3}\frac{c_{KZ}^2 I(x)}{\lambda-2x+3} = \frac{1}{2}\,c_{KZ}^2\,\left.\frac{dI}{dx}\right|_{x=x_{\rm KZ}}, \tag{1.113}$$

where in the last identity we used L'Hôpital's rule. The K-Z constant is therefore

$$c_{\rm KZ} = \sqrt{2\,J\,\left.\frac{dI}{dx}\right|^{-1}_{x=x_{\rm KZ}}} \tag{1.114}$$ eq-KZconst

1.5.1.1 The (spectral) locality criterion

The analysis performed in the previous section assumes that the collision integral is *convergent* on the KZ spectrum. This is however not immediate and needs to be checked a-posteriori. For this, we need to know more informations on the kernels and their asymptotic. So consider the following models:

$$K(\omega_1,\omega_2) = \frac{1}{2}\left[\omega_1^\mu\omega_2^\nu + \omega_1^\nu\omega_2^\mu\right],$$
$$K(\omega_1,\omega_2) = \min(\omega_1,\omega_2)^\mu\,\max(\omega_1,\omega_2)^\nu,$$

where we require $\mu+\nu=\lambda$.

The strategy is the following: first use the δ-function to integrate out ω_3. Then, determine the integrability of integrand as $\omega_2 \to 0$ and $\omega_2 \to \infty$. Following this procedure, one can show [7] that the collision integral is convergent provided

$$x > 1 + \frac{\alpha-d}{\alpha}, \qquad \mu < x < \nu+3. \tag{1.115}$$ bd:splc

These conditions, called the spectral locality criteria, have a very important physical meaning: they tell us when the KZ spectrum is *universal*, i.e. independent of forcing and dissipation in the turbulence limit.

For the KZ-specta, the spectral locality criteria impose two requirements: x_{KZ} must be steeper than the equilibrium spectrum and an interval of locality, $[\mu,\nu+3]$, must exist, i.e. $\mu < \nu+3$. When an interval of locality exists, the KZ exponent is at the midpoint.

Remark 10. *The spectral non-locality does* **not** *present a problem for the applicability of the kinetic equation. However forcing and/or dissipation must be included explicitly.*

1.6 Numerical and Experimental Evidence

In this section, we look at a few examples in which we can actually see wave turbulence, in particular the Kolmogorov-Zhakarov spectrum. This is somewhat surprising for several reasons:

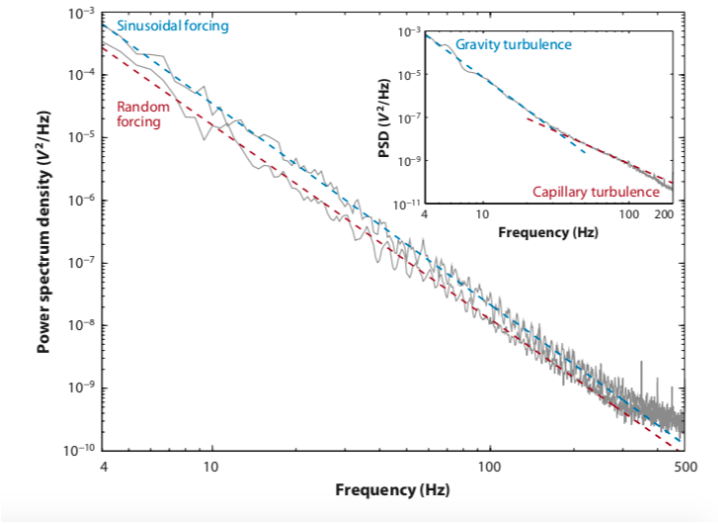

Figure 1.8: Experimental Observations of Weak Capillary Wave Turbulence

1. The asymptotic limit in which the Kinetic Equation arises is not mathematically consistent.

2. Even if the Kinetic Equation is consistent, the system of interest is not necessarily in the relevant regime (weak nonlinearity, long time) for it to apply.

3. Even if the Kinetic Equation is consistent and applicable, the Kolmogorov-Zakarhov spectrum may not be local.

4. Even if the Kinetic Equation is consistent and applicable and the Kolmogorov-Zakharov spectrum is local, the exponent $\frac{\lambda+3}{2}$ could be inconsistent with the assumption of weak nonlinearity as $\omega \to \infty$.

The best experimental evidence of Wave Turbulence occurs in the case of Capillary Wave Turbulence. However, the effects of gravity waves limit the scaling range available under normal conditions. So, experiments performed in space on an A300 Airbus in microgravity generated Figure 1.8, taken from [19]. Not sure if we can have these pictures, but adding them now. These experiments showed that there are in fact 2 regimes, one at low frequency where gravity dominates, and the other at high frequencies where capillarity dominates. Ignoring the lower frequencies, there are in fact clean power laws giving the power spectrum density in terms of the frequency. The power law is present in multiple types of forcing, so it appears from this experimentation that the power law is not dependent on details of the forcing.

On the numerical side, it is difficult to realise "pure" weak wave turbulence. For example, some difficulties arise from the fact that you need to ensure that your numerical grid has sufficient resonances and prevent the boundaries from introducing effects. The Majda-McLaughlin-Tabak (MMT) model proposes a toy model of wave turbulence similar to the NLS with the dispersive term modified so that the time steps can be less fine:

$$i\partial_t \psi = \mathcal{L}^{(1/2)}\psi + \sigma\psi\left|\psi\right|^2 + \mathcal{F}\mathcal{D},$$

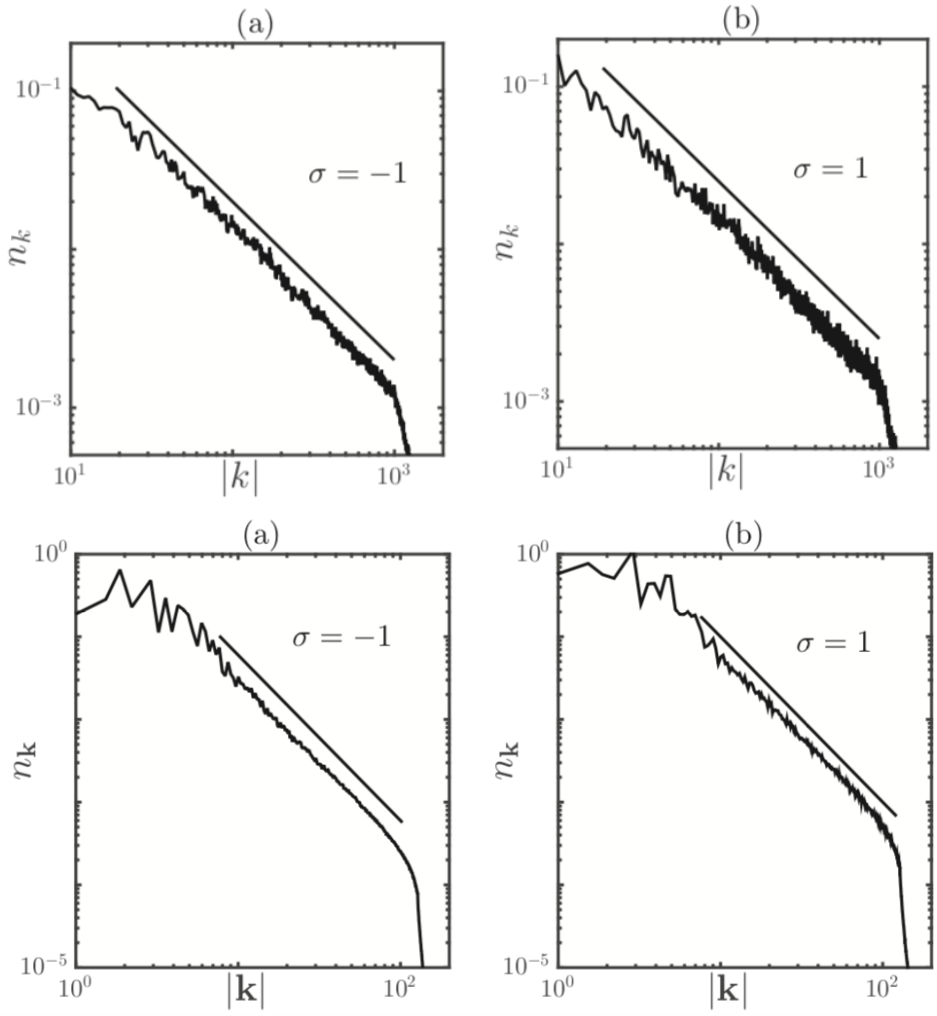

Figure 1.9: Simulations in 1D (top row) and 2D (bottom row) from Sheffield & Rumpf (2017)

MMT

where $\mathcal{L}^{(1/2)}\psi \sim \sqrt{k}\hat{\psi}_{\boldsymbol{k}}$ and $\sigma = \pm 1$. In this case, the Kolmogorov-Zakharov spectrum is then

$$n_{\boldsymbol{k}} = c_{KZ} J^{\frac{1}{3}} k^{-d}.$$

Some numerics using the MMT model in [42] give the predicted scalings both in dimensions 1 and 2 and are shown in Figure (1.9). Note that the slopes in the figures do not depend on the sign of the nonlinearity, which is consistent with the kinetic limit. They used other testable predictions involving the closure mechanism for the 4th order correlation function:

$$\partial_t n_{\boldsymbol{k}} = 2\sigma \int \mathrm{Im} J_{123\boldsymbol{k}} \delta^{\boldsymbol{k}_1\boldsymbol{k}_2}_{\boldsymbol{k}_3\boldsymbol{k}} d\boldsymbol{k}_{123},$$

where

$$J_{123\boldsymbol{k}} \delta^{\boldsymbol{k}_1\boldsymbol{k}_2}_{\boldsymbol{k}_3\boldsymbol{k}} = \langle \hat{\psi}_{\boldsymbol{k}_1} \hat{\psi}_{\boldsymbol{k}_2} \hat{\psi}^*_{\boldsymbol{k}_3} \hat{\psi}^*_{\boldsymbol{k}} \rangle.$$

Assuming that the Kinetic Equation holds for this equation, then it should be the case that

$$\mathrm{Im} J_{123\boldsymbol{k}} \sim 2\pi\sigma F_{123\boldsymbol{k}} \delta(\Omega^{\boldsymbol{k}_1\boldsymbol{k}_2}_{\boldsymbol{k}_3\boldsymbol{k}}),$$

where

$$F_{123\boldsymbol{k}} = n_{\boldsymbol{k}_1} n_{\boldsymbol{k}_2} n_{\boldsymbol{k}_3} + n_{\boldsymbol{k}_1} n_{\boldsymbol{k}_2} n_{\boldsymbol{k}} - n_{\boldsymbol{k}_1} n_{\boldsymbol{k}_3} n_{\boldsymbol{k}} - n_{\boldsymbol{k}_2} n_{\boldsymbol{k}_3} n_{\boldsymbol{k}}.$$

Therefore, some testable predictions include:

- $\mathrm{Im} J_{123\boldsymbol{k}}$ being sharply peaked at resonances.
- $\operatorname{sgn} \mathrm{Im} J_{123\boldsymbol{k}} = \operatorname{sgn} \sigma$.
- $\mathrm{Im} J_{123\boldsymbol{k}} \sim n^3$.
- the time evolution of $\mathrm{Im} J_{123\boldsymbol{k}}$ from uncorrelated initial state.

A sampling of results achieved from trying to observe these predictions is in Figure (1.10). Here, they take $k_1 = 49, k_2 = -4, k_3 = 9$ with $k = 36$ to satisfy resonance. They found that at initial time, the 4th order correlation function is 0, but later it becomes nonzero. The strong nonzero part does appear on the resonant curve, and peaks negatively with the sign of σ. Also, the time evolution of that correlation starts at 0 and builds with quasi-guassianity emerging.

1.7 The Dual Cascade

This section may be somehow linked also to other lectures, e.g. Haynes

In this section, we consider a prototypical example where a dual cascade can be observed: the 2D Navier-Stokes equations which, written in terms of the stream-function $\psi(x, y, t) = \psi(\boldsymbol{x}, t)$, read as

$$\frac{\partial \Delta\psi}{\partial t} + (\boldsymbol{v} \cdot \nabla)\Delta\psi = \nu\Delta(\Delta\psi), \qquad \boldsymbol{x} \in \mathbb{R}^2, \ t \geq 0 \tag{1.116}$$

eq:NS2D

$$\boldsymbol{v} = \nabla^\perp \psi, \tag{1.117}$$

where $\nabla^\perp = (-\partial_y, \partial_x)$. When $\nu = 0$ we have the Euler equations and we observe the conservation of two quantities:

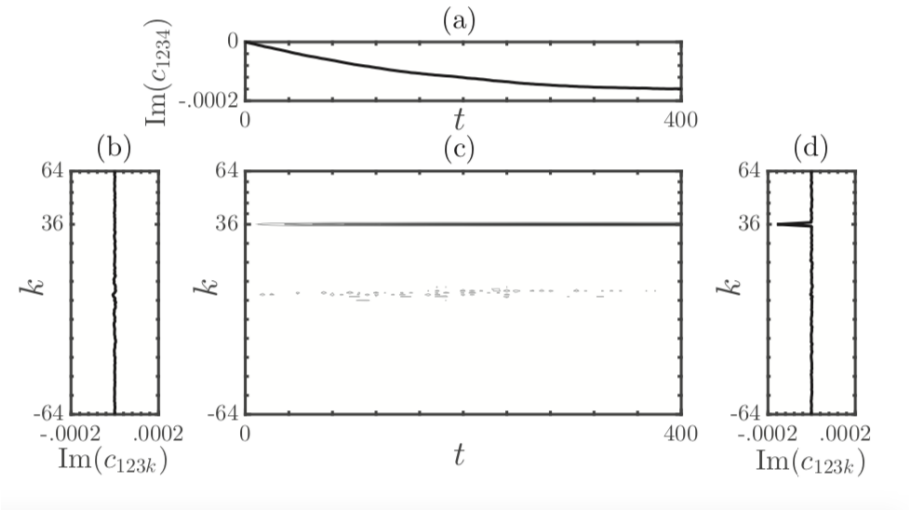

Figure 1.10: Validation of Wave Turbulence Closure Mechanism from Sheffield & Rumpf (2017)

closurepred

- Energy: $E = \frac{1}{2}\int |\nabla\psi|^2 \, d\boldsymbol{x} = \frac{1}{2}\int |\boldsymbol{v}|^2 \, d\boldsymbol{x} = \int E(k)dk.$
- Enstrophy: $\Omega = \int |\Delta\psi|^2 \, d\boldsymbol{x} = \int \left|\nabla^\perp \cdot \boldsymbol{v}\right|^2 d\boldsymbol{x} = \int k^2 E(k)dk.$

We again assumed isotropy to the define the spectral energy density $E(k)$. Let us verify that the two quantities defined above are indeed conserved. Multiplying (1.116) by ψ, integrating in space and performing an integration by parts we get

$$\frac{1}{2}\frac{d}{dt}\int |\nabla\psi|^2 d\boldsymbol{x} = \int \left(\nabla^\perp\psi \cdot \nabla\Delta\psi\right)\psi \; d\boldsymbol{x} = -\int \Delta\psi \left(\nabla^\perp\psi \cdot \nabla\psi\right) = 0, \tag{1.118}$$

which imply the conservation of the energy. Analogously, the conservation of the enstrophy readily follows multiplying (1.116) by $\Delta\psi$.

Other systems where we have the conservation of the energy and (at least) another quantity are, for example, the following:

- Nonlinear Schrodinger equation: conservation of energy and mass.
- Potential vorticity equation: conservation of energy and potential enstrophy.
- Surface water waves: conservation of energy and wave action.

the following remark was not given in the lectures

Remark 11. *For the 2D Euler equations we actually have an infinite set of conserved quantities. Indeed, due to the transport structure of* (1.116) *when* $\nu = 0$*, one has the conservation of*

$$\int F(\Delta\psi)d\boldsymbol{x}, \tag{1.119}$$

for any continuous function F*.*

Having the conservation of energy and enstrophy at hand, we want to investigate the direction of the cascading mechanism for these two quantities. Namely, will the energy (enstrophy) move towards small or large scales? Fjørtoft [21] discovered that the two invariants must be transferred in the opposite direction in the frequency space.

Let us make some preliminary observations to deduce the direction of the cascade. Let k_f be a reference frequency and k_R, k_L higher and lower frequencies respectively (right and left). Denote

$$E(k_f) = J, \qquad E(k_R) = J_R, \qquad E(k_L) = J_L.$$

Assume that the energy split into high and low frequencies as

$$J = J_R + J_L, \tag{1.120}$$

where J_R, J_L are the energy fluxes. This imply that the enstrophy satisfy

$$k_f^2 J = k_R^2 J_R + k_L^2 J_L := J_R^\Omega + J_L^\Omega, \tag{1.121}$$

where J_R^Ω, J_L^Ω are the enstrophy fluxes. Solving the equations in terms of the energy fluxes we get

$$J_L = \frac{k_R^2 - k_f^2}{k_R^2 - k_L^2} J, \qquad J_R = \frac{k_f^2 - k_L^2}{k_R^2 - k_L^2} J. \tag{1.122}$$ eq:energyflux

In terms of enstrophy fluxes the above identities read as

$$J_L^\Omega = k_L^2 \frac{k_R^2 - k_f^2}{k_R^2 - k_L^2} J, \qquad J_R^\Omega = k_R^2 \frac{k_f^2 - k_L^2}{k_R^2 - k_L^2} J. \tag{1.123}$$ eq:enstrophyflux

From (1.122)-(1.123) we deduce that

- $J_L \to J$ and $J_R \to 0$ as $k_R \to \infty$.
- $J_L^\Omega \to 0$ and $J_R^\Omega \to k_f^2 J$ as $k_L \to 0$.

Thus, the energy cannot concentrate in a very high-frequency regime whereas the enstrophy cannot concentrate in a very low-frequency state. This suggests that we should observe an inverse energy cascade and a direct enstrophy cascade, see Figure 1.11. However, these scalings make the "pure" dual cascade very difficult to realise.

Let us now present an elegant formulation of Fjørtoft argument given in Nazarenko's monograph [33], which is rigorous for unforced and inviscid fluids. Define the energy and enstrophy *frequency-centroids* (or center of mass) as

$$k_E = \frac{\int_0^\infty kE(k)dk}{E}, \qquad k_\Omega = \frac{\int_0^\infty k^3 E(k)dk}{\Omega}, \tag{1.124}$$ def:kcentr

where E and Ω are the total energy and enstrophy. The quantities k_E and k_Ω can be considered as the mean frequency-scale at which energy and enstrophy are respectively concentrated. Appealing to the Cauchy-Schwarz inequality we obtain

$$\begin{aligned}\left(\int_0^\infty kE(k)dk\right)^2 &= \left(\int_0^\infty (k\sqrt{E(k)}dk)(\sqrt{E(k)}dk)\right)^2 \\ &\le \left(\int_0^\infty k^2 E(k)dk\right)\left(\int_0^\infty E(k)dk\right) = \Omega E,\end{aligned}$$

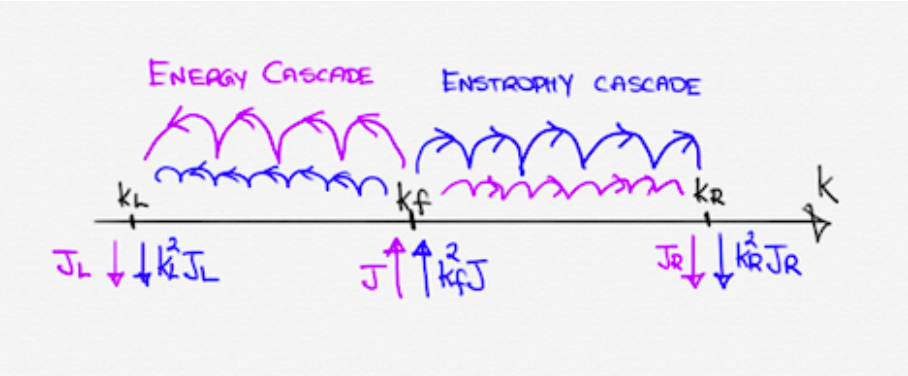

Figure 1.11: Schematic picture of a dual cascade

fig:dualcascade

meaning that

$$k_E \leq \sqrt{\frac{\Omega}{E}}. \tag{1.125}$$

eq-Ecentroi

Arguing similarly for the enstrophy, we have

$$\Omega^2 = \left(\int_0^\infty k^2 E(k)dk\right)^2 = \left(\int_0^\infty (k^{\frac{3}{2}}\sqrt{E(k)}dk)(\sqrt{kE(k)}dk)\right)^2$$
$$\leq \left(\int_0^\infty k^3 E(k)dk\right)\left(\int_0^\infty kE(k)dk\right) = (\Omega k_\Omega)(Ek_E).$$

From the inequality above we deduce that

$$k_\Omega k_E \geq \frac{\Omega}{E}. \tag{1.126}$$

eq-Qcentro

Therefore, combining (1.125) and (1.126) we get

$$k_E \leq \sqrt{\frac{\Omega}{E}}, \qquad k_\Omega \geq \sqrt{\frac{\Omega}{E}}, \qquad k_\Omega k_E \geq \frac{\Omega}{E}.$$

Thus, we obtain the following:

- Thanks to (1.125), the energy cannot accumulate on arbitrarily large frequencies
- From (1.126), if k_E decreases then k_Ω must increase and $k_E \leq k_\Omega$. To have an inverse cascade of energy we must have direct cascade of enstrophy.
- k_Ω is bounded from below, meaning that the enstrophy will not be seen at large spatial scales.

The following is from Nazarenko's book, not included in lecture notes However, from the bounds above we cannot exclude the possibility of having a direct cascade of enstrophy without an inverse cascade of energy. To overcome this problem, we introduce

$$\ell_E = \frac{\int_0^\infty k^{-1}E(k)dk}{E}, \quad \ell_\Omega = \frac{\int_0^\infty kE(k)dk}{\Omega} = k_E\frac{E}{\Omega}, \tag{1.127}$$

def:ellcentr

which are called *length-centroids* since the energy and enstrophy spectrum are multiplied by k^{-1}, that has a measure of a length. In analogy with the frequency centroids, ℓ_E and

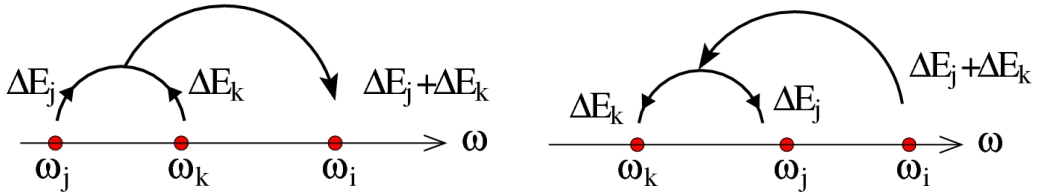

Figure 1.12: Forward transfer and backscatter

:S1S2again

ℓ_Ω are the mean length-scale at which energy and enstrophy are concentrated. Arguing similarly to what was done for k_E and k_Ω, it is not difficult to show that

$$\ell_\Omega \ell_E \geq \frac{\Omega}{E}.$$

Therefore, if ℓ_Ω decreases then ℓ_E must increase. This means that the enstrophy cannot be at arbitrarily small spatial scales without the energy being sent to large ones. Equivalently, we cannot have a direct cascade of enstrophy without an inverse cascade of energy.

1.8 Dynamical phenomena and numerics

In this section we present some dynamical phenomena and numerics related to model problems associated to the 3-wave kinetic equation. We recall that the evolution of the wave $n_{\boldsymbol{k}}$ is given in (1.66). The scaling parameters involved are (d, α, γ) where:

- d is the dimension: $\boldsymbol{k} \in \mathbf{R}^d$
- α is related to the dispersion: $\omega_{\boldsymbol{k}} \sim k^\alpha$
- γ stem from the nonlinearity: $W^{\boldsymbol{k}_1}_{\boldsymbol{k}_2\boldsymbol{k}_3} \sim k^\gamma$

As usual by now, we consider only isotropic systems and we focus on the frequency spectrum N_ω that satisfies (1.98), namely

$$\frac{\partial N_{\omega_1}}{\partial t} = S_1[N_{\omega_1}] + S_2[N_{\omega_1}] + S_3[N_{\omega_1}].$$

The terms S_1, S_2, S_3 are defined in (1.99), (1.101) and (1.103) respectively. S_1 is responsible for the forward-transfer whereas the other two are the backscatter terms. We recall that the main advantage of splitting the right-hand side of (1.98) in this way is that we only have one scaling parameter λ that is

$$\lambda = \frac{2\gamma - \alpha}{\alpha}.$$

The disavantage is that the S_i have slightly different kernels.

To start our discussion, let us consider the c_{KZ} constant given in (1.114). In some model problems, it can be computed exactly. For instance, assume $d = \alpha$ and consider the following toy models:

- Product kernel:

$$L(\omega_1, \omega_2) = (\omega_1\, \omega_2)^{\frac{\lambda}{2}}. \tag{1.128}$$

def:prodK

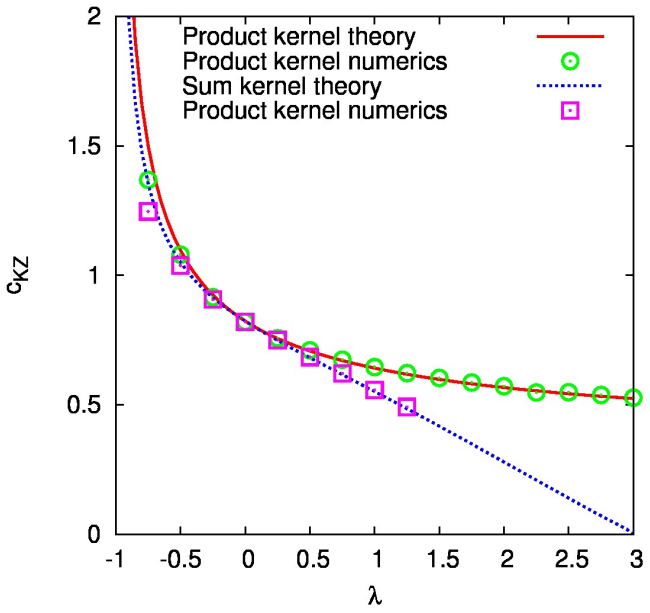

Figure 1.13: Comparison between theoretical and numerical evaluations of the c_{KZ} constant for the kernels (1.128)-(1.129)

fig:cKZnum

- Sum kernel:

$$L(\omega_1, \omega_2) = \frac{1}{2}\left(\omega_1^{\lambda} + \omega_2^{\lambda}\right). \tag{1.129}$$

def:sumK

In Figure 1.13 we compare numerical predictions with the exact calculation that can be done for the kernels defined above. shall we add the exact calculation of c_{KZ} for these kernels? Is it doable by hand?. In view of the exact formulas available, the computation of c_{KZ} for these model problems can be considered as a good numerical test for the code at hand.

1.8.1 Cascade without backscatter

We now consider an example where there is a forward cascade *without* backscatter. This model arise from cluster aggregation problems. Instead of the 3WKE, consider the Smoluchowski equation:

$$\begin{aligned}\frac{\partial N_m}{\partial t} = &\int_0^m dm_1 K(m_1, m-m_1) N_{m_1} N_{m-m_1} \\ &- 2N_m \int_0^{\infty} dm_1 K(m, m_1) N_{m_1} + J\ \delta(m-1),\end{aligned} \tag{1.130}$$

eq:smol

where $N_m(t)$ is the cluster mass distribution while $K(m_1, m_2)$ is the kernel. This model is essentially retaining only the term S_1 in (1.98). Assume that

$$\begin{aligned}&K(am_1, am_2) = a^{\mu+\nu} K(m_1, m_2), \\ &K(m_1, m_2) \sim m_1^{\mu} m_2^{\nu} \qquad m_1 \ll m_2.\end{aligned}$$

In addition, given a typical size $s(t)$ we expect to have a self-similar behavior like

$$N(m,t) \sim s(t)^a F(m/s(t))$$
$$F(x) \sim x^{-y} \qquad x \ll 1.$$

maybe comment more about why?

As shown in Figure 1.14, we see that if we start at large spatial scales (small frequencies), we observe that information travels towards large frequencies.

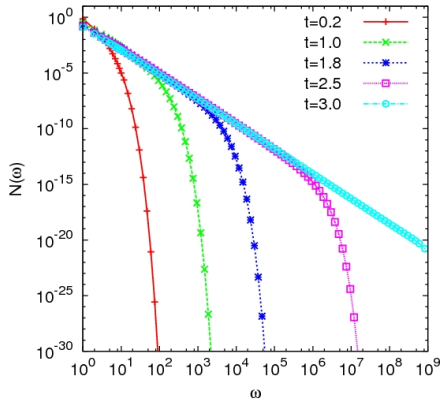

Figure 1.14: Numerical simulation of (1.130) with $K(\omega_1,\omega_2) = (\omega_1\omega_2)^{\frac{3}{2}}$

fig:smol

.

For this cluster-cluster model we also have an analogue of the anomalous dissipation, see (1.8), called *Gelation Transition* Add REF Lushnikov [1977], Ziff [1980]. More precisely, notice that the mass, defined as

$$M(t) = \int_0^\infty m\, N(m,t)\, dm, \tag{1.131}$$

is formally conserved for (1.130). However for $\mu + \nu > 1$, one observes that

$$M(t) < \int_0^\infty m\, N(m,0)\, dm \qquad t > t^*, \tag{1.132}$$

for some t^*. This mechanism is best studied by introducing a cut-off $M_{\max}$, and studying the limit $M_{\max} \to \infty$, a method pioneered by Laurencot in this context REF. In Figure 1.15 we show a numerical simulation with different truncation parameters. As $M_{\max}$ grows, it seems that the loss of the mass happens at a specific time $t^* \sim 3$, with a sharper transition as we increase the value of the cut-off. The cut-off can be considered as a dissipation parameter. The Gelation transition indicates that even if we take $M_{\max} \to \infty$, hence no dissipation, we still observe some dissipative mechanism in the system, in analogy with a large Reynolds number limit in the fluid context. Other phenomenon are also observed:

- If $\nu > 1$ then $t^* = 0$. Add REF(Van Dongen & Ernst [1987]) This is called *instantaneous* gelation.
- It may also *complete*, namely $M(t) = 0$ for $t > 0$. An example when this happens is for the model $K(m_1,m_2) = m_1^{1+\epsilon} + m_2^{1+\epsilon}$ with $\epsilon > 0$.

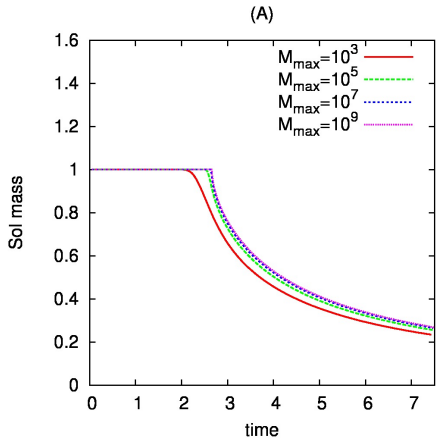

Figure 1.15: $M(t)$ for $K(m_1, m_2) = (m_1 m_2)^{3/4}$

fig:Gelation

Are these some mathematical pathologies? Do that indicates a sort of ill-posedness with that parameters? We should observe that, in some sense, removing the back-scatter from the 3WKE has made the equation simpler but still there are potential ill-posedness. On the other hand, this also means that there are interesting things going on.

In fact, there *are* applications with $\nu > 1$, coming for example from atmospheric science and astrophysics models. From a mathematical point of view, it should make no sense. However, in the literature REF there were numerical simulations comparing their results with observations, and were somehow in agreement. If we try to run a numerical simulation in a case where we expect the instantaneous gelation, see Figure 1.16, we observe the following:

- Introducing a cut-off $M_{\max}$, the *regularized gelation time*, $t^*_{M_{\max}}$, is clearly identifiable.

- $t^*_{M_{\max}}$ *decreases* as $M_{\max}$ increases, which is expected since for the original problem we have instantaneous gelation. In fact, REF Van Dongen & Ernst recovered the result in the limit $M_{\max} \to \infty$.

Remark 12. *The decrease of $t^*_{M_{\max}}$ as $M_{\max}$ is incredibly slow (numerics suggest logarithmic decrease). This can be a justification of why such models are physically reasonable. This is consistent with related results of REF:Krapivsky and Ben-Naim and Krapivsky [2003] on exchange-driven growth. In particular, we shouldn't throw away a particular model "just" because it is ill-posed mathematically.*

If we want to try to understand what instantaneous gelation is doing, we can say that it is an effect that comes from a sort of a runaway absorption of smallest clusters by the large ones. This is clear from the analytically tractable (but non-gelling) marginal kernel, $m_1 + m_2$, with source of monomers. In fact, the case $m_1 + m_2$ it may have a very singular behaviour since it is on the boundary of seeing an instantaneous gelation. For instance, just think of replacing that kernel by $m_1^{1+\epsilon} + m_2^{1+\epsilon}$ for a small ϵ. However, it is easier to treat analytically the case with a source that can sort of mimic some of the interesting behaviour of the instantaneous gelation.

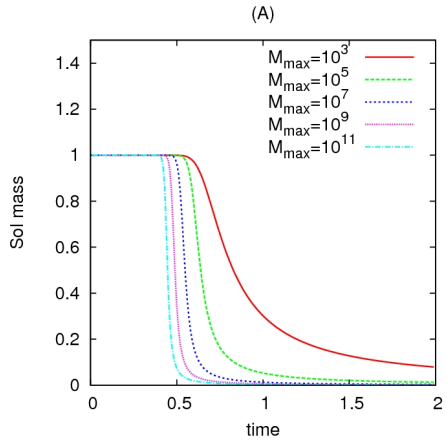

Figure 1.16: $M(t)$ for $K(m_1, m_2) = (m_1 + m_2)^{4/3}$. We have instantaneous gelation for this kernel.

fig:IG

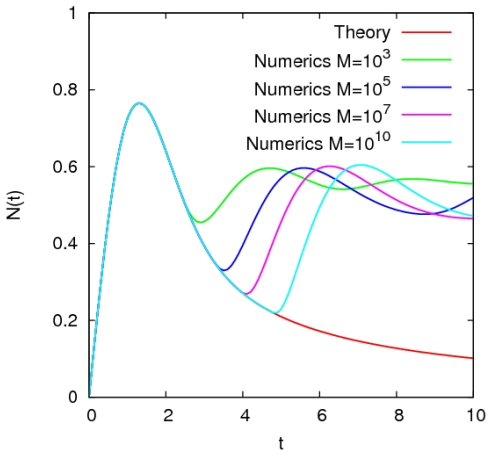

Figure 1.17: Total density, $\int_0^\infty N(m,t)\,dm$ for $K(m_1, m_2) = m_1 + m_2$ and source.

_sumkernel

We can derive an equation for the total mass in the system, which grows like $M(t) \sim t$ just because there is a source. On the other hand, defining $N(t)$ as the integral of density, which is counting the number of particles, we will see that $N(t) \sim 1/t$, see Figure 1.17

The interpreation we can give is that if the exponent $\nu > 1$, then this process where big clusters absorb the smaller ones is extremely efficient. In particular, in a numerical simulation the absorption just diverges with the cut-off, $M_{\max}$. (cf "addition model" (Brilliantov & Krapivsky [1992], Laurencot [1999])). In this kind of system, we will not observe something like a local cascade where there is range of scales where particles merges only with others with nearby sizes. Here, everything is being driven by interaction with the largest particle in the system.

Is it there a similar mechanism for a 3WKE? The analogy would be that the highest frequencies are dominating all of the resonances. We do not know wheter this may true or not, but remember that in our simple model we have neglected the backscatter processes.

With a cut-off, we may also reach a stationary state if a source of monomers is present REF: (Horvai et al [2007]) even though no such state exists in the unregularized system.

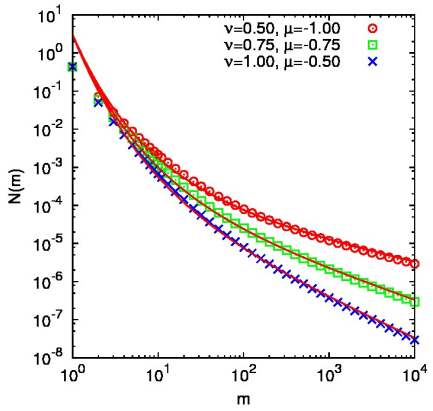

Figure 1.18: Stationary state (theory vs numerics).

fig:SS_M1E4

This stationary state, for $M \gg 1$ has the asymptotic form

$$N_m = \frac{\sqrt{2J\gamma \log M}}{M} M^{m^{-\gamma}} m^{-\nu}, \qquad \gamma = \nu - \mu - 1 \tag{1.133}$$

We have an exponential behaviour for small m and a power law for large m. In particular, it agrees well with numerics without any adjustable parameters, see Figure 1.18.

Remark 13. *Even in the power-law regime, we do not have the KZ spectrum. The amplitude of our spectrum is a function of the cut-off, not universal. In addition, the stationary state* **vanishes** *as $M \to \infty$. The stationary state will not support a constant flux of mass in the limit. But we are forcing, so what happens to the mass flux?*

It turns out that instead of a constant flux propagation through the scales, we have Hopf bifurcation from the stationary state as M is increased. Therefore, our constant mass flux phenomenology stops being the right description. More precisely, we observe the following:

- Semi-analytic linear stability analysis of the exact stationary state shows that the nonlocal stationary state is linearly unstable for large enough M.
- The constant mass flux is replaced by time-periodic pulses.
- The oscillatory behaviour is due to an attracting limit cycle embedded in this very high-dimensional dynamical system. There has been recent mathematical works by REF: Pego, Valazquez, Niethammer

Remark 14. *One may think that an oscillatory behaviour is somewhat counter-intuitive, since it is always implicitly assumed that the system will reach a steady state at long times. However, also in the 2D Euler equations the numerics suggests that the system does reaches a state which oscillates periodically in time rather than a steady state.*

1.8.2 Dissipative anomaly & dynamical scaling

Let us now return to our main subject, namely wave turbulence. We have to insert back the backscatter we removed from the 3WKE. However, it is not clear yet which properties

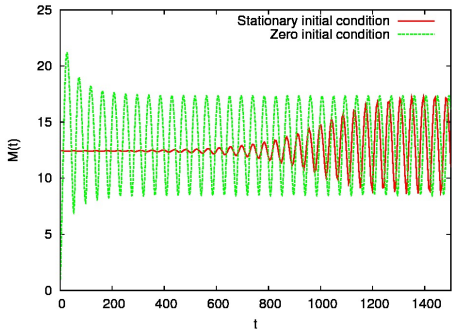

Figure 1.19: Total density, $N(t)$, vs time for $\nu = \frac{3}{2}$, $\mu = -\frac{3}{2}$.

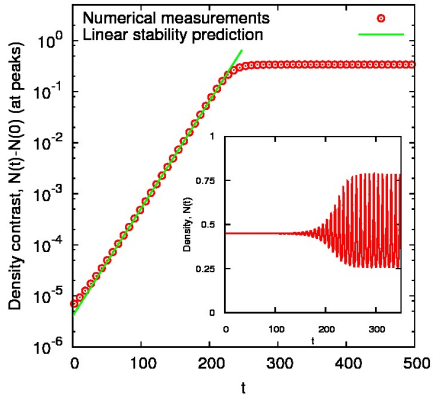

Figure 1.20: Linear stability analysis

observed in the Smoluchovski case are going to be preserved or lost. One may try to have some guess in terms of self-similar solutions. We expect that that this time-evolving solutions are going to *develope wave turbulunce.* In particular, developing wave turbulence refers to the evolution of the spectrum *before* the onset of dissipation. We shall focus on the unforced case since it is easier to analyze.

Consider for instance the numerical simulations shown in Figure 1.14, where we have a 3WKE with kernel $K(\omega_1, \omega_2) = (\omega_1\omega_2)^{\frac{3}{2}}$. For this kernel, the scaling parameter λ, defined in (1.100), is $\lambda = 3$. This corresponds to a finite capacity system and we expect that the cascading process should be observed regardless of the size of the cut-off or the presence of forcing. Indeed, in Figure 1.14 we observe how the system dissipates at higher frequencies even without forcing. Looking at the curve at time $t = 3$ in Figure 1.14, it is an ongoing debate whether the slope that you see in the time evolving solution as you approach this dissipation dissipation time is $(\lambda + 3)/2$, corresponding to a stationary state. The belief it is that it is not exactly this one but close.

As a consinstency check for the numerical simulation, one can actually clearly identify the time $T*$ where the energy dissipation starts, see Figure 1.21.

To distinguish finite and infinite capacity systems, let us consider the stationary KZ spectrum:

$$N_\omega = c_{\mathrm{KZ}} \sqrt{J}\, \omega^{-\frac{\lambda+3}{2}}. \tag{1.134}$$

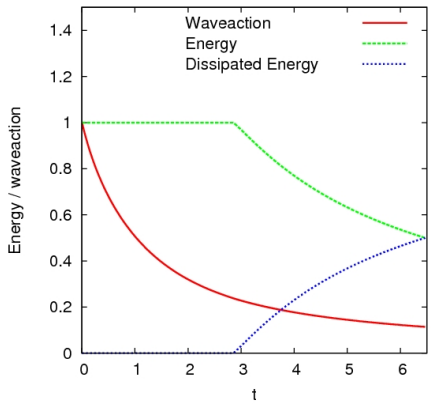

Figure 1.21

fig:diag_PK_1p5

The total energy contained in the spectrum is

$$E = c_{\mathrm{KZ}} \sqrt{J} \int_1^{\Omega} d\omega\, \omega^{-\frac{\lambda+1}{2}}. \tag{1.135}$$

In particular, notice the following:

- E diverges as $\Omega \to \infty$ if $\lambda \leq 1$. This corresponds to the *Infinite Capacity* .
- E finite as $\Omega \to \infty$ if $\lambda > 1$, which is the the *Finite Capacity* case.

As we already mentioned in the last section, the transition occurs at $\lambda = 1$.

In the finite capacity case, the system exhibit a dissipative anomaly as the dissipation scale goes to infinity. For infinite capacity systems, the cascades can absorb as much energy as we want. In Figure **??** we can see a comparison between infinite and finite capacity energy dissipation. As the cut-off increases, the infinite capacity system dissipates later. Instead, the finite capacity one has a sharp transition around time $t = 3$ for sufficiently large cut-off. This is analogous to the gelation transition, except now, instead of mass being lost from a particle system, we have energy being lost from a turbulent cascade as modeled by the 3WKE. There has been a recent paper by REF: Soffer and

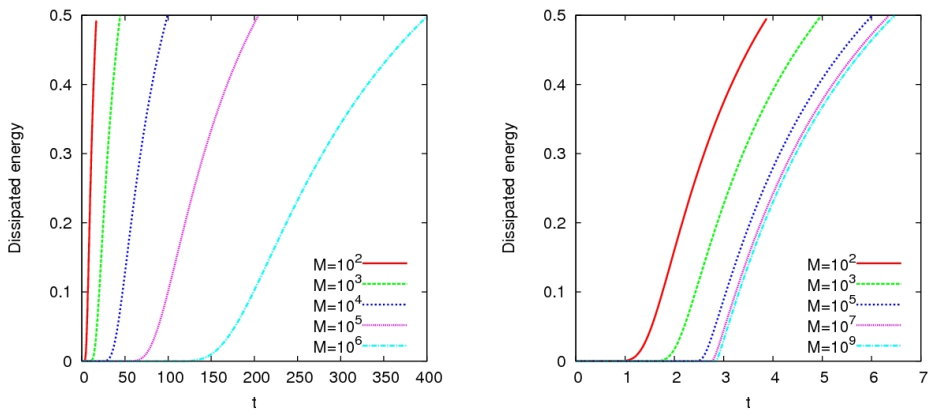

Figure 1.22: A product kernel with $\lambda = 3/4$ on the left and $\lambda = 3/2$ on the right.

fig:dissipation_PK_0p75

Tran where they claim to have established the presence of finite time dissipation for at least a particular case.

To start investigating these transient solutions REF: (Falkovich and Shafarenko, 1991), we need to make some hypotheses. Firts, we assume there exists a typical scale, $s(t)$, such that $N_\omega(t)$ is asymptotically of the form

$$N_\omega(t) \sim s(t)^{-a}\, F(\xi) \qquad \xi = \frac{\omega}{s(t)}. \tag{1.136}$$

This is called the **scaling hypothesis**. We expect to have a self-similar solution because the WKE is scale invariant. Assuming this ansatz, we get that the typical frequency, $s(t)$, and the scaling function, $F(\xi)$, satisfy:

$$\begin{aligned} \frac{ds}{dt} &= s^{\lambda-a+2} \\ -a\,F - \xi\frac{dF}{d\xi} &= S_1[F(\xi)] + S_2[F(\xi)] + S_3[F(\xi)]. \end{aligned}$$

But what is the characteristic time here? From a numerical point of view, it is natural to take ratio of moments and frequency distributions why?. The transient scaling exponent is instead given by the small ξ divergence of the scaling function, namely $F(\xi) \sim A\,\xi^{-x}$.

We are mainly focusing on the unforced case, but it is instructive to see also what happens if we have forcing in this self-similar solutions, see Figure **??** for a numerical simulation. We expect energy to be growing linearly

$$J\,t = \int_0^\infty \omega\, N_\omega\, d\omega = s(t)^{a+2} \int_0^\infty \xi\, F(\xi)\, d\xi. \tag{1.137}$$

If we assume $F(\xi) \sim A\,\xi^{-x}$, balancing leading order terms in the scaling equation leads to:

$$x = \frac{\lambda+3}{2}, \tag{1.138}$$

$$A = \sqrt{2}\left(\left.\frac{dI}{dx}\right|_{x=\frac{\lambda+3}{2}}\right)^{-1/2} = c_{KZ}. \tag{1.139}$$

We thus recovered the KZ exponents, which is basically coming from the conservation of energy maybe I can include that computation about KZ spectrum via conservation of energy. Observe that we may have convergence problem at the origin when $\lambda = 1$, whereas from numerics it is clear we will not have any problem at infinity for all values of λ. Hence, in if $\lambda < 1$, namely infinite capacity system, we should expect to reach the KZ stationary state.

On the other hand, in the unforced case the energy is conserved

$$1 = \int_0^\infty \omega\, N_\omega\, d\omega = s(t)^{a+2} \int_0^\infty \xi\, F(\xi)\, d\xi. \tag{1.140}$$

See Figure 1.24 for a numerical simulation. Arguing as before, assuming $F(\xi) \sim A\,\xi^{-x}$ and balancing leading order terms in the scaling equation, leads to:

$$\begin{aligned} x &= \lambda + 1 \\ A &= \frac{\lambda - 1}{I(\lambda+1)}. \end{aligned}$$

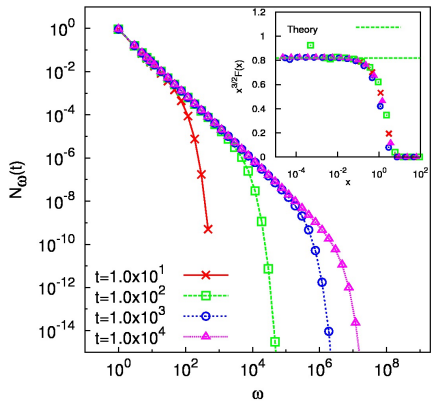

Figure 1.23: Self-similar evolution for the forced case with $L(\omega_1, \omega_2) = 1$. Inset shows scaling function $F(\xi)$ compensated by $x^{3/2}$ and predicted amplitude.

fig:forcedScaling

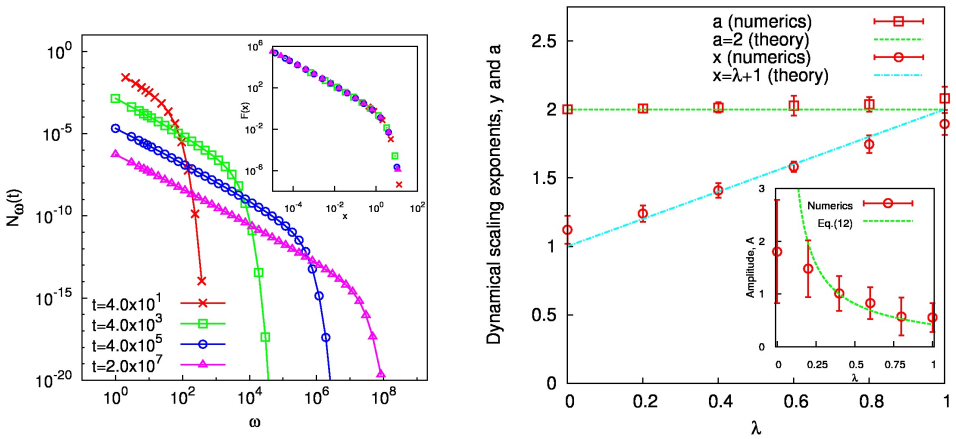

Figure 1.24: Numerical simulations of the self-similar solution in the unforced case

fig:decayScaling

We do not have the KZ exponent coming out. However, we still have a convergence problem at $\lambda = 1$.

The previous argument fails for both forced and unforced cases at $\lambda = 1$, which is the boundary of the finite capacity regime. Let us then consider a finite capacity system. Here we have

$$\int_0^\infty \xi\, F(\xi)\, d\xi$$

diverges at zero, so that the conservation of energy does not determine the dynamical exponent a. These type of self-similar solutions where you cannot determine the scaling exponent by conservation laws, are called of second type REF: Barenblatt?. For finite capacity systems, we therefore observe $s(t) \to \infty$ as $t \to t^*$. If $F(\xi) \sim \xi^{-x}$ as $\xi \to 0$ then the scaling implies that

$$N(\omega, t) \sim s(t)^a \left(\frac{\omega}{s(t)}\right)^{-x} = s(t)^{a+x}\, \omega^{-x} \tag{1.141}$$

as $t \to t^*$. Hence the transient exponent, x must be taken equal to $-a$ if the spectrum is to remain finite as $t \to t^*$. This is true independent of whether we force or not.

On the contrary, for an infinite capacity system we could determine a just by the conservation laws. It is not know a priori how to determine the dynamical exponent a in the finite capacity case. We know that it must be determined by self consistently solving the scaling equation:

$$-a\,F - \xi\frac{dF}{d\xi} = S_1[F(\xi)] + S_2[F(\xi)] + S_3[F(\xi)]. \tag{1.142}$$

Dimensionally, one might guess $a = -\frac{\lambda+3}{2}$, the KZ value. However, overwhelming numerical evidence suggests that this is not so: add all REF Cluster-cluster aggregation (Lee, 2000), MHD turbulence (Galtier et al., 2000), Non-equilibrium BEC (Lacaze et al, 2001), Leith model (CC & Nazarenko, 2004), Generic 3-wave turbulence (CC & Newell, 2010)

The difference it is somehow small, but it is there. See Figure 1.25 for numerical simulations. We can summarize the main observations that can be deduced from the numerics as follows:

- For 3WKE with $K(\omega_1, \omega_2) = (\omega_1\omega_2)^{\lambda/2}$, the transient spectrum is consistently (slightly) steeper than the KZ value.
- KZ spectrum is set up from right to left.
- Finite capacity in itself is not sufficient for the anomaly (e.g. the Smoluchowski equation with product kernel REF to previous section).
- Anisotropy is not necessary but it might help REF:(c.f. Galtier et al. 2005).

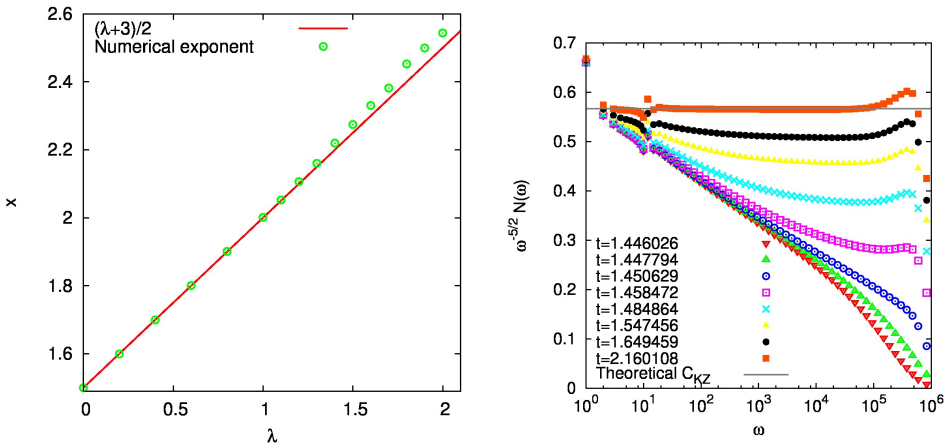

Figure 1.25: Caption

tyAnomaly

1.8.3 Spectral truncations of the wave collision operator

We now turn our attention to a spectrally truncated 3WKE. Thus, we introduce a maximum frequency Ω such that

$$N_\omega = 0, \qquad \text{for all modes having } \omega > \Omega.$$

Then, in sum over triads we only include

$$\omega_j \leq \omega_i < \omega_k \leq \Omega.$$

However we must *choose* how to approximate triads having

$$\omega_j \leq \omega_i < \Omega < \omega_k,$$

which are only relevant for $S_1[N_\omega]$ REF previous section. We have here different options:

- Include them: that is an open truncation. In this case we included a dissipative mechanism.
- Remove them: a closed truncation. This case is conservative.
- Damp them by a factor $0 < \nu < 1$: partially open truncation. Also here we have a dissipative mechanism

There is not an easier choice, and this is becoming complicated because we are trying to put a boundary condition on the energy flux at our dissipation scale Ω. Clearly, this is an artifact of our approximation since there is no real in boundary condition.

The actual truncated equations are the following

$$\frac{dN_i}{dt} = S_i^{(1)}[\mathbf{N},\Omega] + S_i^{(2)}[\mathbf{N},\Omega] + S_i^{(3)}[\mathbf{N},\Omega] - \gamma\, T_i[\mathbf{N},\Omega], \qquad i = 1,2,\ldots\Omega,$$

with the truncated collision integrals given by

$$S_i^{(1)}[\mathbf{N},\Omega] = \sum_{j=1}^{i-1} K_1(j,i-j)\, N_j N_{i-j} - \sum_{j=i+1}^{\Omega} K_1(j-i,i)\, N_i N_{j-i} - \sum_{j=1}^{\Omega-i} K_1(i,j)\, N_i N_j,$$

$$S_i^{(2)}[\mathbf{N},\Omega] = -\sum_{j=1}^{i-1} K_2(j,i-j)\, N_i N_j + \sum_{j=i+1}^{\Omega} K_2(j-i,i)\, N_j N_{j-i} + \sum_{j=1}^{\Omega-i} K_2(i,j)\, N_i N_{i+j},$$

$$S_i^{(3)}[\mathbf{N},\Omega] = -\sum_{j=1}^{i-1} K_3(j,i-j)\, N_i N_{i-j} + \sum_{j=i+1}^{\Omega} K_3(j-i,i)\, N_j N_i + \sum_{j=1}^{\Omega-i} K_3(i,j)\, N_j N_{i+j}.$$

Consider now the dissipative “boundary condition" case. The modified collision integrals $S_i^{(1)}$, $S_i^{(2)}$ and $S_i^{(3)}$ conserve energy. The dissipative “boundary" terms that transfer energy across the cutoff are

$$T_i[\mathbf{N},\Omega] = \gamma \left(\sum_{j=\Omega+1}^{\Omega+i} K_1(j-i,i)\, N_i N_{j-i} + \sum_{j=\Omega-i+1}^{\Omega} K_1(i,j)\, N_i N_j \right).$$

With the open truncation, we will see the KZ solution!, see Figure 1.26. However, the open truncation can produce a **bottleneck** as the solution approaches the dissipative cut-off REF:(Falkovich 1994). However, this bottleneck does not occur for all $L(\omega_1,\omega_2)$ REF???. One also has that the energy flux at Ω is 1.

For a closed truncation, we will observe **thermalisation** REF:(CC and Nazarenko (2004), Cichowlas et al (2005)), see Figure 1.27. The energy is equilibrating as you go near to your numerical cut-off. We will see at large frequencies the equilibrium spectrum. Interestingly enough, thermalisation occurs for all $L(\omega_1,\omega_2)$. Since the energy is conserved for this system, we also know that the energy flux at Ω is 0.

Write something nice to end the chapter

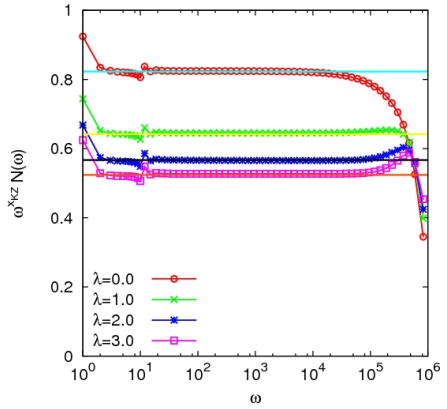

Figure 1.26: Compensated stationary spectra with open truncation. Product kernel: $L(\omega_1, \omega_2) = (\omega_1\omega_2)^{\lambda/2}$.

:bottleneck

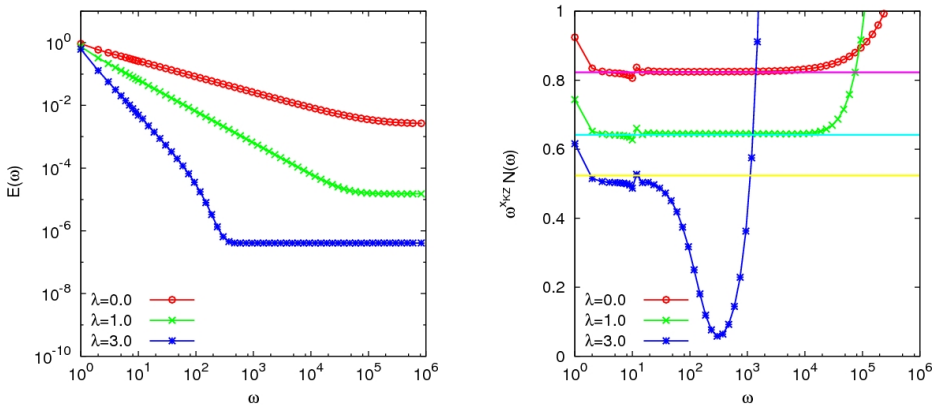

Figure 1.27: Quasi-stationary spectra with closed truncation. Product kernel: $L(\omega_1, \omega_2) = (\omega_1\omega_2)^{\lambda/2}$

malisation2

.

Chapter 2

Wave Turbulence: a Mathematical Perspective

2.1 Introduction

intro to the lecture notes

2.2 Lecture 1: Wave Propagation and Forcing

We begin studying general linear wave equations of the form

$$\partial_t \boldsymbol{u} + L\boldsymbol{u} = \boldsymbol{f} \tag{2.1}$$

In this equation, $\boldsymbol{u}$ is a vector-valued unknown with dependence on time and space, the *wave operator* L is linear and skew-symmetric ($\langle L\boldsymbol{u}, \boldsymbol{v}\rangle = -\langle \boldsymbol{u}, L\boldsymbol{v}\rangle$), and the forcing $\boldsymbol{f}$ is a source term.

When $\boldsymbol{f} = 0$, taking inner products with $\boldsymbol{u}$ and using skew-symmetry:

$$0 = \partial_t \langle \boldsymbol{u}, \boldsymbol{u}\rangle + \langle L\boldsymbol{u}, \boldsymbol{u}\rangle = \partial_t \langle \boldsymbol{u}, \boldsymbol{u}\rangle$$

Hence energy is conserved in the absence of forcing. The superposition principle also holds when $\boldsymbol{f} = 0$. Linear combinations of solutions are also solutions.

It is desirable to determine a set of oscillating modes which solve the equation, known as *waves*. More general solutions can be decomposed into these waves, which are then studied. For instance, when L is a skew-symmetric constant coefficient differential operator in space, we find plane wave solutions of the form $e^{i(\boldsymbol{k}\cdot\boldsymbol{x}-\omega t)}$. We look for a *dispersion relation*, which selects the plane waves that are honest solutions to the wave equation. The dispersion relation is key to characterizing the waves that are seen both in the absence of forcing and in its presence.

2.2.1 Examples of Dispersion Relations

Poincaré waves

Consider the incompressible Euler equations on the domain $\mathbb{T}^3 = [0,1]^3$ with periodic boundary conditions, subject to a Coriolis force in the $\hat{\boldsymbol{z}}$ (vertical) direction.

$$\begin{cases} \partial_t \boldsymbol{u} + (\boldsymbol{u}\cdot\nabla)\boldsymbol{u} + \nabla p + \hat{\boldsymbol{z}}\times\boldsymbol{u} = 0 \\ \nabla\cdot\boldsymbol{u} = 0 \end{cases}$$

Under the assumption that $\boldsymbol{u}$ is small, we may neglect the nonlinearity. Taking the divergence of the first equation and applying $\nabla\cdot\boldsymbol{u} = 0$ produces an equation for the pressure:

$$\Delta p + \nabla\cdot(\hat{\boldsymbol{z}}\times\boldsymbol{u}) = 0.$$

We have $\hat{\boldsymbol{z}}\times\boldsymbol{u} = (-u_2, u_1, 0)$. In Fourier space, the pressure equation becomes

$$-|\boldsymbol{k}|^2\widehat{p} - ik_1\widehat{u}_2 + ik_2\widehat{u}_1 = 0.$$

Note that the incompressibility condition determines u_3 from u_1 and u_2:

$$0 = ik_1\widehat{u}_1 + ik_2\widehat{u}_2 + ik_3\widehat{u}_3.$$

Then we need only to consider the first two components of the velocity. The first two components of ∇p are

$$\widehat{\nabla p} = \begin{pmatrix} ik_1 \\ ik_2 \end{pmatrix}\widehat{p} = \frac{1}{|\boldsymbol{k}|^2}\begin{pmatrix} ik_1(ik_2\widehat{u}_1 - ik_1\widehat{u}_2) \\ ik_2(ik_2\widehat{u}_1 - ik_1\widehat{u}_2) \end{pmatrix} = \frac{1}{|\boldsymbol{k}|^2}\begin{pmatrix} -k_1k_2 & k_1^2 \\ -k_2^2 & k_1k_2 \end{pmatrix}\begin{pmatrix} \widehat{u}_1 \\ \widehat{u}_2 \end{pmatrix}.$$

Moving the linearized equations for u_1 and u_2 to the Fourier domain, we find

$$i\omega\begin{pmatrix} \widehat{u}_1 \\ \widehat{u}_2 \end{pmatrix} + \frac{1}{|\boldsymbol{k}|^2}\begin{pmatrix} -k_1k_2 & k_1^2 \\ -k_2^2 & k_1k_2 \end{pmatrix}\begin{pmatrix} \widehat{u}_1 \\ \widehat{u}_2 \end{pmatrix} + \begin{pmatrix} -\widehat{u}_2 \\ \widehat{u}_1 \end{pmatrix} = 0.$$

Then for plane wave solutions, $i\omega$ must be an eigenvalue of the 2×2 matrix

$$\begin{pmatrix} \frac{k_1k_2}{|\boldsymbol{k}|^2} & 1 - \frac{k_1^2}{|\boldsymbol{k}|^2} \\ \frac{k_2^2}{|\boldsymbol{k}|^2} - 1 & -\frac{k_1k_2}{|\boldsymbol{k}|^2} \end{pmatrix}$$

This means that $i\omega$ must be a root of the characteristic polynomial:

$$\left(-\frac{k_1^2k_2^2}{|\boldsymbol{k}|^4} + (i\omega)^2\right) + \left(1 + \frac{k_1^2k_2^2}{|\boldsymbol{k}|^4} - \frac{k_1^2}{|\boldsymbol{k}|^2} - \frac{k_2^2}{|\boldsymbol{k}|^2}\right) = (i\omega)^2 + \frac{k_3^2}{|\boldsymbol{k}|^2} = 0$$

Hence the dispersion relation is $\omega = \pm\frac{k_3}{|\boldsymbol{k}|}$. The relation determines plane wave solutions $e^{i(\boldsymbol{k}\cdot\boldsymbol{x}-\omega t)}$ to the linearized Euler equations on $\mathbb{T}^3$.

Inertial gravity waves

Consider the linearized shallow water equations with averaged velocity in the vertical directions, horizontal velocity $\boldsymbol{u}$, water height $H+\eta(x,y,t)$, gravity g and varying Coriolis parameter βy. The equations are

$$\begin{cases} \partial_t\eta + \nabla\cdot\boldsymbol{u} = 0 \\ \partial_t\boldsymbol{u} + g\nabla\eta + \beta y\boldsymbol{u}^\perp = 0 \end{cases}$$

The plane wave $e^{i(kx+\ell y-\omega t)}$ is not a good ansatz due to the nonconstant coefficient on the Coriolis term. We instead opt to look for solutions which are plane waves in t and x, $e^{i(kx-\omega t)}(\widehat{\eta}(y), \widehat{u}_1(y), \widehat{u}_2(y))$. Taking Fourier transforms in x and t of our equations,

$$\begin{cases} i\omega\widehat{\eta} + ik\widehat{u}_1 + \partial_y\widehat{u}_2 = 0 \\ i\omega\widehat{u}_1 + ikg\widehat{\eta} - \beta y\widehat{u}_2 = 0 \\ i\omega\widehat{u}_2 + g\partial_y\widehat{\eta} + \beta y\widehat{u}_1 = 0 \end{cases}$$

We can write $\widehat{\eta}$ and $\widehat{u}_1$ in terms of $\widehat{u}_2$. From the second equation, we find

$$\widehat{\eta} = \frac{1}{ikg}(\beta y\widehat{u}_2 - i\omega\widehat{u}_1).$$

The first tells us

$$i\omega\frac{1}{ikg}(\beta y\widehat{u}_2 - i\omega\widehat{u}_1) + ik\widehat{u}_1 + \partial_y\widehat{u}_2 = 0 \quad \Longrightarrow \quad \widehat{u}_1 = \frac{1}{i(\omega^2 - k^2 g)}(kg\partial_y\widehat{u}_2 + \omega\beta y\widehat{u}_2)$$

Using these values for $\widehat{u}_1$ and $\widehat{\eta}$ in the third equation, we find

$$\begin{aligned} 0 &= i\omega\widehat{u}_2 + \frac{1}{ik}\left(\beta(\widehat{u}_2 + y\partial_y\widehat{u}_2) - i\omega\frac{1}{i(\omega^2 - k^2 g)}(kg\partial_y^2\widehat{u}_2 + \omega\beta(\widehat{u}_2 + y\partial_y\widehat{u}_2))\right) \\ &\quad + \beta y\frac{1}{i(\omega^2 - k^2 g)}(kg\partial_y\widehat{u}_2 + \omega\beta y\widehat{u}_2) \\ &= \left(i\omega + \frac{\omega\beta^2 y^2 - \beta kg}{i(\omega^2 - k^2 g)}\right)\widehat{u}_2 - \frac{\omega g}{i(\omega^2 - k^2 g)}\partial_y^2\widehat{u}_2 \end{aligned}$$

Simplifying, we find the relation:

$$0 = (\omega^3 + \omega k^2 g + \beta kg)\widehat{u}_2 + \omega(g\partial_y^2 - \beta^2 y^2)\widehat{u}_2$$

This relation tells us that $\widehat{u}_2$ is in fact an eigenstate of the operator $\partial_y^2 - \frac{\beta^2}{g}y^2$, the harmonic oscillator. This operator has a discrete spectrum of eigenvalues, $\frac{\beta}{\sqrt{g}}(2n+1)$ whose eigenstates are the Hermite functions. Hence we find solutions which are plane waves in x and t and Hermite modes in y which satisfy the dispersion relation:

$$0 = \omega^3 + \omega(k^2 g + \beta\sqrt{g}) + \beta kg$$

This example worked out well in part because the nonconstant coefficient was linear. Equations with more complicated variable coefficients will rarely admit such immediate families of solutions.

Vibrating plates

Consider a thin metal plate with no vertical stress, a linear displacement field in the normal direction z, and negligible tangential inertia compared to the normal inertia. The displacement ζ is described by a linear Föppl-von Kármán equation

$$\partial_t^2\zeta = -\frac{Eh^3}{12(1-\sigma^2)}\Delta^2\zeta$$

where E, h, and σ are constants. Taking a Fourier transform, we find

$$-\omega^2\widehat{\zeta} = -\frac{Eh^3}{12(1-\sigma^2)}|k|^4\widehat{\zeta}$$

and the dispersion relation looks like $\omega \sim \pm|k|^2$ with plane wave solutions.

Surface capillary waves

Consider the linearized equations for capillary waves in a fluid with a free surface with surface tension σ, gravity g, and infinite depth. The vertical perturbation of the fluid is $\eta(x,t)$ and the velocity potential is $\phi(x,z,t)$. The equations are

$$\begin{cases} \partial_t\eta = \partial_z\phi & z=0 \\ g\eta + \partial_t\phi = \sigma\partial_x^2\eta & z=0 \\ \nabla^2\phi = 0 \end{cases}$$

Suppose $\eta(x,t) = e^{i(kx-\omega t)}$. Then the first equation suggests we look for ϕ of the form $\phi(x,z,t) = -i\omega f(z)\eta(x,t)$. Plugging this ansatz into Laplace's equation tells us that

$$f'(z) = k^2 f(z) \qquad \Longrightarrow \qquad f(z) = Ae^{kz} + Be^{-kz}.$$

To obtain a physical solution, we must have $B = 0$. Plugging again into the first equation tells us $A = 1/k$. We have found the velocity potential to be

$$\phi(x,z,t) = -\frac{i\omega}{k}e^{kz}\eta(x,t)$$

Using ϕ and η in the second equation, we find that

$$g\eta - \frac{\omega^2}{k}\eta = -\sigma k^2\eta$$

and multiplying by k/η produces the dispersion relation

$$\omega = \pm\sqrt{gk + \sigma k^3}.$$

2.2.2 Forced waves with discrete spectrum

Consider linear forcing system

$$\begin{cases} \partial_t u + Lu = fe^{i\lambda t} \\ u_{|t=0} = 0 \end{cases} \tag{2.2}$$ general-line

where

- the wave operator L has only **discrete spectrum** which is included in the imaginary axis, i-e L has a countable family of eigenvalues/eigenvectors $(i\omega_n, \psi_n)$ which solve $L\psi_n = i\omega_n\psi_n$ (in mathematical terms, L is skew-adjoint with compact resolvent).
- the forcing term $f(x)e^{i\lambda t}$ is monochromatic with forced frequency λ.

Since the eigenvectors are an orthonormal basis of the energy space L^2, we can make decompositions

$$f(x) = \sum_n f_n \psi_n(x) \quad \text{and} \quad u(t,x) = \sum_n u_n(t)\psi_n(x).$$

Consequently, the coefficients $(u_n)_n$ satisfy the ODEs

$$\partial_t u_n + i\omega_n u_n = f_n e^{i\lambda t},$$

and thus the solution is

$$e^{i\omega_n t} u_n(t) = \int_0^t f_n e^{i(\lambda+\omega_n)s} ds.$$

Two situations with different behaviours appear with the value of $\lambda + \omega_n$:

- **Resonant forcing** $\lambda + \omega_n = 0$ In that case, the solution

  $$e^{i\omega_n t} u_n(t) = f_n t$$

  has a **linear growing in time**. Consequently, the energy growth as

  $$|u_n|^2 = |f_n|^2 t^2.$$

- **Non resonant forcing** $\lambda + \omega_n \neq 0$ In that case, the solution

  $$e^{i\omega_n t} u_n(t) = f_n \frac{e^{i(\lambda+\omega_n)t} - 1}{i(\lambda+\omega_n)}$$

  is **oscillating**. Consequently, the energy is always **bounded in time**

  $$|u_{(k/L)}(t)|^2 = |f_{(k/L)}|^2 \left| \frac{\sin\left[\frac{1}{2}\left(\omega_0 - h\left(\frac{k}{L}\right)\right)t\right]}{\frac{1}{2}\left(\omega_0 - h\left(\frac{k}{L}\right)\right)} \right|^2.$$

If there is no resonant forcing, i-e for all n, $\lambda + \omega_n \neq 0$, then the system is not able to capture energy. If there is some resonant forcing, the energy concentrate on eigenfrequencies. This will be crucial for the wave turbulence theory that we will discuss in next sections.

2.2.3 Forced waves with continuous spectrum

In the examples before, the dynamics are driven by a discrete set of eigenvalues. What happens if the spectrum is not discrete? We will first study this situation on examples.

Schrödinger equation

Consider the Schrödinger equation without potential in the full space

$$i\partial_t \psi + \Delta\psi = 0 \quad \text{on } \mathbb{R}^d. \tag{2.3}$$ dinger-linear

If we look for plane wave solutions $e^{i(\xi\cdot x - \omega t)}$, then ω and ξ must satisfy the dispersion relation $\omega - |\xi|^2 = 0$. Thus the solution can be written as a linear "superposition" of plane waves

$$\psi(t,x) = \frac{1}{2\pi} \int_{\mathbb{R}^d} \hat{\psi}(0,\xi) e^{i(\xi - t|\xi|^2)x} d\xi.$$

When we have have discrete spectrum, the superposition is a sum, here it is an integral and the "coefficients" $\hat{\psi}(0,\xi)$ are the continuous Fourier transform of the initial condition $\psi_{|t=0}$. The dispersion relation $\omega = |\xi|^2$ and the Fourier mode $e^{ix\cdot\xi}$ can be seen as "generalized" eigenvalues / eigenfunctions in the sense that we have the following diagonalisation of the Laplacian

$$-\Delta(e^{ix\cdot\xi}) = |\xi|^2 e^{ix\cdot\xi}.$$

We say "generalised" eigenfunctions since they have infinite L^2 energies $\int |e^{ix\cdot\xi}|^2 d\xi = +\infty$. The spectrum here is $\mathbb{R}^+$.

Homogenous operators of degree 0

Other examples are linked with **homogenous operators of degree** 0. Degree 0 means roughly that no "derivative" acts. As example, the multiplication by a function $\varphi(x)$ is a linear operator of degree 0. To define it correctly, one needs to introduce the notion of symbols of linear operators. Take for example the polynomial differential operator

$$H(x, i\partial) = \sum_j a_j(x)(i\partial_x)^j,$$

freeze the coefficients $a_j(x)$ and take the Fourier transform, it gives

$$h(x,\xi) = \sum_j a_j(x)\xi^j$$

which is called the symbol of H. More generally, the symbol h of an linear operator H is defined by the action of H on Fourier modes

$$He^{ix\cdot\xi} = h(x,\xi)e^{ix\cdot\xi}$$

The symbol is sometimes called the quantification. The operator H associated to a symbol h is called a pseudo-differential operator. It seems natural to definite it by

$$Hu = \mathcal{F}^{-1}(h\mathcal{F}u) \quad \forall u \in L^2$$

for a function u with $\mathcal{F}$ the Fourier transform. This way to associate h and H with the use of Fourier transform is called the Weyl quantification[1]. We say that operator is degree n if its maximal derivative is n, i-e its symbol satisfies

$$|h(x,\xi)| \leq (1 + |\xi|)^n$$

and we say it is homogeneous of degree 0 iff its symbol is homogeneous of degree 0:

$$h(x, \lambda\xi) = h(x,\xi).$$

All the following examples are homogeneous of degree 0:

- multiplication with a function $h(x,\xi) = \varphi(x)$
- internal waves in 2D $h(x,\xi) = \xi_1/|\xi|$

[1]The Weyl quantification is not the only way to associate an operator to a symbol. See for example the Bony quantification for the para-differential calculus

- inertial waves in 2D $h(x,\xi) = \xi_3/|\xi|$

A way to prove that an homogeneous operator of degree 0 has continuous spectrum is to show that one of the variable $x(t)$ or $k(t)$ of the Hamiltonian dynamics related the symbol $h(x,k)$

$$\begin{cases} \dot{x}(t) = \nabla_k h \\ \dot{k}(t) = -\nabla_x h \end{cases}$$

admits an at least linear growth in time. This is a consequence of the Mourre theorem (see Corollary 2.6.3). We will see this on the examples we mentioned above.

2.2.3.0.1 Multiplication by a function in 1D The Hamiltonian dynamics are given by

$$\begin{cases} \dot{x}(t) = 0 \\ \dot{k}(t) = -\partial_x \varphi(x). \end{cases}$$

If $\partial_x \varphi \neq 0$, then $k(t)$ grows linearly and thus there is continuous spectrum. In any dimension, if $\nabla\varphi(x) \neq 0$ for all x, then the whole spectrum is continuous.

2.2.3.0.2 Internal waves The Hamiltonian dynamics of 2D internal waves with affine stratification is given by

$$\begin{cases} \dot{x_1}(t) = \frac{k_3^2}{|k|^3} & \dot{x_3}(t) = \frac{-k_3 k_1}{|k|^3} \\ \dot{k_1}(t) = 0 & \dot{k_3}(t) = 0 \end{cases}$$

The trajectory x_h cannot go to ∞. However, due to the refection on the boundary, k_h can go to ∞. This is the case when one boundary is not horizontal or vertical. The reflection laws on a slope tilted with angle α with respect to the horizontal are

$$\begin{cases} \dfrac{(k_1^r)^2}{|k^r|^2} = \dfrac{(k_1^i)^2}{|k^i|^2} & \textit{(conservation of energy)} \\ \dfrac{k_1^r - k_1^i}{k_3^r - k_3^i} = \tan\alpha & \textit{(zero flux condition)} \end{cases}$$

where (x^i, k^i) refers to the incident ray whereas (x^r, k^r) to the reflected ray.

2.2.4 Forced waves with absolute continuous spectrum

Consider again the linear Schrödinger equation (2.3) in the Fourier space with a **monochromatic forcing**

$$\partial_t \hat{u} + i|\xi|^2 \hat{u} = \hat{f} e^{i\lambda t}.$$

The solution is

$$e^{i|\xi|^2 t}\hat{u}(t,\xi) = \hat{f}\frac{e^{i(\lambda+|\xi|^2)t} - 1}{i(\lambda + |\xi|^2)}$$

In the **continuous spectrum** case, $(\lambda + |\xi|^2)$ can be as small as you want, thus the distinction between resonance and non-resonance doesn't make sense. We will say that $(\lambda + |\xi|^2) = 0$ is a quasi-resonance forcing. The solution in time domain

$$u(t,x) = \int_{\mathbb{R}^d} \hat{f}\frac{e^{i(\lambda+|\xi|^2)t} - 1}{i(\lambda + |\xi|^2)} e^{-i|\xi|^2 t} e^{ix\cdot k} d\xi$$

must be seen as a singular integral. On a test function $\varphi \in L^2$, Parseval's theorem says

$$\begin{aligned}(u,\varphi)_{L^2} &= \frac{1}{2\pi}\int_{\mathbb{R}^d} \frac{e^{i(\lambda+|\xi|^2)t}-1}{i(\lambda+|\xi|^2)} e^{-i|\xi|^2 t}\hat{f}(\xi)\hat{\varphi}^*(\xi)d\xi \\ &= \frac{e^{i\lambda t}}{2i\pi}\int_{\mathbb{R}^d} \frac{1-e^{-i(\lambda+|\xi|^2)t}}{\lambda+|\xi|^2}\hat{f}(\xi)\hat{\varphi}(\xi)d\xi\end{aligned}$$

If the test function and the source are such that $\hat{f}(\xi)\hat{\varphi}(\xi)$ is the indicator function of $[a,b]$ one gets

$$(u,\varphi)_{L^2} = \frac{e^{i\lambda t}}{2i\pi}\int_{\mathbb{R}^d} \frac{1-e^{-i(\lambda+|\xi|^2)t}}{\lambda+|\xi|^2}\mathbf{1}_{[a,b]}d\xi$$

that gives with the change of variable $\mu = (\lambda+|\xi|^2)t$

$$(u,\varphi)_{L^2} = \frac{e^{i\lambda t}}{2i\pi}\int_{\mathbb{R}^d} \frac{1-e^{-i\mu}}{\mu}\mathbf{1}_{[a-|\xi|^2 t, b-|\xi|^2 t]}d\xi$$

and thus

$$(u,\varphi)_{L^2} = \frac{e^{i\lambda t}}{2i\pi}\left[i\pi + \log\left(\frac{b-|\xi|^2}{a-|\xi|^2}\right) + O\left(\frac{1}{t}\right)\right]$$

To have physical meaning, it can be more relevant to look at the energy

$$\frac{1}{2\pi}\int_{\mathbb{R}^d}|\xi|^2|\hat{\psi}(\xi)|^2 d\xi = \frac{1}{2\pi}\int_{\mathbb{R}^d}\left|\frac{1-e^{-i(\lambda+|\xi|^2)t}}{\lambda+|\xi|^2}\right|^2 |\xi|^2|\hat{f}(\xi)|^2 d\xi.$$

Using the symmetry of $|\xi|^2$ and the same change of variable, one gets

$$\frac{1}{2\pi}\int_{\mathbb{R}^d}|\xi|^2|\hat{\psi}(\xi)|^2 d\xi = \frac{t}{2\pi}\int_{\lambda t}^{+\infty}\left|\frac{1-e^{-i\mu}}{\mu}\right|^2 G\left(\frac{\mu}{t}-\lambda\right)d\mu \sim_{t\gg 1} \frac{G(\lambda)}{4}t$$

where $G(x) = \sqrt{x}(|\hat{f}(\sqrt{x})|^2 + |\hat{f}(-\sqrt{x})|^2)$.

Contrary to discrete spectrum case, here the **quasi-resonance** mechanism have the following procedure

1. at the beginning, the force excite a large band around the forcing frequency λ
2. this band shrinks gradually around the forcing frequency λ as time increase,
3. when $t \to \infty$, the **energy grows linearly in time**. What we observe looks like more and more to generalised eigenfunctions which has not L^2 finite energy.

The main difference between quasi-resonance mechanism associated to (absolutely) continuous spectrum and resonance associated to discrete spectrum is the growth of energy. It the first case, it is linear whereas, in the second case, it is quadratic. This is one key-stone of wave-turbulence theory.

2.3 Lecture 2: Random Perturbative Forcing

In the previous section, we have concentrate our effort on additive forcing $\partial_t u + Lu = f$. We have seen that there a growth of energy in longtime scale if the forcing is resonant or quasi-resonant.

- **Resonant forcing.** It corresponds to the case where L have a discrete spectrum and where the forcing excites an eigenvalue. In that case, there is a linear growth of the amplitude of the resonant mode and thus

$$\partial_{tt}^2 \text{Energy} \sim \text{constant}.$$

- **Quasi-resonant forcing.** It corresponds to the case where L have a continuous spectrum and where the exciting frequency are inside the continuous spectrum without being itself an eigenvalue. In that case,

$$\partial_t \text{Energy} \underset{t\gg 1}{\sim} \text{constant}.$$

In this section, we will be interested in **parametric forcing**, i-e a multiplicative forcing

$$\partial_t u + Lu = fu,$$

which induces interactions between the forcing and the solution. Moreover, f will have some **randomness**.

As first example of parametric forcing we will see a periodic perturbation of Schrödinger equation

$$i\partial_t \psi - \Delta\psi = -V_{\text{per}}\psi \quad \text{where } V_{\text{per}} \text{ is periodic}$$

which describe the electrostatic structure in a crystal. When V_{per} is constant, we have seen that we can look for Fourier plane waves $e^{ik\cdot x}$ solutions. Here, since V_{per} is periodic we look for **Bloch waves** $\psi_k(x) = e^{ik\cdot x}u(x)$ solutions where $u(x)$ is a periodic function with same period in the crystal lattice. More precision on Bloch waves can be found in appendix. In particualr, in it appendix, it is explain why the spectrum of $H = -\Delta + V_{\text{per}}$ have a band-gap structure and why the Bloch waves are "generalized eigenfunctions of H.

Then we will considered that the the parametric force is no longer periodic but random. What can we say about the propagation of waves

$$i\partial_t \psi + H\psi = O \quad \text{with} \quad H = -\Delta + V_{\text{rand}}$$

in a random media ? In $\mathbb{R}^d$ with $d \geq 3$, there is a **Anderson's conjecture** bases on experiments which states

- *(weak random parametric forcing.)*

$$V_{\text{rand}} \ll 1 \quad \Rightarrow \quad \mathbb{E}\left[\int |x||\psi(t,x)|^2\right] \underset{t\gg 1}{\sim} D\sqrt{t}$$

  which is typical of **diffusion**,

- *(high random parametric forcing.)*

$$V_{\text{rand}} \gg 1 \quad \Rightarrow \quad \mathbb{E}\left[\int |x||\psi(t,x)|^2\right] \leq C$$

  which is typical of **localization**.

The second case is also true when $d \leq 2$ and V_{rand} not necessary high. In the following, we will focus on the case of weak random parametric forcing.

2.3.1 Linear Perturbation Theory

sec:iteratedDuhamel

The Iterated Duhamel Expansion

Suppose we have the wave operator $L = i\Delta$. Let $\varepsilon > 0$ and consider a small random perturbative forcing $f = i\varepsilon V$. Then we consider the equation

$$\partial_t \psi + L\psi = i\varepsilon V \psi$$

This is $i\partial_t \psi = H\psi$ for the Hamiltonian $H = -\Delta + \varepsilon V$, and then $\psi = e^{-itH}\psi_0$. We will iteratively apply Duhamel's formula to tackle the perturbation. For a single iteration, conjugate by the linear evolution group $e^{it\Delta}$ and then integrate:

$$i\partial_t(e^{it\Delta}\psi) = e^{it\Delta}(\varepsilon V \psi)$$

$$e^{it\Delta}\psi(t) = \psi_0 - i\varepsilon \int_0^t e^{is\Delta}(V\psi(s))\, ds$$

And we find the first iteration, How can H and Δ swap under the integral sign?

$$\psi(t) = e^{-it\Delta}\psi_0 - i\varepsilon \int_0^t e^{-i(t-s)H} V e^{-is\Delta}\psi_0\, ds$$

Applying this formula again to the term under $e^{-i(t-s)H}$ n times, we find

$$\psi(t) = \sum_{n=0}^{N-1} \psi^{(n)}(t) + \delta\psi^{(N)}(t)$$

with the iterated Duhamel terms I don't think the delta notation we wanted works here.

$$\psi^{(n)}(t) = (-i\varepsilon)^n \int e^{is_0\Delta} V e^{is_1\Delta} V \cdots e^{is_n\Delta}\psi_0\, \delta(t - \textstyle\sum s_j) ds_0 ds_1 \cdots ds_n$$

and the remainder Similar concern about H and Δ

$$\delta\psi^{(N)}(t) = (-i\varepsilon) \int_0^t e^{-i(t-s)H} V \psi^{(N-1)}(s)\, ds$$

It is not clear at the outset that this expansion will converge as $N \to \infty$.

Feynmann Diagrams

Now suppose $V = \sum_{\alpha\in\mathbb{Z}^d} V_\alpha$, a sum of independent smooth random variables V_α with support near α and $\mathbb{E}(V_\alpha) = 0$. We also make a summability assumption for each p, q:

$$\mathbb{E}(\textstyle\sum_\alpha \widehat{V}_\alpha(p)\overline{\widehat{V}}_\alpha(q)) = |\widehat{B}(p)|^2\delta_{p-q}$$

where $\widehat{B}$ is a well-behaved, bounded, smooth function.

Then we can decompose $\psi^{(n)}$ into pieces ψ_A where $A = (\alpha_1, \ldots, \alpha_n) \in \mathbb{Z}^{nd}$ using linearity:

$$\psi^{(n)} = \sum_{(\alpha_1,\ldots,\alpha_n)} \psi_A =: \sum_{(\alpha_1,\ldots,\alpha_n)} (-i\varepsilon)^n \int e^{is_0\Delta} V_{\alpha_1} \cdots V_{\alpha_n} e^{is_n\Delta}\psi_0\, \delta(t - \textstyle\sum s_j) ds_0 \cdots ds_n$$

We can think of this as a decomposition into pieces which collide with the potentials at given sequences A of lattice points.

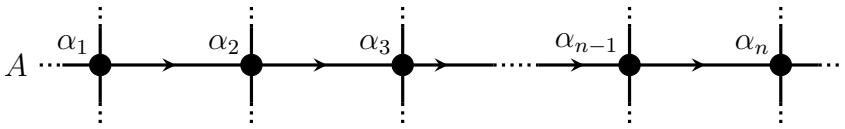

Figure 2.1: A sequence of collisions $A = \{\alpha_1, \ldots, \alpha_n\}$ in the lattice $\mathbb{Z}^d$.

For now, we will only analyze the A's with no repeated indices. We will see that paths with repeated indices admit better estimates than those without repetitions. So our proposed decomposition is

$$\psi = \sum_n \sum_{A \text{ w.o. repetitions}} \psi_A + \text{Repetition remainders} + \text{Duhamel remainder}$$

With this decomposition, we may begin to estimate *observables*: quadratic quantities in ψ. For instance, we can write the L^2 norm:

$$\mathbb{E}(\|\psi(t)\|_2^2) = \sum_{n,m}\sum_{A,B} \mathbb{E}(\psi_A\overline{\psi}_B)$$

where $A = (\alpha_1, \ldots, \alpha_n)$ and $B = (\beta_1, \ldots, \beta_m)$. An observation known as *Wick's rule* tells us that the contribution is 0 whenever B is not a permutation of A. Indeed, then we can use independence of the V_α's to conclude that the expectations are 0. Here, it is important that we have replaced our Hamiltonians by free propagation by $e^{-it\Delta}$ during the Duhamel iteration. This means that the propagators do not depend on V, allowing independent terms to cancel.

So Wick's rule tells us that $B = \pi(A)$ for some permutation π, and we find

$$\mathbb{E}(\|\psi(t)\|_2^2) = \sum_n \sum_{\pi\in S_n} \Big(\sum_{|A|=n} \mathbb{E}(\psi_A\overline{\psi}_{\pi(A)})\Big) =: \sum_n \sum_{\pi\in S_n} \text{Val}(\pi)$$

Remarks:

- This decomposition for the L^2-norm can be similarly performed for any bounded and smooth observable.

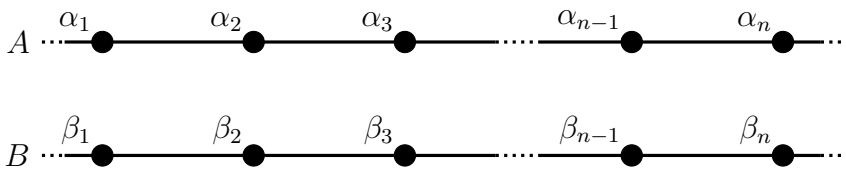

Figure 2.2: An interaction of A and B. By Wick's rule, B must be a permutation of A.

- We can obtain a bound on the Duhamel formula remainder, even though the presence of e^{itH} (which depends on V) prevents us from applying Wick's rule. We apply unitarity of e^{itH} to bound quadratic quantities K in $\delta\psi^{(N)}$:

$$K(\delta\psi^{(N)}(t))^{1/2} \leq Ct \left(\sup_{0\leq s\leq t} \|\varepsilon V \psi^{(N-1)}(s)\|^2 \right)^{1/2}$$

  where C depends on the L^2 norms of ψ and $\psi^{(n)}$ for $n < N$. So the Duhamel remainder is bounded in terms of the iterates. Not sure why C depends on these.

2.3.2 The Kinetic Limit

sec:kineticLimit

We would like to understand the evolution in time of the expectations of observables, i.e. quadratic quantities in $\psi(t)$. It will be helpful for us to note that the time scale for this evolution, known as the *kinetic time scale*, is much greater than the time scale for the oscillations. Which oscillations precisely here? This kinetic time scale is $t = O(\varepsilon^{-2})$.

We will show convergence of the perturbative expansion on this time scale. Moreover, we will show that only the classical collisions matter in this kinetic limit. This is desirable since the kinetic equation holds at the level of classical mechanics.

Ladder graphs

The first terms of $\mathbb{E}(|\psi(t)|^2)$ to estimate are the *ladder graphs*. These are the terms $\mathrm{Val}(\pi) = \mathbb{E}(\psi_A \overline{\psi}_B)$ where $A = B$ and $\pi = \mathrm{Id}_n$. They correspond to Feynmann diagrams where all pairings are connected by vertical edges, or to classical collision histories (meeting at each of the lattice points α_j).

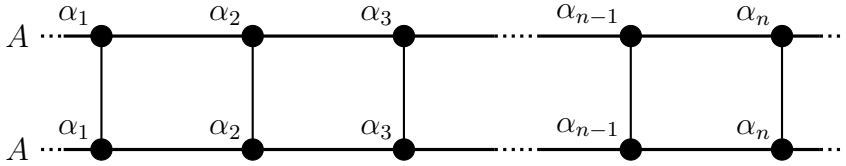

Figure 2.3: A ladder graph, where $A = B$.

We can attempt to estimate these terms naively using the fact that the volume of the

n-simplex $\{(s_0,\dots,s_n) : s_j \geq 0, \sum s_j = t\}$ is $t^n/n!$:

$$\begin{aligned}\mathrm{Val}(\mathrm{Id}_n) = \sum_{|A|=n} \mathbb{E}\Big[(-i\varepsilon)^n \int e^{is_0\Delta} V_{\alpha_1}\cdots V_{\alpha_n} e^{is_n\Delta}\psi_0\,\delta(t-\textstyle\sum s_j)ds_0\cdots ds_n \\ \times (i\varepsilon)^n \int e^{-is_0'\Delta}\overline{V}_{\alpha_1}\cdots\overline{V}_{\alpha_n} e^{-is_n'\Delta}\overline{\psi}_0\,\delta(t-\textstyle\sum s_j')ds_0'\cdots ds_n'\Big]\end{aligned}$$

$$|\mathrm{Val}(\mathrm{Id}_n)| \leq C\varepsilon^{2n}\left(\frac{t^n}{n!}\right)^2 = C\frac{(\varepsilon t)^{2n}}{(n!)^2}$$

Then the scaling is $t = O(\varepsilon^{-1})$, which is not a long enough time scale for our purposes. Note that we can bound the potential terms using the summability assumption we made in the Fourier domain.

If we are more careful and combine the two integrals, we can use the oscillatory nature of the integrand to exploit a quasiresonant mechanism. Similarly to how quasiresonance turned quadratic growth into linear growth in simpler examples, here, we are able to sharpen our bound to:

$$|\mathrm{Val}(\mathrm{Id}_n)| \leq C\varepsilon^{2n}\frac{t^n}{n!} = C\frac{(\varepsilon^2 t)^n}{n!}$$

Then the scaling is $t = O(\varepsilon^{-2})$, and we are in good shape for convergence on the kinetic time scale.

Non-ladder graphs

When π is nontrivial, we have crossings on the Feynmann diagrams corresponding to non-classical interactions. For instance, consider $B = (\alpha_2, \alpha_1, \alpha_3, \dots, \alpha_n)$. It turns out that even one crossing like this gains two powers of ε on the naive bound. In general, the contribution of $\mathrm{Val}(\pi)$ is related to the complexity of π: its number of crossings.

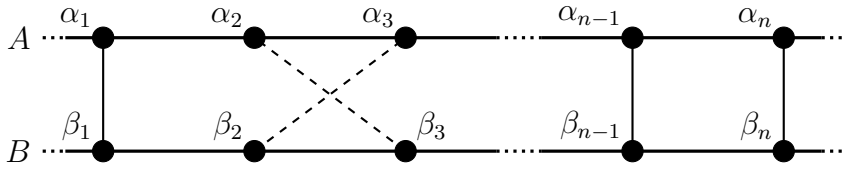

Figure 2.4: Feynmann diagrams with one crossing. ε^2 gain on contribution.

So we estimate

$$\sum_{\pi\neq\mathrm{Id}_n} |\mathrm{Val}(\pi)| \leq \varepsilon^2 n!\frac{(\varepsilon^2 t)^n}{n!} = O(\varepsilon^2)$$

and when $\varepsilon^2 t \ll 1$, we conclude convergence of the series expansion for ψ in to $\psi^{(n)}$ on the kinetic scale. The L^2 norm is bounded as:

$$\mathbb{E}(|\psi(t)|^2) \leq \sum_{n=0}^{N-1}\frac{(\varepsilon^2 t)^n}{n!}\left(1 + n\varepsilon^2 + n!\varepsilon^4\right) + \text{Remainder}$$

where 1 corresponds to ladder graphs, $n\varepsilon^2$ to graphs with one crossing, and $n!\varepsilon^4$ to all other graphs. The Duhamel remainder is bounded using our estimate by $\psi^{(N-1)}$:

$$\text{Remainder} \leq t\frac{(\varepsilon^2 t)^N}{N!}(1 + N\varepsilon^2 + N^2\varepsilon^4 + N!\varepsilon^6)$$

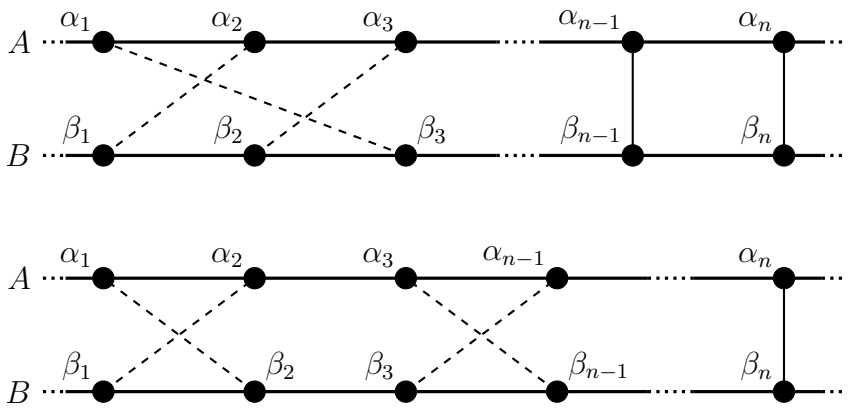

Figure 2.5: Feynmann diagrams with two crossings. ε^4 gain on contribution.

where t is the cost of having a uniform bound, and we extract out the $N^2\varepsilon^4$ term for graphs with two crossings. If we now take

$$N \sim \left| \frac{\log \varepsilon}{\log |\log \varepsilon|} \right|$$

we find convergence of the perturbative expansion as $\varepsilon \to 0$.

Remarks:

- To obtain the limit for diffusive times, a more precise treatment of the remainders is required, the Feynmann diagrams need to be classified more carefully, and there is a renormalization due to the repetitions.
- The perturbative approach we took is not the only option. Another method involves using Bloch waves defined in a weak, distributional sense to pass to the kinetic limit.

2.4 Lecture 3: Weakly Nonlinear Wave Equations

In the linear setting where we have considered linear Schrödinger equation with weak random parametric forcing

$$i\partial_t \psi - \Delta \psi + \varepsilon V = 0,$$

we had a number of key ingredients:

- **Smallness:** Potential was εV for $\varepsilon \ll 1$. This smallness in L^∞ led to a scale separation, which allowed our perturbation expansion.
- **Randomness:** The independence relation allowed us to use Wick's rule, which allowed us to demand pairings on the polynomials in V.
- **Quasiresonant Mechanism:** Despite having a pair of integrals, their oscillations meant that we were able to extract linear growth in t. This allowed convergence of the perturbation expansion on the kinetic time scale $t = O(\varepsilon^{-2})$.
- **Combinatorics:** The analysis of the permutation complexity allows us to discard permutations with crossings and only consider ladder graphs.

- **Kinetic equation:** At order $O(\varepsilon^2)$, we have an identification with Boltzmann equation. This last one can written as

$$(\partial_t + v\nabla_x)f(t,x,v) = \int \sigma(u,v)(f(t,x,u) - (f(t,x,v)du$$

where

  - *Transport:* $v\nabla_x$ comes from the free Schrödinger equation (if we take the Wigner transform of $i\partial_t - \Delta$, one gets $\partial_t + v\nabla_x$) where x is the position and v is the wave number.
  - *Collision operator:* $\int \sigma(u,v)(f(t,x,u) - (f(t,x,v)du$ is a jump process in the frequency space
    * *Cross-section:* $\sigma(u,v) = |\hat{B}(u,v)|^2\delta_{|u|^2-|v|^2}$ where B is related to the random potential
    * *Gain:* $\int \sigma(u,v)f(t,x,u)du$ is the contribution of ladder graphs
    * *Loss term:* $-\int \sigma(u,v)(f(t,x,v)du$ is the contribution of immediate repetitions (pair two adjacent α)

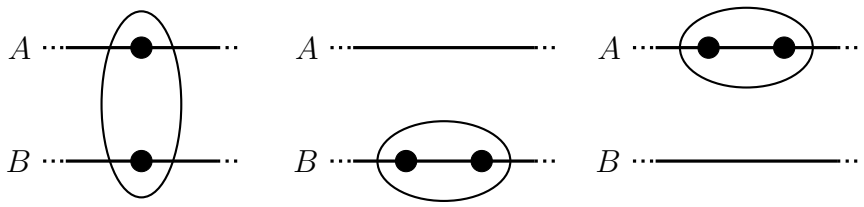

Figure 2.6: Left: gain term. Middle and right: loss terms.

Now, we will shift to the nonlinear case. With $\varepsilon \ll 1$, we write

$$\partial_t \boldsymbol{u} + L\boldsymbol{u} + \varepsilon Q(\boldsymbol{u}) = 0$$

which has weak nonlinearity $\varepsilon Q(\boldsymbol{u})$. When L has discrete spectrum, for example if the previous PDE is cast on a torus, the gaps between two eigenvalues are bounded from below. One can should use filtering method to obtain the envelope equation for each oscillating mode (cf Frederic lecture, where ???). We will be interested in the case where L has continuous spectrum, or almost-continuous spectrum. This is the case for large box limit (when the size of the torus becomes bigger and bigger, the gaps between eigenvalues vanish). For example, we have cubic Nonlinear Schrödinger:

$$(i\partial_t - \Delta)\psi + \varepsilon|\psi|^2\psi = 0$$

We can think of this equation through the lens of the linear wave equations with random forcing by writing $V = |\psi|^2$. But now there is a nonlinear coupling in the forcing.

We would like V to be $O(1)$ in L^∞, and to be random. At the initial time, we will assume randomness. One of the major issues in the analysis will be in propagating the randomness forwards. We will chose our scaling so that $|\psi_0|^2 = O(1)$ in L^∞.

To construct this random initial state, we work in a large box of size R and choose each Fourier mode of ψ_0 to be a Gaussian variable. Here, the spectrum is discrete, consisting of $\frac{k}{R}$ for $k \in \mathbb{Z}^d$. Then, in the perturbation expansion, we will find an expression for $|\psi(t)|^2$ in terms of polynomials in $\widehat{\psi_0}(k)$. This will allow us to use Wick's rule without a priori proving the propagation of randomness.

2.4.1 Nonlinear Perturbation Theory

We will write $a = e^{it\Delta}\psi$ to conjugate by the free propagation. We denote the Fourier modes by a_k for $k \in (\mathbb{Z}/R)^d$. If we write $|\psi|^2\psi = \psi\overline{\psi}\psi$, we can see which terms will need to be convolved on the Fourier side. The NLS becomes:

$$\partial_t a_k = \frac{i\varepsilon}{R^{2d}} \sum_{k=k_1-k_2+k_3} a_{k_1}\overline{a}_{k_2}a_{k_3}e^{it(k_1^2+k_3^2-k_2^2-k^2)} \tag{2.4}$$

The normalization constant $1/R^{2d}$ comes from the normalization in L^∞, R^d as well as the normalizations of the three sums, $1/R^{3d}$.

Integrating this in time, we obtain the analogue of our first Duhamel iteration from the linear case. We can then substitute the equation back in for a_{k_1}, $\overline{a}_{k_2}$, and a_{k_3} to compute the Duhamel expansion.

In this expansion, we are making a splitting from k into three branches k_1, k_2, and k_3. We have the relation $k + k_2 = k_1 + k_3$ from the convolution, and the exponential adds high oscillations unless we are near $k^2 + k_2^2 \sim k_1^2 + k_3^2$, providing quasiresonance.

Contrast this with the linear case, where we found the elementary Duhamel iteration. If we write the corresponding formulas for the Fourier modes, we find

$$\partial_t a_k = i\varepsilon \sum_{k=k_1+k_2} V_{k_1}a_{k_2}e^{it(k_2^2-k^2)}$$

At each step of the iteration, we kept adding to the same term. In the case for the NLS, the iterated Duhamel formula blows up into a tree with many branches where we substitute back in for a_{k_1}, $\overline{a}_{k_2}$, and a_{k_3}.

Figure 2.7: Left: The linear iteration. Right: Nonlinear iteration splitting.

Then observables manifest in pairs of trees with signed edges (corresponding to the presence of a conjugate). We still have a Wick's rule for these trees: the nonzero terms of the expansion may be represented by couples where we pair the end nodes of the trees, pairing conjugated terms with nonconjugated terms and never pairing two nodes stemming from the same direct parent.

In the NLS situation, we may remove trivial branchings such as $k \to (k, k_2, k_2)$ by subtracting a phase shift $\psi \int |\psi|^2$. The potential becomes $\widetilde{V} = |\psi|^2 - \int |\psi|^2$, and these branchings have $a_k\overline{a}_{k_2}a_{k_2} = 0$.

It is important to remark that we still do not have a clear method with which to stop the expansion. We do not have the unitarity of the propagator that we had in the linear case. Still, we can analyze the leading order terms of the expansion.

2.4.2 Leading Order Terms

In the kinetic time scale $t = O(\varepsilon^{-2})$, we can obtain the derivative at time 0 from the term of order ε^2 in the perturbation expansion. Then, we will have to check that the

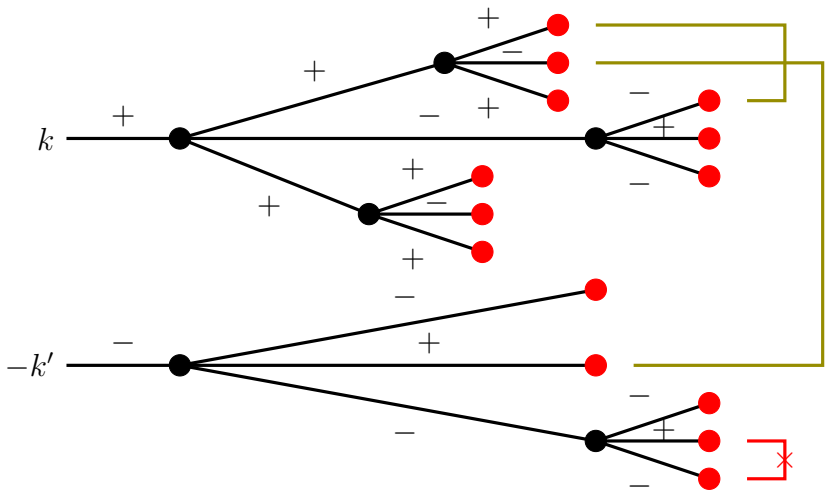

Figure 2.8: A pair of trees with the beginning of a coupling. Signs must be opposite. Due to the phase shift, nodes on the same branch do not couple.

higher order terms can be expressed as "combinations" of these terms of size ε^2. This is in analogy to how the ladder graphs in the linear case contributed the leading order terms, and the higher order terms corresponding to crossings and repetitions could be understood in terms of the ladder graphs.

In the NLS case, there are two types of pairings of trees which contribute to leading order terms. First, we have the "(a)-operations," which are pairings of the same branching: k_j is coupled with $-k'_j$. These are the counterparts of the ladder graphs from the linear setting. Second, we have the "(b)-operations," pairings with one tree with no branchings, and another tree with two branchings. The picture makes it easier to see the pairing, but we record it here as well. Call k the node on the first tree, call k_2 and $-k_3$ the endnodes on the first branching of the second tree, and call $-k_1^1$, k_1^2, and $-k_1^3$ the endnodes of the second branching on the second tree. The coupling is $(k, -k_1^1)$, $(k_1^2, -k_3)$, and $(-k_1^3, k_2)$. This pairing is the counterpart of a repetition from the linear setting.

Figure 2.9: The two leading order tree pairings. Colours indicate the coupling. Left: An (a) operation, the counterpart of the ladder graph. Right: A (b) operation, the counterpart of the repetition.

Using these two kinds of pairings, we can extract all of the order ε^2 terms in the perturbation expansion and take the kinetic limit.

Next, we can look at the order ε^4 terms. These terms either come from diagrams which are composed of (a) and (b) operations, or from diagrams which are not. We can

see that diagrams which are not are necessarily under more constraints for the pairing, and hence contribute less to the expansion. See the examples in Figures ?? and ?? below.

fig:nonregCouple

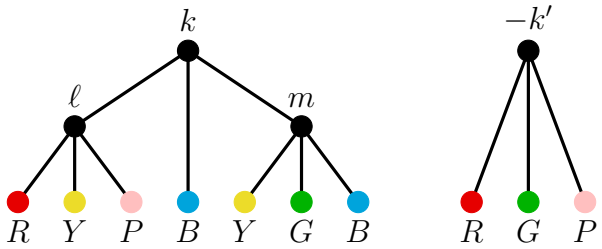

Figure 2.10: Non-regular couple: Not made from (a) and (b) operations.

In Figure ??, we have a coupling of trees which does not originate from composing (a) and (b) operations. Remember that each note corresponds to constraints on the wavenumbers in the iterated Duhamel expansion (where these constraints are demanding some massive convolution). If we write down the constraints imposed on the wavenumbers at each node, we'll find dependencies between the constraints. We get $(d+1)$ at each node, d relations from conservation of momentum ($k + k_2 = k_1 + k_3$) coming from our convolution and 1 relation from conservation of energy ($k^2 + k_2^2 = k_1^2 + k_3^2$) coming from the quasiresonant mechanism. There are 3 distinct nodes, k, ℓ, and m. So we get $3(d+1)$ relations.

fig:regCouple

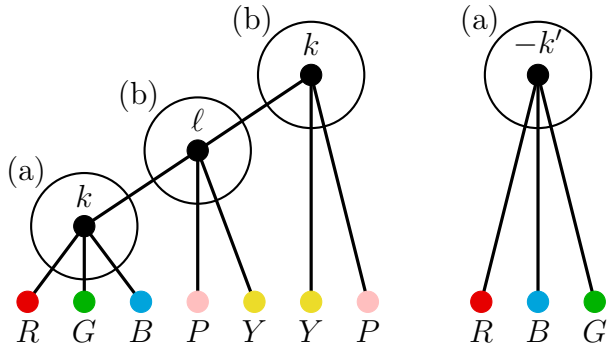

Figure 2.11: Regular couple: Made from two (a) and two (b) operations.

In Figure ??, we have a coupling of trees which originates from composing two (a) and two (b) operations. If we write down the constraints imposed on the wavenumbers at each node, we'll find that the top left and bottom left splitting points contribute the same constraints. We get $2(d+1)$ instead of $3(d+1)$ relations. Since there are less constraints, there are many more possible wavenumbers that obey this coupling. Hence the contribution of these regular terms is much more than the contribution from the non-regular couplings.

2.4.3 The Diffusion Limit

2.5 Lecture 4: Kinetic Equations for Wave Turbulence

add references to chapter of Colm

Our main assumptions are the following:

- Randomness of initial data (so that we may apply Wick's rule)
- Smallness of the nonlinearity: $\varepsilon \ll 1$
- Continuous (or almost continuous) spectrum for the wave operator. In the case of the Laplacian in a box, we must have the box size $R \gg 1$. This is to give us the quasiresonant mechanism.

For short kinetic times, under the appropriate scaling assumptions on ε and R, we use the leading order ε^2 terms in the perturbation expansion to derive a kinetic equation.

For the cubic nonlinear Schrödinger equation, there is no forcing or dissipation, and there is no spatial inhomogeneity. We find the following *4-wave interaction*:

$$\partial_t f = \int f f_1 f_2 f_3 \left(\frac{1}{f} + \frac{1}{f_1} - \frac{1}{f_2} - \frac{1}{f_3}\right) |V|^2 \delta^{k+k_1}_{k_2+k_3} \delta^{|k|^2+|k_1|^2}_{|k_2|^2+|k_3|^2} dk_1 dk_2 dk_3$$

where $f_j = f(k_j)$. (Note that k_1 and k_2 have switched places from the notation in Lecture 3. We should probably fix this!) V represents microscopic interactions, the first delta represents conservation of momentum, and the second delta represents the quasiresonant mechanism. Depending on the original nonlinearity and on the dispersion relation ω, it is also common to find *3-wave interactions*:

$$\partial_t f = \int f f_1 f_2 \left(\frac{1}{f} - \frac{1}{f_1} - \frac{1}{f_2}\right) |V|^2 \delta^{k}_{k_1+k_2} \delta^{\omega_k}_{\omega_{k_1}+\omega_{k_2}} dk_1 dk_2$$

2.5.1 Main Features of the Kinetic Equations

In these notes, we will focus on the 4-wave interactions.

2.5.1.1 Conservation Laws

First, we want to analyze **conservation laws**. For the 4-wave interactions, the conserved quantities may be interpreted as invariants under collisions. We will see that these are 1, k, and ω_k. If we define $Q(f,f)$ to be the right hand side of the 4-wave interaction kinetic equation with no microscopic interactions ($V = 1$), then testing against some ϕ, we can use the symmetry between k and k_1 and then use the symmetry between (k, k_1) and (k_2, k_3) to find:

$$\begin{aligned}
\int Q(f,f)\varphi dk &= \int f f_1 f_2 f_3 \left(\frac{1}{f} + \frac{1}{f_1} - \frac{1}{f_2} - \frac{1}{f_3}\right) \varphi \delta_{\Delta k} \delta_{\Delta\omega} dk dk_1 dk_2 dk_3 \\
&= \int f f_1 f_2 f_3 \left(\frac{1}{f} + \frac{1}{f_1} - \frac{1}{f_2} - \frac{1}{f_3}\right) \left(\frac{\varphi + \varphi_1}{2}\right) \delta_{\Delta k} \delta_{\Delta\omega} dk \cdots dk_3 \\
&= \int f f_1 f_2 f_3 \left(\frac{1}{f} + \frac{1}{f_1} - \frac{1}{f_2} - \frac{1}{f_3}\right) \left(\frac{\varphi + \varphi_1 - \varphi_2 - \varphi_3}{4}\right) \delta_{\Delta k} \delta_{\Delta\omega} dk \cdots dk_3
\end{aligned}$$

Now when $\varphi = 1$, $\int Q(f,f)1dk = 0$, when $\varphi = k$, the first delta kicks in and $\int Q(f,f)kdk = 0$, and when $\varphi = \omega_k$, the second delta kicks in and $\int Q(f,f)\omega_k dk = 0$. Since testing the kinetic equation against any of these quantities makes the right hand side vanish, they provide $d+2$ collision invariants (d comes from testing with k).

Remarks:

- For the 3 wave interactions, there will be no conservation of mass (we don't get a conserved quantity by testing against 1).
- These conservation laws are a key ingredient in taking the diffusive limit.

2.5.1.2 Entropy

Next, we want to see where entropy shows up in the 4-wave interaction kinetic equation. Now, test $Q(f,f)$ against the function $\varphi = 1/f$. We apply the previous identity to find

$$\int Q(f,f)\frac{1}{f}dk = \frac{1}{4}\int ff_1f_2f_3\left(\frac{1}{f}+\frac{1}{f_1}-\frac{1}{f_2}-\frac{1}{f_3}\right)^2\delta_{\Delta k}\delta_{\Delta\omega}dkdk_1dk_2dk_3 \geq 0$$

Since $\partial_t(-\log f) = -Q(f,f)\frac{1}{f}$, we find that

$$\partial_t\left(-\int \log f dk\right) = -\int Q(f,f)\frac{1}{f}dk \leq 0$$

We have found that $-\int \log f dk$ provides a Lyapunov functional for the equation, and thus that the dynamics are irreversible. The entropy is given by $-\log f$. This suggests relaxation to some equilibrium state, which will be characterized by the conserved quantities: the mass, the momentum, and the energy.

2.5.1.3 Mathematical results concerning the Cauchy problem

We enumerate some of the results concerning the Cauchy problems for both the Boltzmann equation and the 4-wave interaction kinetic equation for the purposes of comparison in Figure ??.

Further references:
we may expand a bit more the discussion of these references

- 4-wave interactions, isotropic solutions $f(k) = f(|k|)$:
  - Escobedo-Velazquez
    - Global existence of measure-valued solutions
    - Condensation can occur for infinite time. Most of the energy is transported to high frequencies as $t \to \infty$.
  - Kierkels-Velazquez: Model taking into account the condensate.
- 3-wave interactions, isotropic solutions:
  - Nguyen-Tran: Global existence with dissipation.
  - Soffer-Tran: Special class of solutions with energy flowing at infinity.

kineticEqn

Boltzmann equation	**4 wave interaction kinetic equation**
Conserved quantities: mass $\int f dv$, momentum $\int f v dv$, energy $\int f\|v\|^2 dv$	Same conserved quantities.
Entropy: $\int f \log f dv$. This prevents concentrations.	Entropy: $\int \log f dv$. No information on the large scale. Could possibly allow concentrations?
Global solutions: solutions close to equilibria (Ukai) (Maxwellian distributions) • Spectral information on the linearized collision operator • $\partial_t y = -\lambda y + y^2$ (Fujita-Kato solutions for Navier Stokes)	Equilibria are not nice functions • Conserved quantities (Rayleigh-Jeans) • Even more complicated solutions (Zakharov)
Solutions with finite entropy and energy • Control on entropy and entropy dissipation • Renormalization (Di Perna-Lions)	Entropy bound is bad
Local solutions: $\partial_t f + v \cdot \nabla_x f = Q(f, f)$ $\partial_t y = y^2$. f in some weighted L^∞ space permits local solutions, with blowup after a finite time.	Local solutions: Theorem (Germain-Ionescu-Tran) says that there are local solutions in L^∞_s, $s > 2$, with time $T \gtrsim \|f_0\|^{-2}_{L^\infty_s}$. The proof uses Strichartz estimates with a TT^* argument. What is this last thing?
The derivation is done in the same setting as the derivation of the Boltzmann equation from a system of particles (Lanford) with a perturbation expansion $y = y_0 + \frac{t}{2} y_0^2 + \frac{t^2}{2} y_0^3 + \cdots$	Derivation done with a perturbative expansion (Deng-Hani). Requires a lot of regularity on initial data. Convergence on short kinetic times.

Figure 2.12: Comparison of the Boltzmann and the 4-wave interaction kinetic equation.

2.6 Appendix on Spectral theory

Spectral theory is the generalisation of matrix diagonalisation with general linear operators on infinite dimension space. The infinite dimensional space that we will consider is the space of finite energy

$$L^2 := \left\{ u : \Omega \to \mathbb{C} \,|\, ||u||_{L^2}^2 := \int_\Omega |u|^2 < \infty \right\}$$

where the domain $\Omega \subset \mathbb{R}^d$ could be bounded (including torii) or unbounded. The notation $(\cdot,\cdot)_{L^2}$ stands for the usual inner-product of L^2. In the finite dimension case i-e matrix case (L^2 must be change for $\mathbb{R}^n$), the spectrum is constituted of eigenvalues but in the general it is not necessary the case. Indeed, it is possible to have a continuum of "generalised" eigenvalues or more complicated stuff. Let H a linear operator on L^2 :

$$H : D(H) \to L^2$$

where $D(H)$ is a sub-Hilbert space of L^2 which is dense[2], i-e $\overline{D(H)} = L^2$. We say that H is a **bounded operator** iff there exits a constant $C > 0$ such that $||Hu||_{L^2} \leq C||u||_{L^2}$ for all $u \in L^2$ and we will denote by $\mathcal{L}(L^2, L^2)$ the space of linear bounded operator. Otherwise, we say that the operator H is unbounded. Be careful, unbounded operator has nothing to do with the fact that the domain Ω is bounded or not. For example the Laplacian $H = -\Delta$ with

$$D(-\Delta) = H^2 := \left\{ u \in L^2 \,|\, ||u||_{H^2} := \sqrt{||u||_{L^2}^2 + ||\nabla u||_{L^2}^2 + \sum_{i,j} ||\partial_{x_i}\partial_{x_j} u||_{L^2}^2} \right\}$$

is an unbounded operator.

The **spectrum** of H is defined by the closed set

$$\sigma(H) := \{\lambda \in \mathbb{C} \,|\, \text{the linear operator } H - \lambda Id \text{ is not invertible}\},$$

whereas the set of **"discrete" eigenvalues** is defined by

$$\sigma_d(H) := \{\lambda \in \mathbb{C} \,|\, \dim[\mathrm{Ker}(H - \lambda Id)] \in (0, +\infty)\} \subset \sigma(H),$$

but be not injective is note the sole way to not be invertible. Thus, the spectra is also constituted by

$$\begin{aligned}\sigma_{\text{ess}}(H) &:= \sigma(H)/\sigma_d(H) \\ &= \{\lambda \in \mathbb{C} \,|\, \mathrm{Ker}(H - \lambda Id) = 0 \text{ and } \mathrm{Ran}(H - \lambda Id) \neq X \text{ or } \dim[\mathrm{Ker}(H - \lambda Id)] = +\infty)\},\end{aligned}$$

which is called **essential spectrum**. Noticing that 0 can either be an "eigenvalue" with infinite multiplicity or an accumulation point of the spectrum without being itself an eigenvalue so that it is either in the essential spectrum either not in the spectrum. Showing that there exists essential spectrum could be a difficult task. For the moment, we should focus on operator which only admit discrete spectrum. Infinite linear operator

[2]The set $\overline{A}$ will alway refers to the topological closure of the set A.

behaves like matrix if it has a compact resolvent. The **resolvent** of H in $\omega \notin \sigma(H)$ is defined by

$$R(\omega) := (H - \omega Id)^{-1}.$$

The spectrum can also be seen as the value where the resolvent cannot be a bounded operator of L^2 since

$$||R(\omega)u||_{L^2} = \text{dist}(\omega, \sigma(H))^{-1}||u||_{L^2}.$$

Don't worry about the definition of "**compact**". Intuitively, compact means that it behaves like finite dimension. Rigorously, a compact operator is the strong limit of a sequence of finite rank operators. An infinite linear operator of degree at least one, i-e there at least one derivative, which act on a bounded domain Ω has automatically a compact resolvent[3]. But it is not necessary the case when the domain Ω is unbounded or when it has degree 0. For example, in infinite dimension the identity operator cannot be compact[4].

Proposition 2.6.1. *If H has* **compact resolvent**, *then it spectrum contains only an infinite* **countable sequence of non-null eigenvalues** $(\lambda_j)_j$. *Moreover, the space L^2 admits an orthonormal basis consisting of normalized eigenvectors $(\psi_j)_j$ of H associated to each eigenvalue , i-e solution of*

$$H\psi_j = \lambda_j \psi_j. \tag{2.5}$$ compact-eigen

If H is a compact operator, then it spectrum contains a countable sequence of non-null eigenvalues and possibly 0 which is in the essential spectrum.

For example, if we take $H = -\Delta$ on the torus $\mathbb{T}^d_{L/2\pi} = [0, L/2\pi]^d$, the eigenvalues/eigenfunctions are given by $(\left|\frac{k}{L}\right|^2, e^{i\frac{k\cdot x}{L}}) \in \mathbb{Z}^d_L \times L^2([0, L/2\pi]^d)$ since we have the following diagonalization of the laplacian

$$-\Delta(e^{i\frac{k\cdot x}{L}}) = \left|\frac{k}{L}\right|^2 e^{i\frac{k\cdot x}{L}} \quad \text{for all } k \in \mathbb{Z}.$$

2.6.1 A first excursion in the continuous spectrum world

In the previous example, i-e the laplacian on the torus, the eigenvalues are given by $\left|\frac{k}{L}\right|^2$. When L growth, the distance between the eigenvalues becomes smaller and smaller. At the end, when $L \to \infty$, we expect to see a continuum of spectral values. Indeed, as we already says, on $\mathbb{R}^d$, the Fourier transform of the Laplacian gives

$$-\Delta(e^{i\xi\cdot x}) = |\xi|^2 e^{i\xi\cdot x} \quad \text{for all } \xi \in \mathbb{R}. \tag{2.6}$$ Laplacien-diag

where $|\xi|^2$ are seen as spectral values for all $\xi \in \mathbb{R}$ (i-e $\sigma(-\Delta) = \mathbb{R}^+$) and $e^{i\xi\cdot x}$ the **"generalized" eigenfunctions** associated to $|\xi|^2$. The modes $e^{i\xi\cdot x}$ are not finite energy L^2 but live in a **weighted space**

$$L^2_{-s} = \{\psi \in L^2 \,|\, (1+x^2)^{-\frac{s}{2}}\psi \in L^2\} \text{ for any } s > \frac{1}{2}.$$

[3]More precisely, the resolvent $R(\omega) : L^2 \to D(H)$ could be seen as a bounded isomorphism of L^2. If the embedding $D(H) \to L^2$ is compact, then the resolvent is automatically compact. It is the case, thank to Rellich embeddings, when H has at least one derivative act on a bounded domain Ω.

[4]This one of Riesz theorem.

The usual inner-product of L^2 can extend to the "distribution" product

$$< u, v >_{-s,s} := \int u(x)\overline{v(x)}\,dx = \int \frac{u(x)}{(1+x^2)^{\frac{s}{2}}}\overline{(1+x^2)^{\frac{s}{2}}v(x)}\,dx \quad \forall u \in L^2_{-s}, v \in L^2_s,$$

where

$$L^2_s = \{\psi \in L^2 \,|\, (1+x^2)^{\frac{s}{2}}\psi \in L^2\} \text{ for any } s > \frac{1}{2}$$

is seen as the "dual" space of L^2_{-s}. The diagonalization of the laplacian (2.6) can be read in the weighted functional framework we have just given as

$$< e^{i\xi\cdot x}, -\Delta v >_{-s,s} = |\xi|^2 < e^{i\xi\cdot x}, v >_{-s,s}, \quad \forall v \in L^2_s.$$

Thus, more generally, the definition (2.5) of eigenvectors for compact operator can be generalized our case by

$$< \psi_\xi, Hv >_{-s,s} = \lambda_\xi < \psi_\xi, v >_{-s,s}, \quad \forall v \in L^2_s.$$

This is why we call $\psi_\xi \in L_{-s}$ a "generalized" eigenvector.

A second example is given by operator $H = -\Delta + V(x)$ on $\mathbb{R}^d$ with a V a periodic function on the cell $X = [0, 2\pi)^d$. Instead of looking for Fourier modes superposition, we can look for Bloch modes superposition. A **Bloch mode**, or Bloch wave, for any $k \in X' := [0, 1)^d$ and $m \in \mathbb{N}^*$ the a function

$$e^{ik\cdot x}\phi_{k,m}$$

where $(\phi_{k,m})_m$ is a basis of periodic function of $L^2(X)$ given by the eigenvalues problem

$$\begin{cases} [-(\Delta + 2ik\cdot\nabla - |k|^2) + V]\phi_{k,m} = \lambda_{k,m}\phi_{k,m} \\ \phi_{k,m} \text{ is a periodic function on the cell } X = [0, 2\pi)^d \end{cases} \tag{2.7}$$

It is indeed an eigenvalues problem since the shifted operator $[-(\Delta+2ik\cdot\nabla-|k|^2)+V]$ on the periodic domain X has a compact resolvent. Moreover, since the shifted operator is self-adjoint, the eigenvalues are real. Thus, any function $u \in L^2(\mathbb{R}^d)$ can be be decomposed as a **superposition of Bloch modes**

$$u(x) = \int_{X'} \sum_{m=1}^{\infty} u_{k,m} e^{ik\cdot x}\phi_{k,m}(x)dk \quad \text{with} \quad u_{k,m} = \int_{\mathbb{R}} u(x)e^{-ik\cdot x}\overline{\phi_{k,m}(x)}dx,$$

and the operator H acts on any function $u \in D(H)$ as

$$Hu(x) = \int_{X'} \sum_{m=1}^{\infty} \lambda_{k,m}\, u_{k,m} e^{ik\cdot x}\phi_{k,m}(x)dk \quad \text{since} \quad H(e^{ik\cdot x}\phi_{k,m}(x)) = \lambda_{k,m}\, e^{ik\cdot x}\phi_{k,m}(x).$$

The function $\mathcal{F}_b[u](x,k) = \sum_{m=1}^{\infty} u_{k,m}\phi_{k,m}(x) \in L^2(X \times X')$ is called the Floquet-Bloch transform[5] of u and plays similar role as Fourier transform in case of periodic coefficients.

[5]The Floquet-Bloch can be extend by periodicity on an isometry $L^2(\mathbb{R}^d) \to L^2(\mathbb{R}^d \times \mathbb{R}^d)$.

We can show that the maps $k \mapsto \lambda_{k,m}$, called band functions, are lipshitz such that the spectrum

$$\sigma(H) = \bigcup_{m=1}^{\infty} \left[\min_{k \in X'} \lambda_{k,m}, \max_{k \in X'} \lambda_{k,m} \right]$$

have a band structure. The pairs $(\lambda_{k,m}, e^{ik\cdot x}\phi_{k,m})$ are "generalized" eigenvalues / eigenfunctions associated to $H = -\Delta + V(x)$.

The study of continuous spectrum and its "generalized" eigenvectors is easier for self-adjoint operator. We defined the **adjoint operator** H^* of H by

$$(Hu, v)_{L^2} = (u, H^*v)_{L^2} \quad \forall u \in D(H), v \in D(H^*)$$

with domain

$$D(H^*) :=: \{v \in L^2 \,|\, \exists w \in L^2,\, (Hu, v)_{L^2} = (u, w),\, \forall u \in D(H)\}$$

An operator H is called

- **self-adjoint** iff $Hu = H^*u$ for all $u \in D(H)$,
- **skew-adjoint** iff $Hu = -H^*u$ for all $u \in D(H)$.

Be careful, to show that H is self-adjoint (or skew-adjoint), it is not enough to remark that H is hermitian, i-e $(Hu, v)_{L^2} = (u, Hv)_{L^2}$, (or skew-hermitian, i-e $(Hu, v)_{L^2} = -(u, Hv)_{L^2}$), but it also necessary to ensure that $D(H) = D(H^*)$. If H is hermitian (or skew-hermitian) and if there exists $\omega \in \mathbb{C}$ such that $H - \omega Id$ and $H - \overline{\omega} Id$ are onto, then H is self-adjoint (or skew-adjoint) and $\omega, \overline{\omega} \notin \sigma(H)$. If H is self-adjoint, then the spectrum is real and is included in the closure of numerical range:

$$\sigma(H) \subset \overline{\{(Au, u)_{L^2} \,|\, u \in L^2,\, ||u||_{L^2} = 1\}}.$$

Note that H is self-adjoint iff iH is skew-adjoint. In particular, if H is skew-adjoint, then it spectrum is purely imaginary. When the linear operator is self-adjoint, some tools are devoted to the description of essential spectrum like Weyl's sequences[6], spectral measures or Mourre theory when there exists a commutator estimates. We deal about spectral measure and Mourre theory later on. When the operator is not self-adjoint, the spectrum could becomes unstable by perturbation. It is why, in that context, the notion of pseudo-spectrum[7] could be better.

[6]When the operator is H self-adjoint, Weyl gives a criterium to know if a spectral value is in the discrete spectrum or in the essential spectrum :

- spectrum

$$\sigma(H) = \{\lambda \in \mathbb{R} \,|\, \exists (u_n)_n \subset D(H), ||u_n||_{L^2} = 1 \text{ and } ||(H-\lambda)u_n||_{L^2} \underset{n\to\infty}{\to} 0\},$$

- essential spectrum

$$\sigma_{\text{ess}}(H) = \{\lambda \in \mathbb{R} \,|\, \exists (u_n^\lambda)_n \subset D(H), ||u_n^\lambda||_{L^2} = 1,\, u_n^\lambda \underset{n\to\infty}{\rightharpoonup} 0 \text{ and } ||(H-\lambda)u_n^\lambda||_{L^2} \underset{n\to\infty}{\to} 0\},$$

where $\rightharpoonup$ stands for the L^2-weak limit, i-e $u_n \underset{n\to\infty}{\rightharpoonup} u$ iff $\forall \phi \in L^2, (u_n, \phi) \underset{n\to\infty}{\to} (u, \phi)$. Such a sequence $(u_n^\lambda)_n$ is called a Weyl sequence.

[7]The δ-pseudo-spectrum is

$$\sigma_\delta(H) := \{\lambda \in \mathbb{C} \,|\, \forall u \in L^2, ||R(\lambda)u||_{L^2} > \delta^{-1}||u||_{L^2}\} = \{\lambda \in \mathbb{C} \,|\, \exists P \in \mathcal{L}(L^2, L^2), \forall u \in L^2, ||Pu||_{L^2} < \delta||u||_{L^2},\ \lambda \in \sigma(H+P)\}$$

2.6.2 Spectral measure of self-adjoint operators

To describe more precisely the continuous spectrum of self-adjoint operators, it could be judicious to do some links with **measure theory**. A measure μ can be seen as an integral. We will assume that H is **self adjoint** such that, thank to **spectral theorem**, we can associate at each $u \in D(H)$ a **finite measure** μ_u supported [8] in $\sigma(H) \subset \mathbb{R}$ defined by

$$(Hu, u)_{L^2} = \int_{\sigma(H)} \lambda d\mu_u(\lambda).$$

We can define the polarisation form of the spectral measure

$$d(\mathbb{E}_\lambda u, v)_{L^2} := \frac{1}{2}\left(d\mu_u(\lambda) + d\mu_v(\lambda) - d\mu_{u-v}(\lambda)\right).$$

$\mathbb{E}_\lambda : L^2 \to L^2$ is an orthogonal projection of L^2 which support[9] is the spectrum $\text{supp}(\mathbb{E}_\lambda)_{\lambda\in\mathbb{R}} = \sigma(H)$. The family $(\mathbb{E}_\lambda)_\lambda$ is often called the spectral family associated to H and could be seen as a cumulative distribution function[10]. As we will see later, it can also be seen as the spectral projector on $(-\infty, \lambda]$. The operator can be formally written

$$H = \int_{\sigma(H)} \lambda d\mathbb{E}_\lambda,$$

which rigorously means

$$\begin{cases} D(H) = \{u \in L^2 \,|\, \int_{\sigma(H)} \lambda^2 d\mu_u(\lambda) < +\infty\}, \\ (Hu, v)_{L^2} = \int_{\sigma(H)} \lambda d(\mathbb{E}_\lambda u, v). \end{cases}$$

The easiest spectral measure to construct is the sum of Dirac functions associated to an self-adjoint operator with compact resolvent. Recall that, in that case, H have an infinite countable sequence of real eigenvalues $(\lambda_j)_j$. The spectral measure and the operator are given by

$$\mu_u = \sum_j u(\lambda_j)\delta_{\lambda_j} \quad \text{and} \quad (Hu, v)_{L^2} = \sum_j \lambda_j u(\lambda_j)\overline{v(\lambda_j)}.$$

---

and a δ-pseudo-eigenfunction associated to $\lambda \in \sigma_\delta(H)$ is a function $u \in L^2$ satisfying $||Hu - \lambda u||_{L^2} < \delta$.

[8] The support of a measure μ can be defined as

$$\text{supp}(\mu) := \{S \subset \mathbb{R} \,|\, \int_S d\mu = 0\}$$

[9] The support of a family of spectral projection can be defined as

$$\text{supp}(\mathbb{E}_\lambda)_{\lambda\in\mathbb{R}} = \{\mu \in \mathbb{R} \,|\, \forall \varepsilon > 0,\, \mathbb{E}_{\mu+\varepsilon} - \mathbb{E}_\varepsilon \neq 0\}$$

[10] A spectral family $(\mathbb{E}_\lambda)_\lambda$ is a family of orthogonal projection satisfying:

- the family is non-decreasing $\mathbb{E}_{\lambda_1}\mathbb{E}_{\lambda_1} = \mathbb{E}_{\min(\lambda_1,\lambda_2)}$
- the family is strongly right continuous $\mathbb{E}_{\lambda+0} := \lim_{\varepsilon\to 0^+} \mathbb{E}_{\lambda+\varepsilon} = \mathbb{E}_\lambda$
- $\lim_{\lambda\to-\infty} \mathbb{E}_\lambda = 0$ and $\lim_{\lambda\to+\infty} \mathbb{E}_\lambda = Id$

An other exemple is given by Fourier transform of $H = -\Delta$ on the full space $\mathbb{R}^d$ with continuous spectrum on the positive real $\sigma(H) = \{|\xi|^2 \,|\, \xi \in \mathbb{R}\} = \mathbb{R}^+$. In that case, using the definition of the spectral measure and the Parseval equality, one gets

$$(Hu,u)_{L^2} = \frac{1}{2\pi}(\widehat{Hu},\widehat{u})_{L^2} = \frac{1}{2\pi}\int_{\mathbb{R}^d} |\xi|^2 |\widehat{u}(\xi)|^2\, d\xi = \frac{1}{2\pi}\int_0^\infty |\xi|^2 \left(|\xi|^{d-1}\int_{\mathbb{S}^{d-1}} |\widehat{u}(|\xi|\theta)|^2 d\theta\right) d|\xi|$$

by the change of variable $\lambda = |\xi|^2$, we have

$$(Hu,u)_{L^2} = \frac{1}{2\pi}\int_0^\infty \lambda \left(\sqrt{\lambda}^{d-1}\int_{\mathbb{S}^{d-1}} |\widehat{u}(\sqrt{\lambda}\theta)|^2 d\theta\right) \frac{d\lambda}{2\sqrt{\lambda}}$$

thus we can state

$$d\mu_u(\lambda) = \frac{\sqrt{\lambda}^{d-2}}{4\pi}\int_{\mathbb{S}^{d-1}} |\widehat{u}(\sqrt{\lambda}\theta)|^2 d\theta \tag{2.8}$$ measure-laplacian

to obtained

$$(Hu,u)_{L^2} = \int_{\mathbb{R}^+} \lambda d\mu_u(\lambda).$$

The first example is an example of purely punctual measure whereas the second one is an example of absolutely continuous measure, In general, any measure can be decomposed as

$$\mu = \mu_{pp} + \mu_{ac} + \mu_{sc}$$

where

- μ_{pp} refers to **purely punctual measure**, i-e a sum of Dirac delta function
- μ_{ac} refers to **absolute continuous measure**, i-e there exits a locally integrable function ρ such that for any g

  $$\int_{\mathbb{R}} g d\mu = \int_{\mathbb{R}} g\rho dx$$

  where dx refers to the usual lebesgue measure.
- μ_{sc} refers to **singular continuous measure**, i-e forall $x \in \mathbb{R}$, one gets $\mu_{sc}(\{x\}) = 0$ and there exists a borelian set S such that

  $$\int_{\mathbb{R}/S} dx = 0 \quad \text{and} \quad \mu_{sc}(S) = 0,$$

In consequence we can decompose the spectral measure on this way. It imply a new decomposition of the space L^2

$$L^2 = \mathcal{H}_{pp} \oplus \mathcal{H}_{ac} \oplus \mathcal{H}_{sc}$$

where

- $\mathcal{H}_{pp} := \{u \in L^2 \,|\, \text{the spectral measure } \mu_u \text{ is purely punctual}\}$
- $\mathcal{H}_{ac} := \{u \in L^2 \,|\, \text{the spectral measure } \mu_u \text{ is absolute continuous}\}$
- $\mathcal{H}_{sc} := \{u \in L^2 \,|\, \text{the spectral measure } \mu_u \text{ is singular continuous}\}$

and the spectrum

$$\sigma(H) = \sigma_{pp}(H) \oplus \sigma_{ac}(H) \oplus \sigma_{sc}(H)$$

where

- **(purely ponctual spectrum)** $\sigma_{pp}(H) := \sigma(H_{|\mathcal{H}_{pp}})$
- **(absolute continuous spectrum)** $\sigma_{ac}(H) := \sigma(H_{|\mathcal{H}_{ac}})$
- **(singular continuous spectrum)** $\sigma_{sc}(H) := \sigma(H_{|\mathcal{H}_{sc}})$

Consider the free linear Schrödinger equation

$$\begin{cases} i\partial_t u + Hu = 0, \\ u(0) = u_0 \in L^2. \end{cases} \tag{2.9}$$

Since the operator $-iH$ is skew-adjoint, the Stone theorem sates that there exists a group [11] $(e^{-itH})_{t\in\mathbb{R}}$ of bounded operator of L^2 such that the solution is given by

$$u = e^{-itH} u_0.$$

The long time dynamic is driven by the spectral measure of the initial condition:

- initial condition with purely punctual mesaure $u_0 \in \mathcal{H}_{pp}$

$$\lim_{R\to+\infty} \sup_{t\geq 0} \int_{\mathbb{R}^d/[-R,R]} |e^{-itH} u_0(x)|^2 dx = 0$$

- *(Riemann-Lebesgue)* initial condition with absolutely continuous measure $u_0 \in \mathcal{H}_{ac}$

$$\lim_{t\to+\infty} \int_{[-R,R]} |e^{-itH} u_0(x)|^2 dx = 0$$

- *(RAGE)* initial condition with singular continuous measure $u_0 \in \mathcal{H}_{sc}$

$$\lim_{T\to+\infty} \frac{1}{T} \int_0^T \int_{[-R,R]} |e^{-itH} u_0(x)|^2 dx = 0.$$

As we see in RAGE theorem, the singular continuous spectrum is the bad guy. As we will see later on, the Mourre theory gives a nice tool to have only punctual spectrum or absolute continuous spectrum.

[11] More precisely, the family $(e^{-itH})_{t\in\mathbb{R}}$ is a strongly continuous group of L^2 in the sense that

- $\forall t \in \mathbb{R}$, $e^{-itH} \in \mathcal{L}(L^2, L^2)$,
- e^{-itH} is invertible with $(e^{-itH})^{-1} = e^{+itH}$,
- $e^{-itH} \circ e^{-isH} = e^{-i(t+s)H}$,
- $e^{-itH}_{|t=0} = \mathrm{Id}$ and $\forall u \in L^2, \lim_{t\to 0} ||e^{-itH} u - u|| = 0$.

More generally, the spectral measure of self-adjoint operators is suitable to define a "**functional calculus**" of the operator H: for any real continuous function ϕ, we have

$$\phi(H) = \int_{\mathbb{R}} \phi(\lambda) d\mathbb{E}_\lambda,$$

which is mean

$$\begin{cases} D(\phi(H)) = \{u \in L^2 \mid \int_{\mathbb{R}} \phi(\lambda)^2 d\mu_u(\lambda) < +\infty\}, \\ (\phi(H)u, v)_{L^2} = \int_{\mathbb{R}} \phi(\lambda) d(\mathbb{E}_\lambda u, v). \end{cases}$$

In particular, one gets

$$\sigma(\phi(H)) = \phi(\sigma(H)).$$

If the spectral measure associated to H is absolutely continuous $d\mu_u^H(\lambda) = \rho_u^H(\lambda)d\lambda$ and if ϕ is a non-singular diffeomorphism, then the spectral measure associated to $f(H)$ is also absolutely continuous

$$d\mu_u^{\phi(H)}(\tilde{\lambda}) = \rho_u^{\phi(H)}(\tilde{\lambda})d\tilde{\lambda} \quad \text{with} \quad \rho_u^{\phi(H)}(\tilde{\lambda}) := \left(\frac{\rho_u^H}{\phi'}\right) \circ \phi^{-1}(\tilde{\lambda}).$$

In particular, since we know the spectral measure of $-\Delta$ (see (2.8)), we know the spectral measure of $(-\Delta)^\alpha$ which is

$$d\mu_u^{(-\Delta)^\alpha}(\tilde{\lambda}) = \frac{\tilde{\lambda}^{\frac{d+1}{2\alpha}-1}}{4\pi} \int_{\mathbb{S}^{d-1}} |\widehat{u}(\tilde{\lambda}^{1/2\alpha}\theta)|^2 d\theta$$

Some functions ϕ can be very interesting, for example:

- *(Frequencies cut-off.)* If $\phi = \mathbf{1}_{(a,b]}$, we have the the **spectral projector**

$$\mathbb{E}((a,b]) := \mathbb{E}_b - \mathbb{E}_a = \mathbf{1}_{(a,b]}(H) = \int_a^b d\mathbb{E}_\lambda.$$

- *(Phase shift.)* If $\phi(\lambda) = e^{-it\lambda}$, we have the **propagator**

$$e^{-itH} = \int_{\mathbb{R}} e^{-it\lambda} d\mathbb{E}_\lambda,$$

  which is the flow of the Schrödinger equation $i\partial_t u + Hu = 0$.

- *(Oscillation / resonance.)* If

$$\phi_t(\lambda) = \begin{cases} \frac{1-e^{-i(\omega_0-\lambda)t}}{i(\omega_0-\lambda)} & \text{if } \omega_0 - \lambda \neq 0, \\ t & \text{if } \omega_0 - \lambda = 0. \end{cases}$$

  then we have the **Duhamel formula**, that is to say

$$u(t) = e^{i\omega_0 t}\, \phi_t(H) f = e^{i\omega_0 t} \int_0^t e^{i(s-t)(\omega_0 Id - H)} f ds,$$

  is the solution of the monochromatic forced Schrödinger equation $i\partial_t u + Hu = i f e^{i\omega_0 t}$ with null initial condition and with f a regular enough function.

- *(Resolvent.)* If $\phi(\lambda) = (\lambda - \omega)^{-1}$ for any $\omega \notin \sigma(H)$ we have the **resolvent**

$$R(\omega) := (H - \omega \mathrm{Id})^{-1} = \int_{\mathbb{R}} (\lambda - \omega)^{-1} d\mathbb{E}_\lambda. \tag{2.10}$$ resolvent-sp

The last equation can have a kind of inversion formula, called the **Stone formula**

$$\mathbb{E}((a,b]) = \mathbb{E}_b - \mathbb{E}_a = \frac{-1}{2i\pi} \lim_{\varepsilon \to 0^+} \lim_{\delta \to 0^+} \int_{a+\varepsilon}^{b+\varepsilon} \big[R(\omega - i\delta) - R(\omega + i\delta)\big] d\omega \tag{2.11}$$ Stone

which is particularly suitable to find the spectral projectors and thus the spectrale measure. Note that in the Stone formula, the order of two limits is important. For the discret spectrum, we can obtain the projector on one eigenvalue $\lambda \in \sigma_d(H)$ by

$$\mathbb{E}(\{\lambda\}) := \mathbb{E}_\lambda - \lim_{\varepsilon \to 0} \mathbb{E}_{\lambda - \varepsilon} = \frac{-1}{2i\pi} \int_{\mathcal{C}_\lambda} R(z) dz,$$

where $\mathcal{C}_\lambda$ is any loop which surrounded λ and do not surround or touch an other value of the spectrum. Note also that the rank of $\mathbb{E}(\{\lambda\})$ is the multiplicity $\dim[\mathrm{Ker}(H - \lambda Id)]$ of the eigenvalue λ.

2.6.3 Mourre theory

One goal of Mourre theory is to give a simple way to ensure that there exists essential spectrum which additionally must be absolute continuous. Moreover, it will give a nice way to compute the absolute spectral measure thanks to the resolvent and thus to describe "generalized" eigenfunctions and the long time behavior of forced Schrödinger equation. These is impossible to gives uniform estimates of the resolvent $R(\omega)$ when ω is very closed to the real axis since $||R(\omega)u||_{L^2} = \mathrm{dist}(\omega, \sigma(H))^{-1}||u||_{L^2}$ but it is possible for the weighted resolvent $(1 + D^2)^{-\frac{s}{2}} R(\omega)(1 + D^2)^{-\frac{s}{2}}$ where D is a self-adjoint operator which satisfy a commutator estimate with H. This commutator estimate could be technical to show. It is why we will give a translation in term of escape function associated to the "geometrical optic" approximation of the operator H. "Geometrical optic" can be seen as high frequency study of H and use microlocal analysis.

Mourre-thm **Theorem 2.6.1. (Mourre theorem)** *Let I a closed bounded subset of $\mathbb{R}$. If there exists a self-adjoint operator D, a H-compact operator K, a positive number $\alpha > 0$ and a real function $\chi \in \mathcal{C}^\infty(\mathbb{R})$ with supp$\chi = I$ such that*

$$\begin{cases} \textit{(} H \textit{ is } D\textit{-smooth)} & i[H,D] := i(HD - DH) \in \mathcal{L}(D(H) \cap D(D); L^2) \\ \textit{(commutator estimate)} & \chi(H) i[H,D] \chi(H) \geq \alpha \chi(H) + K \end{cases}$$

then

(i) the discrete spectrum is finite in I,

(ii) the essential spectrum in I only contains absolute continuous spectrum,

(ii) for all $\omega \in I / \sigma_d(H)$, the "boundary values" of the resolvent

$$R(\omega \pm i0) := (H - \omega Id \pm i0)^{-1} = \lim_{\delta \to 0} (H - \omega Id \pm i\delta)^{-1} \in \mathcal{L}(L^2_s, L^2_{-s})$$

are correctly defined in weighted spaces for $s > 1/2$

$$L_s := \{f \in L^2 \,|\, (1+D^2)^{\frac{s}{2}} f \in L^2\} \subset L^2 \subset L_{-s} := \{f \,|\, (1+D^2)^{-\frac{s}{2}} f \in L^2\}.$$

Moreover $\omega \mapsto R(\omega \pm i0)$ *is Hölder continuous*[12]

$$C^{0,\frac{2s-1}{2s}}\big(I/\sigma_p(H),\, \mathcal{L}(L^2_s, L^2_{-s})\,\big).$$

Before describing the hypothesis, let us comment the result. The weighted spaces L^2_{-s} and L^2_s are crucial. Indeed, when $\omega \in I_{\rm ac} := \sigma_{ac}(H) \cap I$, the resolvent $R(\omega \pm i\delta)$ doesn't have a limit in $\mathcal{L}(L^2, L^2)$ as $\delta \to 0$ since $||R(\omega \pm i\delta)u|| = \delta^{-1}||u||$. However,

$$\int R(\omega \pm i\delta) u\overline{u}$$

can have a limit as $\delta \to 0$ when $u \in L_s$. Indeed, for $u \in L_s \cap \mathcal{H}_{ac}$, one gets with (2.10)

$$< \mathbf{1}_{I_{\rm ac}} R(\omega \pm i\delta)u, u >_{-s,s} = \int_{I_{\rm ac}} \frac{\rho_u(\lambda)}{\lambda - \omega \mp i\delta} d\lambda$$

where $d\mu_u(\lambda) = \rho_u(\lambda)d\lambda$ is the (absolutely continuous) spectral measure associated to $u \in \mathcal{H}_{ac}$ and when δ vanish, the left hand side term must be seen as a singular integral

$$\int_{I_{\rm ac}} \frac{\rho_u(\lambda)}{\lambda - \omega \mp i\delta} d\lambda \underset{\delta \to 0}{\to} \pm i\pi\rho_u(\omega) + \mathcal{P}\int_{I_{\rm ac}} \frac{\rho_u(\lambda)}{\lambda - \omega} d\lambda.$$

where we can use the Sokhotski–Plemelj theorem since the function $\lambda \mapsto \rho_u(\lambda)$ is Hölder continuous and where $\mathcal{P}$ refers to Cauchy principal value[13]. Then, by Stone formula (2.11), if the projector $\mathbb{E}_\lambda$ is not seen as a L^2 map but as a map from L_s to L_{-s}, one gets for $(a, b] \in I_{\rm ac}$

$$\mathbb{E}((a,b]) = \frac{1}{2i\pi} \lim_{\delta \to 0} \int_a^b [R(\lambda - i\delta) - R(\lambda + i\delta)] d\lambda = \int_a^b \mathbb{E}'(\lambda) d\lambda$$

with **spectral density**

$$\mathbb{E}'(\lambda) := \frac{1}{2i\pi}[R(\lambda - i0) - R(\lambda + i0)] \in \mathcal{L}(L_s, L_{-s}) \quad \text{for } \lambda \in I_{ac}.$$

[12] A function f is α-Hölder continuous with $\alpha \in (0, 1]$ on I if

$$||f||_{C^{0,\alpha}(I)} := \sup_I |f| + \sup_{x \neq y \in I} \frac{|f(x) - f(y)|}{|x - y|^\alpha}$$

is finite.

[13] If ρ is a Hölder continuous function around ω and integrable on real interval I, the Cauchy principal value can be computed as

$$\mathcal{P}\int_I \frac{\rho(\lambda)}{\lambda - \omega} d\lambda = \int_{I/(\omega-\varepsilon,\omega+\varepsilon)} \frac{\rho(\lambda)}{\lambda - \omega} d\lambda + \int_{\omega-\varepsilon}^{\omega+\varepsilon} \frac{\rho(\lambda) - \rho(\omega)}{\lambda - \omega} d\lambda$$

We can of course extend $\mathbb{E}'(\lambda)$ on $I/\sigma_d(H)$ by taking $\mathbb{E}'(\lambda) = 0$ when $\lambda \notin \sigma(H)$. Consequently, we can define a **functional calculus on weighted space** L_s for ϕ a bounded continuous function supported in I

$$\begin{aligned} < \phi(H)u, v >_{-s,s} &= \int_{I_{\rm ac}} \phi(\lambda) < \mathbb{E}'(\lambda)u, v >_{-s,s} d\lambda \\ &+ \sum_{\lambda_p \in \sigma_d(H)\cap I} \phi(\lambda_p)\big(\mathbb{E}(\{\lambda_p\})u, v\big)_{L^2} \end{aligned} \qquad \forall u, v \in L_s \tag{2.12}$$

functional-c

In particular, we have the spectral measure for $u \in L_s \cap \mathcal{H}_{ac}$

$$d\mu_u(\lambda) = \rho_u(\lambda)d\lambda \quad \text{with} \quad \rho_u(\lambda) =< \mathbb{E}'(\lambda)u, u >_{-s,s} .$$

The following proposition summaries the interesting ideas on spectral measures and "generalized" eigenvectors in the context of Mourre theory.

Proposition 2.6.2. *Let the assumptions of Mourre theorem satisfied on $I = [a, b]$.*

- *If $\lambda \in I \cap \sigma_d(H)$, then*
$$\mu_u(\lambda) = u(\lambda)\delta_\lambda.$$
Moreover for all $u \in L^2$, the eigenvector $u_\lambda := \mathbb{E}(\{\lambda\})u \in \mathcal{H}_{pp}$ is solution of
$$Hu_\lambda = \lambda u_\lambda.$$

- *For all $\lambda \in I/\sigma_p(H)$ and $u \in L_s$, one gets*
$$d\mu_u(\lambda) = \rho_u(\lambda)\, d\lambda$$
with the Hölder continuous function
$$\rho_u(\lambda) := \frac{1}{2i\pi}\big\langle \big[R(\lambda - i0) - R(\lambda + i0)\big]u\,,\, u\big\rangle_{-s,s}.$$
Moreover for all $u \in L_s$ and for $\lambda \in \sigma_{ac}(H)$, the "generalized" eigenvector
$$u_\lambda := \mathbb{E}'(\lambda)u \in L_{-s} \cap \mathcal{H}_{ac}$$
with
$$\mathbb{E}'(\lambda) := \frac{1}{2i\pi}[R(\lambda - i0) - R(\lambda + i0)] \in \mathcal{L}(L_s, L_{-s})$$
is solution of
$$< u_\lambda, H\phi >_{-s,s} = \lambda < u_\lambda, \phi >_{-s,s} \quad \forall \phi \in L_s.$$

The difficult part to ensure the assumptions of Mourre theorem is to show the commutator estimates. This can be done easily with escape functions. For sake of simplicity, we will **assume until the end that the domain Ω is the full space** $\mathbb{R}^d$. To explain what is an escape function, one needs to recall some stuff on symbols of pseudo-differential operator. As we already says, the **symbol** $h \in \mathbb{R}^d \times \mathbb{R}^d$ of the operator H can be defined as it action on Fourier modes
$$He^{ix\cdot\xi} = h(x, \xi)e^{ix\cdot\xi}.$$

Moreover, the dynamic is mainly driven by the maximal derivative part of the operator H so that we can focus on the principal symbol. The **principal symbol** h_0 is defined as the symbol of the maximal derivative part of the operator. More precisely, we say that h_0 is the principal symbol H of degree n_H and h_{-1} it subprincipal symbol if the action of H on rapidly oscillating function is given by the asymptotic expansion

$$He^{i\frac{x\cdot\xi}{\varepsilon}} = \varepsilon^{-n_H}h_0(x,\xi)e^{i\frac{x\cdot\xi}{\varepsilon}} + \varepsilon^{-n_H+1}h_{-1}(x,\xi)e^{i\frac{x\cdot\xi}{\varepsilon}} + O(\varepsilon^{-n_H+2}).$$

We can associate at h_0 an operator $\mathrm{Op}(h_0) := \mathcal{F}^{-1}h_0\mathcal{F}$. One advantage to work with principal symbols is that the remainder $H - \mathrm{Op}(h_0)$ is a H-compact operator. Let us recall the definition of **H-compact operator**. An operator K is H-compact operator iff $D(H) \subset D(K)$ and if there exists $\omega \notin \sigma(H)$ such that the operator $KR(\omega) : L^2 \to L^2$ is a compact operator. In particular, if H and $\mathrm{Op}(h_0)$ are self-adjoint, then they share the same essential spectrum[14]. An other advantage to work with principal symbols rather than full symbols is that we can defined univocally the principal symbol of a composition of operators. If H and D are operators of degree n_H and n_D, then the principal and subprincipal symbols of HD is given by

$$\begin{aligned}HDe^{i\frac{x\cdot\xi}{\varepsilon}} &= \varepsilon^{-(n_H+n_D)}h_0(x,\xi)d_0(x,\xi)e^{i\frac{x\cdot\xi}{\varepsilon}}\\ &+ \varepsilon^{-(n_H+n_D)+1}\Big[h_{-1}(x,\xi)d_0(x,\xi) + h_0(x,\xi)d_{-1}(x,\xi) + \nabla_\xi h_0\cdot\nabla_x d_0(x,\xi)\Big]e^{i\frac{x\cdot\xi}{\varepsilon}} + O(\varepsilon^{-(n_H+n_D)+2}).\end{aligned}$$

where h_0 is the principal symbol of H and d_0 is the principal symbol of D. Similarly, we can define the **symbol of the commutator**

$$i[H,D]e^{i\frac{x\cdot\xi}{\varepsilon}} = \varepsilon^{-(n_H+n_D)+1}\{h_0,d_0\}(x,\xi)e^{i\frac{x\cdot\xi}{\varepsilon}} + O(\varepsilon^{-(n_H+n_D)+2}).$$

where $\{h_0,d_0\}$ is the **Poisson's bracket** defined by

$$\{h_0,d_0\} := (\nabla_\xi h_0\cdot\nabla_x d_0 - \nabla_\xi d_0\cdot\nabla_x h_0).$$

In particular, we see that the commutator $i[H,D]$ is an operator of degree $(n_H+n_D)-1$. The commutator estimate $i[H,D] - K \geq \alpha Id$ with K a H-compact operator can be reads as $\{h_0,d_0\} \geq \alpha$ since $i[H,D] - Op(\{h_0,d_0\})$ is $i[H,D]$-compact and consequently H-compact. Putmann show one part of the theorem (2.6.1) but he need a commutator estimate of kind $i[H,D] \geq \alpha Id$. Mourre add the compact operator K which allows to use analysis on $\mathbb{R}^d\times\mathbb{R}^d$ with principal symbols rather than analysis with abstract operators. For example, if $H = -\Delta$ on the full space $\mathbb{R}^d$, then the generator of dilatations $D = -i(x\cdot\nabla) - Id/2$ is a conjugated operator H which satisfy the assumption of the Mourre theorem 2.6.1 since $\{h_0,d_0\} = -2|\xi|^2$. Constructing by hand such symbol d could be difficult. It is why the following theorem gives an interpretation of d as an escape function of the hamiltonian dynamic associated to H.

pe-theorem **Theorem 2.6.2.** *(Escape function theorem) Let H an operator of principal symbol h_0 and I a bounded closed interval of $\mathbb{R}$. We associate to h_0 it* **hamiltonian dynamic**, *i-e the solution $(x(t),\xi(t)) \in \mathbb{R}^d\times\mathbb{R}^d$ of*

$$\begin{cases}\dot{x} = \nabla_\xi h_0\\ \dot{\xi} = -\nabla_x h_0.\end{cases} \tag{2.13}$$ hamiltoneq

[14] One of Weyl's theorem states that if H and K are closed self-bounded operators and K is H-compact, then $\sigma_{\mathrm{ess}}(H+K) = \sigma_{\mathrm{ess}}(H)$. Sometimes the set $\sigma_{\mathrm{kato}}(H) := \cap_{K\ \mathrm{compact}}\sigma_{\mathrm{ess}}(H+K)$ is called the Kato spectra. When H is self-adjoint, one gets $\sigma_{\mathrm{ess}}(H) = \sigma_{\mathrm{kato}}(H)$, but it is not necessary true when H is not self-adjoint.

with initial condition (x_0, ξ_0) *such that* $h_0(x_0, \xi_0) \in I$. *Assuming first that there exists a global solution* $(x(t), \xi(t))$ *at the previous equation. Assuming then that there exists a function* d_0 *of* $\mathbb{R}^d \times \mathbb{R}^d$ *such that the Poisson's bracket with the principal symbol* h_0 *of* H *is coercive along the trajectories*

$$\{h_0, d_0\}(x(t), \xi(t)) = (\nabla_\xi h_0 \cdot \nabla_x d_0 - \nabla_\xi d_0 \cdot \nabla_x h_0)(x(t), \xi(t)) \geq \alpha > 0 \quad \forall t \gg 1.$$

Such a function is called **an escape function**. *Then,* d_0 *is the symbol of an operator* $D : D(D) \to L^2$ *such that the commutator estimate of Mourre theorem 2.6.1 is satisfied on the interval* I.

We say that d_0 is an escape function since it opposite $-d_0$ is a Lyapunov function in the sense that

$$-\frac{d}{dt} d_0(x(t), \xi(t)) = -\{h_0, d_0\}(x(t), \xi(t)) \leq -\alpha.$$

The flow $(x_0, \xi_0) \mapsto (x(t), \xi(t))$ of the Hamilton equations (2.13) is often called the bicharactersitc. Given one initial condition (x_0, ξ_0), the curve $t \mapsto (x(t), \xi(t))$ is called the **"ray"** from (x_0, ξ_0). It is easy to follow the ray when the domain Ω is unbounded but it could be difficult when the domain is bounded. The rays are solutions to (2.13) until touching the boundary. By matching together rays that meet themselves at the same point of the boundary, one can define a generalized ray as a broken curves which stay in Ω. There are three different ways that he ray $t \mapsto (x(t), \xi(t))$ can touch the boundary and thus three way to extend the ray after the collision.

- *(Reflexion point)* The ray meet non tangentially the boundary on one point. In that case the ray bounce off the boundary in accord with reflection law. For example, if it is ray light, then this law is the Snell-Descartes one.

- *(Diffractive point)* The ray meet tangentially the boundary on one point. In that case the ray don't deviate. In that case the ray don't interact with the boundary.

- *(Slip point)* The ray stay tangent to the boundary in the neighbourhood of this point.

Let H an operator of principal symbol h_0 and I a bounded closed interval of $\mathbb{R}$. If for all $E_0 \in I$, there exits global solution$(x(t), \xi(t))$ the hamiltonian dynamic, i-e the solution of (2.13), with initial condition (x_0, ξ_0) such that $h_0(x_0, \xi_0) \in I$ and there exists $\alpha > 0$, $t_\alpha \geq 0$ and j such that

$$|x_j(t)| \geq \alpha t, \quad \text{or} \quad |\xi_j(t)| \geq \alpha t, \quad \forall t \geq t_\alpha,$$

then the hypothesis of Mourre theorem are satisfied with

$$\begin{cases} D = \operatorname{sign}(x_j(t_\alpha)) x_i & \text{if } |x_j(t)| \geq \alpha t, \\ D = \operatorname{sign}(\xi_j(t_\alpha)) i\partial_{x_j} & \text{if } |\xi_j(t)| \geq \alpha t, \end{cases}$$

and thus H admits essential spectrum (which must be absolutely continus spectrum) in I (and perhaps a finite number of eigenvalue of finite multiplicity).

Proof. The symbol associated to D is

$$\begin{cases} d_0 = \operatorname{sign}(x_j(t_\alpha))x_j & \text{if } |x_j(t)| \geq \alpha t, \\ d_0 = \operatorname{sign}(\xi_j(t_\alpha))\xi_j & \text{if } |\xi_j(t)| \geq \alpha t. \end{cases}$$

Thus, the Poisson's bracket gives

$$\{h_0, d\} = \dot{x}(t) \cdot \nabla_x d_0 + \dot{\xi}(t) \cdot \nabla_\xi d_0 \geq \alpha \quad \forall t \geq t_\alpha.$$

We conclude with escape function theorem 2.6.2. □

2.7 Appendix on Perturbative Estimates

reEstimates

2.7.1 Anne-Laure Dalibard's lecture: Oscillatory integrals

yEstimates

In these notes, we prove the leading order bounds on the perturbative expansion on kinetic time scales presented in Section 2.3.2. First the naive bound will be derived, then oscillatory techniques will be used to derive bounds which permit convergence of the expansion on kinetic time scales $t \sim \varepsilon^{-2}$.

2.7.1.1 Review

Suppose we are in the linear setting, with the Schrödinger equation with random parametric forcing. Let $\varepsilon \ll 1$, ψ_0 an initial state, and $H = -\nabla + \varepsilon V$ where V is a random forcing. The equation of interest is

$$i\partial_t \psi = H\psi \qquad \psi|_{t=0} = \psi_0$$

We assume that $V = \sum_{\alpha \in \mathbb{Z}^d} V_\alpha$ where V_α are random, independent potentials. For all α, $\mathbb{E}(V_\alpha) = 0$. Finally, we need a summability condition: for all p and q,

$$\sum_{\alpha \in \mathbb{Z}^d} \mathbb{E}\left(\widehat{V}_\alpha(p)\overline{\widehat{V}_\alpha(q)}\right) = |\widehat{G}(p)|^2 \delta(p-q)$$

where $G \in \mathcal{S}(\mathbb{R}^d)$, the Schwartz class, and $\operatorname{supp}(\widehat{G}) \subset B(0,R)$ for some $R < 2\pi$.

For an example of a potential satisfying these assumptions, let $G \in \mathcal{S}(\mathbb{R}^d)$, v_α random and independent coefficients with $\mathbb{E}(v_\alpha) = 0$, $\mathbb{E}(|v_\alpha|^2) = 1$, and let $V_\alpha = v_\alpha G(x-\alpha)$. Then $\widehat{V}_\alpha(p) = v_\alpha \widehat{G}(p) e^{ip\alpha}$, and

$$\mathbb{E}\left(\widehat{V}_\alpha(p)\overline{\widehat{V}_\alpha(q)}\right) = \mathbb{E}(|v_\alpha|^2)\widehat{G}_\alpha(p)\overline{\widehat{G}_\alpha(q)}e^{i(p-q)\alpha}$$

Now, using the fact that $\sum_{\alpha \in \mathbb{Z}^d} e^{i(p-q)\alpha} = \delta(p-q)$, we conclude that V satisfies the required summability condition. The other conditions are easily checked.

Recall that in Section 2.3.1 we derived an iterated Duhamel expansion for ψ:

$$\psi(t) = \sum_{n=0}^{N-1} \psi^{(n)}(t) + \delta\psi^{(N)}(t)$$

where the term of order ε^n was given by

$$\psi^{(n)}(t) = (-i\varepsilon)^n \int e^{is_0\Delta} V e^{is_1\Delta} V \cdots e^{is_n\Delta}\psi_0 \, \delta(t - \sum s_j) ds_0 ds_1 \cdots ds_n$$

and the remainder term was

$$\delta\psi^{(N)}(t) = (-i\varepsilon) \int_0^t e^{-i(t-s)H} V \psi^{(N-1)}(s) \, ds$$

This led us to an expansion for observables: the quadratic quantities in ψ. The case that we studied was the L^2 norm:

$$\mathbb{E}(\|\psi(t)\|_2^2) = \sum_n \sum_{\pi \in S_n} \mathrm{Val}(\pi) + \text{ remainders}$$

where Val collects the paired terms with permutation π:

$$\mathrm{Val}(\pi) = \sum_{|A|=n} \mathbb{E}(\psi_A \overline{\psi}_{\pi(A)})$$

To get this, we applied Wick's rule to throw out non-permutation pairs. The goal of this section is to justify this step and to investigate the size of $\mathrm{Val}(\mathrm{Id}_n)$. At first, we will prove the following naive estimate:

$$\mathrm{Val}(\mathrm{Id}_n) \lesssim \varepsilon^{2n} \frac{t^{2n}}{(n!)^2}.$$

This does not stay bounded on the kinetic time scale $t \sim \varepsilon^{-2}$. But exploiting the oscillatory nature of the integrals defining $\psi^{(n)}$, we can sharpen the estimate. For any $a \in (0,1)$, there is a $C_a > 0$ so that

$$\mathrm{Val}(\mathrm{Id}_n) \lesssim \varepsilon^{2n} \frac{(C_a t)^n}{(n!)^a}.$$

When $N \sim \dfrac{|\log \varepsilon|}{|\log|\log \varepsilon||}$, we have $N! \sim \varepsilon^{-1}$. Then for $n \leq N$, the new bound is better than the naive bound.

2.7.1.2 Expansion and Naive Estimate

Recall that we split $\psi^{(n)}$ into a sum of terms representing collisions with a given sequence $A = (\alpha_1, \ldots, \alpha_n)$ of the potentials. This decomposition took the form

$$\psi^{(n)} = \sum_{(\alpha_1,\ldots,\alpha_n)} \psi_A, \quad \psi_A(t) := (-i\varepsilon)^n \int e^{is_0\Delta} V_{\alpha_1} \cdots V_{\alpha_n} e^{is_n\Delta}\psi_0 \, \delta(t - \sum s_j) ds_0 \cdots ds_n$$

With the dispersion relation for Δ, $\omega(p) = p^2$, denote $\omega_i = p_i^2$. We can take a Fourier transform in space of the integrand and get a large convolution:

$$\begin{aligned}
&\mathcal{F}\left(e^{is_0\Delta} V_{\alpha_1} \cdots V_{\alpha_n} e^{is_n\Delta}\psi_0\right) \\
&\quad = \int e^{-is_0\omega} \widehat{V}_{\alpha_1}(p - p_1) e^{-is_1\omega_1} \widehat{V}_{\alpha_2}(p_1 - p_2) \cdots e^{-is_n\omega_n} \widehat{\psi}_0(p_n) dp_1 \cdots dp_n
\end{aligned}$$

which we can use for a formula for the Fourier transform of ψ_A:

$$\widehat{\psi}_A(t,p_0) = (-i\varepsilon)^n \int e^{-i(s_0\omega_0+\cdots+s_n\omega_n)} \prod_{j=1}^{n} \widehat{V}_{\alpha_j}(p_{j-1}-p_j)\widehat{\psi}_0(p_n)\delta(t-\sum s_j)ds_0\cdots ds_n dp_1\cdots dp_n$$

When we take absolute values, the exponential disappears (hence we do not use the oscillations) and the integrals over p and s become decoupled:

$$\begin{aligned}|\widehat{\psi}_A(t)| &\leq \varepsilon^n \int \prod_{j=1}^{n} |\widehat{V}_{\alpha_j}(p_{j-1}-p_j)||\widehat{\psi}_0(p_n)|\delta(t-\sum s_j)ds_0\cdots ds_n dp_1\cdots dp_n \\ &= \varepsilon^n \left(\int \delta(t-\sum s_j)ds_0\cdots ds_n\right)\left(\int \prod_{j=1}^{n} |\widehat{V}_{\alpha_j}(p_{j-1}-p_j)||\widehat{\psi}_0(p_n)|dp_1\cdots dp_n\right)\end{aligned}$$

Now the second integral does not depend on t at all, while the first does not depend on A. The first integral represents the area of an n-simplex:

Lemma 2.7.1. *For each $n \geq 1$, we have*

$$\int_0^\infty \cdots \int_0^\infty \delta(t-\sum s_j)ds_0\cdots ds_n = \frac{t^n}{n!}$$

Proof. The proof is by induction. When $n=1$, this is just $\int_0^t ds_0 = t$.

Suppose the formula holds for n. Then for $n+1$, we have

$$\begin{aligned}&\int_0^\infty \cdots \int_0^\infty \delta(t-\sum s_j)ds_0\cdots ds_{n+1} \\ &= \int_0^t \left(\int_0^\infty \cdots \int_0^\infty \delta((t-s_{n+1})-\textstyle\sum^n s_j)ds_0\cdots ds_n\right) ds_{n+1} \\ &= \int_0^t \frac{(t-s_{n+1})^n}{n!} ds_{n+1} = \frac{t^{n+1}}{(n+1)!}\end{aligned}$$

which proves the result. □

To bound $\mathrm{Val}(\mathrm{Id}_n)$, square this bound and sum over $|A| = n$. The simplex factor does not depend on A, and pulls to the front. By the summability condition on the V, the remaining sum is bounded by a constant independent of t, ε, and n. This leads to

$$\mathbb{E}(\|\psi^{(n)}\|_2^2) \lesssim \left(\frac{\varepsilon^n t^n}{n!}\right)^2.$$

This naive bound will not suffice to show convergence of the perturbative expansion on kinetic time scales. We did not take advantage of how the oscillatory exponential terms interact when paired, we just crudely bounded them by 1.

2.7.1.3 Estimating paired terms

First, we review Wick's rule, which allowed us to restrict to pairing A with permutations of A. Then, we rewrite $\mathrm{Val}(\mathrm{Id}_n)$ and use an oscillatory integral trick.

Using Plancherel, we can write observables in $\psi^{(n)}$ as follows:

$$\mathbb{E}(\|\psi^{(n)}(t)\|^2) = \sum_{|A|=|B|=n} \mathbb{E}(\widehat{\psi}_A(t)\overline{\widehat{\psi}_B(t)}) + \text{remainder}$$

where the sum is over A and B with no repetitions, and for each such A and B we find

$$\mathbb{E}\left(\widehat{\psi}_A(t)\overline{\widehat{\psi}_B(t)}\right) = \varepsilon^{2n}\int e^{i(s_0'\omega_0'+\cdots+s_n'\omega_n'-s_0\omega_0-\cdots-s_n\omega_n)}\mathbb{E}\left[\prod_{j=1}^{n}\widehat{V}_{\alpha_j}(p_{j-1}-p_j)\overline{\widehat{V}_{\beta_j}(p_{j-1}'-p_j')}\right]$$
$$\widehat{\psi}_0(p_n)\overline{\widehat{\psi}_0(p_n')}\delta(t-\textstyle\sum s_j)\delta(t-\sum s_j')d\vec{s}d\vec{p}d\vec{s}'d\vec{p}'$$

where $p_0 = p_0'$ and $\omega_i' = (p_i')^2$.

Because there are no repetitions, the $\widehat{V}_{\alpha_j}$'s are independent from one another, as are the $\widehat{V}_{\beta_j}$'s. If it were also true that $\{\alpha_1,\ldots,\alpha_n\}$ and $\{\beta_1,\ldots,\beta_n\}$ did not contain the same exact collections of indices, we would find an α_k which does not appear among any of the other indices, and so its potential would be independent from every other factor in the product. Then we can pull out an $\mathbb{E}(\widehat{V}_{\alpha_k})$, which is 0 by assumption. Then the entire quantity becomes 0. This shows Wick's rule: the only terms that contribute are terms with $B = \pi(A)$ for some permutation π. So now

$$\mathbb{E}(\|\psi^{(n)}(t)\|_2^2) = \sum_{\pi\in S_n}\Big(\sum_{|A|=n}\mathbb{E}\left(\widehat{\psi}_A(t)\overline{\widehat{\psi}_{\pi(A)}(t)}\right)\Big) = \sum_{\pi\in S_n}\mathrm{Val}(\pi)$$

In this section, we will focus on estimating the leading order term, $\mathrm{Val}(\mathrm{Id}_n)$, which corresponds to the ladder graph Feynmann diagram. In Section 2.7.2, we will estimate the rest of the terms, corresponding to Feynmann diagrams with crossings.

To estimate $\mathrm{Val}(\mathrm{Id}_n)$, begin using our expanded form for the pair of A and B above. Also, write $\delta = \delta(t-\sum s_j)$, $\delta' = \delta(t-\sum s_j')$ for short. We get the following expression for $\mathrm{Val}(\mathrm{Id}_n)$:

$$\varepsilon^{2n}\int e^{i(\vec{s}'\cdot\vec{\omega}'-\vec{s}\cdot\vec{\omega})}\sum_{\alpha_j\in\mathbb{Z}^d}\mathbb{E}\left[\prod_{j=1}^{n}\widehat{V}_{\alpha_j}(p_{j-1}-p_j)\overline{\widehat{V}_{\alpha_j}(p_{j-1}'-p_j')}\right]\widehat{\psi}_0(p_n)\overline{\widehat{\psi}_0(p_n')}\delta\delta' d\vec{s}d\vec{p}d\vec{s}'d\vec{p}'$$

Using independence, the expectation can be pushed inside the product. Up to subsuming a number of the repetition terms that were remainders, the sum can also be pushed inside the product. This allows us to use the summability relation on the V_α. We find that $\mathrm{Val}(\mathrm{Id}_n)$ is equal to

$$\varepsilon^{2n}\int e^{i(\vec{s}'\cdot\vec{\omega}'-\vec{s}\cdot\vec{\omega})}\prod_{j=1}^{n}\left[\sum_{\alpha_j\in\mathbb{Z}^d}\mathbb{E}\left(\widehat{V}_{\alpha_j}(p_{j-1}-p_j)\overline{\widehat{V}_{\alpha_j}(p_{j-1}'-p_j')}\right)\right]\widehat{\psi}_0(p_n)\overline{\widehat{\psi}_0(p_n')}\delta\delta' d\vec{s}d\vec{p}d\vec{s}'d\vec{p}'$$
$$= \varepsilon^{2n}\int e^{i(\vec{s}'\cdot\vec{\omega}'-\vec{s}\cdot\vec{\omega})}\prod_{j=1}^{n}\left[|\widehat{G}(p_{j-1}-p_j)|^2\delta^{p_{j-1}-p_j}_{p_{j-1}'-p_j'}\right]\widehat{\psi}_0(p_n)\overline{\widehat{\psi}_0(p_n')}\delta\delta' d\vec{s}d\vec{p}d\vec{s}'d\vec{p}'$$

But $p_0 = p_0'$, so $p_0 - p_1 = p_0' - p_1'$ implies $p_1 = p_1'$, and so on. $p_j = p_j'$ for all j. We find the formula

$$\mathrm{Val}(\mathrm{Id}_n) = \varepsilon^{2n}\int e^{i(\vec{s}'\cdot\vec{\omega}'-\vec{s}\cdot\vec{\omega})}\prod_{j=1}^{n}\left[|\widehat{G}(p_{j-1}-p_j)|^2\right]|\widehat{\psi}_0(p_n)|^2\delta\delta' d\vec{s}d\vec{p}d\vec{s}'.$$

2.7.1.4 Oscillatory integrals

To handle the oscillating terms and the deltas, the trick is to substitute the deltas for more oscillating terms. In particular, note that for any η, because $e^{-\eta\cdot 0}=1$, we have

$$e^{-\eta(t-\sum s_j)}\delta(t-\sum s_j)=\delta(t-\sum s_j)=\int_{\mathbb{R}} e^{i\mu(t-\sum s_j)}d\mu$$

Then we can estimate the terms which involve the s_j's. We find

$$\begin{aligned}\int \delta(t-\sum s_j)e^{-i\vec{s}\cdot\vec{\omega}}d\vec{s} &= \int_{s_j\geq 0} e^{\eta(t-\sum s_j)}\left(\int_{\mathbb{R}} e^{i\mu(t-\sum s_j)}d\mu\right)e^{-i\vec{s}\cdot\vec{\omega}}d\vec{s}\\ &= e^{\eta t}\int_{\mathbb{R}} e^{i\mu t}\int_{s_j\geq 0} e^{-\sum(\eta+i(\mu+\omega_j))s_j}d\vec{s}d\mu\\ &= e^{\eta t}\int_{\mathbb{R}} e^{i\mu t}\prod_{j=0}^{n}\left[\int_0^\infty e^{-(\eta+i(\mu+\omega_j))s}ds\right]d\mu\\ &= -ie^{\eta t}\int_{\mathbb{R}} e^{i\mu t}\prod_{j=0}^{n}\frac{1}{\mu+\omega_j-i\eta}d\mu\end{aligned}$$

Now, make the following definitions:

$$K(t,\vec{p})=\varepsilon^n e^{\eta t}\int_{\mathbb{R}} e^{i\mu t}\prod_{j=0}^{n}\frac{1}{\mu+\omega_j-i\eta}d\mu,\qquad d\nu(\vec{p})=\prod_{j=1}^{n}|\widehat{G}(p_{j-1}-p_j)|^2|\widehat{\psi}_0(p_n)|^2dp_0\cdots dp_n.$$

Then we find that $\mathrm{Val}(\mathrm{Id}_n)$ is simply written as

$$\mathrm{Val}(\mathrm{Id}_n)=\int |K(t,\vec{p})|^2 d\nu(\vec{p})$$

Then we have a lemma, including a naive bound and a more useful bound:

Lemma 2.7.2. *$K(t,\vec{p})$ is bounded pointwise with the naive bound*

$$|K(t,\vec{p})|\lesssim \varepsilon^n\frac{t^n}{n!}$$

For $a\in(0,1)$, there exists a constant C_a so that we actually find

$$\int |K(t,\vec{p})|^{2-a}d\nu(\vec{p})\leq \varepsilon^{(2-a)n}\frac{(C_a t^{1-a})^n}{(n!)^a}$$

Proof. To prove the naive bound, just estimate

$$|K(t,\vec{p})|\leq \varepsilon^n e^{\eta t}\int_{\mathbb{R}}\frac{d\mu}{|\mu-i\eta|^{n+1}}\leq \varepsilon^n\frac{e^{\eta t}}{\eta^n}\int_{\mathbb{R}}\frac{d\mu}{|\mu-i|^{n+1}}$$

and minimizing η, we find that picking $\eta=n/t$ gives

$$|K(t,\vec{p})|\lesssim \varepsilon^n\frac{t^n e^n}{n^n}\sim\varepsilon^n\frac{t^n}{n!}$$

up to a factor of $\sqrt{n}$ by Stirling's approximation (which is not important).

The second result comes from the same style of estimate done in the quasiresonant forcing case. See Section 2.2.4. □

Need to figure out how precisely to prove this last result, and how to push a to 0.

2.7.2 Roberta Bianchini's lecture: Non-ladder graphs

Chapter 3

Peter Haynes' lecture notes

3.1 Introduction

Intro

These lecture notes correspond to a short 8 hours lecture series by Peter Haynes at Cargèse, Corsica, in August 2021. It is intended to provide an applied view of Atmospheric and Oceanic flows from the UK applied mathematics perspective of use to both the French and UK/US schools.

The lectures focus on fundamental fluid dynamics to describe atmospheric and oceanic flows. A difficulty that arises when studying such flows is related to the enormous spatial and temporal range of scales they span, from the large-scales - which in the context of the Earth's oceans and atmosphere refers to time-scales $T \sim 1\ day$, length-scales of $L \sim 1000\ km$ in the atmosphere and $L \sim 100\ km$ in the ocean - to the small-scales, of the order of a few centimeters, at which dissipation and mixing occur. As a consequence, the full physical equations are too complicated to be solved and it would be unpractical to do so. Therefore, it is crucial to identify the leading order terms in the equations by estimating their magnitudes and finding a simplified version of such equations.

The two main physical processes of significance for atmosphere and oceans are the Earth's rotation, a consequence of the Coriolis force, and stratification due to density gradients which gives rise to a buoyancy force. Large-scale slow evolving flows, referred to as balanced dynamics, satisfy a balance between the Coriolis and the pressure gradient forces, called *geostrophic equilibrium*. By considering such balance, a subset of reduced equations can be found, which constitutes quasi-geostrophic model. This model, initially used in weather forecast models to filter out the fast evolving gravity waves, is too inaccurate for numerical predictions [30]. Small perturbations in the fluid can cause disturbances to the state of equilibrium, giving rise to rich variety of waves, including inertial, gravity, and sound waves. These waves allow for transport of physical quantities (locally), may interact with the mean flow (non-locally), and are crucial in the description of turbulence.

In section 3.2 we proceed by outlining the compressible Navier-Stokes equations describing the most complicated dynamics and by commenting on how physical effects, such as moisture or salinity, may be accounted for. The assumptions and simplifications permissible on the basis of relevant non-dimensional groups are then discussed. Maintaining a focus on waves, we choose to highlight that the vaguely hyperbolic governing equations have five time-derivatives and numerous time-scales. Associated with these time-scales are waves, notably, sound waves and internal gravity waves (also know as inertia gravity

waves), which propagate information and allow for different regions of the flow to communicate locally.

In section 3.3 we make the assumption of weak compressibility, whereby the flow velocity U and sound speed c are such that $U/c \ll 1$, and hydrostatic equilibrium in order to derive the *primitive equations* a five component model with three time-derivatives which ignores sound waves, but retains internal gravity waves. A dispersion relation for the classes of modes captured is obtained by studying its linearisation. The geophysical implications of this dispersion relation are discussed.

Having reduced the full governing equations from a system with 5 to 3 time derivatives, we make further reductions to arrive at the hyperbolic shallow water or Saint-Venant equations in section 3.4. As the title suggests, the reduction made assumes a ratio of the horizontal to vertical length scales that is small. Linearising the shallow water equations the potential vorticity Q, a materially conserved quantity, is introduced and the wave modes supported are discussed. By extending the derivation to cases where boundaries or a weak depth dependency are included variations of the potential vorticity Q and the altered form of the wave modes present are discussed.

Section 3.5 focuses on the spontaneous generation of fast modes, i.e. inertia-gravity waves, by the slowly evolving flow, leading to the breakdown of quasi-geostrophic balance. After showing the non-existence of an invariant slow manifold, resulting in the inevitable generation of gravity waves, we discuss the propagation mechanisms of such waves and their interactions with the mean flow.

Having established that a slowly evolving balanced flow will nevertheless give rise to waves, section 3.6 focuses on wave propagation and wave mean flow interaction. Focusing on the 2D vorticity equation on the β-plane, the dispersion relation for Rossby waves is derived follow by a theoretical description of their interaction with a mean flow. The relevance of this formulation to the quasi-biennial oscillation (QBO) of equatorial zonal winds is explored.

In section 3.7 we discuss the dynamics of a 2D flow on the β-plane. The system is shown to undergo self-organisation with the generation of coherent structures–jets–that are typically observed in geophysical and astrophysical flows. The jet formation mechanisms are briefly discussed together with some useful mathematical models.

Finally, section 3.8 explores the role of moisture and moisture dynamics focusing on the Madden-Julian oscillation, equatorial waves, and aggregated convection.

3.1.1 Motivating examples

MotivatingExamples

From observations of the atmosphere and ocean, we know the large range of phenomena exist and that they do so on a large range of temporal and spatial scales. The most simple example of waves everyone is familiar with are surface water waves. These waves arise at the interface between two fluids, namely water and air, and the change in density of the fluid allows for the waves to propagate at the surface. However, we will not discuss surface waves in this context, focusing rather on waves that occur within the fluid. In

the following we show some examples of phenomena that play an important role in the atmosphere and ocean dynamics and will be treated later in more detail.

Example 1): Storms in the deep ocean generate waves, which propagate towards the shore where they break and generate turbulence. An important aspect of the fluid dynamics is the combination of these two elements: wave propagation on the one hand, which is the way waves travel from the place where they are generated, and turbulence on the other hand, which is a complicated nonlinear fluid motion. There are situations where these two phenomena occur separately, with a first phase of wave generation and propagation, and a second phase in which the flow breaks down into turbulence. In other cases, turbulence and waves co-exist and cannot be separated.

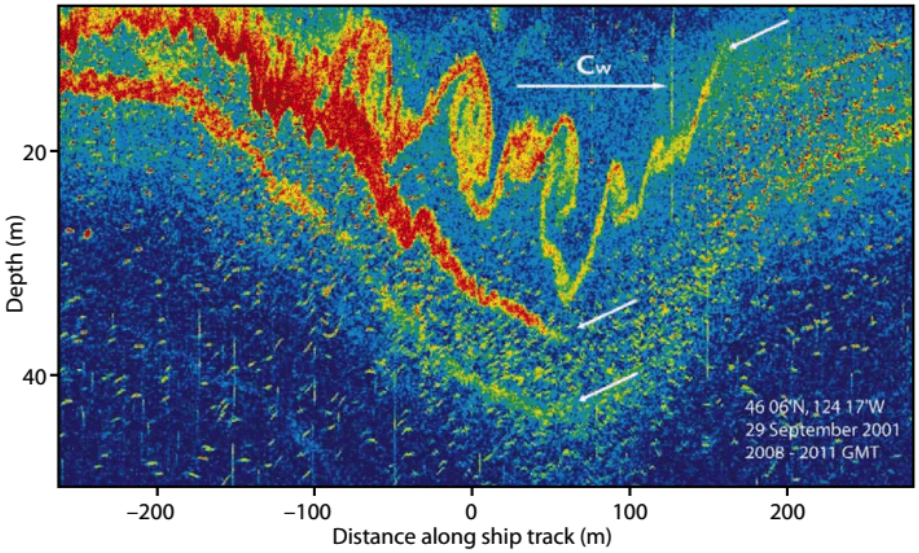

Figure 3.1: Acoustical snapshot of a nonlinear internal gravity wave approaching the Oregon coast. The wave propagates from left to right at speed C_w in this image. Caption and sources copied from [44]

elm_ocean

An example of internal waves breaking into turbulence is visible in figure 3.1, which is an acoustic snapshot captured in the ocean near the Oregon coast [44]. The waves on the left side show rolls up features typically caused by Kelvin-Helmholtz (KH) instability. The KH is a instability of a shear flow, modified by the presence of density stratification. Moving towards the right side, the waves break down into turbulence, characterised by less coherent structures with smaller size. The development of turbulence caused by KH instability is important in explaining the ocean mixing.

Example 2): In the atmosphere, it is possible to see without the need of any instrument the development of the KH instability, when the billows shape the clouds as in the cases shown in figure 3.2. The pattern shows waves similar to the surface waves near to a beach.

Example 3): The KH instability has been studied in the Thorpe tilted tank experiment (originally done in Cambridge in 1971 [48]). The experiment consists of a long horizontal tank filled in with density stratified fluid: a denser layer is in the bottom half, while a lighter fluid is on top of it. When the tank is tilted, the lighter fluid flows towards the lower side of the tank, generating a velocity shear at the interface. Consequently, the Kelvin Helmholtz instability arises at the interface, with billows very similar to the ones observed in the atmosphere (see figure 3.3) [44].

Figure 3.2: Evolution of the Kelvin-Helmholtz instability revealed by clouds. (a) (from http://www-frd.fsl.noaa.gov/mab/scatcat; photo by Brooks Martner), (b) a fog layer on the shore of Nares Strait in the Canadian Arctic (courtesy of Scott McAuliffe, Oregon State University), (c) Ground view of billow clouds (http://www.weathervortex.com/sky-ribbons.htm Caption and sources copied from [44].

fig:KelvinHelm_Exp

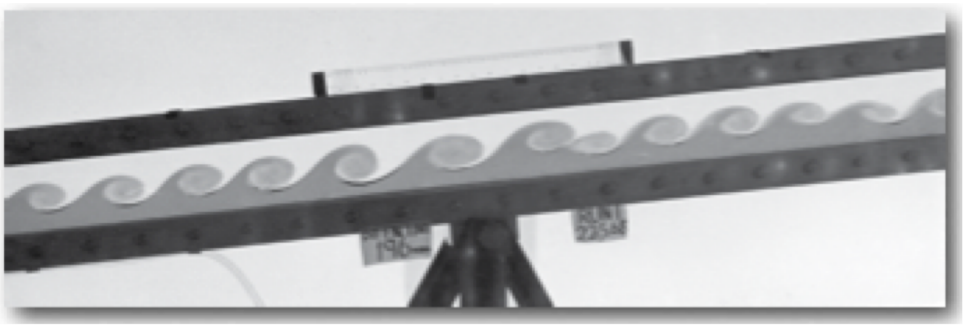

Figure 3.3: Thorpe's titling tank experiment in which a denser fluid (here shown in dark) underlies a lighter fluid. Sources copied from [48].

fig:ThorpeTank_Exp

For many years, laboratory experiments have been the only mean to study these kind of instabilities as they were beyond the computational power of numerical simulations.

However, in most recent years, simulations have improved thanks to the gain in computational power so that they are now capable of effectively simulating the three dimensional nature of the KH instability, including the small-scale breakdown into turbulence. An example showing the life cycle of the fully three-dimensional Kelvin-Helmholtz instability is shown in figure 3.4. The advantage of performing numerical simulations is that they offer access to the full variables in the entire domain, contrary to the laboratory experiment where only some quantities are usually measurable.

Example 4): Another recognisable phenomenon that occurs in the atmosphere is a large thunderstorm convective cloud developing in the tropics. This particular cloud, which is one of the largest persistent thunderstorm extending for almost 20 km in height, is also known as Hector the convector. The name was given by the Australian pilots that, during the second world war, used Hector as a landmark. It forms because of the particular local geometry: two islands just north of Darwin on the Australian coast provide boundaries for the sea breeze setting up a convective system in which moisture rises. This system is of particular interest for studying how chemicals and water vapour are transported from the lower part of the atmosphere to the troposphere and even higher in the stratosphere. Numerical simulations by [14] could capture simultaneously the large scales and small-scale dynamics of the cloud, reaching a resolution of 100 m.

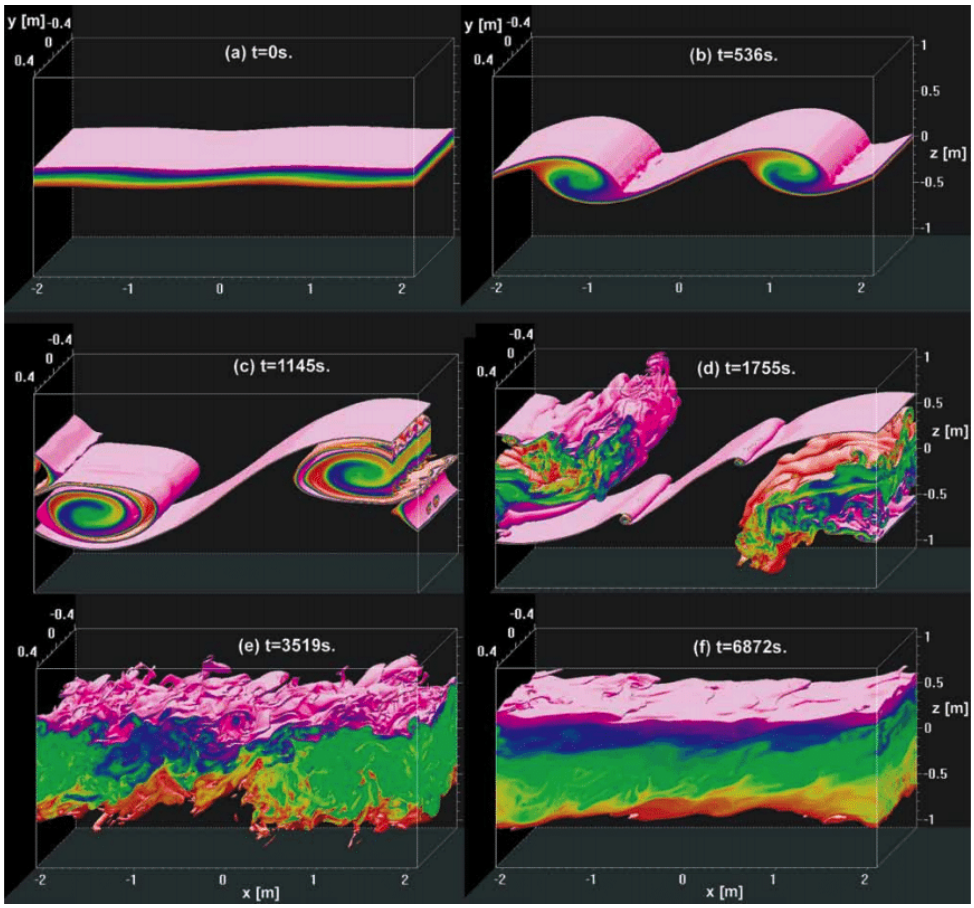

Figure 3.4: Direct numerical simulations of the density field at successive time in the life cycle of a Kelvin-Helmholtz billow train. colors show density in the transition layer; upper and lower homogeneous layers are rendered transparent. (a) The initial state is a two-layer flow, with a lower (dense) layer flowing to the left and an upper layer to the right. a small perturbation is applied. (b) two wavelengths of the primary Kelvin-Helmholtz instability. (c) Kelvin-Helmholtz billows are beginning to pair. Secondary instability is visible in a cutaway at upper right, taking the form of shear-aligned convection rolls. (d) Secondary shear instability forms on the braids. (e) The fully turbulent state. (f) turbulence decays to form sharp layers and random small-scale waves. Sources copied from [44]

horpe_sim

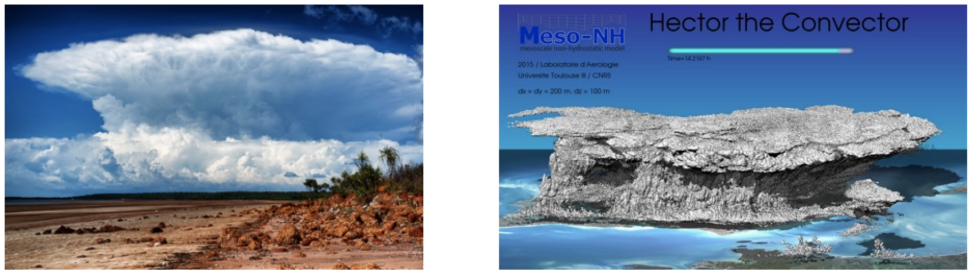

Figure 3.5: Hector the convector reaching stratospheric heights. Sources copied from [14].

_Numerics

Example 6): So far, we have focused on phenomena at the human scales, but with the help of satellite observations we can easily look at even larger scales. For example, figure **??** shows the time-longitude cloudiness in the tropics above Indonesia. Several structures are visible in the plot: waves propagating towards the east, longitudinal heterogeneity

corresponding to over-land regions, variability on the large-scale patterns with a period of around 40 days. The latter is know as the Madden Julian Oscillation, which is a fluctuation associated with variation of convection over the Indian ocean.

Satellite observations have opened new possibilities to investigate space-time structures in the atmosphere and in the ocean that were not possible to observe before.

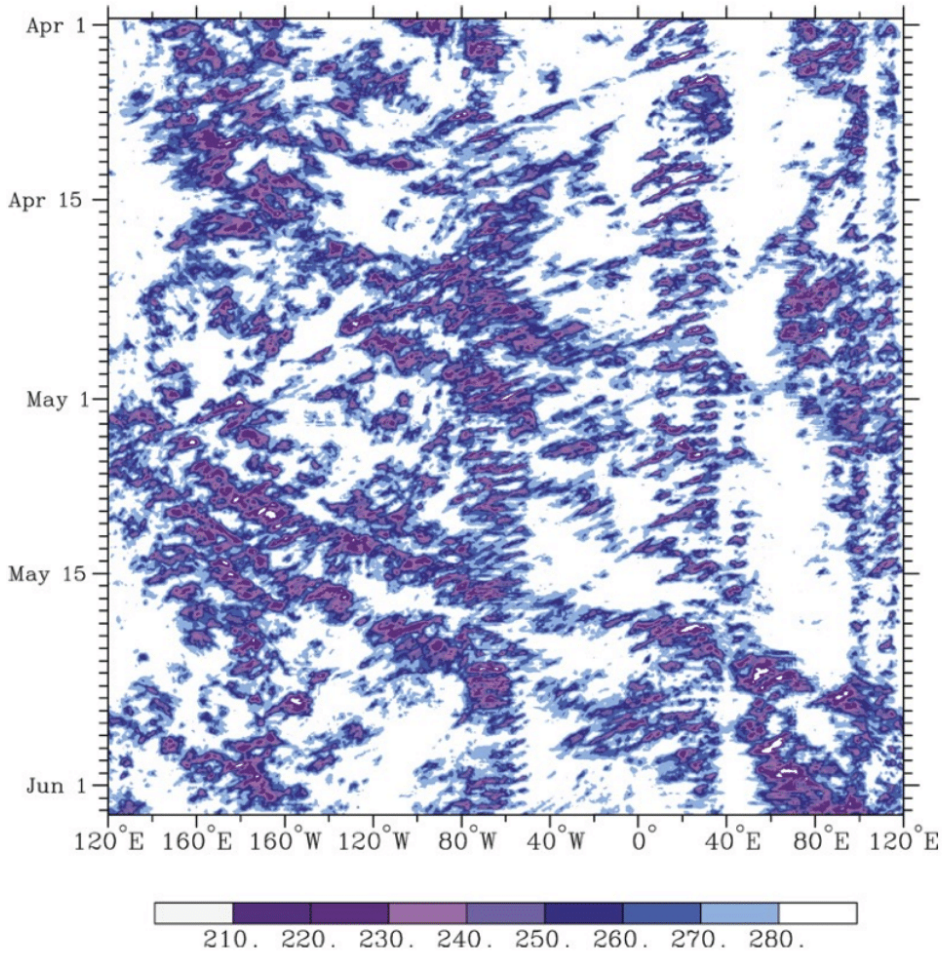

fig:clouds Figure 3.6: Time-longitude showing the cloudiness in the tropics Sources copied from [28]

Questions stemming from all these examples cannot be considered on the human scale and instead require that we consider the large scale/long time dynamics. How the interaction between scales manifests must then be addressed. We proceed in the next section by outlining the governing equations which must allow for all these phenomena, and subsequently by making physically motivated assumptions study particular phenomenon in subsequent sections.

3.2 Mathematical formulation

MathForm

We use $\boldsymbol{x} = (x, y, z)$ to define the longitude, latitude and depth of a fluid layer such as the ocean or atmosphere. Time is denoted by t and the variables $\boldsymbol{u}(\boldsymbol{x}, t), \rho(\boldsymbol{x}, t)$ and $p(\boldsymbol{x}, t)$ denote the velocity vector, density and pressure. $\theta(\boldsymbol{x}, t)$ denotes an entropy like field akin to potential temperature in the context of gaseous fluids, relevant in atmospheric

science. In a rotating frame of reference with constant rotation vector $\boldsymbol{\Omega}$ their evolution is described by

$$\frac{D\boldsymbol{u}}{Dt} + 2\boldsymbol{\Omega} \times \boldsymbol{u} = -\frac{\nabla p}{\rho} + \mathbf{g}, \tag{3.1a}$$

$$\frac{\partial \rho}{\partial t} + \nabla \cdot (\rho \boldsymbol{u}) = 0, \tag{3.1b}$$

$$\frac{\partial \theta}{\partial t} + \nabla \cdot (\theta \boldsymbol{u}) = \mathcal{Q}(\rho, \theta), \tag{3.1c}$$

FullNS where $\mathbf{g}$ denotes the gravity field, $\mathcal{Q}(\rho, \theta)$ a diabatic heating term and centrifugal terms are absorbed into the pressure field p. For model closure (3.1) must accompanied by an appropriate equation of state e.g. $p(\rho, \theta)$. The material derivative, which describes the advection of a fluid parcel is given by

$$\frac{D}{Dt} = \frac{\partial}{\partial t} + (\boldsymbol{u} \cdot \nabla). \tag{3.2}$$

In stating (3.1) we have neglected viscous effects given that typical geophysical flows have a ratio of $\frac{|\boldsymbol{u}\cdot\nabla\boldsymbol{u}|}{|\nu\Delta\boldsymbol{u}|} \sim \frac{UL}{\nu} \ll 1$, where ν is the kinematic viscosity and U, L appropriately chosen velocity and length-scales.

Depending on the physical problem of interest additional complexity may be added to (3.1). The motivation for doing so being that the general equations must allow for all the phenomena reported in subsection 3.1.1. If for example the ocean's dynamics where know to depend strongly on a salinty field $\chi(\boldsymbol{x}, t)$, as is the case in the Mediterranean sea [54], we could require that

$$\frac{D\chi}{Dt} = 0, \tag{3.3}$$

in conjunction with an appropriate modification of the equation of state's functional dependence $p(\rho, \theta, \chi)$. Another scenario of relevance in atmospheric dynamics is the presence of a moisture field, often evoked to explain phenomenon including the biennial Madden Julian oscillation [26, 56]. In such a scenario a moisture field $S(\boldsymbol{x}, t)$ would be required to satisfy

$$\frac{DS}{Dt} = 0, \tag{3.4}$$

along with an appropriate modification of the adiabatic heating term $\mathcal{Q}(\rho, \theta, q)$. The role of moisture, and how it alters the dynamics described by (3.1) will be revisited in more detail in section 3.8.

The approach taken in the following sections is to study particular phenomena by considering physically motivated simplifications of (3.1). More specifically the approach taken will be to consider the linearised behavior of a reduced set of equations about some base state of relevance. This approach allows us to obtain a dispersion relation, from which one can infer the behaviour of various wave modes admitted by the equations. A crucial distinction that will be made when following this approach, is that certain assumptions/reductions reduce the number of time-derivatives present in (3.1). This has the effect of reducing the class wave modes present and thereby altering the means by which transport occurs, i.e. incompressibility $\nabla \cdot \boldsymbol{u} = 0$ excludes sound waves, causing the system to communicate non-locally via the pressure field.

3.3 Primitive equations

PreShallowWater

Given the prominence of rotation and stratification in geophysical flows, we now neglect entropy effects to consider the case of a rotating, stably stratified flow in hydrostatic equilibrium. This serves as a starting point from which we obtain significant dispersion relations that in later sections can be further simplified.

3.3.1 Assumption 1 - The Boussinesq approximation

We assume an incompressible $\nabla \cdot \boldsymbol{u} = 0$ Boussinesq fluid, excluding sound waves on the basis that $U/c \ll 1$ and large variations in pressure or density by restriction to sufficiently shallow fluid layers. We expanded the density field as $\rho(\boldsymbol{x}, t) = \rho_0 + \rho'(\boldsymbol{x}, t)$ about a constant ρ_0 with $\rho'/\rho_0 \ll 1$ and correspondingly the pressure may be split as $p(\boldsymbol{x}, t) = p_0(z) + p'(\boldsymbol{x}, t)$. Substituting and assuming the hydrostatic balance $dp_0(z)/dz + \rho_0 g = 0$, we get at leading order in the vertical momentum balance [1] that

$$
\begin{aligned}
(\rho_0 + \rho')\frac{Dw}{Dt} &= -\frac{\partial p_0}{\partial z} - \frac{\partial p'}{\partial z} - (\rho_0 + \rho')g, \\
\frac{Dw}{Dt} &\approxeq -\frac{1}{\rho_0}\frac{\partial p'}{\partial z} - \frac{\rho'}{\rho_0}g,
\end{aligned}
$$

by retaining density variations occur at leading order only when multiplied by gravity. In the horizontal components of the Navier-Stokes we replace $1/\rho$ by $1/\rho_0$. Taken into account the full equations may be written as

$$
\frac{D\boldsymbol{u}}{Dt} + \mathbf{f} \times \boldsymbol{u} = -\frac{1}{\rho_0}\nabla p' + \frac{\rho'}{\rho_0}\mathbf{g}, \tag{3.5a}
$$

$$
\nabla \cdot \boldsymbol{u} = 0, \tag{3.5b}
$$

$$
\frac{D\rho'}{Dt} = 0, \tag{3.5c}
$$

eq:PreBqNS

where $\mathbf{f} = 2\boldsymbol{\Omega}$. The Boussinesq assumption therefore takes into account the effect of density variations so as to include buoyancy forces. Mathematically this reduction has reduced the set of wave modes described by the equations and introduced non-locality through the pressure field. The implications of this assumption are that where sound waves once propagated information with a limited speed in the hyperbolic system 3.1, p' is now instantaneously determined from $\boldsymbol{u}$ as a solution of the Poisson equation. This has the effect of propagating some information instantaneously in the mixed elliptic-hyperbolic system 3.5. In effect, (3.5) excludes sound waves but retains their implications.

3.3.2 Assumption 2 - Stratified fluid layer

Due to the presence of stratification it is further informative to consider the the density field $\rho'(\boldsymbol{x}, t) = \rho_s(z) + \tilde{\rho}(\boldsymbol{x}, t)$, decomposed in terms of a background density $\rho_s(z)$ and a disturbance density $\tilde{\rho}(\boldsymbol{x}, t)$ usually zero when there is no fluid motion. By doing so, it is possible to quantify the stability of the background state in terms of the Brunt-Vaisala frequency

[1] the vertical component of the Coriolis force is a higher order effect and is thus neglected here

$$N^2 = -\frac{g}{\rho_0}\frac{d\rho_s(z)}{dz}, \tag{3.6}$$

a quantity that is useful when interpreting the stratification strength. For $N^2 > 0$ the density decreases upwards such that a vertically displaced parcel of fluid will return to its original position. Here N refers to the frequency at which this parcel of fluid will oscillation, when returning or deviating from this equilibrium state.

3.3.3 Assumption 3 - Shallow fluid layer

To motivate the final assumptions used to arrive at the *primitive equations*, we first consider the dispersion relation of small amplitude waves for a typical model problem. Taking N to be the buoyancy frequency, describing the stability of a background stratification $\rho_s(z)$ and $\mathbf{f} = f\hat{\mathbf{z}}$ a purely vertical and constant rotation vector, we obtain

$$\omega^2 = \frac{N^2k^2 + f^2m^2}{k^2 + m^2}, \tag{3.7}$$

where $k \sim 1/L$ and $m \sim 1/D$ are the horizontal and vertical wavenumbers respectively. It follows on dimensional grounds that the relative strength of stratification to rotation is given by N/L versus f/D. Given that $N \gg f$ in the atmosphere and ocean, where $f \sim \mathcal{O}(10^{-4})$ and $N \sim \mathcal{O}(10^{-2} - 10^{-3})$ [23, 50], we can deduce that rotation is only of significance in shallow fluid layers when $D \ll L$. However, in such shallow layers vertical velocities will be much smaller than horizontal velocities and for this reason only the Coriolis force associated with horizontal velocities, its vertical component, need be included.

Writing the velocity and rotation vector in terms of their horizontal and vertical components $\boldsymbol{u} = \boldsymbol{u}_h + \boldsymbol{u}_v$, $\mathbf{f} = \mathbf{f}_h + \mathbf{f}_v$ and taking their cross product (accounting for $\mathbf{f}_v \times \boldsymbol{u}_v = 0$) we obtain

$$\mathbf{f} \times \boldsymbol{u} = \mathbf{f}_h \times \boldsymbol{u}_h + \mathbf{f}_h \times \boldsymbol{u}_v + \mathbf{f}_v \times \boldsymbol{u}_h \approxeq \mathbf{f}_v \times \boldsymbol{u}_h. \tag{3.8}$$

This assumes $|\boldsymbol{u}_v| \ll |\boldsymbol{u}_h|$ so that $\mathbf{f}_h \times \boldsymbol{u}_v \approxeq 0$ and that $\mathbf{f}_h \times \boldsymbol{u}_h$ is of higher order in the vertical component of the moment equation so that it may also be neglected. Thus we replace the rotation vector by is vertical component $|\mathbf{f}_v| = 2\Omega \sin\varphi$, where φ denotes the latitude. When considering the region near the equator the first assumption may fail to be valid as $|\mathbf{f}_v| \ll |\mathbf{f}_h|$. Similarly the second assumption may become invalid if $D \gg 1$ such that the hydrostaic approximation ceases to apply.

Collectively these assumptions allow us to write down the so called *primitive equations*

$$\frac{Du}{Dt} + f_v v = \frac{\partial p'}{\partial x}, \tag{3.9a}$$

$$\frac{Dv}{Dt} + f_v u = -\frac{1}{\rho_0}\frac{\partial p'}{\partial y}, \tag{3.9b}$$

$$\frac{\partial p'}{\partial z} = -\rho' g, \tag{3.9c}$$

$$\nabla \cdot \boldsymbol{u} = 0, \tag{3.9d}$$

$$\frac{D\rho'}{Dt} = 0, \tag{3.9e}$$

PrimitiveEqns which are valid in a thin incompressible fluid layer for which the hydrostatic approximation is valid. If the pressure or density were to experience large variations over large vertical length scales, as is the case for cumulus clouds, (3.9) would cease to describe the dynamics. For further details on the reduction to the primitive equations see textbooks [23, 50].

A final approximation of use, is to restrict our attention to a local region of the sphere that can be described in terms of Cartesian co-ordinates. This is achieved by Taylor expanding the vertical rotation vector about a fixed latitude φ_0,

$$f_v(\varphi) \approxeq f + \beta y \approxeq 2\Omega \sin(\varphi_0) + \frac{2\Omega}{a}\cos(\varphi_0) a(\varphi - \varphi_0), \tag{3.10}$$ eq:beta_pl

where Ω is the angular rotation rate and a the radius, in order to replace $f_v \approxeq f + \beta y$ by its local variation correct to first order. This important simplification, termed the β-plane approximation, captures important features including Rossby waves whilst making the equations more tractable.

The primitive equations have 5 prognostic variables, three time derivatives and two instantaneous constraints which include the implication of sound waves non-locally. As such the primitive equations behave like a stack of shallow water equations, which communicate in the vertical through the pressure field.

3.3.4 Dispersion relation for internal gravity waves or inertia-gravity waves

sec:dispertionIGW

In order to understand what type of behaviour we get from (3.9) we consider a background state in hydrostatic equilibrium:

$$\begin{aligned} \boldsymbol{u} &= \mathbf{0}, \\ \rho' &= \rho_s(z), \\ -\frac{\partial p}{\partial z} &- g\rho_s(z) = 0. \end{aligned}$$

Now we consider small disturbances about the background state (here denoted by tilde) and apply a linearisation. The equations become:

$$\begin{aligned} \frac{\partial \tilde{\boldsymbol{u}}}{\partial t} + \mathbf{f} \times \tilde{\boldsymbol{u}} &= -\frac{\nabla \tilde{p}}{\rho_0} + \frac{\tilde{\rho}}{\rho_0}\mathbf{g}, \\ \nabla \cdot \tilde{\boldsymbol{u}} &= 0, \\ \frac{\partial \tilde{\rho}}{\partial t} + \tilde{w}\frac{d\rho_s}{dz} &= 0. \end{aligned}$$

We assume plane waves, that all fields $\propto \exp(i(\mathbf{k}\cdot\boldsymbol{x} - \omega t))$, with the wavevector $\mathbf{k} = (k, l, m)$. For brevity, we replace $\tilde{\boldsymbol{u}}$ by $\tilde{\boldsymbol{u}} e^{i(\mathbf{k}\cdot\boldsymbol{x}-\omega t)}$ and so on. We write the equations in

components:

$$-i\omega\tilde{u} - f\tilde{v} = -i\frac{k\tilde{p}}{\rho_0}, \tag{3.11a}$$
$$-i\omega\tilde{v} + f\tilde{u} = -i\frac{l\tilde{p}}{\rho_0}, \tag{3.11b}$$
$$-i\omega\tilde{w} = -i\frac{m\tilde{p}}{\rho_0} + \tilde{\sigma}, \tag{3.11c}$$
$$-i\omega\tilde{\sigma} + \tilde{w}N^2 = 0, \tag{3.11d}$$
$$k\tilde{u} + l\tilde{v} + m\tilde{w} = 0, \tag{3.11e}$$

where we have replaced $\tilde{\rho}$ by $\tilde{\sigma} = \dfrac{-\tilde{\rho}g}{\rho_0}$. Now starting the algebra we combine (3.11a) & (3.11b)

$$i\omega \times (3.11a) - f(3.11b): \quad (\omega^2 - f^2)\tilde{u} = (k\omega + ilf)\frac{\tilde{p}}{\rho_0},$$
$$i\omega \times (3.11b) + f(3.11a): \quad (\omega^2 - f^2)\tilde{v} = (l\omega + ikf)\frac{\tilde{p}}{\rho_0},$$

and use (3.11e) to eliminate $\tilde{u}, \tilde{v}$

$$\tilde{w} = -\frac{k}{m}\tilde{u} - \frac{l}{m}\tilde{v} \tag{3.12a}$$
$$= -\left(\frac{k}{m}(k\omega + ilf) + \frac{l}{m}(l\omega - ikf)\right) \times \frac{\tilde{p}}{\rho_0(\omega^2 - f^2)} \tag{3.12b}$$
$$= \frac{-(k^2 + l^2)\omega}{\rho_0(\omega^2 - f^2)m}\tilde{p}. \tag{3.12c}$$

Substituting the previous expression for $\tilde{p}$ in (3.11c)

$$-i\omega\tilde{w} = \frac{im^2\tilde{w}(\omega^2 - f^2)}{(k^2 + l^2)w} + \tilde{\sigma}, \tag{3.13}$$

$$\tilde{w} = \frac{\omega(k^2 + l^2)\tilde{\sigma}}{-i(\omega^2(k^2 + l^2 + m^2) - f^2m^2)}, \tag{3.14}$$

and eliminating $\tilde{w}$ using (3.11d) we obtain the dispersion relation for internal gravity waves

$$\omega^2 = \frac{N^2(k^2 + l^2) + f^2m^2}{(k^2 + l^2) + m^2}, \tag{3.15}$$ eq:IGW_dispersion_Rel

where $k, l \sim 1/L$ and $m \sim 1/D$ are the horizontal and vertical wavenumbers respectively. Some important limits of this relation are when

$$(k^2 + l^2) \gg 1 \gg m^2, \quad N^2 \quad \text{dominates} \tag{3.16}$$

and we obtain gravity waves, while for

$$m^2 \gg 1 \gg (k^2 + l^2), \quad f^2 \quad \text{dominates} \tag{3.17}$$

resulting in inertial waves. Another limit (or root) of this dispersion relation is $\omega^2 = 0$. This connects back to the fact that the primitive equations have three time derivatives and thus support three different wave modes, one of which is the zero mode. Given that $m \sim 1/D$ and we require $D \ll L$ for the hydro-static assumption to apply, we cannot approach $m \to 0, D \to \infty$ as our assumptions would break down. For this reason m can not be taken to be too small. A final remark is that the wave frequency must lie between N^2 and f^2, such that they control its upper and lower limits.

To illustrate the difference between group and phase propagation of these waves it is informative to consider a laboratory experiment of stably stratified fluid in which rotation is excluded. Figure 3.7 shows a tank of stably stratified salt water, perturbed at its center by a metal rod suspended on a fishing line. When set in motion the rod creates density fronts, which take the form of beams. In this case the group propagation is along these beams while the phase propagation occurs perpendicular to these beams.

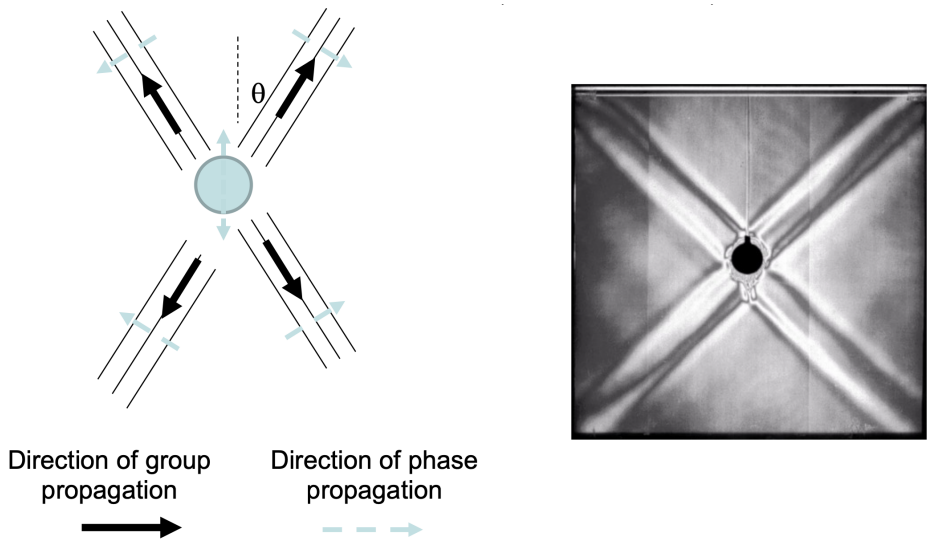

Figure 3.7: An oscillating rod in a tank of stably stratified slated water causes waves to enimate at an angle prescribed by the oscillation frequency. While for oscillation frequencies less that the Brunt-Vaisala frequency N^2 no waves occur. Animation available at GFD-online courtesy of (Satoshi Sakai, Isawo Iizawa, Eiji Aramaki)

fig:SatoshiSakaiGravityWave

To emphasise the notion of group propagation as information propagation, it is informative to consider observations of atmospheric equatorial Kelvin waves as shown in 3.8. In this example, we observe the downward phase propagation of equatorial Kelvin waves from the stratosphere, accompanied by the upward group propagation, a forcing responsible for sustaining these cloud formations? [1].

In the derivation of the dispersion relation and in the discussion of its implications, we have thus far ignored the influence of boundaries. When included boundaries given rise to an interesting set of hybrid wave modes termed kelvin waves. An example of these waves and the pronounced effect rotation has on their dynamics is available at GFD-online courtesy of (Satoshi Sakai, Isawo Iizawa, Eiji Aramaki). In the context of the primitive equations (3.9) the fact that the rotation vector $\mathbf{f}(\varphi)$ varies as a function of latitude

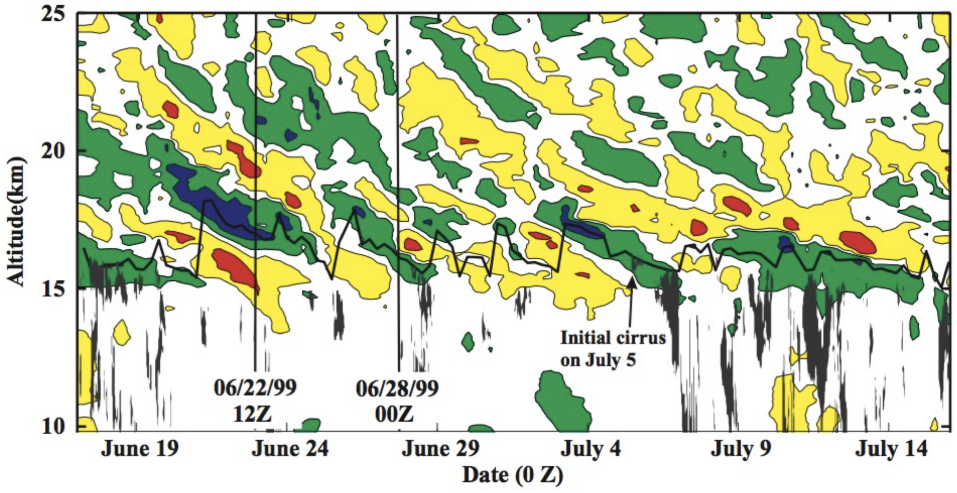

Figure 3.8: Atmospheric equatorial Kelvin waves seen in radiosonde temperature profiles of troposphere cirrus clouds [1].

osphereKW

gives rise to an artificial boundary. This results in a special set of modes termed trapped equatorial Kelvin waves which will be discussed in subsection 3.4.3.

3.4 Shallow water equations

allowWater

Let us consider a thin layer of homogeneous fluid between a rigid bottom and a free surface, as sketched in figure 3.9 where H = constant is the depth of the fluid at rest, $\eta \ll H$ is the disturbance, and therefore $H + \eta$ is the free surface elevation. The two horizontal velocity component (u, v) do not depend on depth. In this way we can describe the system with the so-called *shallow water equations*

$$\frac{D\boldsymbol{u}}{Dt} + \mathbf{f} \times \boldsymbol{u} = \mathbf{g}\nabla\eta, \tag{3.18a}$$ eq:SWmom

$$\frac{\partial \eta}{\partial t} + \nabla \cdot (\boldsymbol{u}(\eta + H)) = 0, \tag{3.18b}$$ eq:SWdensity

eq:SW where the two-dimensional material derivative reduces to

$$\frac{D}{Dt} = \frac{\partial}{\partial t} + u\frac{\partial}{\partial x} + v\frac{\partial}{\partial y}.$$

and $\mathbf{f}$ is purely vertical and constant. Note that the fluid height is directly related to the pressure. We have three time derivatives and the system does not account for any vertical variation. In that sense the shallow water equations can be thought of as describing the evolution of the *primitive equations* (3.9) in a linear regime, for a particular mode, with a fixed vertical structure. An instance where this approach is valuable, is describing the El Nino climate pattern, whereby the first baroclinic mode is an equatorial kelvin mode [50].

These equations are simpler than the full three-dimensional equations (we have reduced the system from 5 to 3 variables), but at the same time they provide a reasonable model for the dynamics of the atmosphere and the oceans [50]. We can reconstruct the system seen in the previous chapter by considering a stack of shallow water layers on top of each other interacting via the hydrostatic equation.

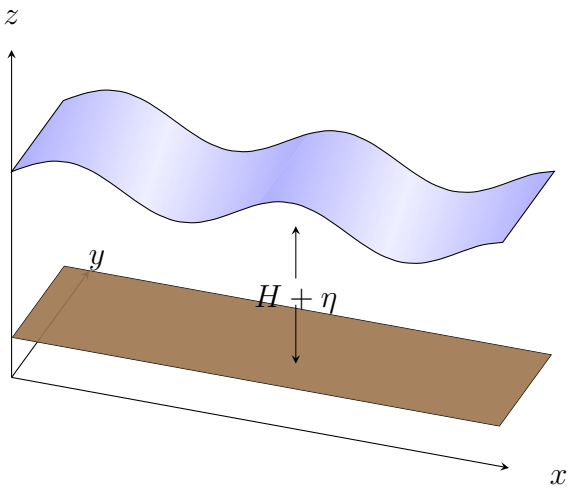

Figure 3.9: Shallow water system

fig:sw

3.4.1 Poincaré waves

The shallow water system of equations admits gravity waves traveling with speed $\sqrt{gH}$. Provided a suitable value for H, shallow water gravity waves share some properties we have already seen for the gravity waves encountered in the 3D continuously stratified system. By linearising (3.18) about a state of rest of the system, we can write the system by components:

$$\frac{\partial u}{\partial t} - fv = -g\frac{\partial \eta}{\partial x} \tag{3.19a}$$ eq:SWlinea

$$\frac{\partial v}{\partial t} + fu = -g\frac{\partial \eta}{\partial y} \tag{3.19b}$$ eq:SWlinea

$$\frac{\partial \eta}{\partial t} + H\left(\frac{\partial u}{\partial x} + \frac{\partial v}{\partial y}\right) = 0. \tag{3.19c}$$ eq:SWlinea

eq:SWlinear By taking the divergence of (3.19a) and (3.19b), we obtain:

$$\frac{\partial}{\partial t}\left(\frac{\partial u}{\partial x} + \frac{\partial v}{\partial y}\right) - f\left(\frac{\partial v}{\partial x} - \frac{\partial u}{\partial y}\right) = -g\left(\frac{\partial^2 \eta}{\partial x^2} + \frac{\partial^2 \eta}{\partial y^2}\right) \tag{3.20}$$ eq:divSW

We then take the time derivative of (3.19c) and substitute (3.20) to obtain

$$\frac{\partial^2 \eta}{\partial t^2} - gH\left(\frac{\partial^2 \eta}{\partial x^2} + \frac{\partial^2 \eta}{\partial y^2}\right) = -fH\left(\frac{\partial v}{\partial x} - \frac{\partial u}{\partial y}\right), \tag{3.21}$$ eq:Ett

where

$$\zeta = \left(\frac{\partial v}{\partial x} - \frac{\partial u}{\partial y}\right) \tag{3.22}$$ eq:vvort

is the vertical vorticity component.

To illustrate that vorticity can be added by stretching and is related to the free surface height. We can also consider the vorticity equation:

$$\frac{\partial \zeta}{\partial t} = -f\left(\frac{\partial u}{\partial x} + \frac{\partial v}{\partial y}\right) = \frac{f}{H}\frac{\partial \eta}{\partial t},$$

obtained by taking the curl of (3.19a) and (3.19b). This is useful to illustrate that

$$\frac{\partial}{\partial t}(\zeta - \frac{f\eta}{H}) = \frac{\partial}{\partial t}(\frac{\partial v}{\partial x} - \frac{\partial u}{\partial y} - \frac{f\eta}{H}) = 0,$$

such that the potential vorticity

$$Q(x,y) = \frac{\partial v}{\partial x} - \frac{\partial u}{\partial y} - \frac{f\eta}{H} \tag{3.23}$$ eq:PotentialVorticityy

is a quantity conserved in time and it is set by the initial conditions. That it is absolute vorticity rather than relative vorticity that's conversed, comes as a consequence of the rotating frame of reference.

Substituting for (3.23) in the right hand side of (3.21), we obtain a closed system for the free surface disturbance:

$$\frac{\partial \eta^2}{\partial t^2} - gH\left(\frac{\partial^2 \eta}{\partial x^2} + \frac{\partial^2 \eta}{\partial y^2}\right) + f^2\eta = -fHQ(x,y). \tag{3.24}$$ eq:eta

The *linearised shallow water system* is described by (3.24). Similarly to what done in section 3.3.4, we can derive the dispersion relation by considering solutions of the form $\eta(x,y,t) = Re(\tilde{\eta}\exp(i\boldsymbol{k}\cdot\boldsymbol{x} - i\omega t))$, for simplicity we consider the one-dimensional case. The dispersion relation for shallow-water gravity waves, also called Poincaré waves, is

$$\omega^2 = c^2k^2 + f^2, \tag{3.25}$$ eq:poincare

where the phase speed is $c = \sqrt{gH}$. Note that if we replace the phase speed with $c = N/m$, we have the same dispersion relation previously found for hydrostatic gravity waves (3.15). This correspondence assumes a fixed vertical wave number $m \sim 1/H \gg k$, as appropriate for a shallow layer of large horizontal extent.

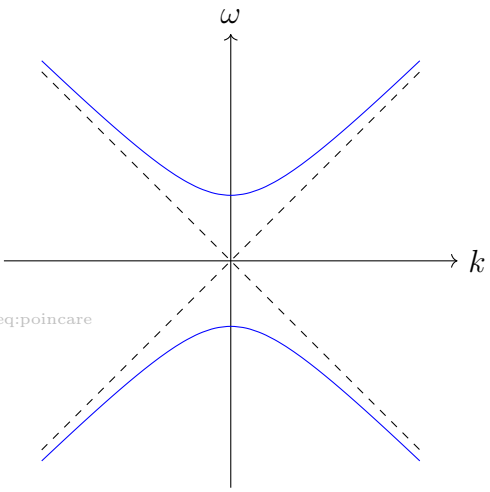

Figure 3.10: Sketch of the inertia-gravity wave dispersion relation

The dispersion relation of inertia-gravity waves is sketched in blue in figure 3.10. The dashed lines show the limit for the non rotating case, where the dispersion relation reduces to $\omega = \pm ck$.

Additionally to the two wave modes $\omega_\pm$, there is a third solution to (3.24), which is the zero frequency mode $\omega = 0$, corresponding to the time-independent flow in geostrophic balance.

3.4.2 Initial value problem ('Rossby adjustment')

Adjustment

If the initial flow is in an imbalanced state, when it is left free to evolve it will reach a state of equilibrium by propagating gravity waves. Given the initial distribution of u, v, and η, one can determine $Q(x,y)$. The waves are generated by the initial condition and will then propagate into the fluid.

For flows where the Rossby number $Ro = U/fL$ is small and therefore the Coriolis term is much larger than the advection term, the shallow water equations can be reduced to

$$-fv = -g\frac{\partial \eta}{\partial x}, \tag{3.26a}$$

$$fu = -g\frac{\partial \eta}{\partial y}, \tag{3.26b}$$

which is known as *geostrophic balance*. Synoptic and larger scale motions in the mid-latitudes are in approximate geostrophic balance. It follows that the steady state is

$$-gH\left(\frac{\partial^2 \eta}{\partial x^2} + \frac{\partial^2 \eta}{\partial y^2}\right) + f^2\eta = -fHQ(x,y), \tag{3.27a}$$

$$u = -\frac{1}{f}g\frac{\partial \eta}{\partial y}, \tag{3.27b}$$

$$v = \frac{1}{f}g\frac{\partial \eta}{\partial x}. \tag{3.27c}$$

We can consider the simple case of an unbounded system. The initial conditions are

$$\eta = \eta_0 \,\mathrm{sgn}(x),$$
$$u = 0,$$
$$v = 0.$$

A sketch of the evolving state is shown in figure 3.11,

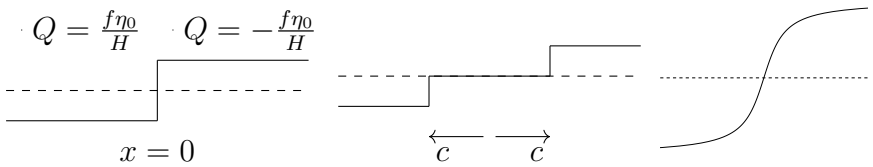

Figure 3.11: evolution of the initial state and radiation of gravity waves away from the disturbance.

fig:IC

The initial state of this flow (which follows from (3.23)) is unbalanced, as we have a discontinuity in the fluid height. $Q(x,y)$ is set by the initial η and has the values indicated in the sketch in the two regions. Note that η also sets the vertical wavelength, After the fluid is let evolve for some time, it will adjust to a stable state by propagating waves in opposite directions, and the discontinuity is smoothed by such propagation.

The final state, reached by the system after the waves propagate away from the source, is

$$\eta = \eta_0 \,\mathrm{sgn}(x)\exp(|x|/L_R) - \eta_0 sgn(x),$$
$$u = 0,$$
$$v = \frac{g}{fL_R}\eta_0 \exp(|x|/L_R),$$

where the Rossby deformation radius L_R representing the length scale at which gravity wave propagation and rotation balance is given by

$$L_R = \frac{\sqrt{gH}}{f} = c/f. \tag{3.30}$$

Alternatively this parameter can be understood as the length scale for which rotation becomes important. In general the Rossby deformation radius is dependent on the vertical structure as c and f are implicitly determined by H. Further details of this problem and the Rossby deformation radius are given in chapter 3 of [50] and chapter 7 of [23].

3.4.3 Kelvin waves - horizontal boundaries

elvinWaves

Let us now consider gravity waves in a domain with a rigid lateral boundary at $y = 0$ (similar to the case of the ocean near the coastline). This boundary imposes then no-penetration condition $v = 0$ for $y = 0$.

By setting $v = 0$ everywhere, we can look for wave-like solutions of the linearised shallow water equations (3.19) that satisfy this zero velocity condition

$$\frac{\partial u}{\partial t} = -g\frac{\partial \eta}{\partial x} \tag{3.31a}$$ eq:KelvinXV0

$$fu = -g\frac{\partial \eta}{\partial y} \tag{3.31b}$$ eq:KelvinYV0

$$\frac{\partial \eta}{\partial t} + H\frac{\partial u}{\partial x} = 0. \tag{3.31c}$$ eq:Kelvin

which lead to the wave equation

$$\frac{\partial^2 \eta}{\partial t^2} - gH\frac{\partial^2 \eta}{\partial x^2} = 0.$$

The solutions for the surface elevation will be of the form $\eta = A(x-ct, y)+B(x+ct, y)$. There is a flow in x direction in geostrophic balance with the surface elevation along y and it follows from (3.31a) that the solution for the velocity can be written as $u = g/cA(x - ct, y) - g/cB(x + ct, y)$. We can substitute the two solutions in (3.31b) and find the values of A and B

$$\frac{fg}{c}\left(A(x-ct,y) - B(x+ct,y)\right) = -g\left(\frac{\partial A}{\partial y}(x-ct,y) + \frac{\partial B}{\partial y}(x+ct,y)\right).$$

It follows that

$$\frac{\partial A}{\partial y} = -\frac{f}{c}A, \qquad \frac{\partial B}{\partial y} = \frac{f}{c}B,$$

with solutions

$$A = \exp\frac{-fy}{c}, \qquad B = \exp\frac{fy}{c},$$

For $y > 0$, the solution for B grows exponentially and therefore we reject it, which leave us with the solutions

$$\eta = A(x-ct, y), \qquad u = \frac{g}{c}A(x-ct, y). \tag{3.32a}$$

Waves propagating along the wall and according to the sign of f they travel eastward or westward.

An example of these waves and the pronounced effect rotation has on their dynamics is available at GFD-online courtesy of (Satoshi Sakai, Isawo Iizawa, Eiji Aramaki). In this experiment a square tank is equipped with a dipper that generates waves. In the absence of rotation, the waves emanate outwards from the source, but when included the rotation introduces a very strong asymmetry and waves propagate along the boundary. The resonant tide phenomena observed in the 1950's in both Holland and the UK constitutes another example of Kelvin waves. In this particular circumstance a high tide coincided with waves from the mid north sea/Atlantic resulting in substantial flooding of both low-lying coastlines. The presence of Kelvin waves is also used to explain the higher tides experienced by the French coast of the English channel. In the context of the primitive equations (3.9) the fact that the rotation vector $\mathbf{f}(\varphi)$ varies as a function of latitude gives rise to an artificial boundary for $\varphi \approxeq 0$. This results in a special set of modes termed trapped equatorial Kelvin waves, whose topological invariance has been argued by [15].

3.4.4 Slow modes - non-flat lower/vertical boundary

sec:SlowModesTopoGraph

The study of the shallow water equations in the lectures thus far have focused on inertia gravity waves, induced by the combined effects of gravity and rotation and Kelvin waves which balance the influence of the Coriolis force and horizontal topographic boundaries. In this section, we demonstrate how incorporating a non-flat boundary with a weak latitudinal depth dependence gives rise to a special slow mode termed a *topographic Rossby wave*, whose vorticity is materially conserved rather than being simply invariant in time. In the context of the derived dispersion relation 3.3.4, this slow mode corresponds to the modification of the geostrophically balanced flow due to a non constant thickness.

Although Rossby waves are typically considered using the β-plane approximation, which includes a latitudinal dependency of the Coriolis force, such waves can also arise due to the presence of a spatially varying lower boundary, such as mountains for atmospheric flows and the sea-bed for oceanic flows.

To demonstrate the material conservation of vorticty we turn now our attention to the full shallow water equations again

$$\frac{\partial u}{\partial t} + u\frac{\partial u}{\partial x} + v\frac{\partial u}{\partial y} - fv = -g\frac{\partial \eta}{\partial x} \tag{3.33a}$$ eq:R1

$$\frac{\partial v}{\partial t} + u\frac{\partial v}{\partial x} + v\frac{\partial v}{\partial y} + fu = -g\frac{\partial \eta}{\partial y} \tag{3.33b}$$ eq:R2

$$\frac{\partial \eta}{\partial t} + \nabla \cdot (\boldsymbol{u}(H+\eta)) = 0 \tag{3.33c}$$ eq:R3

where we have re-introduced the non-linear terms. By subtracting $\partial/\partial x$ of (3.33b) from $\partial/\partial y$ of (3.33a) and using the definition of vertical vorticity (3.22) we get:

$$\frac{\partial \zeta}{\partial t} + u\frac{\partial \zeta}{\partial x} + v\frac{\partial \zeta}{\partial y} + f\left(\frac{\partial u}{\partial x} + \frac{\partial v}{\partial y}\right) + \zeta\left(\frac{\partial u}{\partial x} + \frac{\partial v}{\partial y}\right) = 0 \tag{3.34}$$

By re-arranging (3.33c)

$$\frac{D(\eta + H)}{Dt} + \left(\frac{\partial u}{\partial x} + \frac{\partial v}{\partial y}\right)(H+\eta) = 0, \tag{3.35}$$

and eliminating the divergence in both expressions we can combine the two into

$$\frac{1}{(\zeta+f)}\frac{D(\zeta+f)}{Dt} = \frac{1}{(H+\eta)}\frac{D(H+\eta)}{Dt}, \tag{3.36}$$

which can be written as

$$\frac{DQ(\boldsymbol{x},t)}{Dt} = 0, \text{ where } \quad Q(\boldsymbol{x},t) = \frac{\zeta+f}{H+\eta}, \tag{3.37}$$ eq:NLPotentialVorticityy

in terms of absolute vorticity, combining vorticity induced by rotation with that induced by the thickness of the fluid layer. Contrasting (3.23) with (3.37) we see that the latter also depends on the velocity field, rather than exclusively its rate of change. This implies that for (3.37) fluid parcels remember their initial condition while for (3.23) it is merely the general fluid motion. The nonlinearity in (3.37) also captures a richer behaviour provided $Q(\boldsymbol{x},t)$ has spatial gradients. While for the linearised case the flow is completely determined by $Q(x,y)$.

To derive the dispersion relation for the slow mode with non-zero frequency, we consider a basic state of a fluid at rest $\zeta = 0, \eta = 0$ in a domain whose depth depends on the latitude y such that the vorticity is $Q = f/H(y)$. In contrast to previous sections, the linearised shallow water equations will now gain an advective term. We now define $\Phi = g\eta$ and write the linearised set of equation as

$$\frac{\partial u}{\partial t} - fv = -\frac{\partial \Phi}{\partial x}, \tag{3.38a}$$ eq:add-a

$$\frac{\partial v}{\partial t} + fu = -\frac{\partial \Phi}{\partial y}, \tag{3.38b}$$ eq:add-b

$$\frac{\partial \Phi}{\partial t} + g\frac{\partial (uH)}{\partial x} + g\frac{\partial (vH)}{\partial y} = 0, \tag{3.38c}$$ eq:add-c

where the conservation of mass has been multiplied by g and $H(y)$ does not depend on x. As already done several times before, we can subtract the y derivative of (3.38a) from the x derivative of (3.38b)

$$\frac{\partial}{\partial t}\left(\frac{\partial v}{\partial x} - \frac{\partial u}{\partial y}\right) + f\left(\frac{\partial u}{\partial x} + \frac{\partial v}{\partial y}\right) = 0, \tag{3.39}$$

combine it with the third equation

$$\frac{\partial}{\partial t}\left(\frac{\partial v}{\partial x} - \frac{\partial u}{\partial y}\right) - \frac{f}{gH}\left(\frac{\partial \Phi}{\partial t} + g\frac{\partial H}{\partial y}v\right) = 0, \tag{3.40}$$

and re-arrange the time derivatives on the left-hand side to get

$$\frac{\partial}{\partial t}\left(\frac{\partial v}{\partial x} - \frac{\partial u}{\partial y} - \frac{f\Phi}{gH}\right) = \frac{f}{H}\frac{\partial H}{\partial y}v. \tag{3.41}$$

By taking the time derivative of (3.38b) and substituting for $\partial u/\partial t$ from (3.38a), we obtain

$$\frac{\partial^2 v}{\partial t^2} = -\frac{\partial^2 \Phi}{\partial y \partial t} - f^2 v + f\frac{\partial \Phi}{\partial x}. \tag{3.42}$$ eq:add-2

Now we take the time derivative of (3.42) and substitute (3.38c) to get

$$\frac{\partial^3 v}{\partial t^3} + f^2 \frac{\partial v}{\partial t} = gH \frac{\partial}{\partial y}\frac{\partial}{\partial t}\left(\frac{\partial u}{\partial x} + \frac{\partial v}{\partial y}\right) + \frac{\partial}{\partial y}\frac{\partial}{\partial t}\left(g\frac{\partial H}{\partial y}v\right) + f\frac{\partial}{\partial x}\frac{\partial \Phi}{\partial t}, \tag{3.43}$$

which can be re-written as

$$\frac{\partial^3 v}{\partial t^3} + f^2 \frac{\partial v}{\partial t} - g\frac{\partial^2}{\partial y^2}\frac{\partial (Hv)}{\partial t} = \frac{\partial}{\partial x}\frac{\partial}{\partial t}\left(gH\frac{\partial u}{\partial y} + f\Phi\right), \tag{3.44}$$

and then into

$$\frac{\partial^3 v}{\partial t^3} + f^2 \frac{\partial v}{\partial t} - g\frac{\partial^2}{\partial y^2}\frac{\partial (Hv)}{\partial t} = gH\frac{\partial^2}{\partial x^2}\frac{\partial v}{\partial t} - g\frac{\partial H}{\partial y}f\frac{\partial v}{\partial x}, \tag{3.45}$$

and finally

$$\frac{\partial}{\partial t}\left(\frac{\partial^2 v}{\partial t^2} + f^2 v - g\frac{\partial^2 (Hv)}{\partial y^2} - gH\frac{\partial^2 v}{\partial x^2}\right) = -g\frac{\partial H}{\partial y}f\frac{\partial v}{\partial x}. \tag{3.46}$$ eq:TopogRo

To simply the analysis we consider the case of a weakly sloped lower boundary $H(y) = H_0 + \epsilon\gamma y$, with $\epsilon L\gamma/H_0 << 1$, where L is the width of the domain in the y direction assumed to be large compared with the vertical depth. As we shall demonstrate this yields an additional slow $\mathcal{O}(\epsilon)$ mode in the dispersion relation, corresponding to a branch of topographic Rossby waves.

As previous we look for plane wave solutions to (3.46) of the form $v(x, y, t) \propto v(y)\exp(ikx + i\omega t)$. After substitution we obtain at leading order in ϵ that

$$\frac{\partial^2 v}{\partial y^2} = \left(k^2 + \frac{f^2 - \omega^2}{gH_0}\right)v + \mathcal{O}(\epsilon), \tag{3.47a}$$

$$= -l^2 v + \mathcal{O}(\epsilon), \tag{3.47b}$$

subject to the assumption that $\omega \gg \epsilon$,given that other order one terms would be present should this not hold. The values of l^2 are determined by the quantization condition

$$\omega^2 = gH_0(k^2 + l^2) + f^2, \tag{3.48}$$

a two-branches dispersion relation (as per the standard case see (3.25)) along with the small frequency or *slow solution* $\omega \cong \mathcal{O}(\epsilon)$. In this case, terms of $\mathcal{O}(\epsilon)$ and terms $\propto \omega$ on the left hand side remain become $\mathcal{O}(\epsilon^2)$ such that only the left hand side is retained. Substituting the plane wave Ansatz we have

$$\frac{\partial^2 v}{\partial y^2} = \big(k^2 + \frac{f^2}{gH_o} + \frac{\gamma f k}{H_0}\frac{1}{\Omega}\big)v + \mathcal{O}(\epsilon^2), \text{ where } \Omega = (\omega/\epsilon). \tag{3.49}$$

Gathering the terms as previous l is determined by the quantization condition

$$\Omega = -\frac{\gamma f k}{H_0(k^2 + l^2 + f^2/(gH_0))}. \tag{3.50}$$ eq:Dispersi

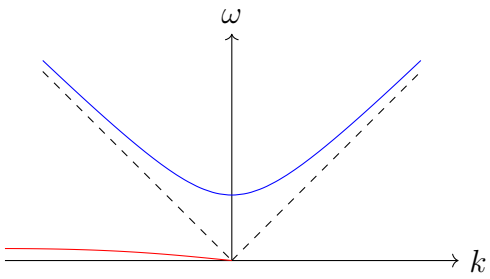

Figure 3.12: Sketch of the inertia-gravity wave and topographic Rossby waves dispersion relation.

fig:Rossby

A sketch of the modified dispersion relation pertaining to the case of $H'(y) \sim \mathcal{O}(\epsilon)$, is shown figure 3.12. Introducing a latitudinal dependency to the depth causes the zero-frequency mode, which was a flat curve in the case of flat bottom, to become small but non-zero. Note that the Rossby waves are not symmetric with respect to the wavenumber and only exist in the negative side. This means that they only propagate in one direction eastward in the northern hemisphere and westward in the southern hemisphere. There is a separation of the linear scales if the bottom surface deformation is small.

3.4.5 Derivation of equations for slow motion

In the previous sections we have seen that having rotation, stratification and a non-constant lower boundary gives rise to: A) Two *fast modes*, typically inertia-gravity waves, with frequencies $\pm\omega \geq \pm f$. By propagating information away from disturbed regions, these waves induce a Rossby adjustment 3.4.2 leading to a near geostrophic balance. B) One *slow mode* with $\omega \ll f$ constituting a slow modification of the geostrophic balance, typically through the propagation of topographic Rossby waves. In this section we consider the motion on this slower timescale to derive a single prognostic equation with one $\frac{\partial}{\partial t}$ rather than three.

We start from the shallow water equations with $\Phi = g\eta$ as in the previous section, and perform a scale analysis taking U as a typical horizontal velocity magnitude, L as a typical horizontal length, and T as a typical time scale.

$$\frac{\partial u}{\partial t} + u\frac{\partial u}{\partial x} + v\frac{\partial u}{\partial y} - fv = -\frac{\partial \Phi}{\partial x}, \tag{3.51a}$$ eq:S1

$$\frac{\partial v}{\partial t} + u\frac{\partial v}{\partial x} + v\frac{\partial v}{\partial y} + fu = -\frac{\partial \Phi}{\partial y}, \tag{3.51b}$$ eq:S2

$$UT^{-1} \quad U^2/L \qquad fU \qquad fU \quad \text{typical magnitudes} \tag{3.51c}$$

(3.51d)

To evaluate the relative importance of the first two terms with respect to the third one, we can define the Rossby number as the ratio between the different magnitudes of the terms

$$Ro = \frac{1}{fT}, \quad \frac{U}{fL}. \tag{3.52}$$

When $Ro \ll 1$, as is the case for the earth, the flow is close to geostrophic balance and we can linearise about this state. Expanding the velocities as $u = u_0 + Ro\, u_1 + \mathcal{O}(Ro^2)$ and $v = v_0 + Ro\, v_1 + \mathcal{O}(Ro^2)$, at the leading order in Ro the geostrophic balance (also justifiable by the Taylor-Proudman theorem) is

$$v_0 = v_g = \frac{1}{f}\frac{\partial \Phi}{\partial x}, \tag{3.53a}$$

$$u_0 = u_g = -\frac{1}{f}\frac{\partial \Phi}{\partial y}, \tag{3.53b}$$

$$\nabla \cdot u_0 = 0, \tag{3.53c}$$ eq:Geostro

where u_g is the 0-th order geostrophic velocity. To evaluate the importance of terms proportional to the free surface height η, appearing on the right hand side of (3.51a),(3.51b) and in the conservation of mass, we consider the non-dimensionalised continuity equation

$$Ro\big(\frac{\partial \Phi}{\partial t} + \nabla \cdot (\boldsymbol{u}\Phi)\big) + \nabla \cdot (\boldsymbol{u}H(y))\frac{L_R^2}{L^2} = 0, \tag{3.54}$$

where

$$H_0 H(y) = H_0 + \epsilon H_1(y), \tag{3.55}$$

and $L_R = \sqrt{gH_0}/f$ is the Rossby deformation radius. For $Ro \ll \frac{L_R^2}{L^2}$ and $L \sim L_R$ it follows that variations of the free surface height $\eta/H_0 \ll 1$, such that terms involving

time-derivatives are small. For this reason, corrections of Φ are higher order and we do not consider its expansion. Similarly for consistency we must assume that $\epsilon \sim Ro$.

Returning to dimensional form, we now consider the first order expansion

$$\frac{\partial u_0}{\partial t} + (\boldsymbol{u}_0 \cdot \nabla) u_0 - f v_1 = 0, \tag{3.56a}$$ eq:g1

$$\frac{\partial v_0}{\partial t} + (\boldsymbol{u}_0 \cdot \nabla) v_0 + f u_1 = 0, \tag{3.56b}$$ eq:g2

$$\frac{\partial \Phi}{\partial t} + g H_0 \nabla \cdot \boldsymbol{u}_1 + \boldsymbol{u}_0 \cdot \nabla g H_1 = 0, \tag{3.56c}$$ eq:g3

where $\nabla \cdot (\boldsymbol{u}_0 \Phi) = 0$ because of the definition of geostrophic balance. We now want to re-write $\nabla \cdot \boldsymbol{u}_1$ in terms of $\boldsymbol{u}_0$. We can use (3.56a) and (3.56b) to get an expression for $\boldsymbol{u}_1$

$$\nabla \cdot \boldsymbol{u}_1 = \frac{1}{f}\frac{\partial}{\partial x}\left(-\frac{\partial v_0}{\partial t} - (\boldsymbol{u}_0 \cdot \nabla) v_0\right) + \frac{1}{f}\frac{\partial}{\partial y}\left(\frac{\partial u_0}{\partial t} + (\boldsymbol{u}_0 \cdot \nabla) u_0\right), \tag{3.57}$$ eq:nlu

and substituting (3.57) into (3.56c), we obtain

$$\frac{\partial}{\partial t}\left(\frac{\partial v_0}{\partial x} - \frac{\partial u_0}{\partial y} - \frac{f\Phi}{g H_0}\right) - \frac{f \boldsymbol{u}_0}{H_0} \cdot \nabla H_1 + (\boldsymbol{u}_0 \cdot \nabla)\left(\frac{\partial v_0}{\partial x} - \frac{\partial u_0}{\partial y}\right) + \frac{\partial \boldsymbol{u}_0}{\partial x} \cdot \nabla v_0 - \frac{\partial \boldsymbol{u}_0}{\partial y} \cdot \nabla u_0 = 0. \tag{3.58}$$

This step doesn't follow unless $H_1 = H_1/f$ or something?? From Peter hand written notes: we add the last term in 3.53 ($-f^2\Phi/gH_0$) and ignore higher order terms in Φ. Rewritten in terms of Φ (using the gesotrophic equations (3.53c)) and replacing subscript zero by subscript g we obtain

$$\frac{\partial}{\partial t}\left(\frac{\partial^2 \Phi}{\partial x^2} + \frac{\partial^2 \Phi}{\partial y^2} - \frac{f^2 \Phi}{g H_0}\right) - \boldsymbol{u}_g \cdot \nabla\left(\frac{f H_1}{H_0}\right) + \boldsymbol{u}_g \cdot \nabla\left(\frac{\partial^2 \Phi}{\partial x^2} + \frac{\partial^2 \Phi}{\partial y^2} - \frac{f^2 \Phi}{g H_0}\right) = 0, \tag{3.59}$$

which can be written in the more compact form

$$\underbrace{\left(\frac{\partial}{\partial t} + \boldsymbol{u}_g \cdot \nabla\right)}_{\frac{D_g}{Dt}} \underbrace{\left(\frac{\partial^2 \Phi}{\partial x^2} + \frac{\partial^2 \Phi}{\partial y^2} - \frac{f^2 \Phi}{g H_0} - \frac{f H_1}{H_0}\right)}_{Q} = 0. \tag{3.60}$$ eq:PVY

We have again a potential vorticity (PV) equation, termed the *quasigeostrophic potential vorticity equation*

$$\frac{D_g Q}{Dt} = 0, \tag{3.61}$$ eq:QuasiGeoPV

with the PV expression for Q including and extra term that takes into account the height variation of the lower boundary. Marching (3.61) forwards in time gives a rule for updating P, which is conserved along the geostrophic flow $\boldsymbol{u}_g$. Similarly by solving the elliptic equation

$$Q = \frac{\partial^2 \Phi}{\partial x^2} + \frac{\partial^2 \Phi}{\partial y^2} - \frac{f^2 \Phi}{g H_0} - \frac{f H_1}{H_0}, \tag{3.62}$$

for Φ, subject to suitable boundary conditions, we can in turn instantaneously determine the geostrophic velocity $\boldsymbol{u}_g$ and any other flow quantities.

This structure is common to a large family of models, for example spherical geometries, three-dimensional models, and non-linearity of the inversion operator (with higher order corrections). In contrast to the shallow water equations, we now have only one time derivative, and thus only one class of wave modes is described by (3.61). Thus is the slow topographic Rossby-wave we consider in the previous section.

3.4.6 3-D geostrophic flow on the β-plane

To demonstrate how the form of the potential vorticty equation varies in accordance with different physical scenarios, we now consider a more general system with variations in depth z, due to stratification, and variations in latitude y due to the Coriolis force (here captured by the β-plane approximation (3.10)). This approximation renders the equations more tractable but equally, captures a potential vorticty gradient in the background state, thus allowing for Rossby waves. This is in contrast to the previous section, where Rossby waves arose as a consequence of the fluid depth depending on y.

To account for stratification we write the density and pressure fields in terms of their hydrostatic and non-hydrostatic components $\rho'(\boldsymbol{x},t) = \rho'_s(z) + \tilde{\rho}(\boldsymbol{x},t)$, $p'(\boldsymbol{x},t) = p'_s(z) + \tilde{p}(\boldsymbol{x},t)$ respectively, while ρ_0 is used to denote a background density. Similarly the velocity field is decomposed as $\boldsymbol{u} = \boldsymbol{u}_g + \boldsymbol{u}_a$, in terms of its geostrophic

$$\boldsymbol{u}_g = \left(\frac{1}{f_0}\frac{\partial\Phi}{\partial x}, -\frac{1}{f_0}\frac{\partial\Phi}{\partial y}, 0\right), \quad \text{where} \quad \Phi = -\tilde{p}/\rho_0, \tag{3.63}$$

and ageostrophic components $\boldsymbol{u}_a$. The latter accounting for the flow induced when $\nabla\tilde{\rho} \neq 0$. Due to the assumption of $Ro \ll 1$ we have $|\boldsymbol{u}_a| \ll |\boldsymbol{u}_g|$. Following [50] (chapter 5), who proceed with their derivation from the Boussinesq primitive equations (3.9), the potential vorticity equation in this scenario is given by

$$\left(\frac{\partial}{\partial t} + \boldsymbol{u}_g\cdot\nabla\right)\frac{1}{f_0}\left(\frac{\partial^2\Phi}{\partial x^2} + \frac{\partial^2\Phi}{\partial y^2} + \frac{\partial}{\partial z}\frac{f_0^2}{N^2}\frac{\partial\Phi}{\partial z} + \beta y\right) = 0, \tag{3.64}$$

eq:PVbeta

where the term $N^2 = -\frac{g}{\rho_0}\frac{d\rho'_s}{dz}$ gives information about the background density. This form of quasi-geostrophic equation hides the ageostrophic circulation $\boldsymbol{u}_a$, however its velocity component w_a can be recovered from the density equation

$$\left(\frac{\partial}{\partial t} + \boldsymbol{u}_g\cdot\nabla\right)\tilde{\rho} - w_a\frac{\rho_0}{g}N^2 = 0 \tag{3.65}$$

while its horizontal components (u_a, v_a) follow from the continuity condition. In the case of rigid vertical boundaries $w_a = 0$ and then

$$\frac{D_g}{Dt}\tilde{\rho} = 0. \tag{3.66}$$

such that the time evolution of $\tilde{\rho}$ on the boundaries must be included in boundary conditions on Φ. Alternatively for the case of a non-rigid vertical boundary an appropriate kinematic condition for the free surface must be satisfied. The physical interpretation of this model follows from the terms comprising the materially conserved potentially vorticity

$$Q = \underbrace{\frac{\partial^2\Phi}{\partial x^2} + \frac{\partial^2\Phi}{\partial y^2}}_{\text{relative vorticity}} + \underbrace{\frac{\partial}{\partial z}\frac{f_0^2}{N^2}\frac{\partial\Phi}{\partial z}}_{\text{stretching term}} + \underbrace{\beta y}_{\text{planetary vorticity}}. \tag{3.67}$$

eq:PV_3D

3.4.7 Models comparison and examples

odelsRecap

As evidenced by the previous two sections, there is a general class of models of the form

$$\frac{D}{Dt}Q = 0, \qquad \psi = L(Q - f), \tag{3.68}$$

for which a materially conserved quantity Q, akin to the potential vorticity is evolved by the geostrophic flow. The specifics of the particular flow are contained within the form of the elliptic operator (which allows the determination of other flow quantities) and are given by

$$\text{2D:} \qquad L = \left(\frac{\partial^2}{\partial x^2} + \frac{\partial^2}{\partial y^2}\right)^{-1} \tag{3.69a}$$

$$\text{2D-SWE:} \qquad L = \left(\frac{\partial^2}{\partial x^2} + \frac{\partial^2}{\partial y^2} - \frac{1}{L_R^2}\right)^{-1} \tag{3.69b}$$

$$\text{3D-QG:} \qquad L = \left(\frac{\partial^2}{\partial x^2} + \frac{\partial^2}{\partial y^2} + \frac{f^2}{N^2}\frac{\partial^2}{\partial z^2}\right)^{-1} \tag{3.69c}$$

$$\text{2D-SQG:} \qquad L = \left(\frac{\partial^2}{\partial x^2} + \frac{\partial^2}{\partial y^2}\right)^{-1/2} \tag{3.69d}$$

for the 2D vortex dipole, 2D shallow water equations, 3D quasi-geostrophic flow (assuming f, N are both constant) and the surface quasi-geostrophic flow respectively. While routinely used by atmospheric fluid dynamicists open questions still exits about the well posedness of these equations.

3.4.7.1 2D versus SQG

To highlight the differences between these systems, we can take a look at some examples of 2D and SQG turbulence.

Two-dimensional turbulence is a useful mathematical tool to approximately describe large-scale motion in the ocean and atmosphere. In two-dimensional turbulence the small scale structures are passive whereas in surface-quasi geostrophic turbulence the small scales become active and this different behaviour is then reflected in the spectra.

The surface quasi-geostrophic (SQG) system can be derived from 2D system by adding boundary conditions. When the effect of boundaries dominates over the fluid interior, one obtains the SQG system with the exponent of L now $-1/2$. In this sense, SQG is more 'local' and more potentially singular than 2D model. Both of these aspects are reflected by the Green's function of a point vortex, which behaves as $\sim 1/|\boldsymbol{x}|$ and $\sim \log(|\boldsymbol{x}|)$ for the SQG and 2D flows respectively.

By comparing numerical simulations of 2D and SQG turbulence (figure 3.13), one notices that both present vortical structures. The main difference lies in the fact that while active down to the small scales in SQG, these structures are passive in 2D turbulence.

Another nice example where the active/passive dynamics is recognizable is the vortex dynamics that develops from a smooth elliptical initial density/temperature perturbation (see figure 3.14). When the same initial state is let evolve under the SQG and 2D flow, filaments are shed from the vortex after some time in both cases. It only in SQG however, that the shear instability also appears along the filaments as can be seen in figure 3.14 for $t = 26$. In 2D, no such instability is present and the vortex evolves towards a more

symmetrical form. As we will shall see in more detail in section 3.5, the slow dynamics is the vortex dynamics but it also allows for waves irrespective of the initial conditions prescribed.

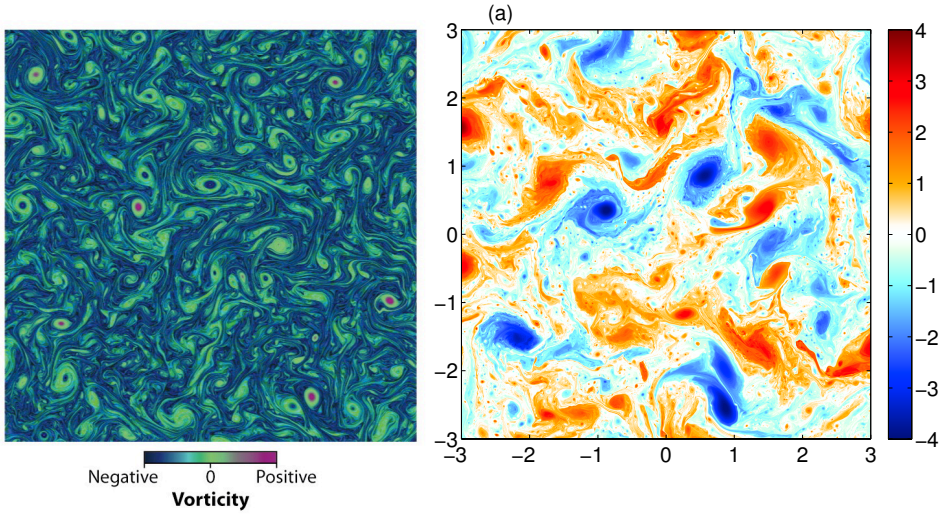

Figure 3.13: Comparison between 2D and SQG turbulence. Left: Snapshot of a vorticity field in a high-resolution numerical simulation of the 2D Navier-Stokes equations. Caption and sources copied from [2]. Right: surface quasi-geostrophic (SQG) turbulence. The plot shows surface buoyancy (an advected scalar analogous to the vorticity) in a freely-decaying simulation at a resolution of 1024×1024. Note that the vortices at all scales develop from a filament instability. Caption and sources copied from [29]

fig:2Dturbulence

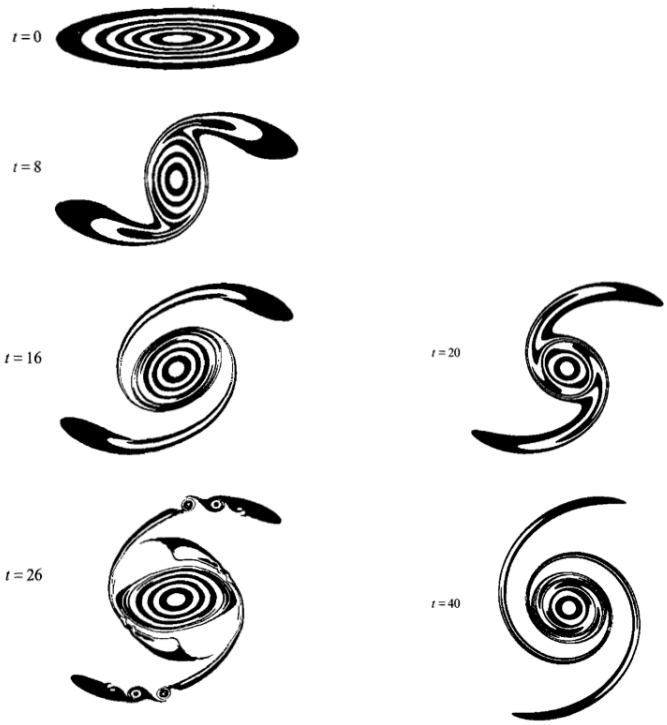

Figure 3.14: Evolution of an eccentric ellipse-like density perturbation (in terms of its temperature field) by the SQG flow (left) and 2D flow (right). Only in the SQG flow does the spinning vortex undergo a shear instability which leads to smaller scale vortices being shed. Caption and sources copied from [24]

:2Dvortices

3.4.7.2 3D-QG

To illustrate the common features of 2D and QG turbulence, [49] performed a series of simulations whereby QG turbulence simulations were forced at large scales (figure 3.15 right) to demonstrate a direct cascade of enstrophy from large to small scales, and forced at small scales produce an inverse cascade of energy to larger scales (figure 3.15 left). This dual cascade phenomena being characteristic of 2D turbulence [2]. In both cases vortices organise in elongated coherent vertical structures. This is due to an anisotropy linked to horizontal advection. This preferential direction along which the flow organise, shows how quasi-geostrophic turbulence (also referred to as Charney turbulence) behaves similarly to 2D turbulence.

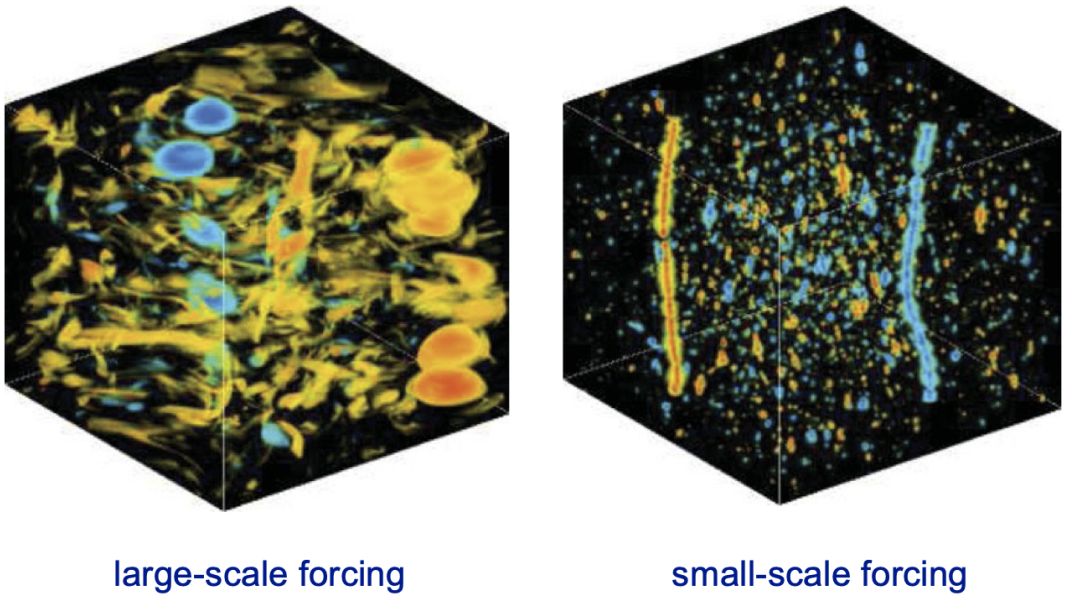

Figure 3.15: Snapshots of potential vorticity field of high resolution numerical simulation of 3D-QG with large-scale forcing (left) and small-scale forcing (right). Both simulations show self-orgnisation leading to dominating vertical structures with opposing signs, albeit more elongated for smaller scale forcing. Simulations from [49]

fig:3DQG

3.4.7.3 Vortices in the ocean

An example of coherent vortices in a stratified rotating flow are shown in figure 3.16. The Mediterranean sea where it extends into the Atlantic ocean provides a salty plume of water at around 1000 meters below the surface. This represents some sort of potential vorticity Q anomaly, which, then breaks up into eddies lasting a long time (they can even be observed on the other side of the Atlantic). As expected from the QG equations, these anticyclonic eddies can be seen in the velocity field (plot on the lower left), and have a corresponding structure in their stratification (density or temperature) field as well. Although the QG equations capture some of these dynamics, it is complicated to point to which process is the cause and which one is the consequence, as they evolve following $D_g Q/Dt$ and determined as prognostic variables from one another.

3.4.7.4 Vortices in the stratosphere

Following the Australian wildfire in 2020, smoke released into the atmosphere and gave rise to long lived vortices (several months), which circumnavigated the southern hemisphere (see figure 3.17). What was unusual about this event, was that it induced a stratospheric perturbation of the same order of magnitude as a volcanic eruption [27]. It is thought that the generation of anti-cyclonic vortices, occurred due to the particulate composition (carbon) of the smoke clouds, which led to substantial radiative heating. In the context of the potential vorticity equations, we have an extra forcing term that results into a coherent circulation of the vortex retaining the smoke in the atmosphere [27].

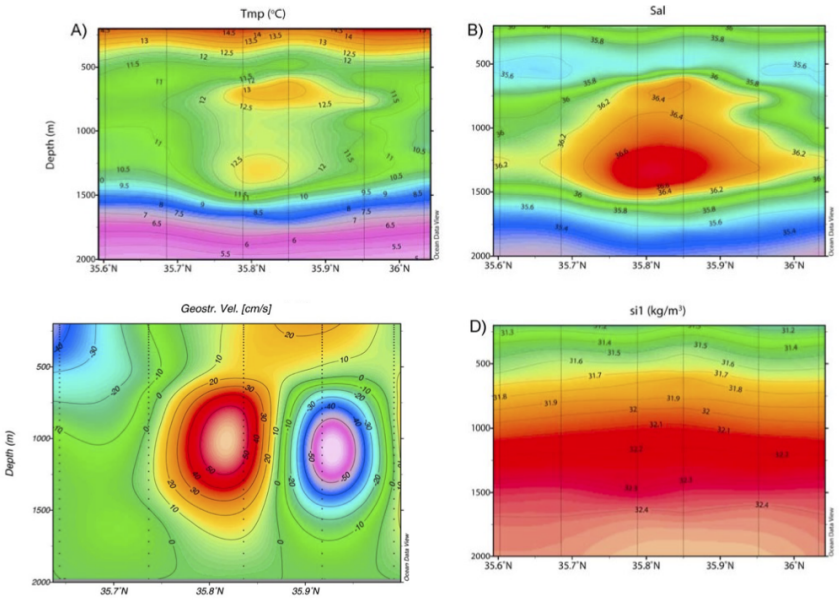

Figure 3.16: Vertical sections (latitude in degrees versus depth in meters) of (a) temperature, (b) salinity. (c) Geostrophic velocity across meddy, (d) density anomaly referenced at 1000 m depth [4]

fig:meddies

3.5 Spontaneous wave generation

pontaneous

So far, we have reduced our initial system of five freely evolving fields (*primitive equations*), given by five prognostic equations, to a system of three freely evolving fields (*shallow water equations*), given by three prognostic equations, to a system where we only have one prognostic equation and one evolving field. The potential-vorticity equation. From a dynamical systems perspective, we could now imagine our phase space as being simply a curve along which the system evolves *slowly*. But how precise is this picture? We can proceed in two ways.

3.5.1 Ertel's potential vorticity

The first approach, is to verify whether these equations are well-posed, meaning if we give the initial conditions, does the system remains well-behaved and definable for all successive times? An exact results is provided by Ertel's potential vorticity [50]. Given a hyrdodynamic invariant $\chi(\boldsymbol{x}, t)$ such that $D\chi/Dt = 0$, this statement says that for an inviscid fluid

$$\rho \frac{DQ}{Dt} = \nabla\chi \cdot \nabla p \times \nabla\rho^{-1}, \quad \text{when} \quad Q = \frac{\boldsymbol{\zeta_g} \cdot \nabla\chi}{\rho}. \tag{3.70}$$

By choosing the invariant χ to be a function of pressure and density only (typically potential temperature is used), we have $\nabla\chi \cdot (\nabla p \times \nabla\rho^{-1}) = 0$ such that $DQ/Dt = 0$. Consequently we can find a potential vorticity, without making any small Rossby number assumption, that is conserved. The caveat however, is that we cannot, without approximation, deduce the velocity, density or pressure fields directly from Q and thus are unable to determine the evolution of the flow.

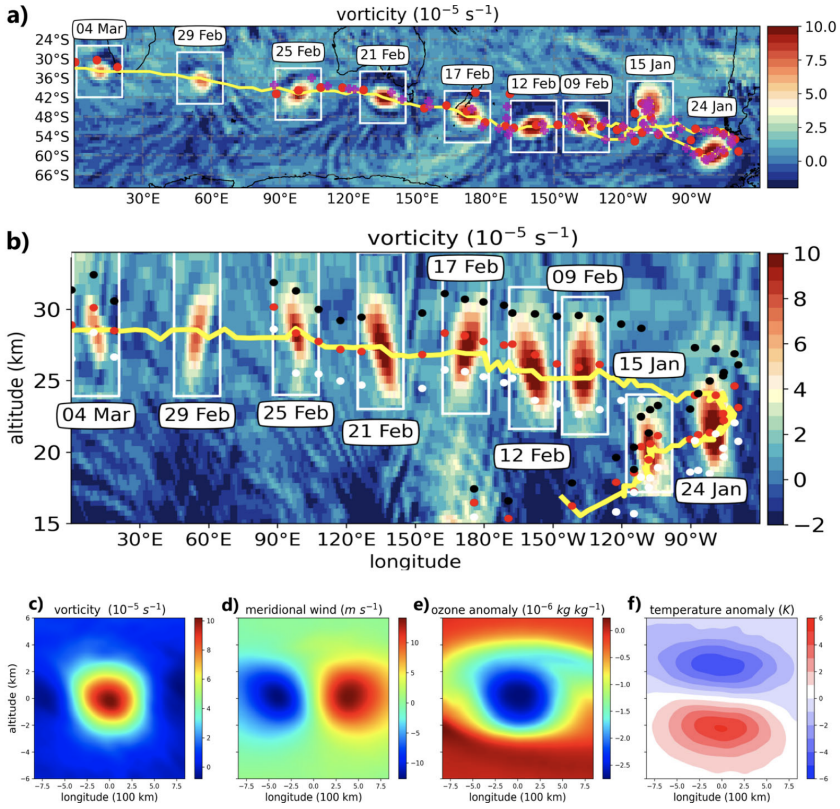

Figure 3.17: Spatio-temporal evolution and thermodynamic properties of the vortex generated by Australian wildfires in 2020. (a) Composite horizontal sections of the vortex in terms of its vorticity. (b) Corresponding vertical sections. (c-e) Composition of the vorticity, meridional wind, ozone and temperature anomalies in the longitude altitude plane [27].

fig:AustraliaWildfire

Because of the complexity of the problem, we can use an *approximate result* instead, where we consider some inversion operator L such that LQ gives us all the other flow quantities ($\boldsymbol{u}$, ρ, etc.). In this slow flow approximation, once we know L, we can predict the evolution of the system. However, there are two main limitations of considering these slow equations. The first is that in order to find a expression for the operator L, we typically must assume geostrophic $Ro \ll 1$ and hydrostatic balance. Should we try to generalise L for less restrictive assumptions the equations break down and finite-time singularities arise. An example of this is frontogenesis, whereby contrasts in velocity and buoyancy in a rapidly rotating fluid are concentrated into frontal regions [25, 45]. The second problem is that while the equations do not include the evolution of gravity waves, as they are fast evolving features (quasi-geostrophic approximation filters out gravity waves), both simulations [13] and models [52] report that even for well balanced initial data, the slow flow gives rise to a fast motion.

3.5.2 Breakdown of quasi-geostrophic balance

sec:BreakdownQGBal

The second approach to determining the precision of this picture is to prove, for the Boussinesq primitive equations (3.5), the existence of a 'slow' manifold [53], as sketched in figure 3.18. If such a manifold exists, it implies that a suitable initialisation can provide

a result that is inertia-gravity wave free, which in-turn justifies the description of the slow balanced flow by a model of reduced dimensionality. Although this is an attractive idea, we demonstrate in this section that even for $Ro \ll 1$, exponentially small inertia-gravity waves (IGWs) are excited, and hence the non-existence of an invariant slow manifold [52, 53]. Crucially this implies that the time-scale separation between a slow motion in hyrdostatic and geostrophic balance and fast inertia-gravity waves, is not exact.

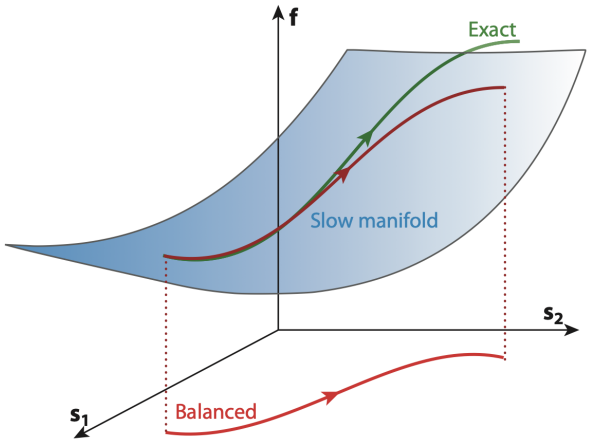

Figure 3.18: Schematic of the slow-manifold, in terms of slow $\boldsymbol{s}_1, \boldsymbol{s}_2$ and fast $\boldsymbol{f}$ state space variables. The slow manifold is often implicitly assumed to be the exactly invariant manifold, capturing the adjustment due to fast IGWs whilst simultaneously devoid of fast motion [53].

Due to the existence of an exact three dimensional solution, we consider Boussinesq primitive equations, for an inviscid fluid with rotation vector $\boldsymbol{f}$ constant and in the vertical. For the case of background stratification

$$\rho' = \rho_s(z) + \tilde{\rho}(\boldsymbol{x}, t), \quad p' = p_s(z) + \tilde{p}(\boldsymbol{x}, t), \tag{3.71}$$

and a uniform shear, (3.5) admits the solution

$$(u, v, w, \phi, B) = (\Sigma y, 0, 0, -\frac{1}{2} f_0 \Sigma y^2, 0), \tag{3.72}$$

eq:ShearSolution

where $\Phi = \tilde{p}/\rho_0$ and $B = -g\tilde{\rho}/\rho_0$ are used to denote the geopotential and buoyancy respectively and $-\Sigma$ is the constant vorticity of the uniform shear flow. Substituting (3.72) into (3.5) we look for plane wave solutions of the form

$$(u', v', w', \phi', B') = (u(t), v(t), w(t), \phi(t), B(t)) \exp^{i(k(x-\Sigma y t)+ly+mz)}, \tag{3.73}$$

eq:ShearPert

with a time-dependent wavenumber $k(t)$. Due to the particular form of (3.73), the nonlinear terms vanish such that the full PDE transforms into a set of linear ordinary differential equations (ODE)

$$\dot{u} + (\Sigma - f)v = -ik\phi, \tag{3.74}$$
$$\dot{v} + fu = -i(l - \Sigma kt)\phi, \tag{3.75}$$
$$\dot{w} - b = -im\phi, \tag{3.76}$$
$$\dot{b} + N^2 w = 0, \tag{3.77}$$
$$ku + (l - \Sigma kt)v + mw = 0, \tag{3.78}$$ eq:ShearDis

where $N^2 = -\frac{g}{\rho_0}\frac{\partial \rho_s}{\partial z}$, the buoyancy frequency is assumed to be constant. The disturbance solution is such that advection can only occur perpendicular to the plane $\boldsymbol{k}(t) \cdot \boldsymbol{x} = const.$ This ensures that disturbance quantities remain constant on a given plane. (3.78) which describes the evolution of five quantities, with four time-derivatives and one constraint equation. These can be written as a third order ODE. Due to the fact that the potential vorticity is constant in the basic state, we can further reduce this to the following second order, albeit non-autonomous, ODE

$$\ddot{\zeta} + b(t)\dot{\zeta} + c(t)\zeta = N^2 \frac{k^2 + (l - \Sigma kt)^2}{k^2 + (l - \Sigma kt)^2 + m^2}, \tag{3.79}$$ eq:Spontan

with

$$b(t) = \frac{2\Sigma k m^2 (l - \Sigma kt)}{[k^2 + (l - \Sigma kt)^2][k^2 + (l - \Sigma kt)^2 + m^2]}, \tag{3.80}$$
$$c(t) = \frac{(f - \Sigma)m^2}{k^2 + (l - \Sigma kt)^2 + m^2}\Big[f - \frac{2\Sigma k^2}{k^2 + (l - \Sigma kt)^2}\Big] + \frac{N^2[k^2 + (l - \Sigma kt)^2]}{k^2 + (l - \Sigma kt)^2 + m^2}, \tag{3.81}$$

where f is the Coriolis frequency and N the constant Brunt-Väisälä frequency (see [52] for details and derivation).

To consider the slow balanced motion we re-introduce the Rossby number, here defined as

$$\epsilon = \frac{|\Sigma|}{f} \ll 1, \tag{3.82}$$

to be a small parameter. A measure of the separation between the slow motion and IGWs this allows us to consider departures from the slow balanced motion. We define the Prandtl number and aspect ratio as

$$S = N^2/f^2, \quad \delta = m/k, \tag{3.83}$$

both formally $\mathcal{O}(1)$ and introduce the Froude number

$$F = \frac{|\Sigma|\delta}{N} = \epsilon \frac{\delta}{S^{1/2}} \ll 1, \tag{3.84}$$

also considered a small parameter, which implies than gravity wave inertia is much greater than the flow inertia induced by shear. Reflecting the fast rotation and strong stratification of the atmosphere and oceans, we focus on the quasi-geostrophic limit $\epsilon \ll 1, F = \mathcal{O}(\epsilon) \ll 1$ thus ensuring a formal frequency separation [53].

Finally by rescaling time $t \to t/|\Sigma|$ and choosing the origin of time such that $l = 0$, we obtain

$$\epsilon^2\big[\ddot{\zeta} + b(t)\dot{\zeta}\big] + c(t)\zeta = S\frac{1 + t^2}{1 + \delta^2 + t^2}, \tag{3.85}$$ eq:scaledOI

with

$$b(t) = \frac{-2\delta^2 t}{(1+t^2)(1+\delta^2+t^2)}, \tag{3.86}$$

$$c(t) = \frac{\delta^2(1\pm\epsilon)}{1+\delta^2+t^2}\left[1 \pm \frac{2\epsilon}{1+t^2}\right] + \frac{S(1+t^2)}{1+\delta^2+t^2}, \tag{3.87}$$

where the choice of sign $\pm$ distinguishes between anticyclonic ϵ and cyclonic shear $-\epsilon$. In this limit we can proceed in a standard way and perform a formal perturbation expansion in powers of ϵ. This yields the asymptotic but not convergent solution

$$\zeta_{bal} = \zeta_0 + \epsilon\zeta_1 + \mathcal{O}(\epsilon^2), \tag{3.88}$$

with

$$\zeta_0 = \frac{1+t^2}{1+\delta^2/S+t^2}, \quad \zeta_1 = \frac{\pm\delta^2(3+t^2}{S(1+\delta^2/S+t^2)}. \tag{3.89}$$

Alternatively we may consider the limit $t \gg 1$

$$\epsilon^2\ddot{\zeta} + S\zeta \approxeq S. \tag{3.90}$$

This limit is preferable as it leads to an unambiguous separation of the balanced motion and IGWs. The solution in this limit is given by

$$\zeta \sim 1 + C^{\pm}\cos(S^{1/2}t/\epsilon + \varphi^{\pm}), \tag{3.91}$$

eq:LargeT_limit

where $C^{\pm}, \varphi^{\pm} \in \mathbb{R}$ and the signs refer to the limits $t \to \pm\infty$. The constant term corresponds to the slow balanced motion, which is steady in the limit $|t| \to \infty$, as the effect of rotation vanishes. The rapidly oscillating term corresponds to the IGWs. While it is possible to prescribe $C^- = 0$ for $t \to -\infty$ this would require $C^- \neq 0$. This suggests that a connection formula exists for $C^+, \varphi^+ \iff C^-, \varphi^-$ which in-turn implies non-vanishing inertia gravity waves and thus the non-existence of an invariant slow manifold. Indeed by initialising (3.85) with ζ_{bal} and time integrating from $-T$ to T, for T sufficiently large, it is possible to numerically demonstrate the generation of IGWs in this model, despite starting from a well balanced state, as shown in figure 3.19.

In order to determine the amplitude of the IGWs generated it remains to calculate the constants defining the connection formula (3.91). While inertia gravity waves are not captured by ζ_{bal}, due to the exponentially small terms which arise, they can be determined by computing a WKB solution to (3.85) of the form

$$\zeta = \zeta_{igw} = (g_0 + \epsilon g_1 + \ldots)\exp(i\epsilon^{-1}\int_0^t \omega(t')dt'). \tag{3.92}$$

Substituting this expression into (3.85) and solving we find that the frequency, corresponding to inertia-gravity waves, is given by

$$\omega = \pm S^{1/2}(\frac{1+\delta^2/S+t^2}{1+\delta^2+t^2})^{1/2}. \tag{3.93}$$

The generation of IGWs is associated with the break down of the perturbation expansion solution, indicated by the dashed line in figure 3.19, which leads to the largest value of

$$\exp(i\epsilon^{-1}|Im\int_0^t \omega(t')dt'|). \tag{3.94}$$

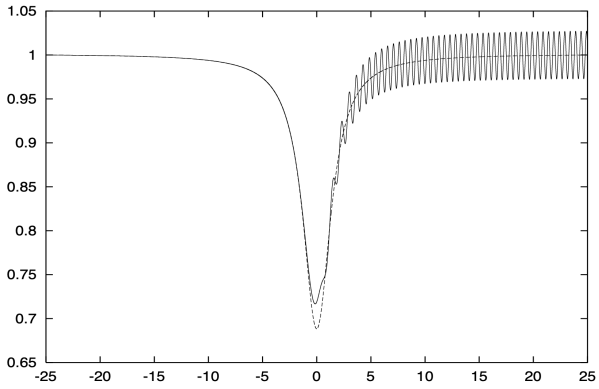

Figure 3.19: Time evolution of (3.85) for $S = \delta^2 = 10$ and $\epsilon = 0.25$. The true solution (solid line) remains well balanced and close to the approximate solutions (dashed line) until we reach $t \approxeq 0$, at which point the Stokes' line is reached at the generation of IGWs occurs [52].

fig:spontaneous_IGWs

For ζ_{bal} the singularity occurs for complex values of t given by the Stokes line

$$t = \pm t^* = \pm i(1 + \delta^2/S)^{1/2}, \tag{3.95}$$

at which the asymptotic solutions changes from exponentially small to exponentially large. By re-scaling and considering solutions near the singularity t^* and then matching with the balanced solutions it is possible to calculate the connection formula [52].

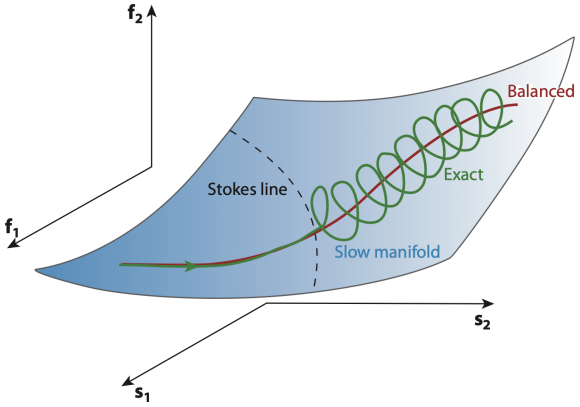

Figure 3.20: Upon crossing the Stokes-line the asymptotic solution changes from being exponentially small to exponentially large. By considering the WKB solution of (3.85) the oscillation amplitude is found to scale $\sim \exp(-\alpha/\epsilon)$ [53].

fig:StokesLine_SlowManifold

Having calculated the form of $\zeta = \zeta_{bal} + \zeta_{igw}$ we can take the limit $t \to \infty$, and comparing with the expression for (3.91) to find that

$$C^+ \approxeq \frac{2|K|}{S^{1/4}} \frac{e^{-\alpha/\epsilon}}{\epsilon^{1/2}}, \tag{3.96}$$

where $|K| \sim \mathcal{O}(1)$ is a constant. This establishes that IGWs exponentially small in Rossby number lead to the breakdown of quasi-geostrophic balance, and conversely that

IGW generation increases with increasing Rossby number. That no exact invariant slow manifold exists to describe this slow balanced motion for the particular case of the sheared Boussinesq equations is also consistent with the theory of dissipationless dynamical systems. This is in contrast for dissipative dynamical systems for which attracting slow manifolds can be routinely obtained [53].

Due to the small amplitudes and lengthscales of these waves, the numerical simulations (for $Ro \ll 1$ to ensure a balanced motion) which are required to capture exponentially small terms, become delicate. Nevertheless it is possible to exploit scenarios where only locally is $Ro \geq 1$ so as to conduct numerical observations of spontaneous wave generation. Using this idea [13] conducted simulations of ocean turbulence modelled by the primitive equations, subject to the Boussinesq and hydrostatic assumption. In their model IGWs are generated at the vertical surface, propagate downwards into the deep ocean where $Ro \ll 1$. Figure 3.21 shows a snapshot of the vertical velocity taken in the lower half of the domain, isolating the quasi-geostrophic and IGW contributions. Similarly figure 3.22 shows the latter stages of the evolution of a IGW wave-packet at 12h intervals. The appearance of larger vertical velocities is found to coincide with regions of strong relative vorticity. In both case the IGW motion is notably of a much smaller scale.

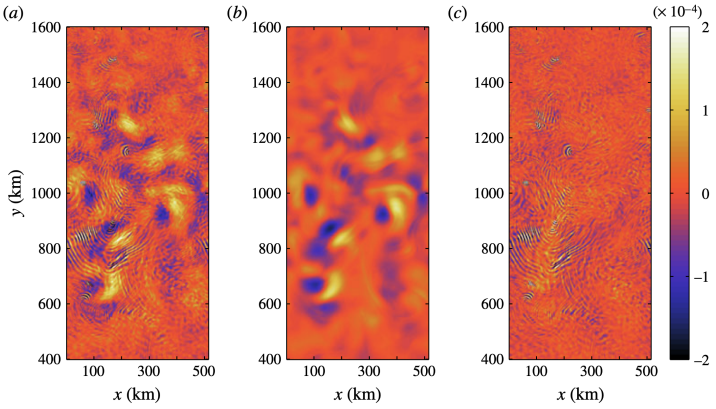

Figure 3.21: Large scale dynamics of the primitive equations arising from a baroclinic instability in terms of vertical velocity (measured in ms^{-1}). (a) total vertical velocity, (b) quasi-geostrophic contribution, (c) unbalanced motion contribution [13]

ocity_IGW

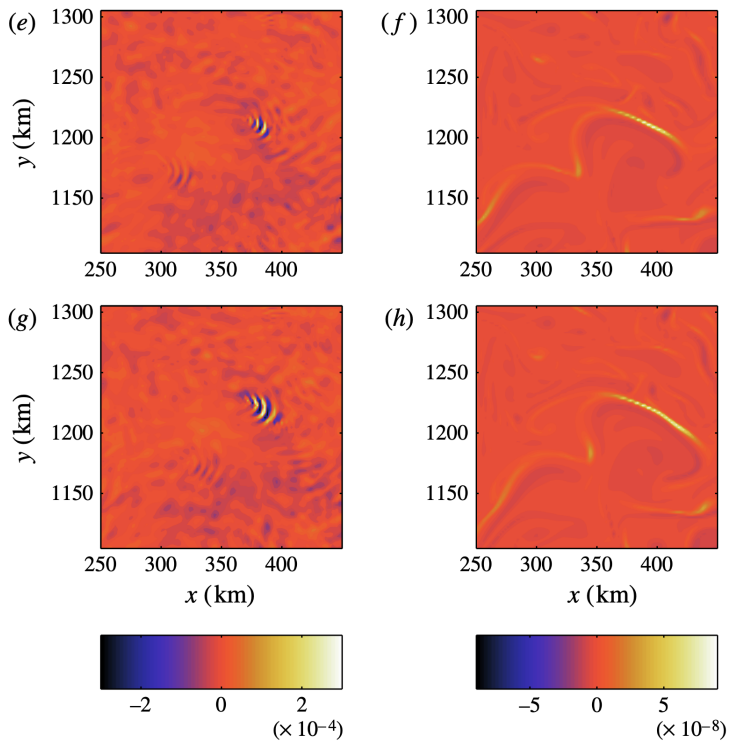

Figure 3.22: Generation and evolution of a IGW wave-packet by a vorticity filament from top to bottom. Left: unbalanced vertical vorticity, right: surface relative vorticity [13]

_WavepacketsVorticity_IGW

3.6 Wave propagation and wave mean-flow interaction

sec:WaveMeanFlow

To motivate this section and highlight the need to account for wave-mean flow interaction we start by considering slow waves, in a system with one time derivative, and subsequently make comparisons between observations and theoretical predictions. Rather than considering the full rotation vector $\boldsymbol{f}(\varphi)$ which has latitudinal dependence λ we restrict our analysis to its vertical component on the so called β-plane (see definition (3.10)). Making this approximation, the 2D vorticity equation on the β-plane is given by

$$\frac{\partial \zeta}{\partial t} + \boldsymbol{u}\cdot\nabla\zeta + \beta v = \mathcal{D}, \quad \text{where} \quad \zeta = \Delta\psi, \quad \boldsymbol{u} = (-\frac{\partial\psi}{\partial y}, \frac{\partial\psi}{\partial x}), \tag{3.97}$$

eq:2dVortic

and $\mathcal{D}$ is assumed to be a known linear dissipative term. Considering the case where the background state is at rest $\boldsymbol{u} = 0$ we linearise (3.97) and consider perturbations here denoted by tilde

$$\frac{\partial \tilde{\zeta}}{\partial t} + \beta\frac{\partial \tilde{\psi}}{\partial x} = 0. \tag{3.98}$$

Assuming these perturbations take the form of plane waves, that is $\tilde{\psi} = Re(\hat{\psi}\exp(i(kx + ly - \omega t)))$, we obtain the dispersion relation for Rossby waves

$$\omega = -\frac{\beta k}{k^2 + l^2}, \tag{3.99}$$

eq:disp_Ro

whose phase speed is always westward but their group speed can be eastward or westwards. As per section 3.4.4 in which variations of the fluid depth depending on latitude y were considered to investigate slow modes, we require that $\beta \neq 0$ to obtain Rossby waves.

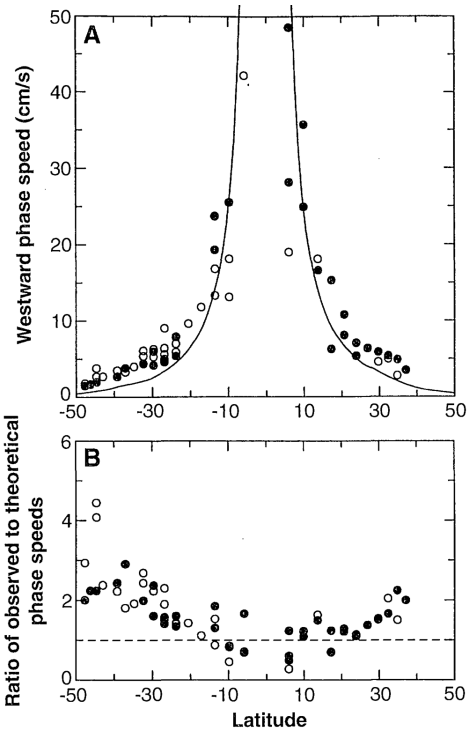

Figure 3.23: Comparison between theoretically predicted and observed Rossby wave phase speeds [5]. Hollow circles (Atlantic Ocean), solid dots (Pacific Ocean) and solid line (theoretical prediction). Theory and observation are found to systematically disagree outside the tropical latitudes $\pm 10^o$.

haseSpeeds

From (3.99) it can also be seen that their phase speed depends on latitude as confirmed in figure 3.23. Alternatively had we considered the shallow water equations, for which the vorticity $\zeta = \Delta^2\psi - \psi/L_R^2$, where $L_R^2 = gH/f_0^2$ is the Rossby radius of deformation, we would instead obtain

$$\omega = -\frac{\beta k}{k^2 + l^2 + 1/L_R^2}. \tag{3.100}$$

These waves are an essential communicator of information in the atmosphere and oceans, and describe the transient adjustment of the oceans circulation to large scale forcing [5]. Figure 3.23 compares theoretical predictions and observations from satellite altimetery at different latitudes for Rossby wave phase speeds. While the comparison is good for tropical latitudes $\pm 10^o$, their is systematic discrepancy for other latitudes

To understand the interaction of Rossby waves with the mean flow, we now consider perturbations to the basic flow $\boldsymbol{u} = (U(y), 0)$ in order to derive a wave activity relation for the quasi-geostrophic equations. This equation will serve to describe the propagation and dissipation of Rossby waves. The perturbed vorticity equation for this scenario is given by

$$\underbrace{\frac{\partial \tilde{\zeta}}{\partial t}}_{\text{L}} + \underbrace{U(y)\frac{\partial \tilde{\zeta}}{\partial x}}_{\text{L}} + \underbrace{(\beta - \frac{\partial^2 U}{\partial y^2})\tilde{v}}_{\text{L}} + \underbrace{\tilde{\boldsymbol{u}} \cdot \nabla \tilde{\zeta}}_{\text{NL}} = \underbrace{\tilde{D}}_{\text{L}} \tag{3.101}$$

eq:disturbance

where L, NL denote linear and nonlinear terms respectively. Introducing the overbar $\bar{()}$ and prime $()'$ notation, to denote the x mean and x dependent fluctuations about the

mean respectively we write the linearised equations as

$$\frac{\partial \zeta'}{\partial t} + U\frac{\partial \zeta'}{\partial x} + \bar{\zeta}_y v' = D'. \tag{3.102}$$

To demonstrate that waves can gain or loose energy from the mean flow in a reversible wave we multiply the previous expression by ζ', and average in x to obtain

$$\frac{\partial}{\partial t}(\frac{1}{2}\bar{\zeta'^2}) + \bar{\zeta}_y \overline{v'\zeta'} = \overline{\zeta' D'}, \tag{3.103}$$

eq:qprime_

where it is implicitly assumed that primed quantities are periodic in x. From the Taylor identity we have that

$$\begin{aligned}
\overline{v'\zeta'} &= \frac{\partial}{\partial y}(-\overline{u'v'}), \\
\overline{v'(\frac{\partial v'}{\partial x} - \frac{\partial u'}{\partial y})} &= \frac{\partial}{\partial y}(-\overline{u'v'}) + \overline{\frac{\partial v'}{\partial y}u'}, \\
&= -\frac{\partial}{\partial y}(\overline{u'v'}),
\end{aligned}$$

implying that the eddy momentum flux convergence is equal to the meridional flux of eddy potential vorticity (the last step follows from the horizontal divergence). Assuming the mean quantities are varying slowly in time (such as a flow in geostrophic balance), allows us to write (3.103) as a wave activity conservation relation

eq:Taylor_ID

$$\frac{\partial}{\partial t}(\frac{1}{2}\frac{\bar{\zeta'^2}}{\bar{\zeta}_y}) + \frac{\partial}{\partial y}(-\overline{u'v'}) = \overline{\frac{\zeta'}{\bar{\zeta}_y} D'}, \tag{3.104}$$

eq:Taylor_

$$\frac{\partial}{\partial t}(\mathcal{A}) + \frac{\partial}{\partial y}(\mathcal{F}) = \mathcal{D}_{\mathcal{A}}, \tag{3.105}$$

eq:wave_er

where $\mathcal{A}$ represents a wave activity density, $\mathcal{F}$ a wave flux and $\mathcal{D}$ dissipation of wave activity. We note that in contrast to the analysis carried out in 3.5.2, these results are independent of the WKB assumption, in that we do not require scale separation. Nevertheless it is helpful that (3.105) be consistent when there is scale separation. This is ensured by satisfying the group velocity property $\langle \mathcal{F} \rangle = \langle \mathcal{A} \rangle c_g$, where $\langle . \rangle$ is used to denote a phase average. This removes the gauge freedom in $\mathcal{F}$, defined only up to a constant/divergence free wave flux.

It is noteworthy that the term quadratic in $\boldsymbol{u}$ is akin to a Reynolds stress terms. Typically these appear when considering fluctuations about a mean in turbulent flows. For this particular case the terms resemble those obtained if $v \cong 0$ for the quasi-geostrophic equations. Much like the Reynolds stresses, this terms plays the role of extracting energy from the mean flow, suggesting an intimate connection between the propagation of waves and the forcing of the mean flow. Indeed for $\overline{u'v'} < 0$ we have northward group propagation and conversely southward group propagation for $\overline{u'v'} > 0$. Generally these relations between group propagation and eddy fluxes hold only under the usual $Ro \ll 1$ assumption.

To expand on the connection with group propagation we consider the forcing of a mean flow in x due to waves. Writing the x component of the primitive equations as

$$\frac{\partial u}{\partial t} + \frac{\partial}{\partial x}(u^2) + \frac{\partial}{\partial y}(uv) - fv = -\frac{\partial}{\partial x}(p/\rho), \tag{3.106}$$

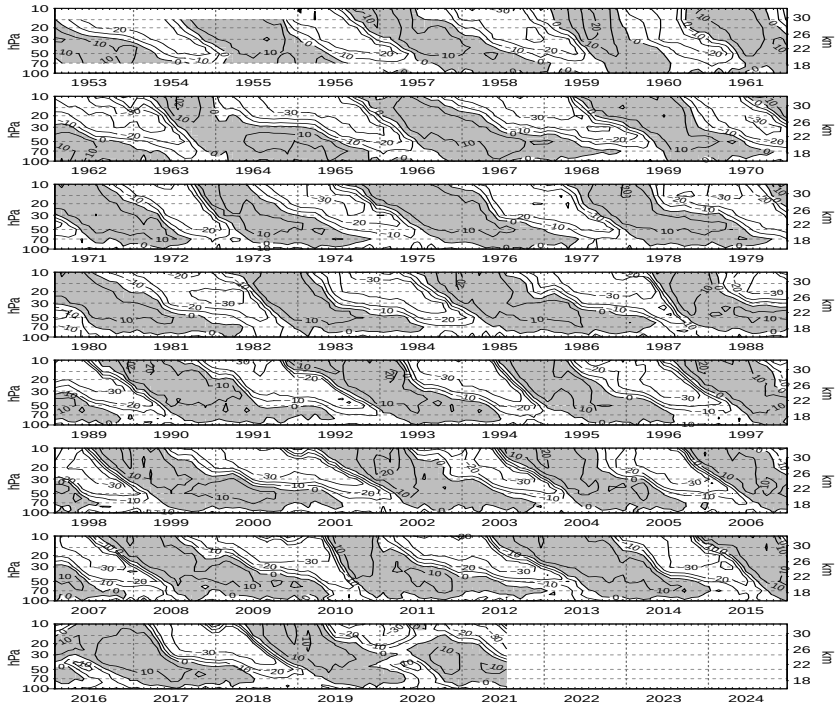

Figure 3.24: Time-height section of monthly mean zonal winds (m/s) at equatorial stations: Canton Island, $3^oS/172^oW$ (Jan 1953 - Aug 1967), Gan/Maledive Islands, $1^oS/73^oE$ (Sep 1967 - Dec 1975) and Singapore, $1^oN/104^oE$ (since Jan 1976) Source:Fu-Berlin Atmospheric Dynamics Group

eries_FUB

expanding variables as $\chi = \bar{\chi} + \chi'$ in terms of their mean and fluctuating components, and averaging in x we have

$$\frac{\partial \bar{u}}{\partial t} = -\frac{\partial}{\partial y}(\overline{u'v'}) = \frac{\partial}{\partial y}(\mathcal{F}^{(y)}), \tag{3.107}$$

eq:meanflow_energy

where the terms on the right hand side are the momentum flux and wave activity flux respectively. From this we have that the force experienced by the mean flow is equal to the divergence of wave activity flux. Or alternatively the force acting on the mean flow due to the eddies. Combining expressions (3.105) and (3.107) we arrive at the *non acceleration theorem*

$$\frac{\partial \bar{u}}{\partial t} = \mathcal{D}_{\mathcal{A}} - \frac{\partial \mathcal{A}}{\partial t}, \tag{3.108}$$

eq:non_acceleration_theorem

which implies that unsteadiness or dissipation are essential in order to induce a force on the mean flow. While (3.108) applies generally, the form of terms $\mathcal{D}_{\mathcal{A}}, \mathcal{A}$ including their sign may differ when considering different scenarios such as stratification for example. In particular it is worth noting that the right hand side of (3.107) is a non-local function of its argument $\boldsymbol{u}$, thus it captures the non-rotating component of the system including internal gravity waves (should stratification be included), but makes it challenging to predict the dependence of $\overline{u'v'}$ on $\bar{u}$.

As discussed by [37] this interaction of multiple internal waves with a mean flow can be used to explain phenomena including the quasi-biennial oscillation (QBO). Shown in the time-height sections of figure 3.24, this oscillation is seen to represent the alternation of the equatorial zonal wind between easterlies and westerlies.

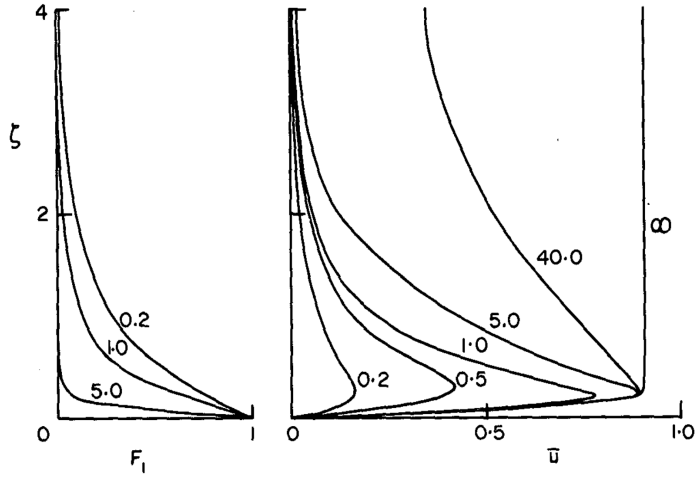

Figure 3.25: Profiles of the mean velocity $\overline{u}$ and wave momentum flux F for a single wave forcing with $\Lambda = 0.1$. The vertical co-ordinate ζ denotes height and the curves are labeled with time [37]. (* ζ is used to denote height in this instance only)

fig:QBO_PLUMB_OneWave

In this case internal gravity waves provide a force on the mean flow causing it to change form. If this change does not result in an equilibrium, we arrive at a situation reminiscent of relaxation oscillations. Whereby the form of the waves supported changes due to the mean flow's change which in turn results in further changes of the waves. To model this phenomena, [37] considered the 2D (x, z) interaction of two internal waves, with and without dissipation, for the primitive equations with uniform mean density. Assuming waves of the form $\psi_i = Re(\hat{\psi}_i(z)\exp(ik_i(x - c_i t)))$, the adjustment of the mean flow is given by

$$\frac{\partial \overline{u}}{\partial t} - \nu \frac{\partial^2 \overline{u}}{\partial z^2} = -\sum_i \frac{\partial F_i}{\partial z}, \tag{3.109}$$

$$F_i(z,t) = F_i(0)\exp(-\int_z^0 \frac{N\mu}{k_i(u(z',t) - c_i)^2} dz'), \quad i = 1, 2, \tag{3.110}$$

eq:Plumb19

where F_i denotes the wave momentum flux, ν the viscosity, N the buoyancy frequency and μ the thermal dissipation rate. Figures 3.25 and 3.26 contrast the results of the model comprising a one and a two wave nonlinear integration for varying degrees of the dissipation parameter Λ. The results of their model highlight that multi-wave interactions and dissipation in the critical layer (see section 3.6.1) are both required to realise this phenomena.

Laboratory realisations of spontaneous flow reversals mimicking the QBO mechanism have been conducted by GFD-online courtesy of (Satoshi Sakai, Isawo Iizawa, Eiji Aramaki). In their experiment a chamber of stratified salt-water is is actuated at its surface by a rubber membrane, thus creating an internal gravity wave and a mean current. When actuated at a sufficiently large amplitude reversals of the mean flow induced are observed.

3.6.1 The Rossby wave critical layer problem

sec:CriticalLayer

In this section, we consider a simple mathematical model to describe Rossby waves propagating in a shear flow. This could be in the extra tropical atmosphere where waves

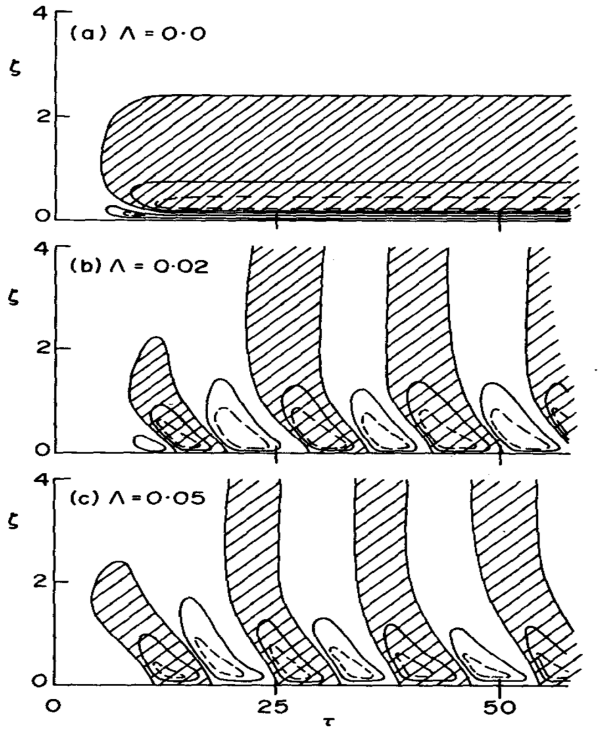

Figure 3.26: Nonlinear integration of the model (3.110) presented in terms of time(τ)-height(ζ) series of the mean zonal velocity $\overline{u}$ for varying values of the dissipation parameter $\Lambda = \frac{\nu N \mu}{kcF_0}$. In the absence of dissipation no critical levels/layers occur and the wave driving is weakened [37]. Only by allowing for dissipation can the waves incident on the critical layer induce a force on the mean flow. (* ζ is used to denote height in this instance only)

Dissipation

propagate upwards from the troposphere to the stratosphere and the background wind, here modeled as a shear flow, changes intensity with height. As we have seen in the previous section, including non-linearity and dissipation is an essential ingredient to resolving the dynamics in these critical layers and thus explaining phenomenon such as the quasi-biennial oscillation [37].

The simple model considered consists of the flow configuration schematized in figure 3.27, where the flow $U(y)$ is eastward and increases for positive y and is westward and decreases for negative y with a change of sign at $y = 0$. At the top of the figure, there is a wave source, which generates Rossby waves propagating towards the bottom of the figure with a defined phase speed c. In this situation, Rossby waves can propagate only if the flow speed is greater than the phase speed. When they reach the critical layer of speed inversion $y = 0$, waves will get trapped at the latitude and cannot propagate in the region where we have a mean flow in the opposite direction (only evanescent waves exist here with decaying amplitude). In the narrow region around the critical line, the streamlines are closed and assume the typical pattern named *Kelvin's cat's eye*.

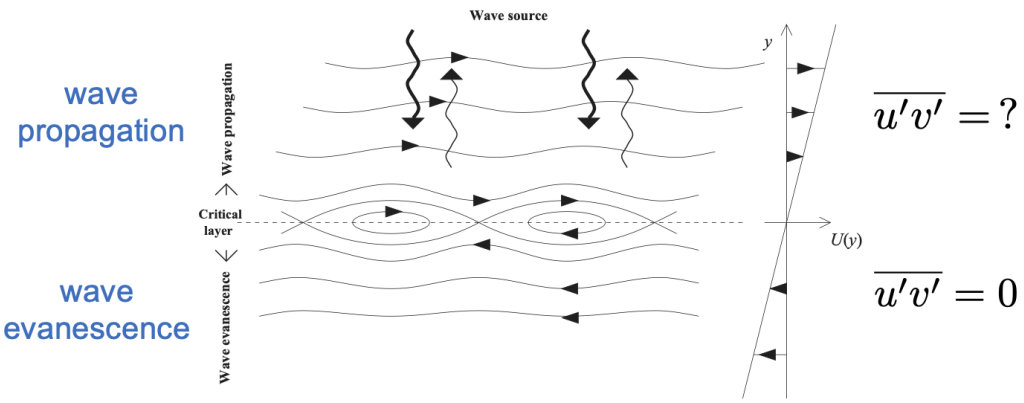

Figure 3.27: Schematic diagram of Rossby-wave propagation on a shear flow $U(y)$ with a critical line. Figure and caption taken from [35].

fig:cat-eye

To determine the waves contribution to the mean flow in terms of the momentum flux $\overline{u'v'}$, we define the streamfunction ψ such that the relative vorticity is $\zeta' = \Delta\psi'$, and assume the waves propagate steadily in the x direction such that their contribution to the streamfunction can be written in the form $\psi' = Re(\hat{\psi}(y) \exp ik(x - ct))$. Then the linearised and dissipativeless part of equation (3.101) for this system reads

$$\frac{\partial^2 \hat{\psi}}{\partial y^2} - k^2 \hat{\psi} = \hat{\psi} \frac{(\beta - \frac{\partial^2 U(y)}{\partial y^2})}{U(y) - c} \tag{3.111}$$

eq:cat1

with k small. The differential equation (3.111) has a singularity in $U = c$ (with $c = 0$ in the particular example considered here). Such singularities can arise in a system when the equations are simplified via approximations that neglect some terms. In this case it is the neglect of higher order nonlinear and dissipative terms, akin to those observed in the study of boundary layers, which we must now include to correctly resolve the flow. Nevertheless, it is worth emphasising that outside the singular region the approximations made hold since the effects of the neglected terms are small. Close to the critical layer, which can be described as a region of defined small thickness in the vicinity to the line

$U = c$, other physical processes need to be included. Which of the processes is dominant and should be added back into the system to resolve the system? All the terms ignored are those necessary to have a forcing by the waves on the mean flow. It follows that such forcing can only happen in the critical layer, where non-linearities and/or dissipation become important.

Considering $U(y) = \Lambda y$, with $\Lambda > 0$, $c = 0$, and k small, (3.111) reduces to

$$\frac{\partial^2 \hat{\psi}}{\partial y^2} = \hat{\psi}\frac{\beta}{\Lambda y}. \tag{3.112}$$

eq:catex2

Near $y = 0$ we have a mild singularity with $\hat{\psi} \sim O(1)$ and $\frac{\partial \psi}{\partial y} \sim \mathcal{O}(\log|y|)$. Taking a Frobenius expansion we can find two solutions, one for positive and one for negative y

$$y > 0: \quad \hat{\psi} = \epsilon\left(A\left(1 + \frac{\beta y}{\Lambda}\log|y| + ...\right) + B_+(y + ...)\right), \tag{3.113}$$

$$y < 0: \quad \hat{\psi} = \epsilon\left(A\left(1 + \frac{\beta y}{\Lambda}\log|y| + ...\right) + B_-(y + ...)\right), \tag{3.114}$$

where we neglected higher order terms and it is understood that each solution must decay as $y \to \pm\infty$. To determine the relation between the coefficients B_+ and B_-, the solutions must match at $y = 0$ to ensure continuity. This demands that we consider the possible balances arising for (3.101) in the critical layer. Letting $V(0) = k\hat{\psi}$, we have

$$\text{linear dynamics:} \quad V(0)\beta \sim \Lambda y k \zeta, \tag{3.115}$$

$$\text{non linear dynamics:} \quad u\frac{\partial \zeta}{\partial x} \sim V(0)\log|y|\frac{V(0)\beta}{\Lambda y}, \tag{3.116}$$

$$v\frac{\partial \zeta}{\partial y} \sim V^2(0)\frac{\beta}{\Lambda k y^2}, \tag{3.117}$$

implying that the non linear terms cannot be neglected when $V(0)/(\Lambda k y^2) \sim 1$. Owning to the assumed smallness of the dissipation term $\mathcal{D} \sim \alpha\zeta'$, it is subdominant to the nonlinear terms. An estimate for the width of the critical layer is thus given by the balance between the linear and non linear terms

$$y \approx \left(\frac{V(0)}{k\Lambda}\right)^{1/2}, \tag{3.118}$$

and corresponds to the width of the closed streamline region in figure 3.27. We can re-scale the equations by considering the small parameter ϵ, such that the thickness of the critical layer is $O(\epsilon^{1/2})$. If $V(0) = \epsilon V$, then

$$y = \epsilon^{1/2}Y, \quad t = \epsilon^{-1/2}T, \quad \zeta = \epsilon^{-1/2}\Xi. \tag{3.119}$$

The non dimensional equation describing the evolution within the critical layer is

$$\frac{\partial \Xi}{\partial T} + Y\frac{\partial \Xi}{\partial X} + V\frac{\partial \Xi}{\partial Y} = 0, \tag{3.120}$$

where V is only a function of x and is not changing rapidly within the critical layer. We can now match the flow outside the critical layer (approaching it from the two sides)

$$\left[\frac{\partial \psi}{\partial y}\right]_{0_-}^{0^+} = B_+ - B_- = \int_{-\infty}^{+\infty} \Xi dY, \tag{3.121}$$

by enforcing exponential decay for $y < 0$ setting $A = \lambda B_-$ and that $\mu A + \nu B_+ = \hat{\psi}(0)$, where λ, μ, ν are known constants. We now have all the necessary information to determine the constants B_+ and B_-. a few sentences needed here to connect the analysis with the following example.

The the momentum flux $\overline{u'v'}$ is a measure of the wave propagation. The critical layer at first acts like an absorber of the waves and eventually as a reflector, as schematically represented in figure 3.28. In regions where $\overline{u'v'} > 0$, waves propagate southward, and the opposite, i.e. waves propagate northward, where $\overline{u'v'} < 0$. The vorticity controls whether the layer is absorbing or reflecting.

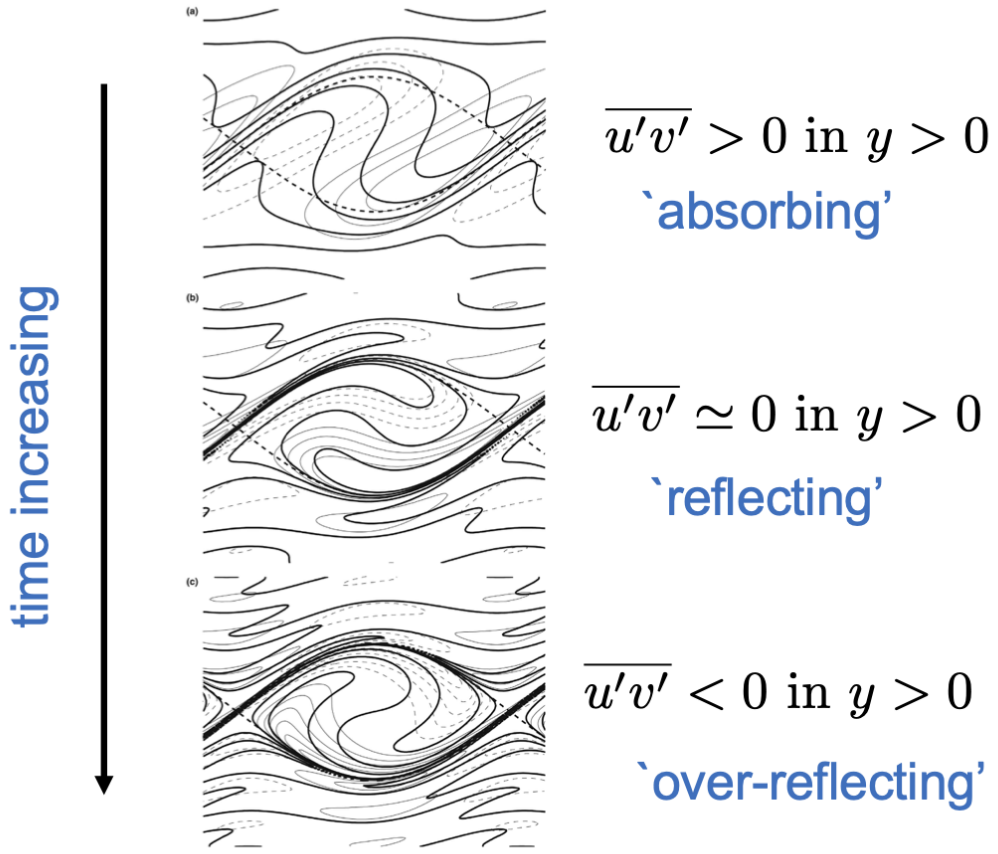

Figure 3.28: Time evolution of the vorticity field in the critical layer. Thick dotted curves are the bounding close streamlines. Thick solid curves are contours of absolute vorticity $\zeta + \beta y$. Thin curves are contours of wave relative vorticity ζ', with solid curve indicating positive values and dashed curves indicating negative values. Figure and caption adapted from Encyclopedia of Atmospheric Science [35].

fig:cat-evolution

When the distortion of the streamline in the critical layer is so strong that it becomes irreversible, there is a wave breaking phenomenon that can lead to geostrophic turbulence. An example of Rossby wave breaking is shown in figure 3.29. Numerical simulations by [31] indicate that when small-scale instabilities are allowed to grow the potential vorticity field Q is rearranged irreversibly. The mixing of vorticity in the critical layer implies a negative anomaly in the flow. There is an analogy between the potential vorticity and

the velocity of the flow, shown in figure 3.29(b) and (c).

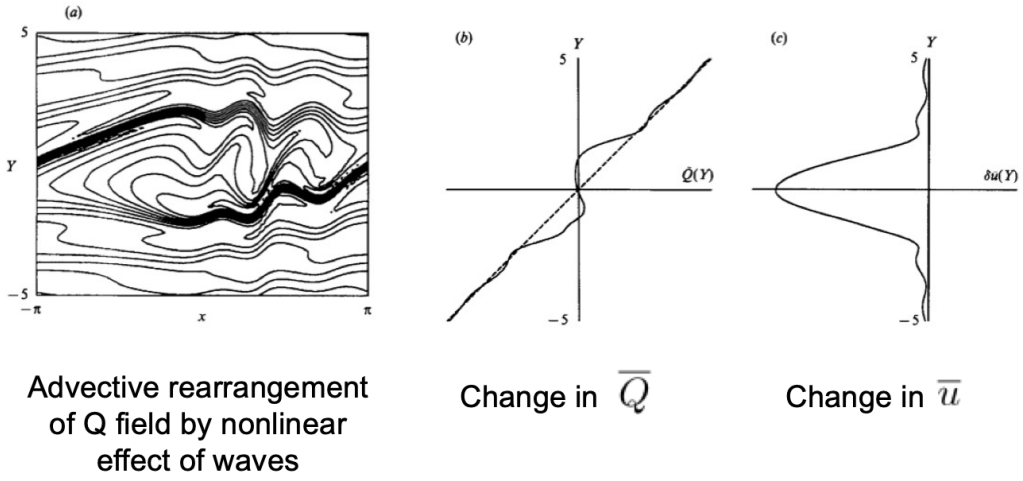

Figure 3.29: (a) Coutours of Q or ζ in the narrow critical layer region of an inviscid, nonlinear Rossby-wave critical layer simulations. (b) Eulerian-mean initial (dashed) and present (solid) $\overline{Q}(y)$ profiles. (c) Eulerian-mean flow change $\delta\overline{u}(y)$ that results from the rearrangement. Figures and caption taken from [31].

fig:cat-QU

3.7 2D flow on a β-plane

sec:jets

Let us consider again the vorticity equation for a 2D flow on a β- plane

$$\frac{\partial \zeta}{\partial t} + \boldsymbol{u}\cdot\nabla\zeta + \beta\frac{\partial \psi}{\partial x} = \xi + D\zeta, \tag{3.122}$$

eq:vorticityJet

where we have introduced an additional forcing term ξ, which could be a stochastic forcing, and the dissipation that can be expressed as hyperviscosity $D = \nu_n\Delta^n$. The relative vorticity and velocity are expressed in terms of the stream function as

$$\zeta = \Delta\psi, \quad \boldsymbol{u} = \left(-\frac{\partial \psi}{\partial y}, \frac{\partial \psi}{\partial x}\right). \tag{3.123}$$

This system has no pre-imposed mean flow, so the initial state has no particular structure or pre-imposed length scales. Letting the flow evolve under (3.122) in a doubly-periodic domain, subject to a small scale stochastic forcing, the flow naturally assembles into a set of jets as shown in figure 3.30. The eddy mean flow interaction has organised the flow in a series of alternating jets, presenting an asymmetry with narrow eastward jets, associated with a sharp jump in the potential vorticity, and broader westward jets, associated with a constant potential vorticity. Because they are mostly organised along the east-west direction, they are also called *zonal jets*. Due to its ability to capture the formation and dynamics of such jets, the β-plane is a particularly useful model given its simplicity. In contrast to the 3D primitive equations, which generate turbulence via its internal dynamics (the interaction between a slow balanced flow and the fast internal gravity waves) a stochastic forcing must be applied.

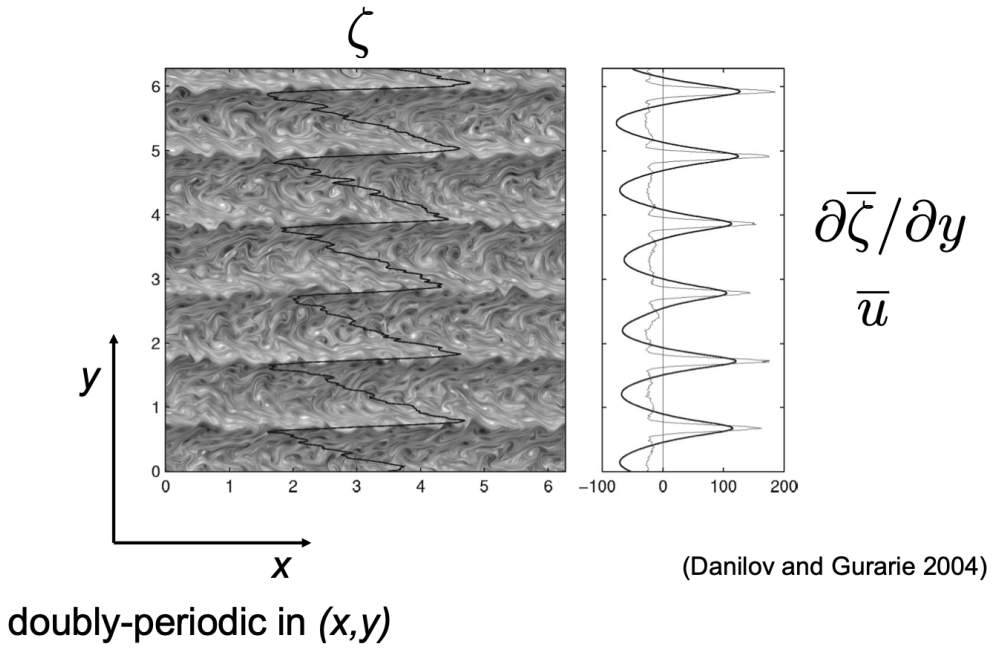

Figure 3.30: Snapshot of the vorticity field with superimposed instantaneous zonal mean vorticity profile. Right panel, $\langle d\zeta(y)/dy\rangle$ (thin line) averaged over 100 units centered around the snapshot time and zonal velocity (thick line) multiplied with 100 to fit the same axes. Figure and caption reproduced from [12].

fig:jets

β-plane jets were initially discovered in the '70s in the seminar paper by [40], and research has since focused on the mechanisms responsible for the formation and maintenance of such jets. The classical explanation relies on there being an upscale energy cascade in 2D turbulence (see review [2]). Energy is injected at smaller scales by the forcing, then is transferred to larger scales until it reaches a scale at which the β effect becomes important. This halts the upscale cascade with the consequent formation of these jets, exemplifying self-organisation with the creation of long-lived coherent structures. Some examples of jets are the typical structures on Jupiter, as it can be seen in frame (a) of figure 3.31.

Jets are also important for atmospheric and ocean flows and despite being observed in several locations they are still not well understood. A combination of model and observational data in figure 3.31(b) show multiple jet structures in the Southern Ocean. Observations by [11] of flow as a function of latitude and depth are shown in figure 3.31(c), where red marks the eastward and blue the westward flow, revealing that the jets are rather deep.

3.7.1 Energy and length scales

sec:jetsenergy

To estimate relevant length scales for the jet systems, we can consider the ratio between the terms in the vorticity equation (3.122). The ratio between the advection and the β term gives the *Rhine scale*

$$L_{Rh} = \left(\frac{U}{\beta}\right)^{1/2}, \tag{3.124}$$

(a)

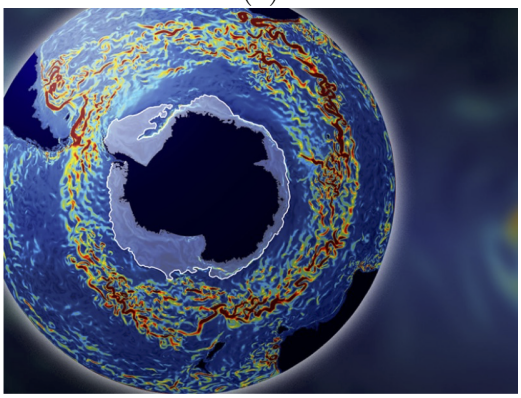

(b)

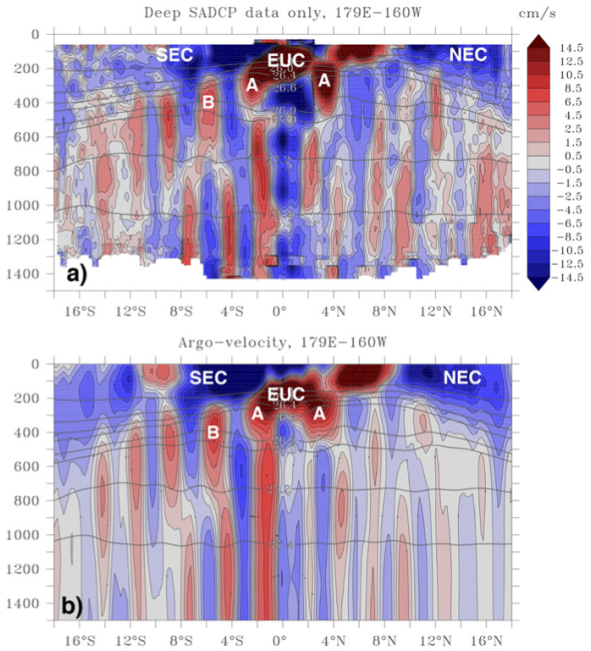

(c)

Figure 3.31: (a) Jets and vortices on Jupiter captured by the Juno mission (source NASA JPL). (b) Map showing the speed of the clockwise Antarctic Circumpolar Current on May 12, 2006, increasing from slow-moving water (blue) to water moving more than one mile per hour (dark red). The map is obtained via a state-of-the-art ocean circulation model to produce estimates of ocean conditions of greatly increased accuracy. The model can merge sparse observations of the Southern Ocean and fill in the blanks to describe the flow in places where no observations have been taken. Figure from Mazloff/San Diego Supercomputer Centre. (c) frame-a) Mean zonal currents in the Equatorial Ocean as a function of depth and latitude. frame-b) Mean absolute geostrophic zonal currents. Figure and caption adapted from [11].

fig:jetEX

which is related to the latitudinal scale of the jet. The typical velocity U could be, for example, the square root of the mean kinetic energy, or the strength of the mean flow. Another problem is that the Rhine scale is not predictive, in the sense that it gives the width of the jet but only from the measured quantities of the flow, i.e. we require a good estimate of U a-priori.

Another important parameter is the given input energy rate ϵ, and the related scales and energy are

$$L_\epsilon = \left(\frac{\epsilon}{\beta^3}\right)^{1/5}, \quad E_\epsilon = \left(\frac{\epsilon^2}{\beta}\right)^{2/5}, \tag{3.125}$$

which indicates the scales at which the eddies forced at input scales will feel the β-term. L_ϵ is analogous of the Ozmidov scale in stratified turbulence. Given a damping rate μ, the ratio between the energy input rate and the dissipation rate gives the total energy

$$E_\mu = \frac{\epsilon}{\mu}, \tag{3.126}$$

which can also give an estimate for the Rhine scale

$$L_{Rh,\mu} = \left(\frac{\epsilon}{\mu\beta^2}\right)^{1/4} . \tag{3.127}$$

The scale interval between $L_{Rh,\mu}$ and L_ϵ is defined as *zonostrophic inertial range*. The ratio between the two defines the *zonostrophy parameter*

$$R_\beta = \frac{L_{Rh,\mu}}{L_\epsilon} = \left(\frac{\epsilon\beta^2}{\mu^5}\right)^{1/20} . \tag{3.128}$$

If R_β is small there is no jet formation, if it is large strong and persistent jets can form.

A long term evolution of the energy and vorticity field is shown in figure 3.32. This illustrates that following jet formation at the beginning, there is an inverse cascade where jets merge until a final equilibrium is reached. The energy is equally partitioned between the mean flow and the eddies. For the frictionless run ($\mu = 0$), the total energy keeps increasing and the flow is unsteady. The jets in this case are observed to undergo repeated merging events and because the energy keeps increasing, the zonostrophy also increases leading to the jets becoming stronger and stronger.

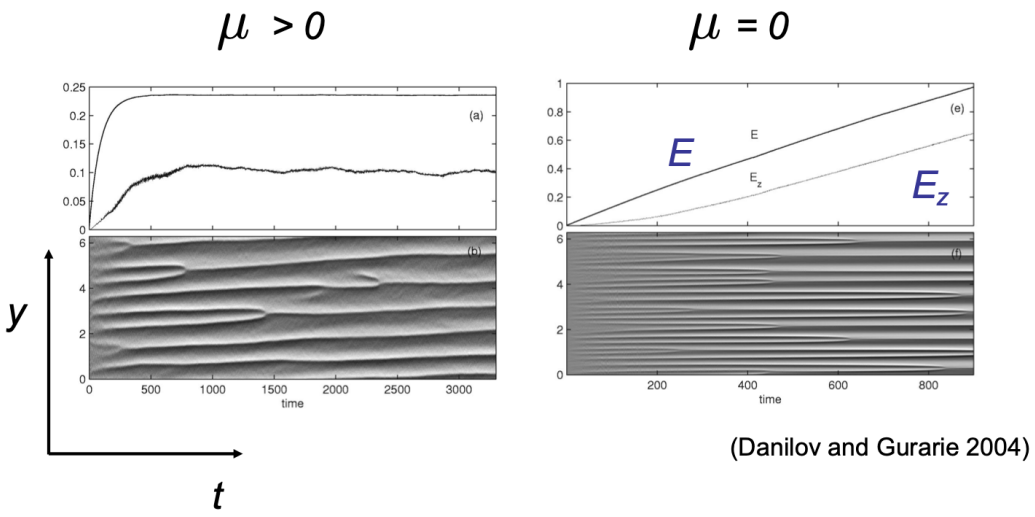

Figure 3.32: Long term evolution of energy frames (a), (e) and the corresponding zonal vorticity frames (b),(f). Left bottom-drag run $\mu > 0$ and right the frictionless run $\mu = 0$. E is the total energy, and E_z the energy in the zonal flow. Figures and captions are taken from [12].

fig:jetEvo

3.7.2 Jet formation mechanisms

sec:JetFormation

So far, we have described some properties of the jets and looked at their time evolution, without discussing how such jets can form. There are two alternative ways of thinking of the effect of waves on the mean flow, which can be used to describe jet formation [17].

The first one is a *momentum flux description*. This description considers the quantity $\overline{u'v'}$, which is related to wave propagation as a long term momentum transport

$$\frac{\partial \overline{u}}{\partial t} = -\frac{\partial}{\partial y}\left(\overline{u'v'}\right) . \tag{3.129}$$

There is a force exerted on the flow where the waves are being generated, and the effect of such force is transmitted by momentum flux through wave propagation to the region where waves are dissipated, which is where the flow changes.

The second way of thinking is a *potential vorticity (PV) flux description*. In this description, the flow changes are related to the local mixing of potential vorticity (here equivalent to the relative vorticity ζ)

$$\frac{\partial \overline{\zeta}}{\partial t} = -\frac{\partial}{\partial y}\left(\overline{v'\zeta'}\right), \tag{3.130}$$

via the Taylor identity (see 3.104). A schematic way of representing this mechanism, drawn in figure 3.33, relies on the fact that jets have constant potential vorticity between them. In regions of strong mixing the background gradient of PV is weakened, facilitating further mixing. Conversely it is strengthened where the background gradient of PV is large, inhibiting further mixing. This leads to a positive feedback giving rise to a self-reinforcing mechanism, closely related to the Philips effect [17]. PV gradients are large in eastward jets and small in westward jets. In this way, we have the formation of a potential vorticity staircase, which is equivalent to a set of jets.

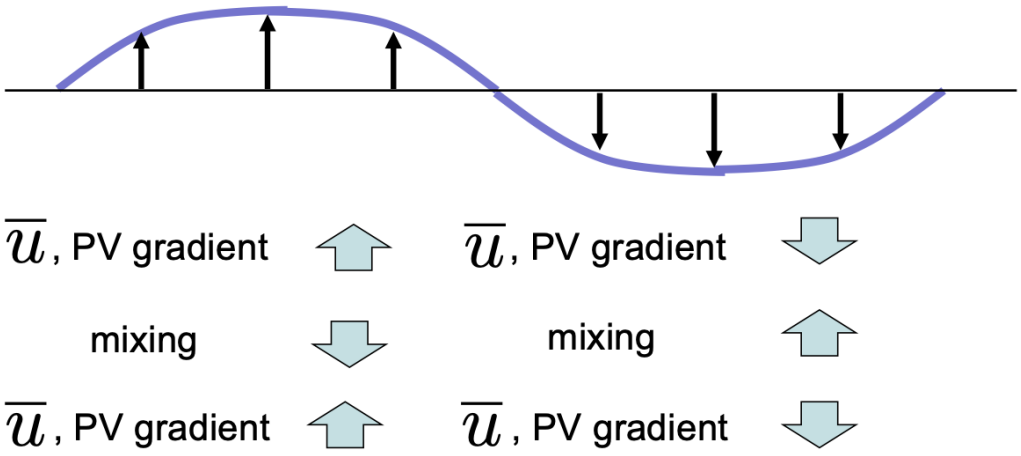

Figure 3.33: PV mechanism for jet formation, whereby the self-reinforcement of PV gradients arises due to decreased mixing.

-jets-sketch

Figure 3.34 sketches and example of how the PV staircase forms. The red dashed line shows the initial PV profile, and the red solid line is the final PV. In the top drawing, the eddies mix the PV, resulting in regions higher and lower gradients depending on whether mixing is favoured of inhibited. The self-reinforcing mechanism further increases and decreases the mixing in such regions, so that the more extreme situation depicted in the bottom drawing can occur. Here, the velocity field has reached the state of asymmetric zonal jets, and steep potential vorticity gradients are co-located with jet core regions.

Such staircase formation is indeed reproduced by numerical simulations [12] and [41] (see figure 3.35). The PV profile reveals a time evolution from a linear to a staircase shape, where the size of the constant regions is expanding, as it can be seen from the plot of latitude potential vorticity in time (figure 3.35 (f)).

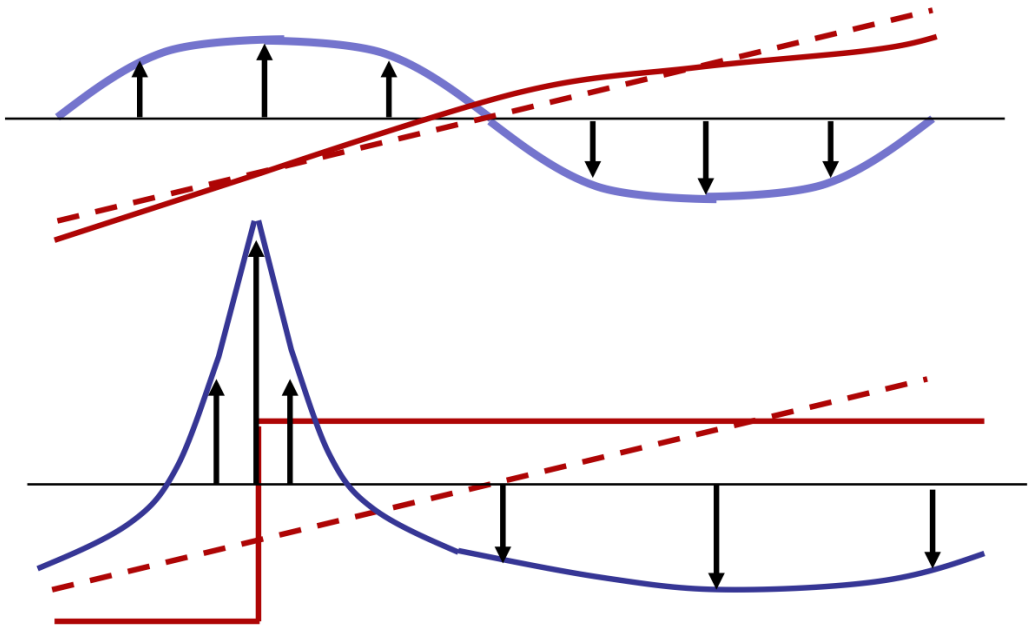

Figure 3.34: Sketch of the staircase formation in PV. The initial PV profile is indicated by a dashed red line, and it's development by a solid red line.

fig:PV-staircase-sketch

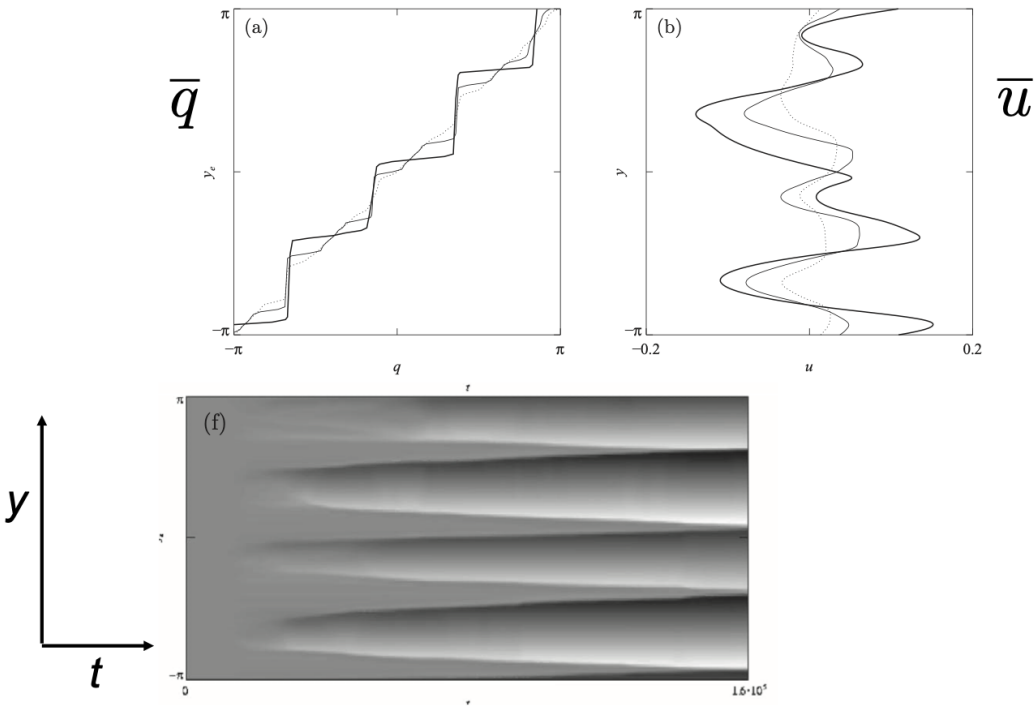

Figure 3.35: Time evolution of $\overline{q}$ (here used to denote the potential vorticity Q) (a), $\overline{u}$ (b) profiles, and latitude PV anomaly (f). In (a) and (b), the dotted line marks the initial state, the continuous line the intermediate state and the bold line the final state. Figure from [41].

fig:PV-staircase-simulations

3.7.3 Theoretical models of jet formation

The vorticity equation of the β-plane system (3.122), includes the advective nonlinearity $\boldsymbol{u}\cdot\nabla\zeta$ describing the interactions between different wave numbers, for example $\mathbf{k_1}+\mathbf{k_2}=\mathbf{k_3}$ is one possible resonance. Due to the complexity of these equation, some simplifications must be adopted to make them more accessible. A possible approach, is to describe only the statistically relevant quantities needed to reproduce the large-scale features and to parametrize the smaller-scales. In this way, the computational costs are reduced, and numerical models can simulate the flow without completely neglecting the scales that they cannot resolve.

Due to the tendency of 2D turbulence, to favour an upscale cascade of energy and an inverse cascade of enstrophy [2], we proceed by outlining a variation of (3.122), denoted here and in subsequent sections the nonlinear model (NL)

$$\frac{\partial\zeta}{\partial t}+J(\psi,\zeta)+\beta\frac{\partial\psi}{\partial x}=\xi-\mu\zeta+D\zeta,\quad\text{where}\quad D=\nu_n\Delta^n\zeta, \tag{3.131}$$

μ is a constant and ξ a random (in space and time) isentropic forcing. The first linear term $\mu\zeta$ dissipates energy at large scales and the second enstrophy build up a small scales via a hyperviscoisty ν_n. The nonlinearity has been expressed in terms of the Jacobian $J(f,g)=f_xg_y-f_yg_x$ and the vorticity in terms of $\zeta=\Delta\psi$.

Applying the Reynolds decomposition the flow can be expressed in terms of its mean and fluctuating components

$$\psi(x,y,t)=\overline{\psi}(y,t)+\psi'(x,y,t). \tag{3.132}$$

By assuming $\overline{\xi}=0$ because the forcing is statistically homogeneous, the zonal mean zonal flow $U(y,t)=\overline{u(y,t)}$ equation is

$$\frac{\partial U}{\partial t}=\overline{v'\zeta'}-\mu U+DU, \tag{3.133}$$ eq:NL-mean

and for the disturbance part, we get the eddy vorticity equation

$$\frac{\partial\zeta'}{\partial t}+U\frac{\partial\zeta'}{\partial x}+\left(\beta-\frac{\partial^2U}{\partial y}\right)\frac{\partial\psi'}{\partial x}+\left[\frac{\partial\psi'}{\partial x}\frac{\partial\zeta'}{\partial y}-\frac{\partial\psi'}{\partial y}\frac{\partial\zeta'}{\partial x}-\frac{\partial}{\partial y}\left(\overline{\frac{\partial\psi'}{\partial x}\zeta'}\right)\right]=\xi-\mu\zeta'+D\zeta'. \tag{3.134}$$ eq:NL-eddies

where the relation between the zonal mean vorticity and zonal mean zonal flow $\overline{\zeta}=-\partial_yU$ has been used to simply the previous expressions. The system considered so far is nonlinear and allows interactions between waves and the mean flow as well as wave-wave interactions. One way of simplifying the nonlinear equations is given by the *quasilinear (QL) approximation*, whereby the term in the square brackets in (3.134), representing wave-wave interactions, is set to be equal to zero. This widely used method removes the wave-wave interactions that lead to the formation of a new wave number, whilst interactions of the type $k_x-k_x=0$ (waves leading to a mean flow) and $k_x+0=k_x$ (wave-mean flow interactions) are still allowed. In practice, (3.133) remains the same as it only includes wave-mean flow interaction in the wave momentum flux convergence term $\overline{v'\zeta'}$. This simplification leaves us with linear operators, of the form

$$\frac{\partial\zeta'}{\partial t}+L\zeta'=\xi-\mu\zeta'+D\zeta',\quad\text{where}\quad L=\left[(\beta-\partial_y^2U)\Delta^{-1}+U\right]\frac{\partial}{\partial x}. \tag{3.135}$$ eq:QLzeta

A particular model that has been investigated [9] is to make the further assumption that the system is excited by a stochastic in time force, where the noise is δ-correlated, statistically homogeneous in x and has the property

$$\langle \xi(\mathbf{x_1}, t_1)\xi(\mathbf{x_2}, t_2)\rangle = \delta(t_2 - t_1)\Xi(x_1 - x_2, y_1, y_2), \tag{3.136}$$

where the angular brackets denote an ensemble average, and Ξ denotes a two point correlation function [8]. This approach focuses on finding equations for statistical averages. The two-point correlation function of the vorticity can be written as

$$\langle \zeta'(\mathbf{x_1}, t_1)\zeta'(\mathbf{x_2}, t_2)\rangle = Z(x_1 - x_2, y_1, y_2, t). \tag{3.137}$$ eq:2corrZet

We seek an evolution equation for (3.137) in the form

$$\frac{\partial Z}{\partial t} = \left\langle \zeta'(\mathbf{x_1}, t_1)\frac{\partial \zeta'}{\partial t}(\mathbf{x_2}, t_2) + \frac{\partial \zeta'}{\partial t}(\mathbf{x_1}, t_1)\zeta'(\mathbf{x_2}, t_2)\right\rangle. \tag{3.138}$$ eq:Zt

By using (3.135) to express the time derivatives in (3.138), we obtain

$$\frac{\partial Z}{\partial t} = \langle \zeta_1' \left(\xi_2 - L_2\zeta_2' - \mu\zeta_2' + D_2\zeta_2'\right) + \zeta_2' \left(\xi_1 - L_1\zeta_1' - \mu\zeta_1' + D_1\zeta_1'\right)\rangle, \tag{3.139}$$ eq:Zt_expa

where the subscripts refer to the quantities evaluated at point 1 or 2. There is an important assumption about the interpretation of statistical average? I didn't understand this point. Include a small aside to clarify this. We can write the analogous for a stochastic 1D differential equation

$$\frac{dX}{dt} = \xi < \xi(t_1)\xi(t_2) >= \delta(t_1 - t_2). \tag{3.140}$$

The interpretation would be

$$d(X_t^2) = 2X_t dW_t (dW_t)^2 \tag{3.141}$$

where $(dW_t)^2$ is some deterministic quantity dt, and since there is no statistical correlation between dW_t and dt

$$< d(X_t)^2 >= \underbrace{< 2X_t dW_t >}_{=0} dt \tag{3.142}$$

Take a look at the appendix of [46] for a detailed explanation. Expanding (3.139) we can write

$$\frac{\partial Z}{\partial t} = \Xi - 2\mu Z + \langle \zeta_1' D_2\zeta_2' + \zeta_2' D_1\zeta_1' - \zeta_2' L_1\zeta_1' - \zeta_1' L_2\zeta_2'\rangle, \tag{3.143}$$ eq:Zt_expa

where $\langle \zeta_1'\xi_2 + \zeta_2'\xi_1\rangle = \Xi$ follows from the assumption of ergodicity and that the system and forcing are uncorrelated (see appendix B.4 of [9]). Simplifying further we obtain

$$\frac{\partial U}{\partial t} = \frac{1}{2}(\Delta_1^{-1} - \Delta_2^{-1})\frac{\partial}{\partial x}Z(0, y, y, t) - \mu U + DU, \tag{3.144}$$ eq:NL-mean

along with

$$\frac{\partial Z}{\partial t} + \left[\Delta_1^{-1}L_1 - \Delta_2^{-1}L_2\right]\frac{\partial Z}{\partial x} = \Xi - 2\mu Z + (D_1 + D_2)Z, \tag{3.145}$$

which is a closed equation expressing $\partial U/\partial t$ and $\partial Z/\partial t$ in terms of its first U and second cumulants Z. The main assumption used in the model, and that which we have used

to close the model in obtaining (3.144) from (3.133), is that if there is an equivalence between the x average in the initial equation

$$\frac{\partial U}{\partial t} = \overline{v'\zeta'}, \tag{3.146}$$

and the statistical average

$$\langle v'(x_1, y_1, t)\zeta'(x_2, y_2, t)\rangle\Big|_{\substack{x_1=x_2=0\\ y_1=y_2=y}}, \tag{3.147}$$

then we can rename it as

$$\langle v'(x_1, y_1, t)\zeta'(x_2, y_2, t)\rangle = \frac{1}{2}\big(\overline{v_1'\zeta_2'} + \overline{v_2'\zeta_1'}\big). \tag{3.148}$$

As shown in chapter 6 of [9], from this it follows that

$$\overline{v'\zeta'} = \frac{1}{2}(\Delta_1^{-1} - \Delta_2^{-1})\frac{\partial}{\partial x}Z(0, y, y, t). \tag{3.149}$$

This model is called CE_2, which stands for closure at second order in the cumulant expansion. Authors [20] and [46] used the CE_2 model to demonstrate the *zonostrophic instability*. If we assume $\psi(x, y_1 - y_2)$ homogeneous and that Z is non zero, it can be shown that by adding a small perturbation to the flow U and to Z, under certain circumstances the flow is unstable to a sinusoidal mode in y which represents the growth of jet-like disturbances.

A comparison of simulations run using the nonlinear model, quasilinear model, and CE_2 model is shown in figure 3.36. The state is initialised by some random initial conditions and for all three models the flow self-organises into jets. However, there are significant difference in the models.

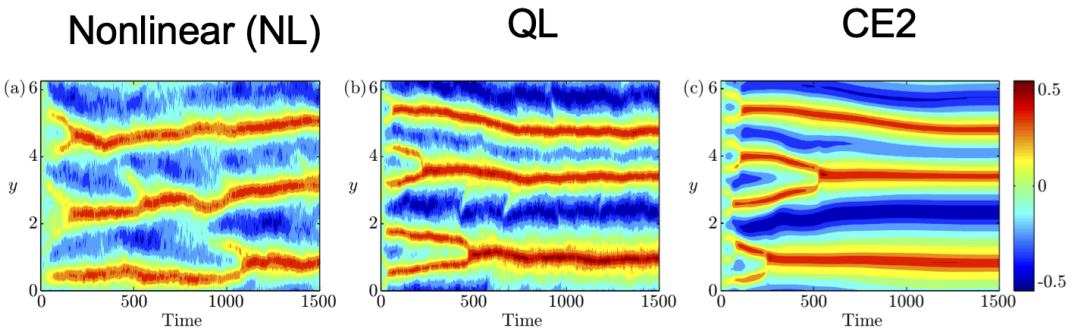

Figure 3.36: Latitude-time plots showing the zonal mean of the zonal velocity field from numerical integration of (a) a nonlinear model, (b) a quasilinear model, (c) a CE_2 model. Identical parameters were used in all three models in which we observe the spontaneous formation of 3 eastward jets. Figure from [9] adapted from [8].

NL-QL-CE

3.7.3.1 Jets variability

Variability

After the jets are formed in the flow, they show different behaviours in terms of their spatio-temporal evolution. The jet variability has been studied in detail by [9]. Three

typical jet evolutions obtained from long-time simulations of the nonlinear model are shown in figure 3.37. In the upper plot, a single jet forms and maintains an approximately constant amplitude over the entire duration of the simulation, except for small fluctuations. The jet moves at different latitudes, without any preferential direction. This behaviour is defined as *randomly wandering*. The middle plot shows a second behaviour, in which jets are merge and split over time, the total number of jets changing throughout. This is referred to as a *merging and nucleating* behaviour. In addition to these first two jet behaviour, which are also found in observations and other studies, a third one has been discovered by [9], here shown in figure 3.37(c). In this case, the jet is observed to systematically move to lower or higher latitudes and sometimes reverse direction in a *jet migration*. This last behaviour is deterministic and has a symmetry breaking in the latitudinal coordinate. The nonlinear and quasilinear models can be compared by run-

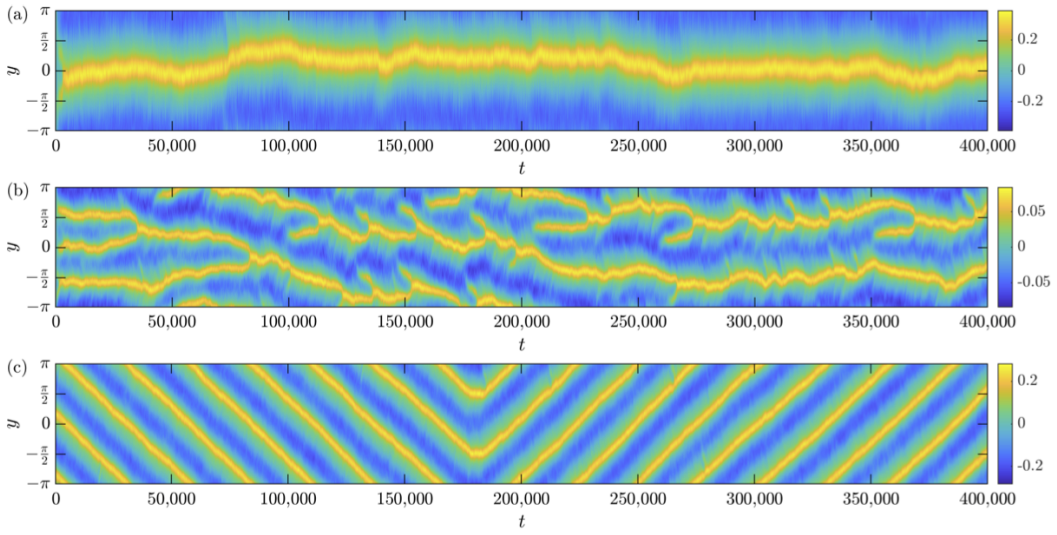

Figure 3.37: Fundamental types of zonal jet variability regimes observed in the NL model. (a) Randomly wandering behaviour, (b) merging and nucleating behaviour, and (c) migrating behaviour. Figure from [9]

fig:jetsExample

ning simulations where the jet variability is changed by acting on the zonostrophy of the system. The jet variability can be studied as a function of the β parameter by linearly increasing the Rhines wavenumber, which is the inverse of the Rhines scale $k_{Rh} = L_{Rh}^{-1}$. The effect of increasing k_{Rh} is that the number of jets increases, as shown in figure 3.38 frames (a) and (c) for the nonlinear and quasilinear models respectively. The increase in the number of jets is a complicated process subject to a strong variability. The nonlinear model also shows an intermittent migrating behaviour of the jet which does not appear in the quasilinear model, where only the merging and nucleation behaviour can be observed. The zonal mean flow index, $\mathrm{zmf}(t)$, is a dimensionless quantity equal to the fraction of the total kinetic energy that is distributed in the zonal mean zonal flow

$$\mathrm{zmf}(t) = \frac{\left\langle \overline{|\psi|}^2 \right\rangle}{\langle |\psi|^2 \rangle} \tag{3.150}$$

eq:zmf

This parameter is shown in the bottom plot in figure 3.38. A more in depth analysis of the spontaneous transitions and how they relate to zonostrophy has revealed a correlation

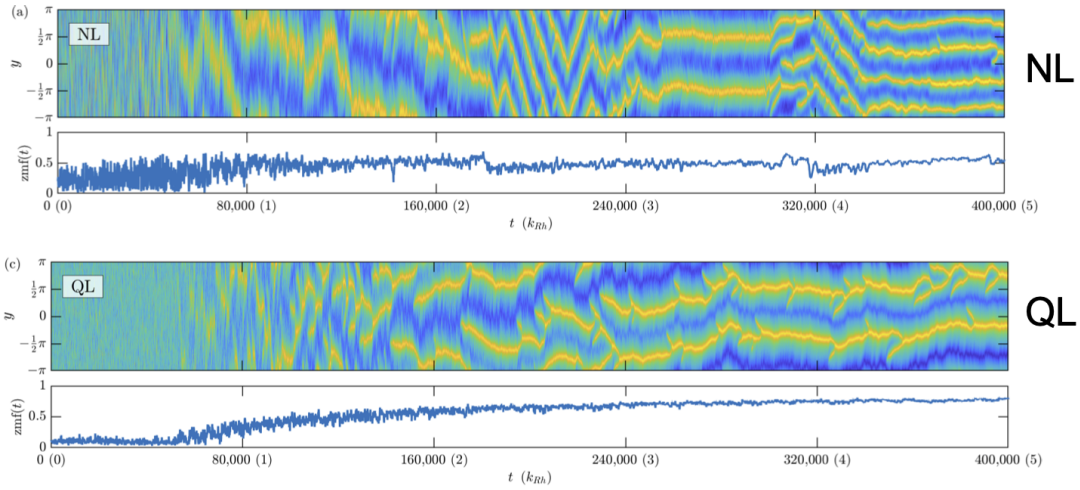

Figure 3.38: Zonal jet variability regimes observed as the Rhines wavenumber is linearly varied in time over the range $0 \leq k_{Rh} \leq 5$. Figure (a) used the NL model while figure (c) used the QL model. The inverse Rhines length scale $k_{Rh} = L_{Rh}^{-1}$ is linearly increased. The top figures show a latitude-time plot of the time evolution of the zonal mean zonal velocity field, while the bottom plot shows the corresponding evolution of the zmf index (3.150). Figure and caption adapted from [9]

fig:jetsBeta

between the two. In figure 3.39, four simulations at different values of R_β are compared. What emerges is a negative correlation between transitions and R_β, with more frequent transitions occurring for the lowest values of the zonostrophy parameter.

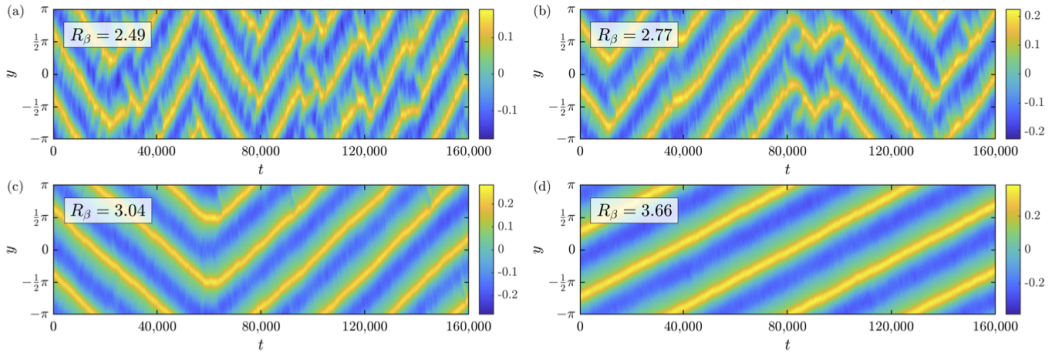

Figure 3.39: The influence of the zonostrophy parameter R_β on the frequency of regime transitions. Latitude-time plots showing the zonal mean zonal velocity field are selected for four simulations in which fast jet migration behaviour is observed. Figure and caption adapted from [9]

fig:jetsZono

Another interesting feature, adding to the complexity of the jet variability, is hysteresis. In runs where β is first increased and then decreased with all other parameters the same, NL and QL simulations both show hysteresis, as can be seen in figure 3.40. Very different jet evolutions are observed depending on the run. Similarly, hysteresis is also observed in the CE_2 model, as shown in figure 3.41. In this case, not only is the number of jets that forms different when β is decreased, but their direction of migration is also reversed.

One question that arises is: is the variability always directly generated by the stochas-

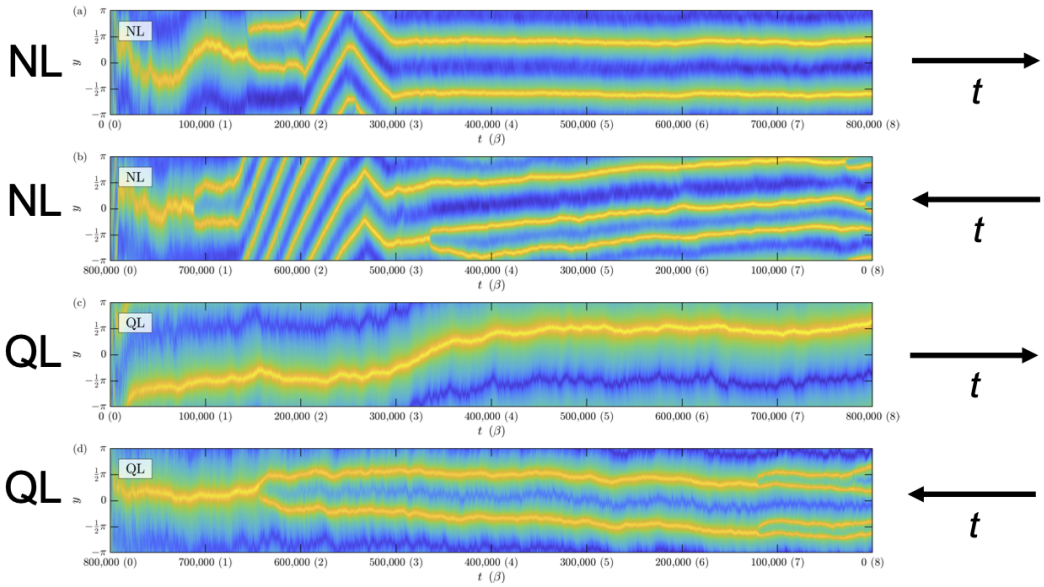

Figure 3.40: Hysteresis observed as the parameter β is linearly varied in time over the range $0 \leq \beta \leq 8$. Figures (a) and (b) used the NL model while figures (c) and (d) used the QL model. β is linearly increased in figures (a) and (c) while in figures (b) and (d) it is linearly decreased and the direction of time is reversed. Figure and caption adapted from [9]

fig:jetshysteresis

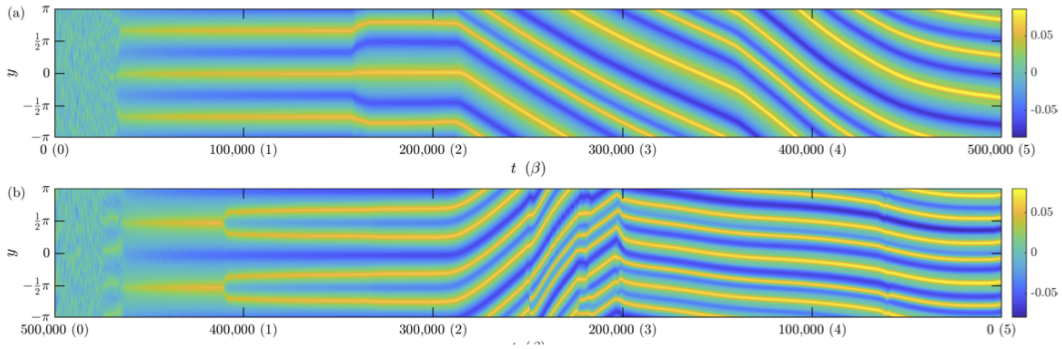

Figure 3.41: Hysteresis observed as the parameter β is linearly varied in time over the range $0 \leq \beta \leq 5$ in the CE_2 model. β is linearly increased in figure (a) and linearly decreased in figure (b), where the direction of time is also reversed. Figure and caption adapted from [9]

fig:jetshysteresisCE2

tic forcing or is the system behaving in a deterministic way? For the system considered so far, the QL is explicitly stochastic whilst the CE_2 model is deterministic. Therefore, deterministic regimes and chaotic systems could be captured by the CE_2 model. Machine learning and other data-driven techniques can help answering this question and understanding the nature of the jet variability [36].

A test of what effect the stochastic forcing has on a system is conducted by comparing two different set of simulations. In the first one, the forcing remains invariant but a small perturbation is added to the system. The difference between the runs shows an exponential divergence (see figure 3.42), as one could expect for the evolution of a chaotic system, which would have a divergence in the Lyapunov exponent. A second set of runs, where

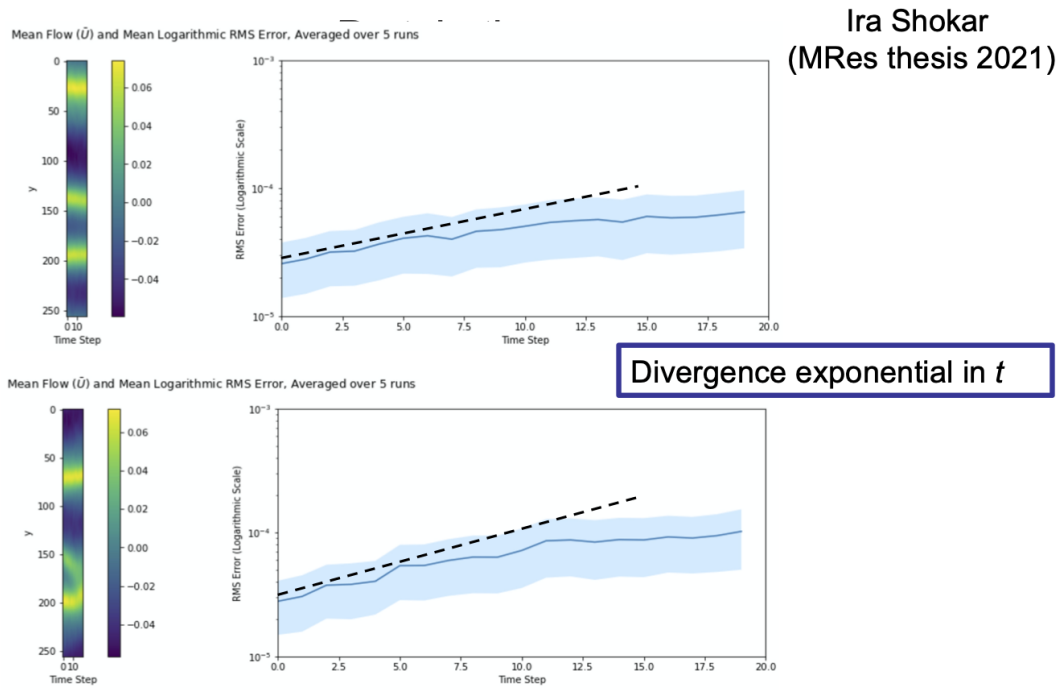

Figure 3.42: Comparison between two runs that only differ in their initial conditions. The color plots on the left show the mean flow, averaged over 5 runs. On the right the mean difference between runs is shown in the solid blue line, with the standard deviation envelope shown in lighter blue. Figure and caption adapted from [43]

the flow is unperturbed but the forcing is different, are shown in figure 3.43. Differently from the previous case, the time evolution assumes a random-walk behaviour and there is a growth in the error.

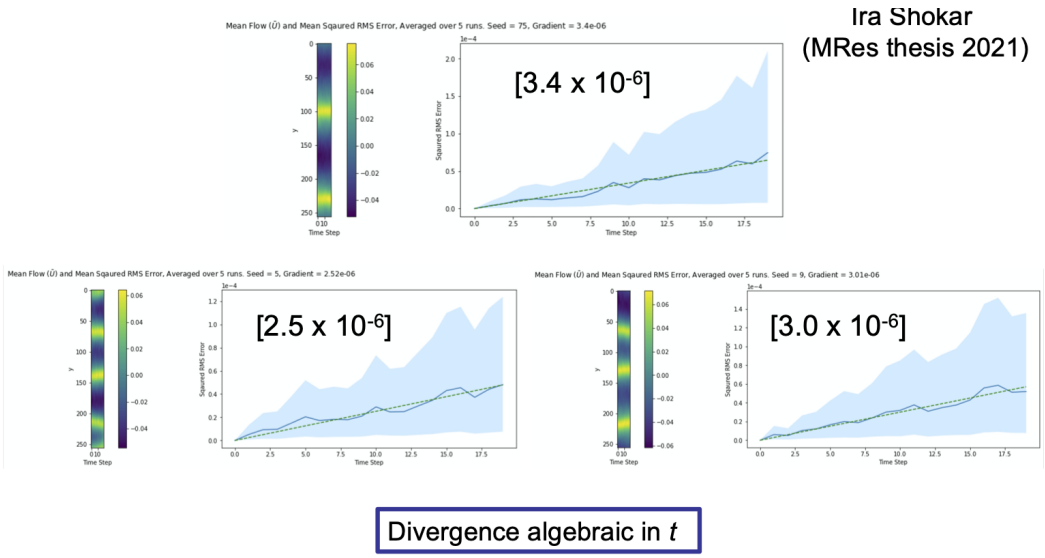

Figure 3.43: The color plots on the left show the mean flow averaged over the 5 runs. On the right we see the mean difference between runs shown in the solid blue line, with the standard deviation envelope shown in lighter blue. In this case, at time $t = 0$ the runs were initialised with a different random forcing, all other initial conditions remained the same. The green dashed line shows the gradient, determined via regression to represent the diffusion rate, characterised by the diffusion constant. Figure and caption adapted from [43]

fig:stoc-variant

3.8 Moist dynamics

sec:moist

The topics covered so far, discussing the basics of the atmosphere and ocean dynamics are based on dry dynamical theories that do not consider moist processes. When water vapour in the atmosphere condenses, it releases heat, which impacts the circulation, especially in tropical regions. Moreover, condensation leads to the formation of clouds and successively to rain, both phenomena affecting the weather and climate evolution. Yet, most of the traditional geophysical fluid dynamics do not treat moist dynamics. It is becoming more and more essential to develop 'wet' dynamics, since the water vapour percentage in the atmosphere increases with global warming, and therefore it will potentially change the circulation.

In this chapter, we will introduce the topic of moist dynamics, discussing the Madden-Julian Oscillation as the manifestation of a 'moisture' mode [38]. Different convection models are discussed, and the basic ideas for developing an analytical model are introduced. A recent review article on the topic can be found in [51].

3.8.1 The Madden-Julian oscillation

The Madden-Julian oscillation (MJO) is a global scale disturbance related to the large-scale convective fluctuations and associated vertically overturning circulation anomalies with a periodicity of 30-60 days [26]. The MJO impacts the weather and climate, playing an important role in the Indian Ocean dynamics. Therefore, an accurate description of this phenomenon is necessary to improve the models and add predictability to the weather

forecasts.

Figure 3.44 show a time-longitude plot of the precipitations in the tropics, where the effects of MJO are most apparent. Several time-space structures are recognizable in the plot with different phase propagation directions. An interplay of different scale phenomena is well visible in the figure. The MJO globally moves eastward with the large-scale convective envelope within which smaller-scale disturbances are observed to move in both directions. For example, Kelvin waves (propagating eastward) are superposed to inertia-gravity waves and Rossby waves that propagate in the opposite direction (westward) [38].

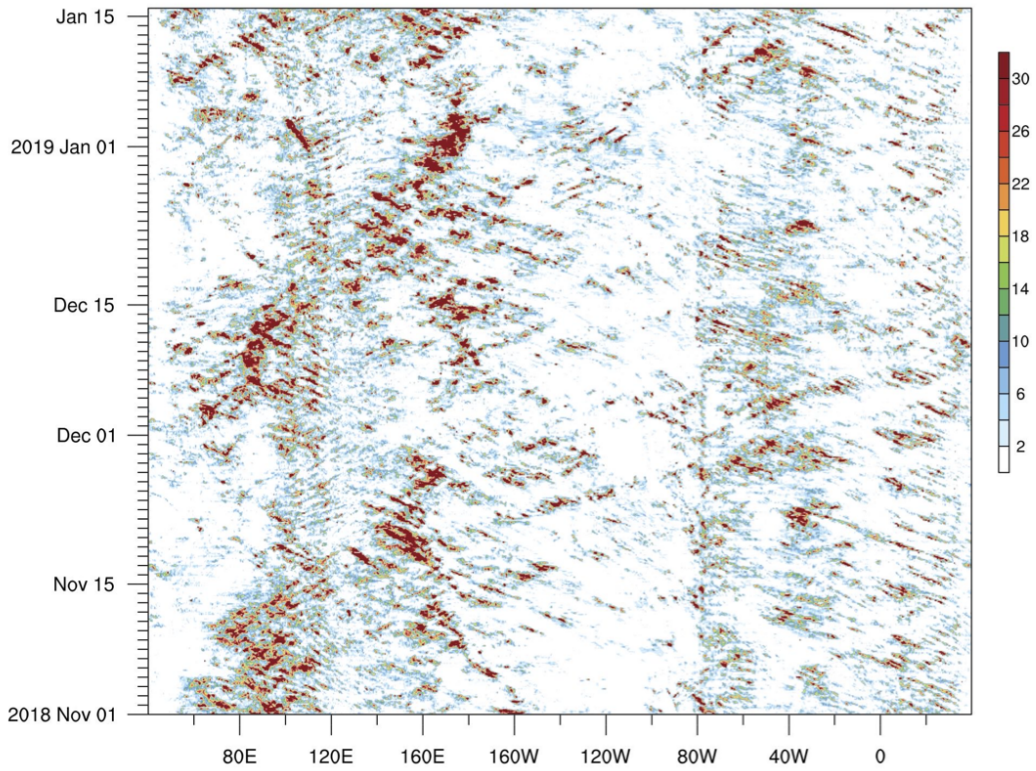

Figure 3.44: Time-longitude evolution of precipitation based on the NASA Global Precipitation Measurement. Figure and caption adapted from [26]

In section 3.4, we have analysed the shallow water equations and the family of waves that can be described by the equations. We now consider the equatorial-β plane, where $f = \beta y$ and $f_0 = 0$ is the equator. In this system, equatorially trapped solutions, which decay away from the equator exist and can be written as

$$\frac{\sqrt{gh_e}}{\beta}\left(\frac{\omega^2}{gh_e} - k^2 - \frac{k}{\omega}\beta\right) = 2n+1, \quad n = 0, 1, 2, \ldots \tag{3.151}$$ eq:equatoredispersion

which has three classes of solutions corresponding to eastward and westward propagating inertia-gravity waves plus equatorial Rossby waves [28]. The dispersion relation for the three types of waves is plotted in figure 3.45 for adimensional frequency $\omega^* = \omega/(\beta\sqrt{gh_e})^{1/2}$ and wavenumber $k^* = k(\sqrt{gh_e}/\beta)^{1/2}$. The solution for $n = 0$ is a particular case, for which the waves behave as Rossby waves for negative wavenumber and as inertia-gravity waves for positive wavenumbers. Such wave is called *mixed Rossby-gravity*.

The equatorial Kelvin wave is an analogous of the costally trapped Kelvin wave we have previously seen and it only propagates towards the East.

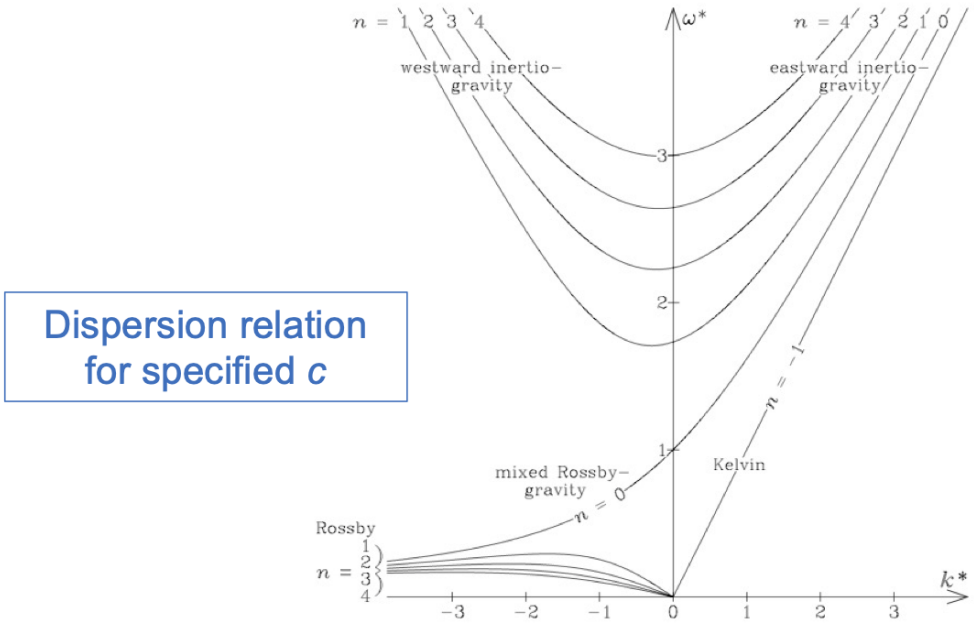

Figure 3.45: Dispersion curves for equatorial waves as a function of the nondimensional frequency, ω^*, and nondimensional zonal wave number, k^*. Figure and caption adapted from [28]

fig:equatorial-dispersion

There is a correspondence between the theoretical dispersion relation (3.151) and observations in the cloudiness disturbances, shown in figure 3.46. The match is obtained by setting the values of the phase speed c. The waves appear to be slower than what is predicted by the dry dynamics, i.e. the dynamics where moisture effects are neglected. The motion of gravity waves in the tropics is associated very strongly with precipitations, which provides heating, and therefore one needs to modify the equations to take into account the effect of moisture. The left plot in figure 3.46 shows a peak in the bottom right sector, corresponding to the MJO. 20-30 years ago, someone put forward the idea that the MJO could be explained as a slow Kelvin mode due to the effect of moisture. However, this hypothesis has been discarded, and a theory explaining MJO is still lacking.

3.8.2 Moist shallow water equations

sec:moistSW

Can we include the moisture in the equatorial $\beta-$plane shallow water equations to make a link between the dry equations given in section 3.4 and the hydrology cycle?

A simple approach consists in rewriting the shallow water equations as

$$\frac{\partial \boldsymbol{u}}{\partial t} + \boldsymbol{u}\cdot\nabla\boldsymbol{u} + \beta y \mathbf{e_z}\times\boldsymbol{u} = -g\nabla\eta, \tag{3.152}$$

$$\frac{\partial \eta}{\partial t} + \nabla\cdot(\boldsymbol{u}\eta) = S(r,\eta), \tag{3.153}$$

$$\frac{\partial r}{\partial t} + \nabla\cdot(\boldsymbol{u}r) = R(r,\eta), \tag{3.154}$$

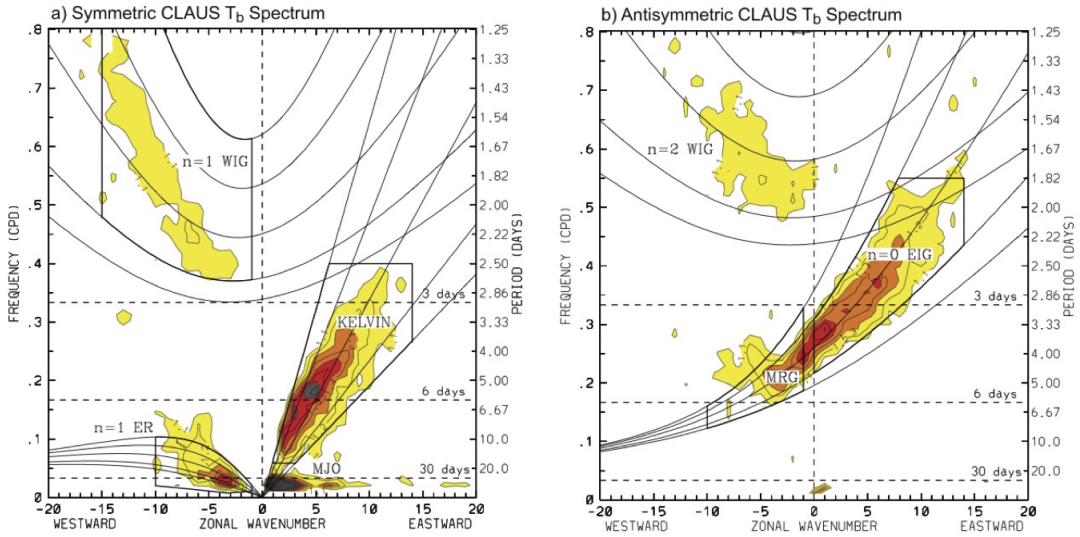

Figure 3.46: Wave number–frequency power spectrum of the (a) symmetric and (b) antisymmetric component of tropical cloudiness. Figure and caption adapted from [28]

s-dispersion

where there is an additional moisture variable r. $S(r, \eta)$ includes the latent and radiative heating, and $R(r, \eta)$ precipitations combined with evaporation. In this way, we have built a simple system with which it is possible to investigate moist effects. From the extra equation a new mode should arise, a *moisture mode*, which manifests in the atmosphere as the MJO.

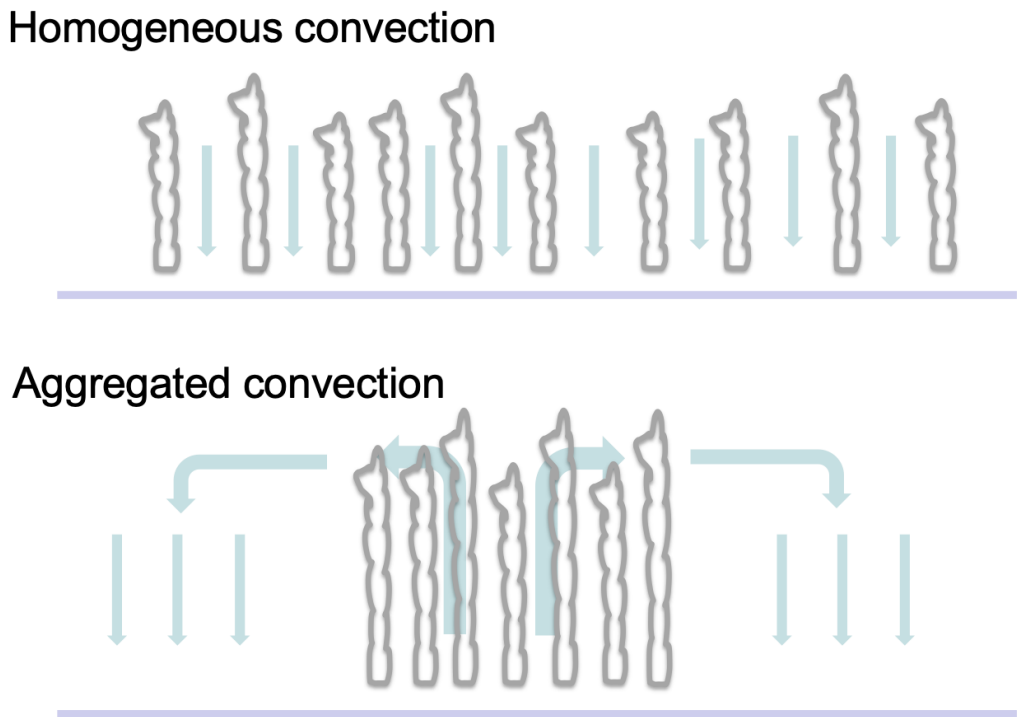

Figure 3.47: Sketch of homogeneous vs. aggregate convection.

g:aggregate

3.8.3 Numerical simulations including convection

Simulations including convection are usually done over a homogeneous domain in a periodic box, where convection is happening more or less randomly everywhere maintaining a statistically equilibrium. As it can be seen in the sketch in figure 3.47, in this situation there is a rise where clouds are situated and then sinking motions outside the clouds. Under some circumstances, aggregation can happen so that convection becomes more organised and localised in some specific regions. In such regions there will be a large-scale upwelling motions and subsiding in other regions (see figure 3.47). The state-of-the-art models can resolve (or better represent) convection. They have a spatial resolution of about 2-3 km and have turbulent parametrization and can give some representation about the convection scale flow.

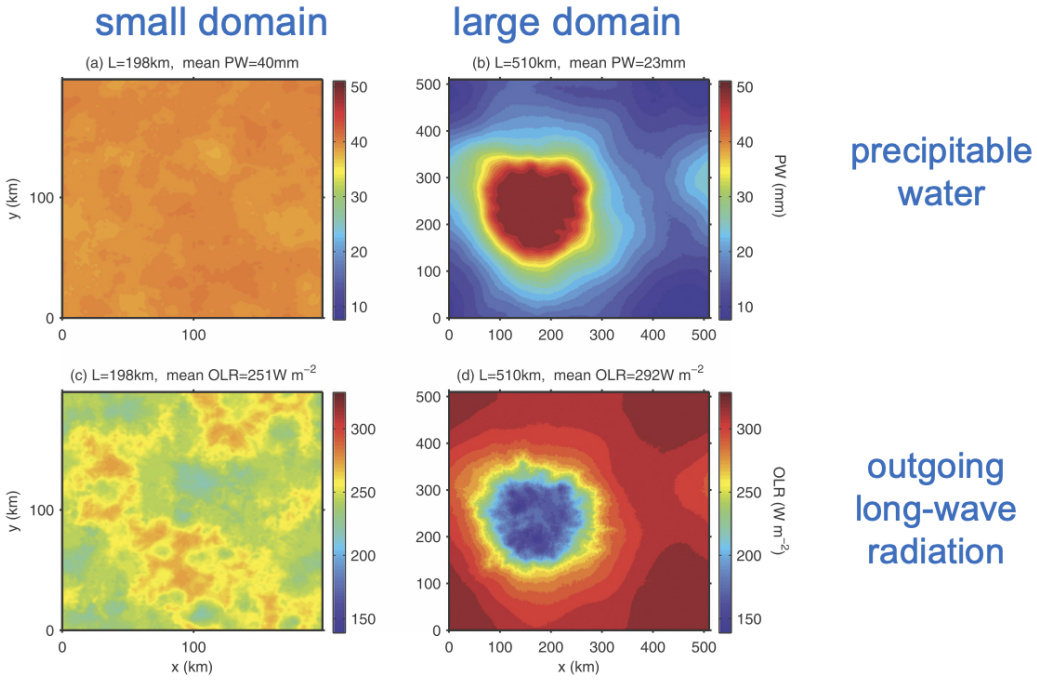

Figure 3.48: Daily mean (a),(b) precipitable water (PW) and (c),(d) outgoing longwave radiation (OLR) after 60 days in two simulations with the same resolution $dx = 2$km but different domain sizes L = (a),(c) 198 and (b),(d) 510km. Figure and caption taken from [32]

fig:model-convection

An example of such models is shown in figure 3.49 taken from [32]. On a rather small domain (plots on the left) the moisture stays homogeneous, whilst moisture self-aggregates when the domain is large enough resulting in localised areas where convection is very strong and precipitations occur. A theory proposed is that aggregation could be related to the MJO.

An extremely simple mathematical model for aggregation was proposed in [10]. In this model, the authors assume that the organisation can be explained on the basis of the moisture field alone. The equations they derived, similar to the Allen-Cahn equation, is the following

$$\frac{\partial r}{\partial t} - k\nabla^2 r = R(r) \quad \text{and} \quad \int R dx dy = R_0, \tag{3.155}$$

with k the eddy diffusivity. It is a bistable system with two possible stable states and an unstable state in between.

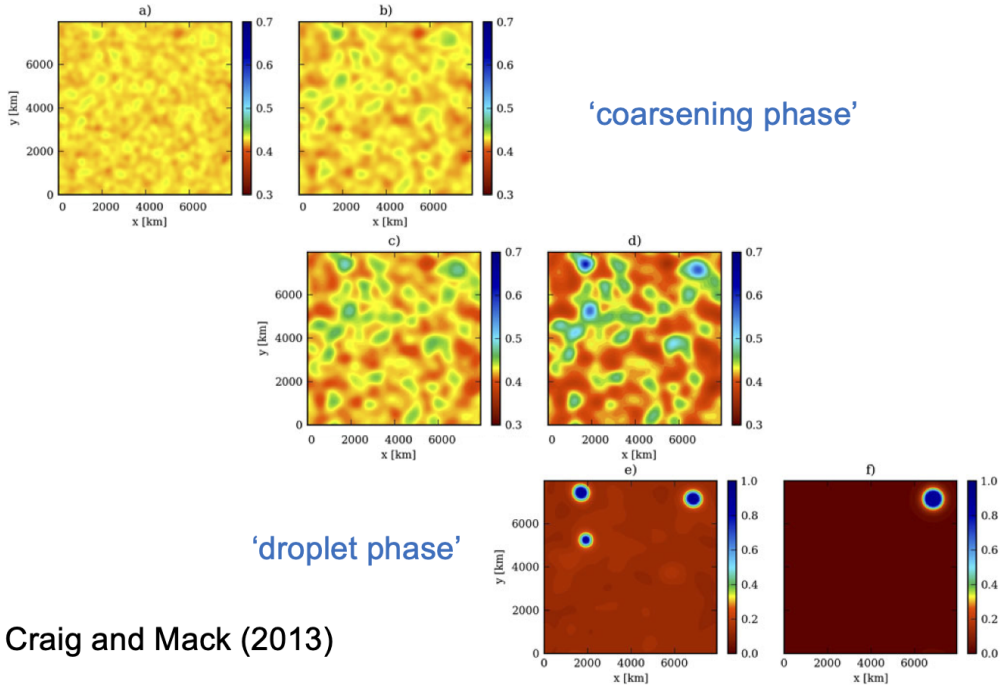

Figure 3.49: Snapshots of the horizontal distribution of the integrated moisture content normalized by its saturation value, daily for days 1 to 4, and at days 8 and 50, for a representative simulation. Figure and caption taken from [10]

The resulting moisture content is shown in figure 3.49 taken from [10]. Three different stages can be recognised at successive times. A *diffusive stage*, where the moisture field becomes smooth after being initialised with random noise. A *coarsening stage*, where small-scale merges creating larger scale-features. A final *droplet stage*, in which we have the aggregation in some regions.

A limitation of this model is that it does not include any dynamical interaction.

The discussion about moist dynamics given in this section, far from being exhaustive, aims to provide the reader with some basic knowledge about a fairly unexplored area of geophysical fluid dynamics. The effects of moisture on the dynamics are general circulation are much more poorly understood than the thermodynamic aspects and are therefore an area where new research can be developed.

Chapter 4

Frédéric Rousset's lecture notes

These lecture notes provide a summary of the Atmospheric and Oceanic Fluid Dynamics PDEs course given by Frédéric Rousset at the Mathematical Fluid Dynamics Summer School in Cargèse, 2021.

4.1 Ekman layers in rotating fluids

4.1.1 Introduction

This section will aim to discuss some simplified models in geophysical fluids. The final goal will be to perform some rigorous analysis on these models, and try to illustrate some mathematical techniques that we may use to study them. When considering geophysical fluids, there are often two important phenomena that we must consider. These are waves and, when considering problems with some small viscosity, boundary layers. We will start by looking at boundary layers.

We will study the *Ekman layer* in rotating fluids to begin. Let us consider the incompressible Navier-Stokes equations in a rotating system with isentropic viscosity, namely

$$\left\{ \begin{array}{rcl} \partial_t \boldsymbol{u} + (\boldsymbol{u}\cdot\nabla)\boldsymbol{u} + \frac{1}{\mathrm{Ro}}\boldsymbol{e}\times\boldsymbol{u} + \nabla p &=& \frac{\mathrm{E}}{\mathrm{Ro}}\Delta\boldsymbol{u} \\ \nabla\cdot\boldsymbol{u} &=& 0, \end{array} \right. \tag{4.1}$$

eqn:NS-1

on some spatial domain Ω, for positive time, where Ro is the Rossby number and E is the Ekman number. Both are non-dimensional. The vector $\boldsymbol{e} = (0,\, 0,\, 1)^{\mathrm{T}}$ represents the Coriolis force. We suppose that Ro and E/Ro are small, so we will denote $\varepsilon = \mathrm{Ro}$ and consider $\mathrm{E}/\mathrm{Ro} = \beta\varepsilon$ with $\beta \sim 1$ a constant. Note that at leading order, the gradient of the pressure will be of order $1/\varepsilon$, so we will pull this factor out for ease of notation. These scaled equations come from a nondimensionalization of the original equations, using the assumption that the effects of rotation will have a leading order effect on the flow. There isn't a natural scaling for pressure so its scale is chosen to balance the leading order terms. Analogously, in the Navier-Stokes equations without rotation, pressure is often chosen to scale with the advective term. After simplification, the equation becomes

$$\partial_t \boldsymbol{u}^\varepsilon + (\boldsymbol{u}^\varepsilon\cdot\nabla)\boldsymbol{u}^\varepsilon + \frac{1}{\varepsilon}\boldsymbol{e}\times\boldsymbol{u}^\varepsilon + \frac{1}{\varepsilon}\nabla p^\varepsilon = \beta\varepsilon\Delta\boldsymbol{u}^\varepsilon. \tag{4.2}$$

Remark 15. *In geophysical fluids it is sometimes more natural to take a different form of the viscosity by modelling turbulent effects. A variant of these equations is thus obtained by replacing $\beta\varepsilon\Delta\boldsymbol{u}$ by the turbulent viscous tensor $\varepsilon\partial_z^2 u + \nu_H\Delta_y u$, where $\nu_H \sim 1$.*

We will denote the coordinates $\boldsymbol{x} \in \Omega$ where $\boldsymbol{x} = (\boldsymbol{y}, z)$ with $\boldsymbol{y} = (y_1, y_2)$ and z, respectively its horizontal and vertical components. An example of a possible, and one which we will consider here, is $\Omega = \mathbb{R}^2 \times (0,1)$. Another domain that we will study is $\Omega = \mathbb{T}^2 \times (0,1)$ where $\mathbb{T}$ denotes periodic boundary conditions in the $\boldsymbol{y}$ variable. We impose the no-slip boundary condition $\boldsymbol{u}|_{z=0,1} = \boldsymbol{0}$.

Let us consider the behaviour of $\boldsymbol{u}^\varepsilon$ as ε goes to 0. From the general PDEs perspective, there are two ways to tackle this kind of problem:

- Using compactness arguments from uniform estimates; this can be quite arduous for non linear PDEs as the estimates that you can obtain are often quite weak, leading to weak convergence from which it is difficult to obtain the limit.
- Justifying a multi-scale asymptotic expansion.

The aim of this section will be to focus on the second method, in the case where we take into account two scales for the space variable.

Remark 16. *Notice that from (4.1) we can obtain the following energy estimate*

$$\frac{1}{2}\frac{\mathrm{d}}{\mathrm{d}t}\|\boldsymbol{u}^\varepsilon\|_{L^2}^2 + \beta\varepsilon\|\nabla\boldsymbol{u}^\varepsilon\|_{L^2}^2 = 0, \tag{4.3}$$

eqn:energy

which translates the dissipation of physical energy in this case.

Formal proof of remark. By taking the dot product of (4.3) with $\boldsymbol{u}^\varepsilon$ and integrating over Ω, one has

$$\int_\Omega \partial_t\boldsymbol{u}^\varepsilon\cdot\boldsymbol{u}^\varepsilon + (\boldsymbol{u}^\varepsilon\cdot\nabla)\boldsymbol{u}^\varepsilon\cdot\boldsymbol{u}^\varepsilon - \beta\varepsilon\Delta\boldsymbol{u}^\varepsilon\cdot\boldsymbol{u}^\varepsilon + \frac{1}{\varepsilon}\boldsymbol{e}\times\boldsymbol{u}^\varepsilon\cdot\boldsymbol{u}^\varepsilon + \frac{1}{\varepsilon}\nabla p^\varepsilon\cdot\boldsymbol{u}^\varepsilon = 0.$$

Considering individual terms within this equation, we have

$$\int_\Omega \partial_t\boldsymbol{u}^\varepsilon\cdot\boldsymbol{u}^\varepsilon = \frac{1}{2}\frac{\mathrm{d}}{\mathrm{d}t}\int_\Omega |\boldsymbol{u}^\varepsilon|^2.$$

Most of the other terms vanish. Integration by parts along with both the given boundary condition and the incompressibility of $\boldsymbol{u}^\varepsilon$ implies

$$\int_\Omega (\boldsymbol{u}^\varepsilon\cdot\nabla)\boldsymbol{u}^\varepsilon\cdot\boldsymbol{u}^\varepsilon = -\int_\Omega \nabla\cdot\boldsymbol{u}^\varepsilon\,\frac{|\boldsymbol{u}^\varepsilon|^2}{2} = 0.$$

For the same reasons, one has

$$\int_\Omega \nabla p^\varepsilon\cdot\boldsymbol{u}^\varepsilon = -\int_\Omega p^\varepsilon\nabla\cdot\boldsymbol{u}^\varepsilon = 0.$$

The Coriolis term automatically vanishes since

$$\boldsymbol{e}\times\boldsymbol{u}^\varepsilon\cdot\boldsymbol{u}^\varepsilon = 0.$$

Finally, an integration by parts provides

$$\int_\Omega \Delta\boldsymbol{u}^\varepsilon\cdot\boldsymbol{u}^\varepsilon = -\int_\Omega |\nabla\boldsymbol{u}^\varepsilon|^2.$$

□

Formally, we thus have the energy conservation property, which we can use prove global existence of weak solutions to the Navier-Stokes equation. Let us recall the following famous result.

Theorem 4.1.1 (Leray). *For any $\varepsilon > 0$ and $\boldsymbol{u}^\varepsilon(0) \in L^2(\Omega)$ with free divergence, there exists at least one weak solution $\boldsymbol{u}^\varepsilon$ to the incompressible Navier-Stokes equation in a rotating system such that*

$$\|\boldsymbol{u}^\varepsilon(t)\|_{L^2}^2 + 2\beta\varepsilon \int_0^t \|\nabla \boldsymbol{u}^\varepsilon(s)\|_{L^2}^2 \,\mathrm{d}s \leq \|\boldsymbol{u}^\varepsilon(0)\|_{L^2}^2.$$

Remark 17. *Let us emphasize that the result does not include uniqueness. The notion of weak solution must at least ensure that the latter estimate is well defined. Here to be a weak solution means that*

$$\boldsymbol{u}^\varepsilon \in L^\infty(\mathbb{R}_+; L^2(\Omega)) \cap L^2(\mathbb{R}_+; H^1(\Omega)).$$

The first part is referring to how the solution remains in L^2 and is bounded by the initial condition, and the second that the gradient exists and its square is integrable with respect to space and time. Notice that results for strong solutions also hold, but would imply a finite time of existence depending on ε. Therefore to use this result would require to prove that there exists an interval of time independent of ε in order to perform our study. In fact, the way to obtain a stronger solution is to try to justify the asymptotic expansion as mentioned above. Instead, we will describe the limit of any Leray weak solution.

If we assume that $\boldsymbol{u}^\varepsilon \to \boldsymbol{u}^0$ as $\varepsilon \to 0$, in a sufficiently strong sense, then $\boldsymbol{u}^0$ should solve the following system of equations, know as *geostrophic balance*,

$$\begin{cases} \boldsymbol{e} \times \boldsymbol{u}^0 + \nabla p^0 &= \boldsymbol{0} \\ \nabla \cdot \boldsymbol{u}^0 &= 0 \\ u_3^0|_{z=0,1} &= 0, \end{cases}$$

where $\boldsymbol{u} = (u_1, u_2, u_3)^{\mathrm{T}}$, with eventual extra indices. Explicitly, we may write the first equation as

$$\begin{pmatrix} -u_2^0 \\ u_1^0 \\ 0 \end{pmatrix} + \begin{pmatrix} \partial_1 p^0 \\ \partial_2 p^0 \\ \partial_z p^0 \end{pmatrix} = \boldsymbol{0}. \tag{4.4}$$ eq:tp

Since $\partial_z p^0 = 0$, the pressure is independent of z; hence by (4.4), u_1^0 and u_2^0 are also independent of z. Furthermore, looking at (4.4), we observe that $\nabla_{\boldsymbol{y}} \cdot \boldsymbol{u}_{\boldsymbol{y}}^0 = 0$. Since $\boldsymbol{u}^0$ is divergence free, we obtain that u_3^0 is independent of z too. By our choice of boundary conditions, necessarily there is $u_3^0 = 0$, and so we have shown that the velocity field is indeed of the form

$$\boldsymbol{u}^0(t, \boldsymbol{x}) = \begin{pmatrix} u_1^0(t, \boldsymbol{y}) \\ u_2^0(t, \boldsymbol{y}) \\ 0 \end{pmatrix}.$$

The Dirichlet boundary condition cannot be satisfied by such a limit. Therefore, there must be a boundary layer.

4.1.2 Multiscale expansion with boundary layers

A boundary layer is a region in the domain which is governed by different equations to the interior region, in order to satisfy given boundary conditions. These regions are typically thin in the direction perpendicular to the boundary. Drawing upon another physical situation as an example, the flow of air past an aerofoil/plane wing is fast (hundreds of kilometres per hour) but must reduce to zero relative to the boundary of the aerofoil, and this reduction is achieved close to the boundary. In our case, the flow in the interior region as already stated above is close to geostrophic balance, and we expect diffusive effects to be strong close to the boundary. The following method of solution consists of expressing the solution as an asymptotic expansion where each successive term is small ($O(\varepsilon)$) compared to the previous term, and then further split into components which satisfy the interior and boundary layer equations. The idea behind an asymptotic expansion is that substitution into the governing equations and looking at terms of the same order in ε yields simpler equations for each term in the expansion, which when put back together give a solution which will have a small error.

Given the dependence of the solution on ε, let us call $\boldsymbol{u} = \boldsymbol{u}^\varepsilon$. In the following we generically denote, with possible indices,

$$\boldsymbol{U} = \begin{pmatrix} \boldsymbol{u} \\ p \end{pmatrix}.$$

Consider the following two spatial scales expansion: let us write the approximate solution $\boldsymbol{U}^{\mathrm{app}}$ with some corrector $\boldsymbol{\mathcal{C}}$:

$$\boldsymbol{U}^{\mathrm{app}} = \sum_{k=0}^{M} \varepsilon^k \boldsymbol{U}^k \left(t, \boldsymbol{x}, \frac{z}{\varepsilon}, \frac{1-z}{\varepsilon} \right) + \boldsymbol{\mathcal{C}},$$

where we decompose the functions as interior and boundary layer parts, as follows

$$\boldsymbol{u}^k \left(t, \boldsymbol{x}, \frac{z}{\varepsilon}, \frac{1-z}{\varepsilon} \right) = \boldsymbol{u}^{k,\mathrm{int}}(t, \boldsymbol{x}) + \boldsymbol{u}^{k,\mathrm{b},0} \left(t, \boldsymbol{y}, \frac{z}{\varepsilon} \right) + \boldsymbol{u}^{k,\mathrm{b},1} \left(t, \boldsymbol{y}, \frac{1-z}{\varepsilon} \right).$$

The term $\boldsymbol{\mathcal{C}}$ is a corrector, the properties of which will be specified further in the proof of Theorem 4.1.2. The coordinates z/ε and $(1-z)/\varepsilon$ will be henceforth labeled as the *inner variable* Z, which takes the value of 0 at each of the boundaries. The interior and boundary layer solutions $\boldsymbol{u}^{k,\mathrm{int}}, \boldsymbol{u}^{k,b,i}$ must satisfy certain boundary and continuity conditions in order to provide us with a reasonable solution to our system of equations throughout the domain. To ensure the boundary conditions are satisfied, we require that

$$\boldsymbol{u}^{k,\mathrm{int}}(t, \boldsymbol{y}, i) + \boldsymbol{u}^{k,\mathrm{b},i}(t, \boldsymbol{y}, 0) = \boldsymbol{0},$$

and that the boundary layer functions are not felt at infinity,

$$\forall \alpha, \boldsymbol{\beta}, \qquad \sup_{t \in [0,T]} \left\| \partial_t^\alpha \partial_{\boldsymbol{y}}^{\boldsymbol{\beta}} \boldsymbol{u}^{k,\mathrm{b},i}(t, \cdot, Z) \right\|_{L^2} \lesssim e^{-c_0 Z}.$$

We also require that these functions have sufficiently many derivatives so that an error of $O(\varepsilon^{M-1})$ can be achieved, that is to say

$$\forall n, \qquad \boldsymbol{u}^{k,\mathrm{int}}, \boldsymbol{u}^{k,\mathrm{b},i} \in H^n(\Omega),$$

Let us define

$$\mathbf{NS}^\varepsilon(\boldsymbol{U}) = \partial_t \boldsymbol{u} + (\boldsymbol{u}\cdot\nabla)\boldsymbol{u} + \frac{1}{\varepsilon}\nabla p + \frac{1}{\varepsilon}\boldsymbol{e}\times\boldsymbol{u} - \beta\varepsilon\Delta\boldsymbol{u}.$$

We will prove the following result.

p-soln-exist **Theorem 4.1.2.** *For any $M \in \mathbb{N}^*$ and $s > 0$ there exists such an element $\boldsymbol{U}^{\rm app}$ satisfying*

$$\left\{\begin{array}{rcl} \mathbf{NS}^\varepsilon(\boldsymbol{U}^{\rm app}) & = & \begin{pmatrix}\boldsymbol{R}^\varepsilon\\ 0\end{pmatrix}\\ \boldsymbol{u}^{\rm app}|_{z=0,1} & = & \mathbf{0}, \end{array}\right.$$

with

$$\|\boldsymbol{R}^\varepsilon\|_{H^s} \leq \varepsilon^{M-s-3/2}.$$

Proof. In what follows we generically denote, with a possible extra index,

$$\mathbb{U} = \begin{pmatrix}\boldsymbol{U}^{\rm int}\\ \boldsymbol{U}^{\rm b,0}\\ \boldsymbol{U}^{\rm b,1}\end{pmatrix}.$$

Let us consider the following iterative scheme, for $1 \leq k \leq M-1$,

$$\left\{\begin{array}{rcl} \mathbb{L}\mathbb{U}^0 & = & \mathbf{0}\\ \mathbb{L}\mathbb{U}^{k+1} & = & \mathbb{F}\left((\mathbb{U}^j)_{j\leq k}\right), \end{array}\right.$$

where the operator $\mathbb{L}$ is defined as

$$\mathbb{L}\mathbb{U} = \begin{pmatrix}\boldsymbol{L}^{\rm int}\boldsymbol{U}^{\rm int}\\ \boldsymbol{L}^{{\rm b},i}\boldsymbol{U}^{{\rm b},i}\end{pmatrix}$$

with

$$\boldsymbol{L}^{\rm int}\boldsymbol{U}^{\rm int} = \begin{pmatrix}\boldsymbol{e}\times\boldsymbol{u}^{\rm int} + \nabla p^{\rm int}\\ \nabla\cdot\boldsymbol{u}^{\rm int}\end{pmatrix}, \qquad \boldsymbol{L}^{{\rm b},i}\boldsymbol{U}^{{\rm b},i} = \begin{pmatrix}-u_2^{{\rm b},i} + \partial_1 p^{{\rm b},i} - \partial_Z^2 u_1^{{\rm b},i}\\ u_1^{{\rm b},i} + \partial_2 p^{{\rm b},i} - \partial_Z^2 u_2^{{\rm b},i}\\ \pm\partial_Z p^{{\rm b},i}\\ \pm\partial_Z u_3^{{\rm b},i}\end{pmatrix},$$

on a set of functions satisfying the boundary compatibility conditions

$$\boldsymbol{u}^{\rm int}|_{z=i} + \boldsymbol{u}^{{\rm b},i}|_{Z=0} = \mathbf{0}. \tag{4.5}$$ eq:bcond

The scheme defined here comes from factorizing the equation by the powers of ε in the interior and boundary layers parts respectively, and provides in particular the map $\mathbb{F}$ which is not explicited here. Specifically, given that in the boundary layer the vertical scale of interest is order $Z = z/\varepsilon$, the diffusion is the same magnitude as the Coriolis and pressure terms here. This scheme requires in particular $\mathbb{F}\left((\mathbb{U}^j)_{j\leq k}\right)$ to be in the range of $\mathbb{L}$. The key step to justifying the iteration is therefore to understand the kernel and the image of this operator.

• Initially, let us look at the kernel of $\mathbb{L}$ satisfying the boundary compatibility conditions, meaning the set of $(\boldsymbol{U}^{\rm int}, \boldsymbol{U}^{{\rm b},i})$ satisfying (4.5) and such that

$$\boldsymbol{L}^{\rm int}\boldsymbol{U}^{\rm int} = \mathbf{0}, \qquad \boldsymbol{L}^{{\rm b},i}\boldsymbol{U}^{{\rm b},i} = \mathbf{0}.$$

The first equality means that the interior flow satisfies the geostrophic balance and the divergence free condition, which we know to imply that the pressure is independent of the z coordinate. The second relation gives information for the boundary layer functions; using the third and fourth components of $\boldsymbol{L}^{\mathrm{b},i}$, along with the decay at infinity of the velocity and pressure fields, we have that $u_3^{\mathrm{b},i} = 0$ and $p^{\mathrm{b},i} = 0$. To consider the boundary condition, we impose that there must be no vertical interior velocity, meaning that $u_3^{\mathrm{int}} = 0$.

Following this, along with the boundary conditions, we find that the first and second components of $\boldsymbol{L}^{\mathrm{b},i}$ are, along with the boundary conditions,

$$\partial_Z^2 \boldsymbol{u}_{\boldsymbol{y}}^{\mathrm{b},i} = (\boldsymbol{u}_{\boldsymbol{y}}^{\mathrm{b},i})^{\perp} \qquad \text{with} \qquad \boldsymbol{u}_{\boldsymbol{y}}^{\mathrm{b},i}|_{Z=0} = -\boldsymbol{u}_{\boldsymbol{y}}^{\mathrm{int}}(t,\boldsymbol{y}).$$

This ordinary differential equation (ODE) admits the following solution

$$\boldsymbol{u}_{\boldsymbol{y}}^{\mathrm{b},i}(t,\boldsymbol{y},Z) = -e^{-Z/\sqrt{2}}\left(\boldsymbol{u}_{\boldsymbol{y}}^{\mathrm{int}}(t,\boldsymbol{y})\cos\left(Z/\sqrt{2}\right) + (\boldsymbol{u}_{\boldsymbol{y}}^{\mathrm{int}})^{\perp}(t,\boldsymbol{y})\sin\left(Z/\sqrt{2}\right)\right), \tag{4.6}$$

eq:ekman

which is the Ekman layer.

• Now let us describe the image of $\mathbb{L}$. To do requires us to solve

$$\boldsymbol{L}^{\mathrm{int}}\boldsymbol{U}^{\mathrm{int}} = \boldsymbol{F}^{\mathrm{int}}(t,\boldsymbol{y},z),$$
$$\boldsymbol{L}^{\mathrm{b},i}\boldsymbol{U}^{\mathrm{b},i} = \boldsymbol{F}^{\mathrm{b},i}(t,\boldsymbol{y},Z),$$

with respect to the boundary conditions (4.5), where $\boldsymbol{F}^{\mathrm{int}}$ is given in $H^s(\Omega)$ and $\boldsymbol{F}^{\mathrm{b},i}$ is exponentially decaying with respect to Z. We decompose the velocity and divergence parts of the force terms as follows

$$\boldsymbol{F}^{\mathrm{int}} = (\boldsymbol{F}_{\boldsymbol{u}}^{\mathrm{int}}, F_{\mathrm{d}}^{\mathrm{int}})^{\mathrm{T}} \in \mathbb{R}^3 \times \mathbb{R}, \quad \boldsymbol{F}^{\mathrm{b},i} = (\boldsymbol{F}_{\boldsymbol{y}}^{\mathrm{b},i}, F_Z^{\mathrm{b},i}, F_{\mathrm{d}}^{\mathrm{b},i})^{\mathrm{T}} \in \mathbb{R}^2 \times \mathbb{R} \times \mathbb{R}.$$

The system is written, for the interior part,

$$\begin{cases} \boldsymbol{e} \times \boldsymbol{u}^{\mathrm{int}} + \nabla p^{\mathrm{int}} &= \boldsymbol{F}_{\boldsymbol{u}}^{\mathrm{int}} \\ \nabla \cdot \boldsymbol{u}^{\mathrm{int}} &= F_{\mathrm{d}}^{\mathrm{int}}, \end{cases}$$

and for the boundary layer part

$$\begin{cases} (\boldsymbol{u}_{\boldsymbol{y}}^{\mathrm{b},i})^{\perp} + \nabla_{\boldsymbol{y}} p^{\mathrm{b},i} - \partial_Z^2 \boldsymbol{u}_{\boldsymbol{y}}^{\mathrm{b},i} &= \boldsymbol{F}_{\boldsymbol{y}}^{\mathrm{b},i} \\ \pm \partial_Z p^{\mathrm{b},i} &= F_Z^{\mathrm{b},i} \\ \pm \partial_Z u_Z^{\mathrm{b},i} &= F_{\mathrm{d}}^{\mathrm{b},i}. \end{cases}$$

The latter equalities impose

$$p^{\mathrm{b},i} = \mp \int_Z^{+\infty} F_Z^{\mathrm{b},i}\,\mathrm{d}Z', \qquad u_Z^{\mathrm{b},i} = -\int_Z^{+\infty} F_{\mathrm{d}}^{\mathrm{b},i}\,\mathrm{d}Z',$$

and the relation (4.5) implies

$$u_z^{\mathrm{int}}|_{z=i} = \int_0^{+\infty} F_{\mathrm{d}}^{\mathrm{b},i}\,\mathrm{d}Z$$

For the interior part, the pressure satisfies

$$\partial_z p^{\mathrm{int}} = \left(\boldsymbol{F}_{\boldsymbol{u}}^{\mathrm{int}}\right)_z, \tag{4.7}$$

which implies that $p^{\rm int}$ is of the form $f(z)+\tilde{p}^{\rm int}(t,\boldsymbol{y})$. Hence we have

$$\left(\boldsymbol{u}_{\boldsymbol{y}}^{\rm int}\right)^{\perp}=\left(\boldsymbol{F}_{\boldsymbol{u}}^{\rm int}\right)_{\boldsymbol{y}}-\nabla_{\boldsymbol{y}}\tilde{p}^{\rm int},$$

the curl of which provides

$$\partial_1 u_1^{\rm int}+\partial_2 u_2^{\rm int}=\left(\partial_1\boldsymbol{F}_{\boldsymbol{u}}^{\rm int}\right)_2-\left(\partial_2\boldsymbol{F}_{\boldsymbol{u}}^{\rm int}\right)_1.$$

Combined with $\nabla\cdot\boldsymbol{u}^{\rm int}=F_{\rm d}^{\rm int}$, one finds

$$\partial_z u_z^{\rm int}=-\left[\left(\partial_1\boldsymbol{F}_{\boldsymbol{u}}^{\rm int}\right)_2-\left(\partial_2\boldsymbol{F}_{\boldsymbol{u}}^{\rm int}\right)_1\right]+F_{\rm d}^{\rm int}.$$

From the first equation on the boundary part, one can determine $\left(\boldsymbol{u}_{\boldsymbol{y}}^{{\rm b},i}\right)^{\perp}$ by solving an ODE with a decaying part, and matching the tangential boundary condition

$$u_z^{\rm int}|_{z=0}=\int_0^{+\infty}F_{\rm d}^{{\rm b},0}\,{\rm d}Z,\qquad u_z^{\rm int}|_{z=1}=-\int_0^{+\infty}F_{\rm d}^{{\rm b},1}\,{\rm d}Z,$$

from which emerges the constraint

$$\int_0^1 F_{\rm d}^{\rm int}-\int_0^1\left(\partial_1\boldsymbol{F}_{\boldsymbol{u}}^{\rm int}\right)_2-\left(\partial_2\boldsymbol{F}_{\boldsymbol{u}}^{\rm int}\right)_1=\int_0^{+\infty}F_{\rm d}^{{\rm b},0}+\int_0^{+\infty}F_{\rm d}^{{\rm b},1}. \tag{4.8}$$ eq:constraint

• Let us compute the terms of the scheme. From the preliminaries we now know that $\mathbb{U}_0$ must be of the form

$$\boldsymbol{u}^{0,{\rm int}}=\begin{pmatrix}\boldsymbol{u}_{\boldsymbol{y}}^{0,{\rm int}}(t,\boldsymbol{y})\\0\end{pmatrix},$$

and that $\boldsymbol{u}^{0,{\rm b}}$ is given by the Ekman layer (4.6). Let us set

$$\mathbb{F}(\mathbb{U}^0):=\begin{pmatrix}\boldsymbol{F}_{\boldsymbol{u}}^{\rm int}\\F_{\rm d}^{\rm int}\\\boldsymbol{F}_{\boldsymbol{y}}^{{\rm b},i}\\F_Z^{{\rm b},i}\\F_{\rm d}^{{\rm b},i}\end{pmatrix}=\begin{pmatrix}\partial_t\boldsymbol{u}^{0,{\rm int}}+(\boldsymbol{u}^{0,{\rm int}}\cdot\nabla)\boldsymbol{u}^{0,{\rm int}}-\nu_H\Delta_{\boldsymbol{y}}\boldsymbol{u}^{0,{\rm int}}\\0\\\partial_t\boldsymbol{u}_{\boldsymbol{y}}^{0,{\rm b},i}+\left(\left(\boldsymbol{u}_{\boldsymbol{y}}^{0,{\rm int}}+\boldsymbol{u}_{\boldsymbol{y}}^{0,{\rm b},i}\right)\cdot\nabla_{\boldsymbol{y}}\right)\boldsymbol{u}^{0,{\rm b},i}+\left(\boldsymbol{u}_{\boldsymbol{y}}^{0,{\rm b},i}\cdot\nabla_{\boldsymbol{y}}\right)\left(\boldsymbol{u}^{0,{\rm int}}+\boldsymbol{u}^{0,{\rm b},i}\right)\\0\\\mp\nabla_{\boldsymbol{y}}\cdot\boldsymbol{u}^{0,{\rm b},i}\end{pmatrix}.$$

Remark 18. *Let us take a look at the expansion of the product of the interior and boundary parts of the maps we consider, to justify the expression of $\boldsymbol{F}_{\boldsymbol{y}}^{{\rm b},i}$. For generic $f=f^{\rm int}+f^{b}$ and $g=g^{\rm int}+g^{\rm b}$, with Taylor decomposition head terms of the following form*

$$f^{\rm int}(t,\boldsymbol{y},z)=f^{\rm int}(t,\boldsymbol{y},0)+z\tilde{f}^{\rm int}(t,\boldsymbol{y}),$$

the products of the form $z\tilde{f}^{\rm int}g^{\rm b}$ are equivalent to $\varepsilon Ze^{-Z/\sqrt{2}}$, so that the expansion of the product of f and g is

$$f^{\rm int}g^{\rm int}+\underbrace{f^{\rm int}|_{z=0}\,g^{\rm b}+f^{\rm b}g^{\rm int}|_{z=0}}_{\textit{boundary layer part}}+f^{\rm b}g^{\rm b}+\ \textit{higher order terms.}$$

The boundary layer part of this multiplication is dominated by the the boundary layer function multiplied by the interior function evaluated at the boundary. This means that the terms coming from the z-derivatives, which are order $1/\varepsilon$, don't appear above due to multiplication by the vertical velocity at the boundary which is 0.

By condition (4.8) on the range of $\mathbb{L}$ and taking the 2D curl of $\boldsymbol{F}_{\boldsymbol{u}}^{\rm int}$ as follows

$$\int_0^1 \nabla_{\boldsymbol{y}} \times (\partial_t \boldsymbol{u}_{\boldsymbol{y}}^{0,\rm int} + (\boldsymbol{u}_{\boldsymbol{y}}^{0,\rm int} \cdot \nabla_{\boldsymbol{y}}) \boldsymbol{u}^{0,\rm int}) = - \int_0^{+\infty} \nabla_{\boldsymbol{y}} \cdot (\boldsymbol{u}_{\boldsymbol{y}}^{0,\rm b,0} + \boldsymbol{u}_{\boldsymbol{y}}^{0,\rm b,1}) \, \mathrm{d}Z$$

provides

$$\partial_t \omega^{0,\rm int} + (\boldsymbol{u}_{\boldsymbol{y}}^{0,\rm int} \cdot \nabla_{\boldsymbol{y}}) \omega^{0,\rm int} = -\sqrt{2}\, \omega^{0,\rm int},$$

where $\omega^{0,\rm int}$ is the 2D curl of $\boldsymbol{u}_{\boldsymbol{y}}^{0,\rm int}$ defined as

$$\omega^{0,\rm int} = \nabla_{\boldsymbol{y}} \times \boldsymbol{u}_{\boldsymbol{y}}^{0,\rm int} = \partial_1 u_2^{0,\rm int} - \partial_2 u_1^{0,\rm int},$$

and the boundary layer terms are

$$\boldsymbol{V}^E(t,\boldsymbol{y},Z) := \boldsymbol{u}_{\boldsymbol{y}}^{0,\rm b,i}(t,\boldsymbol{y},Z) = e^{-Z/\sqrt{2}} \left(\boldsymbol{u}_{\boldsymbol{y}}^{0,\rm int}(t,\boldsymbol{y}) \cos\left(Z/\sqrt{2}\right) + \left(\boldsymbol{u}_{\boldsymbol{y}}^{0,\rm int}(t,\boldsymbol{y})\right)^{\perp} \sin\left(Z/\sqrt{2}\right) \right).$$

[picture of Ekman spiral solution here]

Now passing to the velocity formulation shows that $\boldsymbol{u}^{0,\rm int}$ must solve

$$\left\{ \begin{array}{rcl} \partial_t \boldsymbol{u}_{\boldsymbol{y}}^{0,\rm int} + \left(\boldsymbol{u}_{\boldsymbol{y}}^{0,\rm int} \cdot \nabla_{\boldsymbol{y}}\right) \boldsymbol{u}_{\boldsymbol{y}}^{0,\rm int} + \sqrt{2} \boldsymbol{u}_{\boldsymbol{y}}^{0,\rm int} + \nabla_{\boldsymbol{y}} p^{0,\rm int} &=& \boldsymbol{0} \\ \nabla_{\boldsymbol{y}} \cdot \boldsymbol{u}_{\boldsymbol{y}}^{0,\rm int} &=& 0. \end{array} \right. \tag{4.9}$$

eq:damped

which is a 2D Euler equation with damping, related to the Ekman pumping phenomenon [?, ref?]. We admit here that this equation is well-posed, so that $\mathbb{U}^1$ is determined up to the choice of an element of the kernel of $\mathbb{L}$.

For the next orders, $\mathbb{U}^k$ are also determined up to elements of $\operatorname{Ker} \mathbb{L}$, and since $\mathbb{L}\mathbb{U}^k = \mathbb{F}(\mathbb{U}^j : 0 \leq j \leq k-1)$, $\boldsymbol{u}^{k,\rm int}$ also solves a linearized version of the damped Euler equation (4.9) about $\boldsymbol{u}_{\boldsymbol{y}}^{0,\rm int}$.

The last step is the construction of the corrector $\boldsymbol{\mathcal{C}}$. Let us denote

$$\boldsymbol{V}^{\rm app} := \sum_{k=0}^{M} \varepsilon^k \boldsymbol{U}^k,$$

which satisfies $\boldsymbol{V}^{\rm app}|_{z=0,1} = O\left(e^{-1/\varepsilon}\right)$ and $\nabla \cdot \boldsymbol{V}^{\rm app} = \mathbb{R}_{\rm d}^{\varepsilon}$ with $\|R_{\rm d}^{\varepsilon}\|_{H^s} = O\left(\varepsilon^{M-1-s}\right)$. We (admit that) we can choose $\boldsymbol{\mathcal{C}}$ such that

$$\left\{ \begin{array}{rcl} \nabla \cdot \boldsymbol{\mathcal{C}} &=& -R_{\rm d}^{\varepsilon} \\ \boldsymbol{\mathcal{C}}|_{z=0,1} &=& O\left(e^{-1/\varepsilon}\right) \end{array} \right.$$

□

From a physical oceanography perspective the Ekman layer comes from wind stress which is forcing the ocean surface, rather than the requirement of zero velocity at the boundary which was used here. Also, the Ekman pumping alluded to above is the mechanism by which wind stress forcing causes a downward (upward) flow of water due to convergence (divergence) of surface waters.

Now we can wonder in which sense $\boldsymbol{u}^{\varepsilon}$ does converge to $\boldsymbol{u}^{\rm app}$. The following results provides an answer.

Theorem 4.1.3 (Grenier & Masmoudi [??]). *Let $T > 0$. Set*

$$R_0 := \sup_{\substack{t\in[0,T]\\ \boldsymbol{y}\in\mathbb{T}^2}} 2\int_0^{+\infty} Z\partial_Z \boldsymbol{V}^{\mathrm{E}}(t,\boldsymbol{y},Z)\,\mathrm{d}Z,$$

with $\boldsymbol{V}^{\mathrm{E}}$ the Ekman layer defined in (4.6).

If

$$R_0 < 0 \tag{4.10}$$ eq:condR0

and if

$$\|\boldsymbol{u}_0^\varepsilon - \boldsymbol{u}^{0,\mathrm{int}}|_{t=0}\|_{L^2} \underset{\varepsilon\to 0}{\longrightarrow} 0, \tag{4.11}$$ eq:convhyp

then

$$\sup_{[0,T]} \|\boldsymbol{u}^\varepsilon - \boldsymbol{u}^{0,\mathrm{int}}\|_{L^2} \underset{\varepsilon\to 0}{\longrightarrow} 0.$$

Remark 19.

- *As a consequence,*

$$\sup_{[0,T]} \|\boldsymbol{u}^\varepsilon - \boldsymbol{u}^{0,\mathrm{int}}\|_{L^2} \underset{\varepsilon\to \infty}{\longrightarrow} 0.$$

  That is to say that $\boldsymbol{u}^\varepsilon$ converges to the solution of the damped incompressible 2D Euler equation.

- *We can prove more. In fact*

$$\|\boldsymbol{u}^\varepsilon - \boldsymbol{u}^{\mathrm{app}}\|_{H^s} \leq \varepsilon^{M-3/2}, \quad M \geq 2,$$

  if we ask condition (4.11) to hold in H^s spaces. In particular it follows uniform convergence of $\boldsymbol{u}^\varepsilon$, by Sobolev embedding for $s > 1/2$.

- *The condition (4.10) is a well-prepared data assumption. If $\boldsymbol{u}_0^{\mathrm{int}}$ satisfies (4.10) then it is satisfied for small times.*

- *If we take the anisotropic viscosity $\varepsilon\partial_Z^2 + \nu_H\Delta_{\boldsymbol{y}}$ then this latter condition is automatically satisfied for small times and is not required, see Remark 20.*

Proof. Set $\boldsymbol{v} = \boldsymbol{u}^\varepsilon - \boldsymbol{u}^{\mathrm{app}}$. Then $\boldsymbol{v}$ solves the system,

$$\begin{cases} \partial_t\boldsymbol{v} + \boldsymbol{u}^{\mathrm{app}}\cdot\nabla\boldsymbol{v} + \boldsymbol{v}\cdot\nabla\boldsymbol{u}^{\mathrm{app}} + \boldsymbol{v}\cdot\nabla\boldsymbol{v} + \nabla p &= \varepsilon\Delta\boldsymbol{v} + \boldsymbol{R}^\varepsilon \\ \nabla\cdot\boldsymbol{v} &= 0 \\ \boldsymbol{v}|_{z=0,1} &= 0, \end{cases}$$

for $\boldsymbol{R}^\varepsilon$ that satisfies $\sup_{[0,T]}\|\boldsymbol{R}^\varepsilon\|_{L^2} \to 0$ as $\varepsilon \to 0$. We then make the following energy estimate, again by dot multiplying with $\boldsymbol{v}$ and integrating over Ω. Firstly we obtain,

$$\frac{\mathrm{d}}{\mathrm{d}t}\frac{1}{2}\int_\Omega |\boldsymbol{v}|^2\,\mathrm{d}x + \int_\Omega (\boldsymbol{u}^{\mathrm{app}}\cdot\nabla\boldsymbol{v})\cdot\boldsymbol{v} + (\boldsymbol{v}\cdot\nabla\boldsymbol{v})\cdot\boldsymbol{v} + \nabla p\cdot\boldsymbol{v} - \varepsilon\Delta\boldsymbol{v}\cdot\boldsymbol{v}\,\mathrm{d}\boldsymbol{x}$$
$$= \int_\Omega \boldsymbol{R}^\varepsilon\cdot\boldsymbol{v} - (\boldsymbol{v}\cdot\nabla\boldsymbol{u}^{\mathrm{app}})\cdot\boldsymbol{v}\,\mathrm{d}\boldsymbol{x}, \tag{4.12}$$ eqn:GM-2

for which all terms simplify one way or another, except the remainder term that we bound using Cauchy-Schwarz and Young inequality, namely $ab \leq (a^2+b^2)/2$, so that we have,

$$\int_\Omega \boldsymbol{R}^\varepsilon \cdot \boldsymbol{v}\,\mathrm{d}\boldsymbol{x} \leq \frac{1}{2}(\|\boldsymbol{R}^\varepsilon\|_{L^2}^2 + \|\boldsymbol{v}\|_{L^2}^2).$$

The final term of (4.12) requires use of the form of $\boldsymbol{u}^{\mathrm{app}}$. If we expand this then we have separate contributions from the interior and boundary layer parts. Treating the boundary layer parts first, we have that the magnitude of the gradient in these regions is dominated by the vertical derivative. For the boundary at $z=0$,

$$\int_\Omega (\boldsymbol{v}\cdot\nabla \boldsymbol{u}^{0,\mathrm{b},0})\cdot\boldsymbol{v}\,\mathrm{d}\boldsymbol{x} \sim \left|\frac{1}{\varepsilon}\int_\Omega v_3 \partial_Z \boldsymbol{u}^{0,\mathrm{b},0}\left(t,\boldsymbol{y},\frac{z}{\varepsilon}\right)\cdot\boldsymbol{v}\,\mathrm{d}\boldsymbol{x}\right|, \tag{4.13}$$

eqn:bounda

and similarly for the boundary layer at $z=1$. Now we notice that we can use Cauchy-Schwarz again, and that $\boldsymbol{v}|_{z=0}=\boldsymbol{0}$, to obtain,

$$\begin{aligned}|\boldsymbol{v}(t,\boldsymbol{y},z)| &= \left|\int_0^z \partial_z \boldsymbol{v}(t,\boldsymbol{y},w)\,\mathrm{d}w\right| \\ &\leq z^{1/2}\left(\int_0^z |\partial_z\boldsymbol{v}(t,\boldsymbol{y},w)|^2\,\mathrm{d}w\right)^{1/2},\end{aligned}$$

which can then be substituted into the previous equation,

$$\begin{aligned}\left|\frac{1}{\varepsilon}\int_\Omega v_3\partial_Z\boldsymbol{u}^{0,\mathrm{b},0}\left(t,\boldsymbol{y},\frac{z}{\varepsilon}\right)\cdot\boldsymbol{v}\,\mathrm{d}\boldsymbol{x}\right| &\leq \frac{1}{\varepsilon}\int_\Omega |\boldsymbol{v}|^2\left|\partial_Z\boldsymbol{u}^{0,\mathrm{b},0}\left(t,\boldsymbol{y},\frac{z}{\varepsilon}\right)\right|\,\mathrm{d}\boldsymbol{x} \\ &\leq \frac{1}{\varepsilon}\int_\Omega z\left(\int_0^z |\partial_z\boldsymbol{v}(t,\boldsymbol{y},w)|^2\,\mathrm{d}w\right)\left|\partial_Z\boldsymbol{u}^{0,\mathrm{b},0}\left(t,\boldsymbol{y},\frac{z}{\varepsilon}\right)\right|\,\mathrm{d}\boldsymbol{x} \\ &\leq \sup_{\substack{t\in[0,T]\\ \boldsymbol{y}\in\mathbb{T}^2}}\left(\int_0^1 \frac{z}{\varepsilon}\left|\partial_Z\boldsymbol{u}^{0,\mathrm{b},0}\left(t,\boldsymbol{y},\frac{z}{\varepsilon}\right)\right|\,\mathrm{d}z\right)\int_\Omega |\partial_z\boldsymbol{v}|^2\,\mathrm{d}\boldsymbol{x} \\ &\leq \varepsilon\sup_{\substack{t\in[0,T]\\ \boldsymbol{y}\in\mathbb{T}^2}}\left(\int_0^\infty Z|\partial_Z\boldsymbol{u}^{0,\mathrm{b},0}(t,\boldsymbol{y},Z)|\,\mathrm{d}Z\right)\int_\Omega |\partial_z\boldsymbol{v}|^2\,\mathrm{d}\boldsymbol{x} \\ &\leq \frac{\varepsilon R_0}{2}\|\partial_z\boldsymbol{v}\|_{L^2}^2.\end{aligned}$$

We also get the same contribution from the other boundary layer. Now returning to the contribution from the interior part, since $\boldsymbol{u}^{0,\mathrm{int}}$ is independent of ε we can find a constant C, dependent on the supremum of gradients of $\boldsymbol{u}^{0,\mathrm{int}}$ (so also independent of ε) such that,

$$\int_\Omega (\boldsymbol{v}\cdot\nabla\boldsymbol{u}^{0,\mathrm{int}})\cdot\boldsymbol{v}\,\mathrm{d}\boldsymbol{x} \leq C\|\boldsymbol{v}\|_{L^2}^2.$$

Putting this all together and using the assumption that $R_0<1$ we have,

$$\begin{aligned}\frac{\mathrm{d}}{\mathrm{d}t}\frac{1}{2}\|\boldsymbol{v}\|_{L^2}^2 + \varepsilon(1-R_0)\|\nabla\boldsymbol{v}\|_{L^2}^2 &\leq \frac{1}{2}\left(\|\boldsymbol{R}^\varepsilon\|_{L^2}^2 + \|\boldsymbol{v}\|_{L^2}^2\right) + C\|\boldsymbol{v}\|_{L^2}^2 \\ \frac{\mathrm{d}}{\mathrm{d}t}\|\boldsymbol{v}\|_{L^2}^2 &\leq \|\boldsymbol{R}^\varepsilon\|_{L^2}^2 + D\|\boldsymbol{v}\|_{L^2}^2\end{aligned}$$

where $D = 2C + 1$. We can now use Grönwall's inequality to give,

$$\|\boldsymbol{v}(t)\|_{L^2}^2 \leq \|\boldsymbol{v}|_{t=0}\|_{L^2}^2 e^{Dt} + e^{Dt} \int_0^t \|\boldsymbol{R}^\varepsilon\|_{L^2}^2 \,\mathrm{d}s.$$

Since both $\|\boldsymbol{v}|_{t=0}\|_{L^2}$ and $\|\boldsymbol{R}^\varepsilon\|_{L^2}$ vanish as ε goes to zero, this concludes the proof. □

rk:R0 **Remark 20.** *In the case of anisotropic vorticity, $\varepsilon\partial_z^2 + \nu_H \Delta_{\boldsymbol{y}}$, we firstly replace the energy dissipation term $\varepsilon \int_\Omega |\nabla \boldsymbol{v}|^2 \,\mathrm{d}\boldsymbol{x}$ by $\varepsilon \int_\Omega |\partial_Z \boldsymbol{v}|^2 \,\mathrm{d}\boldsymbol{x} + \nu_H \int_\Omega |\nabla_{\boldsymbol{y}} \boldsymbol{v}|^2 \,\mathrm{d}\boldsymbol{x}$. Also, going on from equation (4.13) we can try to make use of the anisotropy by noticing that $\boldsymbol{u}^{0,\mathrm{b},0}$ has no vertical component, so the dot product with $\boldsymbol{v}$ leaves behind only $\boldsymbol{v}_{\boldsymbol{y}}$. In particular, we have that this equation is instead less than or equal to*

$$\begin{aligned}
\frac{1}{\varepsilon} \int_\Omega z \left(\int_0^z |\partial_z v_3(t, \boldsymbol{y}, w)|^2 \,\mathrm{d}w \right)^{1/2} \left(\int_0^z |\partial_z \boldsymbol{v}_{\boldsymbol{y}}(t, \boldsymbol{y}, w)|^2 \,\mathrm{d}w \right)^{1/2} \left| \partial_Z \boldsymbol{u}^{0,\mathrm{b},0} \left(t, \boldsymbol{y}, \frac{z}{\varepsilon} \right) \right| \,\mathrm{d}\boldsymbol{x} \\
&\leq \varepsilon \frac{R_0}{2} \|\partial_z v_3\|_{L^2} \|\partial_z \boldsymbol{v}_{\boldsymbol{y}}\|_{L^2} \\
&\leq \varepsilon \frac{R_0}{2} \|\nabla_{\boldsymbol{y}} \boldsymbol{v}\|_{L^2} \|\partial_z \boldsymbol{v}\|_{L^2} \\
&\leq \frac{\varepsilon}{4} \|\partial_z \boldsymbol{v}\|_{L^2}^2 + \frac{C}{2} R_0^2 \varepsilon \|\nabla_{\boldsymbol{y}} \boldsymbol{v}\|_{L^2}^2.
\end{aligned}$$

Finally taking into account the second boundary layer too we see that a similar energy estimate can be made for the anisotropic case without the need for $R_0 < 1$, instead requiring that $\nu_H - C R_0^2 \varepsilon > 0$, which is true for ε sufficiently small.

4.2 Sizes of boundary layers

The following section will address the question of how to compute the sizes of boundary layers in different geophysical fluids, and will give us a general recipe to do so. In geophysical fluids, these boundary layers will often come from the linear part of the equation.

Linear systems with boundary and initial conditions take the form:

$$\begin{cases}
L^\varepsilon(\partial_t, \partial_y, \partial_z) U &= F \quad \text{for } z > 0, \\
B(\partial_t, \partial_y, \partial_z) U_{|z=0} &= g, \\
U_{|t=0} &= U_0.
\end{cases}$$

We note the following general facts about such systems.

- Before considering the dependence on ε, let us suppose that is fixed and so we can ignore it for now. This allows us to consider minimal well-posedness assumptions for such PDEs.

- The Cauchy problem satisfies the system

$$\begin{cases}
L(\partial_t, \partial_y, \partial_z) U &= F \quad \text{for } t > 0, \boldsymbol{y} \in \mathbb{R}^2, z \in \mathbb{R}, \\
U_{|t=0} &= U_0.
\end{cases}$$

For the Cauchy case, we may look for a solution which takes the form of a linear superposition of plane waves. Plane waves take the form $U = \mathrm{e}^{(\gamma t + i\tau t)}\mathrm{e}^{i\boldsymbol{\xi}\cdot\boldsymbol{x}}$ where $\boldsymbol{x} = (\boldsymbol{y}, z)$. We can find one non-zero solution of this form, which satisfies

$$D(\gamma + i\tau, i\boldsymbol{\xi}) := \det L^*(\gamma + i\tau, i\boldsymbol{\xi}) = 0. \tag{4.14}$$

For well-posedness, this must also satisfy the assumptions that

$$\begin{cases} D(\gamma + i\tau, i\boldsymbol{\xi}) = 0 \implies \gamma = 0, \\ \gamma \geq 0. \end{cases} \tag{4.15}$$ eqn:LEwell

Usually, there is also homogeneity, such that if $D(\gamma_0 + i\tau_0, i\boldsymbol{\xi}_0) = 0$ for $\gamma_0 > 0$ then $D(\lambda^\alpha(\gamma_0 + i\tau_0), i\lambda^\beta\boldsymbol{\xi}_0) = \lambda D(\gamma_0 + i\tau_0, i\boldsymbol{\xi}_0) = 0 \implies$ ill-posed.

We can reduce the linear system of equations to

$$\begin{cases} LU = F \quad \text{for } z > 0, t \in \mathbb{R}, \\ BU_{|z=0} = g, \end{cases}$$

such that $F, g_{|t<0} = 0$, which will allow us to take Fourier transforms. We also want $U_{|t<0} = 0$. We take a Laplace transform in time and a Fourier transform in space, noting that the operators L, B, F, g will now denote the transforms, the system becomes an ODE in z:

$$\begin{cases} L(\gamma + i\tau, i\eta, \partial_z)v = F, \\ B(\gamma + i\tau, i\eta, \partial_z)v_{|z=0} = g. \end{cases}$$

Assuming that L is not of first order in z, we transform into

$$\begin{cases} \partial_z V = G(\gamma + i\tau, i\eta)V + \mathbb{F}, \\ \Gamma V_{|z=0} = \mathfrak{G}. \end{cases}$$

lem:eigenvalues **Lemma 4.2.1.** *Assuming (4.15), G for $\gamma > 0$ has no eigenvalues on the imaginary axis.*

Proof. If $i\mu$ is an eigenvalue of G then $\det L(\gamma + i\tau, i\eta, i\mu) = 0 \implies \gamma = 0$ by (4.15). □

Remark 21. *The number of positive (N^+) and negative (N^-) eigenvalues is independent of the parameters $\gamma > 0$, τ and η.*

A consequence of Lemma 4.2.1 is that $\exists\, \Pi_\pm$ projectors such that $G\Pi_\pm(\gamma, \tau, \eta) = \Pi_\pm G$. Call $G_\pm = \Pi_\pm G$ and decompose V such that $V = V_+ + V_-$ where $V_+ \in \mathrm{Im}\,(\Pi_+)$ and $V_- \in \mathrm{Im}\,(\Pi_-)$. Now our system of equations may be written in the form

$$\begin{cases} \partial_z V_+ = G_+V_+ + \Pi_+ + \mathbb{F} & z > 0, \\ \partial_z V_- = G_-V_- + \Pi_+\mathbb{F} & z > 0, \\ \Gamma(V_+ + V_-)_{|z=0} = g \end{cases}$$

We have now obtained a system of constant coefficient linear ODEs, so we can solve using the exponential of the matrices, and the fact that $G_\pm$ has only eigenvalues of positive

(negative) real part. That is to say, $G_+ \to \boldsymbol{\mathcal{C}}_+ := \sigma(G_+) \subset \{\mathrm{Re}\lambda > 0\}$ and $G_- \to \boldsymbol{\mathcal{C}}_- := \sigma(G_-) \subset \{\mathrm{Re}\lambda < 0\}$. We find that

$$\left\{\begin{array}{rcl} \Pi_+ & = & \int_{\partial \boldsymbol{\mathcal{C}}_+} (\lambda - G)^{-1}\, d\lambda, \\ V_+(z) & = & -\int_z^\infty \mathrm{e}^{(z-y)G_+} \Pi_+ \mathbb{F}(y) dy, \\ V_-(z) & = & \mathrm{e}^{-zG_-} v^0 + \int_0^z \mathrm{e}^{(z-y)G_-} \Pi_- \mathbb{F}(y) dy, \end{array}\right.$$

with v^0 currently free but required to satisfy the necessary condition that $\Gamma v^0 = g + \Gamma \int_0^\infty \mathrm{e}^{-yG_+} \mathbb{F}_+(y) dy$, in order to satisfy the boundary condition. We note the following facts and consequences:

- $\Gamma : \mathrm{Im}\ \Pi_- \to \mathrm{Im}\ \Gamma$ is an isomorphism,
- $\mathrm{rank}\ \Gamma = N$,
- $\Delta(\gamma, \tau, \eta) = \det\left({}^{\Gamma}/_{\mathrm{Im}\ \Pi_-}\right) \neq 0$ (Lopatinski condition).

We will now study three short examples.

- **The heat equation.** For this example, the system of equations is written

$$\left\{\begin{array}{rcl} \partial_t u - \Delta u & = & F, \\ u_{|z=0} & = & 0. \end{array}\right.$$

  Taking the Laplace transform:

$$\left\{\begin{array}{rcl} \left(\gamma + iz + |\eta|^2\right) u - \partial_z^2 u & = & F, \\ u_{|z=0} & = & 0. \end{array}\right.$$

  We may then rewrite this as

$$\left\{\begin{array}{rcccl} \partial_z V & = & GV + \begin{pmatrix} 0 \\ F \end{pmatrix} G & = & \begin{pmatrix} 0 & 1 \\ \gamma + i\tau + |\eta|^2 & 0 \end{pmatrix}, \\ \Gamma V & = & \begin{pmatrix} v_1 \\ 0 \end{pmatrix} & = & 0, \end{array}\right.$$

  where $V = \begin{pmatrix} v_1 \\ v_2 \end{pmatrix} = \begin{pmatrix} u \\ d_z u \end{pmatrix}$.

  We find eigenvalues $\mu = \pm\sqrt{\gamma + |\eta|^2 + i\tau}$ which are not on the imaginary axis. $N_- = 1$ and the Lopatinski condition holds $\iff$ $\Gamma R_- \neq 0$, where R_- is the eigenvector associated to the negative eigenvalue.

- **General hyperbolic systems.** For general hyperbolic systems,

$$\partial_z u + \sum_{k=1}^d A_k \frac{\partial U}{\partial x_k} = F, \text{ for } t = x_d > 0,$$

  $A(\boldsymbol{\xi}) = \sum_{k=1}^d \xi_k A_k$ has real eigenvalues. If A_d is invertible, it is an exercise to show that N_- is equal to the number of positive eigenvalues of A_d.

- **Including ε.** Suppose that we now reintroduce our dependence on ε. In this example, our system is still

$$\left\{\begin{array}{rcl} \partial_z V_+ &=& G_+^\varepsilon(\gamma+i\tau,\eta)V_+ + \mathbb{F}_+, \\ \partial_z V_- &=& G_-^\varepsilon(\gamma+i\tau,\eta)V_- + \mathbb{F}_-, \\ \Gamma(V_+ + V_-)_{|z=0} &=& g \end{array}\right. \tag{4.16}$$

eqn:ch2ex3

What happens as $\varepsilon \to 0$? If there is an eigenvalue μ^ε of G^ε such that $|\mu^\varepsilon| \to 0$ as $\varepsilon \to 0$, then (4.16) becomes

$$\left\{\begin{array}{rcl} \partial_z v_-^{\mathrm{b},\varepsilon} &=& \mu^\varepsilon v_-^{\mathrm{b},\varepsilon} + (\ldots) \\ \partial_z v_-^{\mathrm{g},\varepsilon} &=& G^\varepsilon v_-^{\mathrm{g},\varepsilon} + (\ldots), \end{array}\right.$$

hence we cannot use this component to match the boundary condition and so we must have a boundary layer here. The size of the boundary layer will be

$$\mu^\varepsilon \sim -\frac{C}{\varepsilon^\alpha} \text{ as } \varepsilon \to 0 \text{ with } \alpha > 0.$$

A good boundary layer scaling is $v_-^{\mathrm{b},\varepsilon}\left(\frac{z}{\varepsilon^\alpha}\right)$.

We study now the solutions of $D(\gamma+i\tau, i\eta, \mu) = 0$ with $\mathrm{Re}\mu^\varepsilon < 0$ in order to find a general recipe to get the sizes of boundary layers. If $\exists\ \mu_i^\varepsilon$ such that $|\mu_i^\varepsilon| \to \infty$ as $\varepsilon \to 0$ this will give us the scaling of the boundary layer. Supposing that $|\mu^\varepsilon| \sim C/\varepsilon^\alpha$ as $\varepsilon \to 0$, then the boundary layer will be of size ε^α. [REFS - ??-Grenier and ??-T. Paul]

We study three further examples to find the sizes of boundary layers in the given geophysical systems.

- **Ekman Layer.** Does our recipe give us back the correct scaling?

$$\left\{\begin{array}{rcl} \partial_t \boldsymbol{u} + \dfrac{\boldsymbol{e}\times\boldsymbol{u}}{\varepsilon} + \dfrac{\nabla p}{\varepsilon} &=& \varepsilon\Delta\boldsymbol{u}, \quad z>0 \\ \nabla\cdot\boldsymbol{u} &=& 0 \end{array}\right.$$

We get

$$\varepsilon^2 D^\varepsilon(\gamma+i\tau, i\eta, \mu) = \varepsilon^2 \det \begin{pmatrix} \gamma+i\tau+\varepsilon|\eta|^2-\varepsilon\mu^2 & -\frac{1}{\varepsilon} & 0 & \frac{i\eta_1}{\varepsilon} \\ \frac{1}{\varepsilon} & (\gamma+\ldots) & 0 & \frac{i\eta_2}{\varepsilon} \\ 0 & 0 & (\gamma+\ldots) & -\frac{\mu}{\varepsilon} \\ \eta_1 & \eta_2 & -i\mu & 0 \end{pmatrix}$$
$$= \varepsilon^2(\gamma+i\tau+\varepsilon|\eta|^2-\varepsilon\mu^2)^2(\mu^2-|\eta|^2)+\mu^2 = 0.$$

Do there exist eigenvalues $\mu \to \infty$ as $\varepsilon \to 0$? Indeed we see that there are, given that we have a sixth order polynomial whose leading terms are multiplied by the ε^2 term. The general procedure to solve this would be to look for solutions $\nu = 1/\mu \to 0$. We describe with respect to ε the behaviour close to 0 of the roots of the polynomial. In general this will require a Newton polygon to solve, which allows one to describe all the branches that occur. Look for a change of variables $\nu = t\varepsilon^\alpha$, where $\alpha \in \mathbb{Q}$. Write the coeffecients of the double polynomial in ν, α. Suppose you may write a

term in your polynomial in the form $a_{ij}\nu^i\varepsilon^j$, with $a_{ij} \neq 0$, A general recipe is to find the convex envelope of the set of points in ij-space; α is then given by the slope of the polygon's edges (thus we many find as many α as there are edges). However, it is often much quicker to solve this directly.

If we look for $\mu^\varepsilon = C/\varepsilon^\alpha$ then at leading order, the balance is

$$\varepsilon^2\varepsilon^2 C^6/\varepsilon^{6\alpha} + C^2/\varepsilon^{2\alpha} = 0$$

so that $\alpha = 1$, which is exactly the Ekman layer.

- **Munk layer.** In this example, we will consider a model of wind-driven ocean circulation. The 2D equations,

$$\left\{\begin{array}{rcl} \partial_t\omega + \boldsymbol{u}\cdot\nabla\omega + \frac{r}{2}\omega + \beta u_2 - \nu\Delta\omega - \beta\mathrm{curl}\psi &=& 0, \\ \omega &=& \partial_x u_2 - \partial_y u_1, \\ \nabla\cdot\boldsymbol{u} &=& 0, \end{array}\right. \tag{4.17}$$

eq:munklayer

can be obtained from the 3D rotating incompressible Navier-Stokes equations with forcing, a free surface, and a geometry effect (in this case, this is the term $\beta\mathrm{curl}\psi$, which describes a wind forcing). We also have an Ekman pumping term, $\frac{r}{2}\omega$, and again a representation of the Coriolis force, βu_2. [ref: Desjardins+Grenier for derivation, with rigid boundary approximation]

The domain in this example will be $\chi_W(y) \leq x \leq \chi_E(y)$ [diagram to add]. We scale $\beta = 1/\varepsilon$ with ν, r fixed.

The linear part of this equation is

$$\partial_t w + \frac{r}{2}w + \frac{1}{\varepsilon}u_2 - \nu\Delta w = 0. \tag{4.18}$$

To find $D^\varepsilon(\gamma + i\tau, i\eta, \mu)$, we look for solutions of the form $\mathrm{e}^{(\gamma+i\tau)t}\mathrm{e}^{\mu x}\mathrm{e}^{i\eta y}$ with $\mathrm{Re}\mu < 0, x > 0$. We obtain

$$(\gamma + i\tau) + \frac{r}{2} + \frac{1}{\varepsilon}\frac{\mu}{\mu^2 - \eta^2} - \nu(\mu^2 - \eta^2) = 0 \tag{4.19}$$

since $\partial_k w = \Delta u_2$ [details in recording]. Multiplying through:

$$\varepsilon(\gamma + i\tau)(\mu^2 - \eta^2) + \frac{r}{2}\varepsilon(\mu^2 - \eta^2) + \mu - \nu\varepsilon(\mu^2 - |\eta|^2)^2 = 0. \tag{4.20}$$

Try a solution to this equation of the form $\mu^\varepsilon = c/\varepsilon^\alpha$. The leading balance of the equation is then

$$c/\varepsilon^\alpha - \varepsilon c^4/\varepsilon^{4\alpha} = 0 \implies \alpha = 1/3, c^3 = 1, \tag{4.21}$$

giving us a boundary layer of size $\varepsilon^{1/3}$. If we looked for $x < 0$, we could obtain the Stommel layer.

- **Spherical boundary layers.** For this example, the linear equation is

$$\left\{\begin{array}{rcl} \partial_t\boldsymbol{u} + \frac{1}{\varepsilon}\begin{pmatrix}\sin\theta\\0\\\cos\theta\end{pmatrix} + \frac{1}{\varepsilon}\nabla p &=& \varepsilon\Delta\boldsymbol{u}, \\ \nabla\cdot\boldsymbol{u} &=& 0. \end{array}\right. \tag{4.22}$$

eq:spher_BL

We look for solutions of the form $\mathrm{e}^{(\gamma+i\tau)t}\mathrm{e}^{-\mu x}\mathrm{e}^{i\eta_1 y}\mathrm{e}^{i\eta_2 z}$ satisfying $|\mu^\varepsilon| \to \infty, |\eta_2^\varepsilon| \to \infty$ with $\eta_2^\varepsilon = |\mu^\varepsilon|^{1/2}$, to take into account the geometrical constraint of the sphere.

We get, with $\boldsymbol{\eta} = (\eta_1, \eta_2)$,

$$D^\varepsilon(\gamma + i\tau, i\boldsymbol{\eta}, \mu) = \varepsilon^2(|\boldsymbol{\eta}|^2 - \mu^2)(\gamma + i\tau + \varepsilon(|\boldsymbol{\eta}|^2 - \mu^2))^2 \\ - (\sin\theta)^2\mu^2 + (\cos\theta)^2\eta_2^2 + 2i\mu\eta_2\cos\theta\sin\theta = 0. \quad (4.23)$$

The balance of the leading terms will depend on whether or not our domain is close to the equator.

- Fixing $\theta \neq 0$ with $\eta_2 = \mu^{1/2}$, we find leading terms $-\varepsilon^4\mu^6 = (\sin\theta)^2\mu^2$ which gives a boundary layer of size $\left(\dfrac{\varepsilon}{|\sin(\theta)|}\right)^{1/2}$.
- For $\theta = \varepsilon^\gamma \to 0$ as $\varepsilon \to 0$, a change in the leading terms occurs when $\gamma = 2/5$.
- At the equator, when $\theta = 0$, we have leading orders $-\varepsilon^4\mu^6 + \mu = 0$. For $\mu = c/\varepsilon^\alpha$, this gives $\alpha = 4/5$.

Rigorous studies for these kinds of layers are still few and far between. Even for the linear systems, the boundaries layers can be very degenerate, so even for these seemingly simple linear PDEs, it is not always clear that they are well-posed. The justification, once the boundaries layers are well-posed, of the expansion with the boundary layer of size larger than ε is also unclear.

4.3 Waves

The aim of this lecture is to study waves in the rotating fluid system. Different from the two previous lectures though, here we will omit boundary layers by considering the periodic domain $\mathbb{T}^3$. The rotating fluid equations that we consider are

$$\left\{\begin{array}{rcl} \partial_t \boldsymbol{u}^\varepsilon + (\boldsymbol{u}^\varepsilon \cdot \nabla)\,\boldsymbol{u}^\varepsilon + \dfrac{1}{\varepsilon}\boldsymbol{e} \times \boldsymbol{u}^\varepsilon + \dfrac{1}{\varepsilon}\nabla p^\varepsilon &=& 0 \\ \nabla \cdot \boldsymbol{u}^\varepsilon &=& 0 \\ \boldsymbol{u}^\varepsilon|_{t=0} &=& \boldsymbol{u}_0. \end{array}\right. \quad (4.24)$$

eq:rf

Additionally the viscous terms are not included as they are not important for the present analysis. The framework we will use to study the equations is fairly general, so the incompressible limit of non-rotating equations will also be considered on the same domain. These equations (after scaling analogously to the previous equations) will be

$$\left\{\begin{array}{rcl} \partial_t\rho^\varepsilon + \nabla\cdot(\rho^\varepsilon\boldsymbol{u}^\varepsilon) &=& 0 \\ \partial_t\boldsymbol{u}^\varepsilon + (\boldsymbol{u}^\varepsilon\cdot\nabla)\boldsymbol{u}^\varepsilon + \dfrac{1}{\varepsilon^2}\nabla\rho^\varepsilon &=& 0. \end{array}\right.$$

Remark 22. *Here we have considered the following barotropic pressure law.*

$$p(\rho) = \frac{1}{2}\rho^2.$$

The ε which appears is the Mach number, defined as the ratio of velocity scale to the speed of sound. These equations describe acoustic waves, and also share some similarity with the nondimensional shallow water equations; in 2 dimensions they are equivalent upon replacing ρ^ε with h^ε.

We consider a perturbation of the homogeneous density profile

$$\rho^\varepsilon = 1 + \varepsilon R^\varepsilon,$$

such that the equations on R^ε writes

$$\left\{\begin{array}{rcl} \partial_t R^\varepsilon + (\boldsymbol{u}^\varepsilon \cdot \nabla) R^\varepsilon + \dfrac{1}{\varepsilon}\nabla \cdot \boldsymbol{u}^\varepsilon + R^\varepsilon \nabla \cdot \boldsymbol{u}^\varepsilon &=& 0 \\ \partial_t \boldsymbol{u}^\varepsilon + (\boldsymbol{u}^\varepsilon \cdot \nabla) \boldsymbol{u}^\varepsilon + \dfrac{1}{\varepsilon}\nabla R^\varepsilon &=& 0 \\ \boldsymbol{u}^\varepsilon|_{t=0} &=& \boldsymbol{u}_0 \\ R^\varepsilon|_{t=0} &=& R_0, \end{array}\right. \tag{4.25}$$ eq:ceeps

where $\boldsymbol{u}^\varepsilon$ is not asked to satisfy the divergence free condition. If $\boldsymbol{u}^\varepsilon$ and R^ε converge, we expect their limits to be in the kernel of the singular in ε parts of the equation. In the present case, it would mean that

$$\nabla \cdot \boldsymbol{u}^0 = 0, \qquad \nabla R^0 = \boldsymbol{0},$$

i.e. the limit or $\boldsymbol{u}^\varepsilon$ should satisfy the incompressibility condition and the perturbation R^ε should converge toward a constant.

There are 2 different ways to approach these sets of equations, so we will use different techniques for each. Firstly though, since we are ignoring viscous effects, the equations are able to exhibit a singularity in finite time, and so we need to first ensure that the solution is smooth enough for an interval of time that doesn't depend on ε.

4.3.1 Uniform existence results

Let us consider a general class of system including linear and nonlinear parts, using the formal notation $L(D)$ to denote a Fourier multiplier associated to $L(i\xi)$, *i.e.* a linear operator such that

$$\widehat{L(D)f}(\xi) = L(i\xi)\hat{f}(\xi).$$

For instance, $2\pi i\xi_j$ is the Fourier multiplier for $D = \partial_{x_j}$. The linear part considered is singular such that the general equation is written

$$A^0(\varepsilon \boldsymbol{V})\partial_t \boldsymbol{V} + \frac{1}{\varepsilon}L(D)\boldsymbol{V} + A(\boldsymbol{V}, D)\boldsymbol{V} = 0, \tag{4.26}$$ eqn:generalSystem

with everything depending smoothly on $\boldsymbol{V}$. We also assume the following:

- $A^0(\boldsymbol{U})$ is symmetric positive definite for any $\boldsymbol{U}$ and there exist constants $0 < c_0 < K$ such that
$$\forall \boldsymbol{U} \in B(0,1), \quad c_0 I_N \leq A^0(\boldsymbol{U}) \leq K I_N;$$
- L is skew-symmetric and of order p, meaning that the operator $L(D)$ will consume p derivatives, with estimate
$$\|L(D)\boldsymbol{V}\|_{H^s} \leq C\|\boldsymbol{V}\|_{H^{s+p}}, \quad \forall s;$$

- The latter operator is of the form

$$A(\boldsymbol{V}, D) = \sum_{j=1}^{d} B^j(D) A^j(\boldsymbol{V}) Bj(D) \partial_j \boldsymbol{V},$$

  with $A^j(\boldsymbol{V})$ symmetric matrices and B^j zero order symmetric, which will take no additional derivatives when composed with a differential operator.

Remark 23. *One important consequence of these assumptions is that the derivatives commute with $L(D)$ and B_j.*

Now let us introduce the Leray decomposition of a vector field. A given $\boldsymbol{u}$ can be decomposed into the sum of an irrotational vector field, which can be written in a unique way as the gradient of a scalar field ψ, and a divergence free vector field $\boldsymbol{v}$,

$$\boldsymbol{u} = \nabla\psi + \boldsymbol{v}.$$

This is similar to the Helmholtz decomposition which may be more familiar in the applied literature,

$$\boldsymbol{u} = \nabla\psi + \nabla \times \boldsymbol{A},$$

but is slightly different in that $\boldsymbol{v}$ is unique, whereas $\boldsymbol{A}$ is not. With this introduced, the Leray projector is defined as the projection of a vector field onto its divergence free component.

$$\mathbb{P} : \boldsymbol{u} \mapsto \boldsymbol{v}.$$

If we apply this operator to the rotating fluid equation (4.24) we obtain

$$\partial_t \boldsymbol{u}^\varepsilon + \frac{1}{\varepsilon}\mathbb{P}\left(\boldsymbol{e} \times \mathbb{P}(\boldsymbol{u}^\varepsilon)\right) + \mathbb{P}\left((\boldsymbol{u}^\varepsilon \cdot \nabla)\mathbb{P}(\boldsymbol{u}^\varepsilon)\right) = 0,$$

where we have used the fact that $\nabla \cdot \boldsymbol{u}^\varepsilon = 0$ to add $\mathbb{P}$ where convenient to make the equation look more symmetric. This equation is now of the form (4.26) with

- $L = \mathbb{P}\left(\boldsymbol{e} \times \mathbb{P}(\cdot)\right)$ skew-symmetric;
- $A^0 = I_3$;
- $A(\boldsymbol{u}, D)\boldsymbol{u} = \sum_{j=1}^{d} \mathbb{P}(u_j \partial_j)(\mathbb{P}\boldsymbol{u})$, that is to say $B^j = \mathbb{P}$ and $A^j(\boldsymbol{u}) = u_j I_3$.

thm:gwp **Theorem 4.3.1.** *Let $s > 1 + d/2$. For any $\boldsymbol{V}_0 \in H^s(\mathbb{T}^d)$ there exists $T > 0$ and $\varepsilon_0 > 0$ such that for any $\varepsilon \in (0, \varepsilon_0)$ there exists a unique $\boldsymbol{V}^\varepsilon \in C(0, T; H^s)$ solution of (4.26) such that $\boldsymbol{V}^\varepsilon|_{t=0} = \boldsymbol{V}_0$.*

Reference : [Kleinerman-Majda-Shochet]

Proof. We admit here that for any $\varepsilon > 0$ there exits $T_\varepsilon > 0$ and a unique solution $\boldsymbol{V}^\varepsilon \in C(0, T_\varepsilon; H^s)$. The proof is an energy estimate, and while we can look at general s we assume for simplicity that s is an integer. We get, for any multi-index $\boldsymbol{\alpha}$ such that $|\boldsymbol{\alpha}| \leq s$,

$$A^0(\varepsilon \boldsymbol{V})\partial_t \partial^{\boldsymbol{\alpha}} \boldsymbol{V} + \frac{1}{\varepsilon} L(D)\partial^{\boldsymbol{\alpha}} \boldsymbol{V} + A(\boldsymbol{V}, D)\partial^{\boldsymbol{\alpha}} \boldsymbol{V} = -\boldsymbol{\mathcal{C}}$$

with the commutator term defined as

$$\boldsymbol{\mathcal{C}} = \underbrace{[\partial^{\boldsymbol{\alpha}}, A^0(\varepsilon \boldsymbol{V})]\partial_t \boldsymbol{V}}_{\boldsymbol{\mathcal{C}}_1} + \underbrace{[\partial^{\boldsymbol{\alpha}}, A(\boldsymbol{V}, D)]\boldsymbol{V}}_{\boldsymbol{\mathcal{C}}_2}.$$

In order to bound $\boldsymbol{\mathcal{C}}_1$, let us compute the following derivative, for any $\boldsymbol{\alpha} = \boldsymbol{\beta} + \boldsymbol{e}_j$,

$$\partial^{\boldsymbol{\alpha}}(A^0(\varepsilon \boldsymbol{V})\partial_t \boldsymbol{V}) = \partial^{\boldsymbol{\beta}} \left(DA^0(\varepsilon \boldsymbol{V}) \cdot \partial_{x_j} \boldsymbol{V} \varepsilon \partial_t \boldsymbol{V} + A^0(\varepsilon \boldsymbol{V}) \partial_t \partial_{x_j} \boldsymbol{V} \right). \tag{4.27}$$ eq:dalpha

With this expression and the tame estimates, see for instance [?], one finds

$$\|\boldsymbol{\mathcal{C}}_1\|_{L^2} \leq \varepsilon \Lambda \left(\|\boldsymbol{V}\|_{H^s} \right) \|\partial_t \boldsymbol{V}\|_{H^{s-1}} \tag{4.28}$$

with Λ a continuous increasing function, depending on the operators of the problem. Then using the equation, one finds

$$\begin{aligned} \|\varepsilon \partial_t \boldsymbol{V}\|_{H^{s-1}} &\leq \|L\boldsymbol{V}\|_{H^{s-1}} + \varepsilon \|A(\boldsymbol{V}, D)\|_{H^{s-1}} \\ &\leq C\|\boldsymbol{V}\|_{H^s} + \Lambda \left(\|\boldsymbol{V}\|_{H^s} \right) \|\boldsymbol{V}\|_{H^s}, \end{aligned}$$

that we can rewrite

$$\|\varepsilon \partial_t \boldsymbol{V}\|_{H^{s-1}} \leq \Lambda(\|\boldsymbol{V}\|_{H^s}) \|\boldsymbol{V}\|_{H^s}. \tag{4.29}$$ eq:ept

Remark 24. *If $A^0 \neq I_N$, we assume $p \leq 1$.*

Also applying directly the same inequality to the second commutator term provides

$$\|\boldsymbol{\mathcal{C}}_2\|_{L^2} \leq \Lambda \left(\|\boldsymbol{V}\|_{H^s} \right) \|\boldsymbol{V}\|_{H^s}.$$

From (4.27) we get

$$\int A^0(\varepsilon \boldsymbol{V}) \partial_t \partial^{\boldsymbol{\alpha}} V \cdot \partial^{\alpha} \boldsymbol{V} + \frac{1}{\varepsilon} \int L(D) \partial^{\boldsymbol{\alpha}} \boldsymbol{V} \cdot \partial^{\boldsymbol{\alpha}} \boldsymbol{V} + \int A(\boldsymbol{V}, D) \partial^{\boldsymbol{\alpha}} \boldsymbol{V} \cdot \partial^{\boldsymbol{\alpha}} \boldsymbol{V} = - \int \boldsymbol{\mathcal{C}} \cdot \partial^{\boldsymbol{\alpha}} \boldsymbol{V}.$$

The integral on $L(D)$ is equal to zero since L is skew-symmetric. Besides, we observe that

$$\frac{\mathrm{d}}{\mathrm{d}t} \int A^0(\varepsilon \boldsymbol{V}) \partial^{\boldsymbol{\alpha}} \boldsymbol{V} \cdot \partial^{\boldsymbol{\alpha}} \boldsymbol{V} = \int A^0(\varepsilon \boldsymbol{V}) \partial_t \partial^{\boldsymbol{\alpha}} \boldsymbol{V} \cdot \partial^{\boldsymbol{\alpha}} \boldsymbol{V} + \varepsilon \underbrace{\int DA^0(\varepsilon \boldsymbol{V}) \partial_t \boldsymbol{V} \partial^{\boldsymbol{\alpha}} \boldsymbol{V} \cdot \partial^{\boldsymbol{\alpha}} \boldsymbol{V}}_{\boldsymbol{\mathcal{C}}_\varepsilon}.$$

Let us bound this latter integral,

$$|\boldsymbol{\mathcal{C}}_\varepsilon| \leq \|DA^0(\varepsilon \boldsymbol{V}) \varepsilon \partial_t \boldsymbol{V}\|_{L^\infty} \|\partial^{\boldsymbol{\alpha}} \boldsymbol{V}\|_{L^2}^2,$$

where we have uniformly bounded ε since it is meant to be very small. Use that $s-1 > d/2$, the smoothness of A^0 and the compactness of the spatial domain to obtain

$$|\boldsymbol{\mathcal{C}}_\varepsilon| \leq \Lambda \left(\|\boldsymbol{V}\|_{H^s} \right) \|\varepsilon \partial_t \boldsymbol{V}\|_{H^{s-1}} \|\boldsymbol{V}\|_{H^s}^2.$$

Now, using estimate (4.29) we can merge different non-decreasing maps Λ and obtain

$$|\boldsymbol{\mathcal{C}}_\varepsilon| \leq \Lambda \left(\|\boldsymbol{V}\|_{H^s} \right) \|\boldsymbol{V}\|_{H^s}^2.$$

It remains to expand $A(\boldsymbol{V}, D)$ and to estimate the following integrals

$$\int B^j(D)A^j(\boldsymbol{V})B^j(D)\partial_j\partial^{\boldsymbol{\alpha}}\boldsymbol{V}\cdot\partial^{\boldsymbol{\alpha}}\boldsymbol{V} = -\int B^j(D)DA^j(\boldsymbol{V})\partial_j\boldsymbol{V}B^j(D)\partial^{\boldsymbol{\alpha}}\boldsymbol{V}\cdot\partial^{\boldsymbol{\alpha}}\boldsymbol{V}$$
$$\leq \Lambda\left(\|\boldsymbol{V}\|_{H^s}\right)\|\boldsymbol{V}\|_{H^s}^2.$$

In summary,

$$\frac{\mathrm{d}}{\mathrm{d}t}\frac{1}{2}\int A^0(\varepsilon\boldsymbol{V})\partial^{\boldsymbol{\alpha}}\boldsymbol{V}\partial^{\boldsymbol{\alpha}} \leq \Lambda\left(\|\boldsymbol{V}\|_{H^s}\right)\|\boldsymbol{V}\|_{H^s}^2.$$

Integrate with respect to time and sum up for $|\boldsymbol{\alpha}| \leq s$ yields

$$\left(\sum_{|\boldsymbol{\alpha}|\leq s}\int A^0(\varepsilon\boldsymbol{V})\partial^{\boldsymbol{\alpha}}\boldsymbol{V}\cdot\partial^{\boldsymbol{\alpha}}\boldsymbol{V}\right)(t) \leq \left(\sum_{|\boldsymbol{\alpha}|\leq s}\int A^0(\varepsilon\boldsymbol{V})\partial^{\boldsymbol{\alpha}}\boldsymbol{V}\cdot\partial^{\boldsymbol{\alpha}}\boldsymbol{V}\right)(0)$$
$$+\int_0^t \Lambda\left(\|\boldsymbol{V}\|_{H^s}\right)\|\boldsymbol{V}(\tau)\|_{H^s}^2\,\mathrm{d}\tau.$$

Thanks to the former assumption on A^0, we can deduce

$$c_0\|\boldsymbol{V}(t)\|_{H^s}^2 \leq K\|\boldsymbol{V}_0\|_{H^s}^2 + \int_0^t \Lambda\left(\|\boldsymbol{V}\|_{H^s}\right)\|\boldsymbol{V}(\tau)\|_{H^s}^2\,\mathrm{d}\tau.$$

Now we can infer that there exists some time of existence uniform with respect to ε. Let us consider $R > 0$ such that

$$\frac{2K}{c_0}\|\boldsymbol{V}_0\|_{H^s} \leq R.$$

From the local existence result we can define

$$T_\varepsilon^* := \sup\{T : \sup_{[0,T]}\|\boldsymbol{V}\|_{H^s}^2 \leq R\}$$

so that either $T_\varepsilon^* = +\infty$ or $T_\varepsilon^* < +\infty$ and $\sup_{[0,T_\varepsilon^*)}\|\boldsymbol{V}\|_{H^s}^2 = R$. Hence any $T > 0$ satisfying

$$\frac{K}{c_0}\|\boldsymbol{V}_0\|_{H^s}^2 + T\Lambda(R^{1/2})R \leq \frac{3}{2}\frac{K}{c_0}\|\boldsymbol{V}_0\|_{H^s}^2$$

also satisfy $T < T_\varepsilon^*$, providing the result. □

The next step is to describe $\boldsymbol{V}^\varepsilon$ when ε goes to 0. There are at least two ways to do it:

- Using the energy estimate and some weak convergence argument;
- Using the filtering method (introduced by Schochet and Grenier), requiring to study the continuous semigroup $e^{tL/\varepsilon}$.

4.3.2 Incompressible limit

As in our first example, let us recall the compressible Euler equations,

$$\left\{\begin{array}{rcl} \partial_t R^\varepsilon + (\boldsymbol{u}^\varepsilon\cdot\nabla)R^\varepsilon + \dfrac{1}{\varepsilon}\nabla\cdot\boldsymbol{u}^\varepsilon + R^\varepsilon\nabla\cdot\boldsymbol{u}^\varepsilon &=& 0\\ \partial_t\boldsymbol{u}^\varepsilon + (\boldsymbol{u}^\varepsilon\cdot\nabla)\,\boldsymbol{u}^\varepsilon + \dfrac{1}{\varepsilon}\nabla R^\varepsilon &=& 0, \end{array}\right. \tag{4.30}$$

eqn:incompEuler

which also writes, while dropping the ε superscript for sake of simplification,

$$\left\{\begin{array}{rcl} \partial_t R + (\boldsymbol{u}\cdot\nabla)\,R + \dfrac{1}{\varepsilon}\nabla\cdot\boldsymbol{u} + R\nabla\cdot\boldsymbol{u} &=& 0\\ (1+\varepsilon R)\partial_t\boldsymbol{u} + (1+\varepsilon R)(\boldsymbol{u}\cdot\nabla)\boldsymbol{u} + \dfrac{1}{\varepsilon}\nabla R + R\nabla R &=& 0, \end{array}\right.$$

where momentum equation has been multiplied by $1+\varepsilon R$ for convenience. Note that this system is also of the form (4.26) with

$$\left\{\begin{array}{ll} \boldsymbol{V} = \begin{pmatrix} R\\ \boldsymbol{u}\end{pmatrix}, & A^0(\varepsilon\boldsymbol{V}) = \begin{pmatrix} 1 & 0\\ 0 & (1+\varepsilon R)\mathrm{Id}\end{pmatrix}, \qquad L(D) = \begin{pmatrix} 0 & \nabla\cdot\\ \nabla & 0\end{pmatrix}\\ B_j = \mathrm{Id}, & A(\boldsymbol{V},\boldsymbol{\xi}) = \sum_{j=1}^d \xi_j A_j(\boldsymbol{V}) = \begin{pmatrix} \boldsymbol{u}\cdot\boldsymbol{\xi} & R\boldsymbol{\xi}^T\\ R\boldsymbol{\xi} & (1+\varepsilon R)\boldsymbol{u}\cdot\boldsymbol{\xi}\mathrm{Id}\end{pmatrix}, \end{array}\right.$$

satisfying indeed $L^* = -L$ and $A(\boldsymbol{V},\boldsymbol{\xi})$ symmetric for any $\boldsymbol{\xi}\in\mathbb{R}^d$. Now we can state the convergence result.

Theorem 4.3.2. *Let $\boldsymbol{V}_0 \in H^s$ for $s > 1+d/2$ and $T>0$ given by the previous result. Then $\boldsymbol{u}^\varepsilon$ converges weakly in $L^2([0,T]\times\mathbb{T}^3)$ to $\boldsymbol{u}$ the solution of the incompressible Euler equation*

$$\left\{\begin{array}{rcl} \partial_t\boldsymbol{u} + (\boldsymbol{u}\cdot\nabla)\,\boldsymbol{u} + \nabla p &=& \boldsymbol{0}\\ \nabla\cdot\boldsymbol{u} &=& 0\\ \boldsymbol{u}|_{t=0} &=& \mathbb{P}(\boldsymbol{u}_0). \end{array}\right.$$

Proof. In what follows, the technique comes from Lions and Masmoudi for the Navier-Stokes equation, see for instance [?].

From the general H^s estimates obtained in the proof of Theorem 4.3.1 we obtain that for any $T>0$ the H^s norm of $\boldsymbol{u}^\varepsilon$ is uniformly bounded with respect to ε. In particular $\boldsymbol{u}^\varepsilon$ converges weakly in H^{s-1} toward some $\boldsymbol{u}$, up to an extraction. By multiplying the first equation of (**??**) and letting ε go to 0 we obtain that $\boldsymbol{u}$ is divergence-free. Besides $\boldsymbol{v}^\varepsilon := \mathbb{P}(\boldsymbol{u}^\varepsilon)$ inherits from the same boundedness of $\boldsymbol{u}^\varepsilon$. Moreover, applying the Leray projector on equation (**??**) provides

$$\left\{\begin{array}{rcl} \partial_t\boldsymbol{v}^\varepsilon + \mathbb{P}\left((\boldsymbol{u}^\varepsilon\cdot\nabla)\,\boldsymbol{u}^\varepsilon\right) &=& \boldsymbol{0}\\ \nabla\cdot\boldsymbol{v}^\varepsilon &=& 0\\ \boldsymbol{v}^\varepsilon|_{t=0} &=& \mathbb{P}(\boldsymbol{u}_0), \end{array}\right. \tag{4.31}$$

eq:pie

since the term $R\nabla R$ also writes $\nabla R^2/2$. We infer that

$$\begin{aligned} \sup_{[0,T]}\|\partial_t\boldsymbol{v}^\varepsilon\|_{H^{s-1}} &\le \|\mathbb{P}\left((\boldsymbol{u}^\varepsilon\cdot\nabla)\boldsymbol{u}^\varepsilon\right)\|_{H^{s-1}}\\ &\le \|\boldsymbol{u}^\varepsilon\|_{H^{s-1}}\|\boldsymbol{u}^\varepsilon\|_{H^s}, \end{aligned}$$

so that Ascoli theorem applies and provide the strong convergence of $\boldsymbol{v}^\varepsilon$ toward some $\boldsymbol{v}$ in $C([0,T];H^\sigma(\mathbb{T}^3))$ for any $\sigma < s$. Since $\mathbb{P}(\boldsymbol{u}) = \boldsymbol{u}$, the continuity of $\mathbb{P}$ and the uniqueness of the limit provide $\boldsymbol{v} = \boldsymbol{u}$. From the weak (resp. strong) convergence of $\boldsymbol{u}^\varepsilon$ (resp. $\boldsymbol{v}^\varepsilon$) and the Leray decomposition

$$\boldsymbol{u}^\varepsilon = \nabla\psi^\varepsilon + \boldsymbol{v}^\varepsilon$$

we obtain that both $\nabla\psi^\varepsilon$ and $\nabla^2\psi^\varepsilon$ converge weakly toward $\mathbf{0}$ in $L^2([0,T]\times\mathbb{T}^3)$. The strong-strong and weak-strong convergences allow to pass to the limit in

$$\mathbb{P}((\boldsymbol{u}^\varepsilon\cdot\nabla)\boldsymbol{u}^\varepsilon) = \mathbb{P}\left(((\nabla\psi^\varepsilon+\boldsymbol{v}^\varepsilon)\cdot\nabla)\,(\nabla\psi^\varepsilon+\boldsymbol{v}^\varepsilon)\right)$$

except for the following term, which actually vanishes,

$$\mathbb{P}\left((\nabla\psi^\varepsilon\cdot\nabla)\,\nabla\psi^\varepsilon\right) = \frac{1}{2}\mathbb{P}\left(\nabla\left|\nabla\psi^\varepsilon\right|^2\right) = \mathbf{0}.$$

Therefore, we obtain as ε goes to zero that the limit $\boldsymbol{u}$ satisfies

$$\left\{\begin{array}{rcl}\partial_t\boldsymbol{u}+\mathbb{P}\left((\boldsymbol{u}\cdot\nabla)\boldsymbol{u}\right) &=& \mathbf{0}\\ \nabla\cdot\boldsymbol{u} &=& 0\\ \boldsymbol{u}|_{t=0} &=& \mathbb{P}(\boldsymbol{u}_0),\end{array}\right.$$

from which one can always recover the pressure. □

4.3.3 Rotating fluids

We use a different strategy called the *filtering method* in order to deal with the rotating fluids equation

$$\partial_t\boldsymbol{u}^\varepsilon + \frac{1}{\varepsilon}L\boldsymbol{u}^\varepsilon + \mathbb{P}\left((\boldsymbol{u}^\varepsilon\cdot\nabla)\,\boldsymbol{u}^\varepsilon\right) = \mathbf{0}$$

where $L\boldsymbol{u}^\varepsilon = \mathbb{P}(\boldsymbol{e}\times\boldsymbol{u}^\varepsilon)$. The filtering method consists in writing $\boldsymbol{u}^\varepsilon = e^{-tL/\varepsilon}\boldsymbol{v}^\varepsilon$. Upon substitution into the previous equation, we find that $\boldsymbol{v}^\varepsilon$ satisfy

$$\partial_t\boldsymbol{v}^\varepsilon + e^{tL/\varepsilon}\mathbb{P}\left(\left(\left(e^{-tL/\varepsilon}\boldsymbol{v}^\varepsilon\right)\cdot\nabla\right)e^{-tL/\varepsilon}\boldsymbol{v}^\varepsilon\right) = \mathbf{0}.$$

Notice that it is equivalent to have $\boldsymbol{u}^\varepsilon$ or $\boldsymbol{v}^\varepsilon$ bounded in $C([0,T];H^s(\mathbb{T}^3))$. Hence here $\partial_t\boldsymbol{v}^\varepsilon$ is bounded in $C([0,T];H^{s-1}(\mathbb{T}^3))$ so that by Ascoli theorem there exists $\boldsymbol{v}$ such that

$$\boldsymbol{v}^\varepsilon \underset{\varepsilon\to 0}{\longrightarrow} \boldsymbol{v} \quad \text{in} \quad C([0,T];H^\sigma(\mathbb{T}^3)), \quad \forall\sigma<s.$$

Therefore we can write $\boldsymbol{u}^\varepsilon = e^{-tL/\varepsilon}\boldsymbol{v} + \boldsymbol{r}^\varepsilon$ with $\boldsymbol{r}^\varepsilon = e^{-tL/\varepsilon}(\boldsymbol{v}^\varepsilon - \boldsymbol{v})$ converging strongly to 0. Let us now decompose

$$\boldsymbol{v} = \underline{\boldsymbol{v}} + \boldsymbol{v}^{\mathrm{os}}$$

with $\underline{\boldsymbol{v}} \in \operatorname{Ker} L$ and $\boldsymbol{v}^{\mathrm{os}} \in (\operatorname{Ker} L)^\perp$, where the kernel describes as

$$\{\boldsymbol{y}\mapsto\boldsymbol{u}(\boldsymbol{y}) : u_z = 0, \nabla\cdot\boldsymbol{u} = 0\}.$$

. In this decomposition $\boldsymbol{v}^{\mathrm{os}}$ represents the oscillatory part coming from waves. So following this we have

$$\begin{aligned}\boldsymbol{u}^\varepsilon &= e^{-tL/\varepsilon}\underline{\boldsymbol{v}} + e^{-tL/\varepsilon}\boldsymbol{v}^{\mathrm{os}} + \boldsymbol{r}^\varepsilon\\ &= \underline{\boldsymbol{v}} + e^{-tL/\varepsilon}\boldsymbol{v}^{\mathrm{os}} + \boldsymbol{r}^\varepsilon,\end{aligned}$$

with both the second and the third terms converging to 0. Hence $\boldsymbol{u}^\varepsilon$ converges weakly to $\underline{\boldsymbol{v}}$.

Denote the bilinear part of the latter equation as

$$\boldsymbol{Q}_\varepsilon(\boldsymbol{v},\boldsymbol{v}) := e^{tL/\varepsilon}\mathbb{P}\left(\left(\left(e^{-tL/\varepsilon}\boldsymbol{v}^\varepsilon\right)\cdot\nabla\right)e^{-tL/\varepsilon}\boldsymbol{v}^\varepsilon\right)$$

which should converge weakly to some $\boldsymbol{Q}(\boldsymbol{v},\boldsymbol{v})$,

$$\boldsymbol{Q}_\varepsilon(\boldsymbol{v},\boldsymbol{v}) \rightharpoonup \boldsymbol{Q}(\boldsymbol{v},\boldsymbol{v}).$$

Using this the limit equation is given by

$$\partial_t\boldsymbol{v} + \boldsymbol{Q}(\boldsymbol{v},\boldsymbol{v}) = 0,$$

the projection of which onto $\operatorname{Ker} L$ is given by

$$\partial_t\underline{\boldsymbol{v}} + \Pi\boldsymbol{Q}(\underline{\boldsymbol{v}}+\boldsymbol{v}^{\mathrm{os}},\underline{\boldsymbol{v}}+\boldsymbol{v}^{\mathrm{os}}) = 0.$$

Here Π is our notation for projection onto the kernel of L. When we expand this bilinear term we first get $\Pi\boldsymbol{Q}(\boldsymbol{v},\boldsymbol{v})$, the bilinear term in 2D Euler, followed by terms which involve the oscillatory part $\boldsymbol{v}^{\mathrm{os}}$. It isn't clear that applying Π to these additional terms will give an equation which is decoupled from the oscillatory part. So the next question is to find out whether these other terms are 0 or not, and this will tell us if there is an interaction between the waves and the mean flow.

Now we start to give a more detailed expression for this bilinear operator using the spectral decomposition of L. As we are working on $\mathbb{T}^3$ we can compute this spectrum using Fourier series. In particular we need to know how the operator acts on $\boldsymbol{u}(\boldsymbol{k})e^{i\boldsymbol{k}\cdot\boldsymbol{x}}$. We can write this as

$$\hat{\boldsymbol{u}}(\boldsymbol{k}) = \frac{\boldsymbol{k}}{|\boldsymbol{k}|}\left(\hat{\boldsymbol{u}}\cdot\frac{\boldsymbol{k}}{|\boldsymbol{k}|}\right)e^{i\boldsymbol{k}\cdot\boldsymbol{x}} + \left(\hat{\boldsymbol{u}} - \boldsymbol{k}\left(\hat{\boldsymbol{u}}\cdot\frac{\boldsymbol{k}}{|\boldsymbol{k}|}\right)\right)e^{i\boldsymbol{k}\cdot\boldsymbol{x}},$$

where we see that in Fourier space,

$$\begin{aligned}
\widehat{\mathbb{P}(\boldsymbol{u})}(\boldsymbol{k}) &= \left(I - \frac{\boldsymbol{k}}{|\boldsymbol{k}|}\otimes\frac{\boldsymbol{k}}{|\boldsymbol{k}|}\right)\hat{\boldsymbol{u}}(\boldsymbol{k})e^{i\boldsymbol{k}\cdot\boldsymbol{x}} \\
\therefore\qquad \widehat{L\boldsymbol{u}}(\boldsymbol{k}) = \widehat{\mathbb{P}(\boldsymbol{e}\times\boldsymbol{u})}(\boldsymbol{k}) &= \left(I - \frac{\boldsymbol{k}}{|\boldsymbol{k}|}\otimes\frac{\boldsymbol{k}}{|\boldsymbol{k}|}\right)\boldsymbol{e}\times\hat{\boldsymbol{u}}(\boldsymbol{k})e^{i\boldsymbol{k}\cdot\boldsymbol{x}} \\
&= \underbrace{\left(I - \frac{\boldsymbol{k}}{|\boldsymbol{k}|}\otimes\frac{\boldsymbol{k}}{|\boldsymbol{k}|}\right)\begin{pmatrix}0&-1&0\\1&0&0\\0&0&0\end{pmatrix}}_{A}\hat{\boldsymbol{u}}(\boldsymbol{k})e^{i\boldsymbol{k}\cdot\boldsymbol{x}}.
\end{aligned}$$

This matrix A has eigenvalues $\{0,\pm ik_3/|\boldsymbol{k}|\}$. The two nonzero eigenvalues correspond to Poincaré waves. Also associated with each of the eigenvalues is an eigenvector which we will write $\boldsymbol{R}^\alpha_{\boldsymbol{k}}$, where $\alpha\in\{0,+,-\}$ tell us which of the eigenvalues this vector is associated with. Now denoting $\lambda^\alpha_{\boldsymbol{k}}\in\{0,\pm k_3/|\boldsymbol{k}|\}$ we can write for a vector $\boldsymbol{f}$

$$\widehat{e^{tL/\varepsilon}\boldsymbol{f}}(\boldsymbol{k}) = \sum_{\alpha\in\{+,-,0\}} e^{it\lambda^\alpha_{\boldsymbol{k}}/\varepsilon}(\hat{\boldsymbol{f}}(\boldsymbol{k})\cdot\boldsymbol{R}^\alpha_{\boldsymbol{k}})\boldsymbol{R}^\alpha_{\boldsymbol{k}}$$

Then we can substitute this into the expression for $\boldsymbol{Q}_\varepsilon(\boldsymbol{v},\boldsymbol{v})$,

$$\widehat{\boldsymbol{Q}_\varepsilon(\boldsymbol{v},\boldsymbol{v})}(\boldsymbol{k}) = \sum_\alpha e^{it\lambda^\alpha_{\boldsymbol{k}}/\varepsilon}(\widehat{\tilde{\boldsymbol{Q}}_\varepsilon(\boldsymbol{v},\boldsymbol{v})}(\boldsymbol{k})\cdot \boldsymbol{R}^\alpha_{\boldsymbol{k}})\boldsymbol{R}^\alpha_{\boldsymbol{k}},$$

where $\tilde{\boldsymbol{Q}}_\varepsilon(\boldsymbol{v},\boldsymbol{v})$ is given by

$$\begin{aligned}\widehat{\tilde{\boldsymbol{Q}}_\varepsilon(\boldsymbol{v},\boldsymbol{v})}(\boldsymbol{k}) &= \sum_{\boldsymbol{l}+\boldsymbol{m}=\boldsymbol{k}} (\widehat{e^{-tL/\varepsilon}\boldsymbol{v}}(\boldsymbol{l})\cdot i\boldsymbol{m})\widehat{e^{-tL/\varepsilon}\boldsymbol{v}}(\boldsymbol{m})\\ &= \sum_{\substack{\boldsymbol{l}+\boldsymbol{m}=\boldsymbol{k}\\ \beta,\gamma}} e^{-it\lambda^\beta_{\boldsymbol{l}}/\varepsilon}(\hat{\boldsymbol{v}}(\boldsymbol{l})\cdot\boldsymbol{R}^\beta_{\boldsymbol{l}})(\boldsymbol{R}^\beta_{\boldsymbol{l}}\cdot i\boldsymbol{m})e^{-it\lambda^\gamma_{\boldsymbol{m}}/\varepsilon}(\hat{\boldsymbol{v}}(\boldsymbol{m})\cdot\boldsymbol{R}^\gamma_{\boldsymbol{m}})\boldsymbol{R}^\gamma_{\boldsymbol{m}}.\end{aligned}$$

Therefore

$$\begin{aligned}\widehat{\boldsymbol{Q}_\varepsilon(\boldsymbol{v},\boldsymbol{v})}(\boldsymbol{k}) &= \sum_{\substack{\boldsymbol{l}+\boldsymbol{m}=\boldsymbol{k}\\ \alpha,\beta,\gamma}} e^{it(\lambda^\alpha_{\boldsymbol{k}}-\lambda^\beta_{\boldsymbol{l}}-\lambda^\gamma_{\boldsymbol{m}})/\varepsilon}(\hat{\boldsymbol{v}}(\boldsymbol{l})\cdot\boldsymbol{R}^\beta_{\boldsymbol{l}})(\boldsymbol{R}^\beta_{\boldsymbol{l}}\cdot i\boldsymbol{m})(\hat{\boldsymbol{v}}(\boldsymbol{m})\cdot\boldsymbol{R}^\gamma_{\boldsymbol{m}})(\boldsymbol{R}^\gamma_{\boldsymbol{m}}\cdot\boldsymbol{R}^\alpha_{\boldsymbol{k}})\boldsymbol{R}^\alpha_{\boldsymbol{k}}\\ &= \sum_{\substack{\boldsymbol{l}+\boldsymbol{m}=\boldsymbol{k}\\ \alpha,\beta,\gamma}} e^{it(\lambda^\alpha_{\boldsymbol{k}}-\lambda^\beta_{\boldsymbol{l}}-\lambda^\gamma_{\boldsymbol{m}})/\varepsilon}\boldsymbol{Q}_{\substack{\boldsymbol{k},\boldsymbol{l},\boldsymbol{m}\\ \alpha,\beta,\gamma}}(\hat{\boldsymbol{v}}(\boldsymbol{l}),\hat{\boldsymbol{v}}(\boldsymbol{m})).\end{aligned}$$

These terms always converge weakly to 0 except for the resonant terms, when $\boldsymbol{k}=\boldsymbol{l}+\boldsymbol{m}$ and $\lambda^\alpha_{\boldsymbol{k}}=\lambda^\beta_{\boldsymbol{l}}+\lambda^\gamma_{\boldsymbol{m}}$, so the limit of $\boldsymbol{Q}_\varepsilon(\boldsymbol{v},\boldsymbol{v})$ can be expressed as

$$\boldsymbol{Q}(\boldsymbol{v},\boldsymbol{v}) = \sum_{\text{resonant set}} \boldsymbol{Q}_{\substack{\boldsymbol{k},\boldsymbol{l},\boldsymbol{m}\\ \alpha,\beta,\gamma}}(\hat{\boldsymbol{v}}(\boldsymbol{l}),\hat{\boldsymbol{v}}(\boldsymbol{m})).$$

The above proves,

Theorem 4.3.3. *$\boldsymbol{u}^\varepsilon = e^{-tL/\varepsilon}\boldsymbol{v}^\varepsilon$ where $\boldsymbol{v}^\varepsilon\to\boldsymbol{v}$ and $\boldsymbol{v}$ solves*

$$\partial_t\boldsymbol{v}+\boldsymbol{Q}(\boldsymbol{v},\boldsymbol{v})=0.$$

To get a better understanding of $\boldsymbol{Q}$ we have the following lemma.

Lemma 4.3.1 (Babin-Mahalov-Nicolaenko)**.**

$$\Pi\boldsymbol{Q}(\boldsymbol{v},\boldsymbol{v}) = \mathbb{P}(\underline{\boldsymbol{v}}\cdot\nabla\underline{\boldsymbol{v}}),$$

therefore $\underline{\boldsymbol{v}}$ solves the 2D incompressible Euler equations, with

$$\underline{\boldsymbol{v}}|_{t=0} = \Pi\boldsymbol{v}_0 = \int_z \boldsymbol{v}_0(y_1,y_2,z)\,\mathrm{d}z.$$

Proof. The resonant set is the set of wavenumbers $\boldsymbol{k},\boldsymbol{l},\boldsymbol{m}$ such that $\boldsymbol{k}=\boldsymbol{l}+\boldsymbol{m}$ and

$$\frac{\pm k_3}{|\boldsymbol{k}|} = \frac{\pm l_3}{|\boldsymbol{l}|} = \frac{\pm m_3}{|\boldsymbol{m}|},$$

with $k_3=0$, as this is given by the initial condition being an integral in the vertical direction. In particular this means that $l_3+m_3=0$ and

$$\frac{\pm l_3}{|\boldsymbol{l}|}+\frac{\pm m_3}{|\boldsymbol{m}|}=0 \quad\text{or}\quad \frac{\pm l_3}{|\boldsymbol{l}|}-\frac{\pm m_3}{|\boldsymbol{m}|}=0.$$

The second of these implies that $|\boldsymbol{l}| = -|\boldsymbol{m}|$ so $\boldsymbol{l} = \boldsymbol{m} = 0$. For the first we have $|\boldsymbol{l}| = |\boldsymbol{m}|$.

It is better now to use a slightly different decomposition of L. To study the oscillatory part of L we can write

$$\widehat{e^{-tL/\varepsilon}\boldsymbol{v}}(\boldsymbol{k}) = c_{\boldsymbol{k}}\hat{\boldsymbol{v}}(\boldsymbol{k}) - \frac{s_{\boldsymbol{k}}}{|\boldsymbol{k}|}\boldsymbol{k}\times\hat{\boldsymbol{v}}(\boldsymbol{k}), \qquad \text{with} \quad c_{\boldsymbol{k}} = \cos\left(\frac{k_3}{|\boldsymbol{k}|}\frac{t}{\varepsilon}\right)$$
$$s_{\boldsymbol{k}} = \sin\left(\frac{k_3}{|\boldsymbol{k}|}\frac{t}{\varepsilon}\right).$$

Then we have that,

$$e^{-tL/\varepsilon}\times\widehat{\operatorname{curl}(e^{-tL/\varepsilon}\boldsymbol{v}) = \sum_{\substack{\boldsymbol{l}+\boldsymbol{m}=\boldsymbol{k}\\ l_3+m_3=0\\ |\boldsymbol{l}|=|\boldsymbol{m}|}} \left(c_{\boldsymbol{l}}\hat{\boldsymbol{v}}(\boldsymbol{l}) - \frac{s_{\boldsymbol{l}}}{|\boldsymbol{l}|}\boldsymbol{l}\times\hat{\boldsymbol{v}}(\boldsymbol{l})\right)\times\boldsymbol{m}$$
$$\times\left(c_{\boldsymbol{m}}\hat{\boldsymbol{v}}(\boldsymbol{m}) - \frac{s_{\boldsymbol{m}}}{|\boldsymbol{m}|}\boldsymbol{m}\times\hat{\boldsymbol{v}}(\boldsymbol{m})\right) + \text{other terms}.$$

The other terms here are those that come from when $l_3 + m_3 \neq 0$ and when $|\boldsymbol{l}| \neq |\boldsymbol{m}|$, which don't concern us here. We will ignore these additional terms now. In this sum each of the summands can be rewritten using the vector triple product as,

$$\left(c_{\boldsymbol{l}}\hat{\boldsymbol{v}}(\boldsymbol{l}) - \frac{s_{\boldsymbol{l}}}{|\boldsymbol{l}|}\boldsymbol{l}\times\hat{\boldsymbol{v}}(\boldsymbol{l})\right)\times(c_{\boldsymbol{m}}\boldsymbol{m}\times\hat{\boldsymbol{v}}(\boldsymbol{m}) + s_{\boldsymbol{m}}|\boldsymbol{m}|\hat{\boldsymbol{v}}(\boldsymbol{m})).$$

Then we have a lot of cancellation giving,

$$\begin{aligned} e^{-tL/\varepsilon}\times\widehat{\operatorname{curl}(e^{-tL/\varepsilon}\boldsymbol{v}) &= \sum c_{\boldsymbol{l}}c_{\boldsymbol{m}}\hat{\boldsymbol{v}}(\boldsymbol{l})\times\boldsymbol{m}\times\hat{\boldsymbol{v}}(\boldsymbol{m}) - s_{\boldsymbol{l}}s_{\boldsymbol{m}}\frac{|\boldsymbol{m}|}{|\boldsymbol{l}|}\boldsymbol{l}\times\hat{\boldsymbol{v}}(\boldsymbol{l})\times\hat{\boldsymbol{v}}(\boldsymbol{m})\\ &= \sum c_{\boldsymbol{l}}^2\hat{\boldsymbol{v}}(\boldsymbol{l})\times(\boldsymbol{m}\times\hat{\boldsymbol{v}}(\boldsymbol{m})) + s_{\boldsymbol{l}}^2(\boldsymbol{l}\times\hat{\boldsymbol{v}}(\boldsymbol{l}))\times\hat{\boldsymbol{v}}(\boldsymbol{m})\\ &= \sum c_{\boldsymbol{l}}^2\hat{\boldsymbol{v}}(\boldsymbol{l})\times(\boldsymbol{m}\times\hat{\boldsymbol{v}}(\boldsymbol{m})) + s_{\boldsymbol{l}}^2(\boldsymbol{m}\times\hat{\boldsymbol{v}}(\boldsymbol{m}))\times\hat{\boldsymbol{v}}(\boldsymbol{l}), \end{aligned}$$

where the last line comes from just swapping $\boldsymbol{l}$ and $\boldsymbol{m}$ in the summation as the sum is symmetric in these terms. Finally this gives,

$$\sum(c_{\boldsymbol{l}}^2 - s_{\boldsymbol{l}}^2)(\hat{\boldsymbol{v}}(\boldsymbol{l})\times(\boldsymbol{m}\times\hat{\boldsymbol{v}}(\boldsymbol{m})).$$

Since $c_{\boldsymbol{l}}^2 - s_{\boldsymbol{l}}^2 = \cos\left(\frac{2l_3}{|\boldsymbol{l}|}\frac{t}{\varepsilon}\right)$ which is oscillating, this completes the proof that $\Pi\boldsymbol{Q}(\boldsymbol{u},\boldsymbol{u}) = \boldsymbol{Q}(\Pi\boldsymbol{u},\Pi\boldsymbol{u})$.

□

We won't go further with these considerations other than noting a few further results. Define $\Pi^{\text{os}} = I - \Pi$, then we can consider the equation for the oscillating flow,

$$\partial_t\boldsymbol{v}^{\text{os}} + \Pi^{\text{os}}(\boldsymbol{Q}(\boldsymbol{v},\boldsymbol{v}^{\text{os}}) + \boldsymbol{Q}(\boldsymbol{v}^{\text{os}},\boldsymbol{v}) + \boldsymbol{Q}(\boldsymbol{v}^{\text{os}},\boldsymbol{v}^{\text{os}})) = 0,$$

and ask whether this equation is truly nonlinear, i.e. if the last term on the left is nonzero. Specifically this being nonzero would present problems such as lack of global existence. In fact, the outcome depends on the geometric situation being considered. It is true that $\Pi^{\text{os}}\boldsymbol{Q}(\boldsymbol{v}^{\text{os}},\boldsymbol{v}^{\text{os}})$ is not always zero. We could study more generally $\Omega = \mathbb{T}^2\times a_3\mathbb{T}$, where we have adjusted the length of the torus in one direction, then the value a_3 with affect the behaviour of the solution. In particular some a_3 with give resonance to the solution, meaning that this term is nonzero, while others won't. We have the following result.

Lemma 4.3.2 (Babin-Mahalov-Nicolaenko)**.** *For almost every a_3, $\Pi^{\mathrm{os}}\boldsymbol{Q}(\boldsymbol{v}^{\mathrm{os}}, \boldsymbol{v}^{\mathrm{os}}) = 0$, i.e. the system is not resonant.*

Another domain that could be considered is when the horizontal domain is unbounded, $\Omega = \mathbb{R}^2 \times \mathbb{T}$. One thing that we might be interested in studying in the convergence of $\boldsymbol{u}^\varepsilon$ to $\boldsymbol{u}$ in this domain. As before, what is always true is that,

$$\boldsymbol{u}^\varepsilon = \Pi \boldsymbol{v} + e^{tL/\varepsilon}(I - \Pi)\boldsymbol{v} + \boldsymbol{r}^\varepsilon,$$

where $\boldsymbol{v}$ is some limit function and $\boldsymbol{r}^\varepsilon$ converges strongly to 0 as $\varepsilon \to 0$. In the previous case the other terms were converging weakly to 0. In the rotating fluid equations we have dispersive waves with the dispersion relation

$$\omega = \frac{k_3}{(|\boldsymbol{\xi}|^2 + k_3^2)^{1/2}} \underset{k_3 \neq 0}{=} \pm \frac{1}{\left(1 + \frac{|\boldsymbol{\xi}|^2}{k_3^2}\right)^{1/2}},$$

where we have made a distinction between the horizontal and vertical wavenumbers. In particular now we can have

$$\omega(\boldsymbol{\xi}) = \frac{1}{(1 + |\boldsymbol{\xi}|)^{1/2}},$$

which has the hessian

$$D^2\omega = -\frac{2|\boldsymbol{\xi}|^2}{(1 + |\boldsymbol{\xi}|^2)^5} \neq 0.$$

This is bounded below for $\boldsymbol{\xi}$ bounded above, $|\det D^2\omega| \geq c_0$ uniformly for $|\boldsymbol{\xi}| \leq R$. The presence of this dispersion, meaning that waves with different wavenumbers travel at different speeds creates energy decay in the system. In this case we have Strichartz's estimates which give strong convergence to 0 of the aforementioned term,

$$e^{tL/\varepsilon}(I - \Pi)\boldsymbol{v} \underset{\epsilon \to 0}{\to} 0.$$

For the incompressible, this observation was due to [Ukai], and for rotating fluids is was due to [Chemin-Desjardins-Gallagher-Grenier].

[more on literature here]

4.4 Stability of the Ekman layer

The aim of this chapter is to describe the optimality of $R_0 < 1$, one of the conditions noted previously in the theorem of Grenier-Masmoudi. We start with the linearized (around the approximate solution $\boldsymbol{u}^{\text{app}}$) rotating fluid equations,

$$\partial_t \boldsymbol{u} + \boldsymbol{u}^{\text{app}} \cdot \nabla \boldsymbol{u} + \boldsymbol{u} \cdot \nabla \boldsymbol{u}^{\text{app}} + \frac{\boldsymbol{e} \times \boldsymbol{u}}{\varepsilon} + \frac{\nabla p}{\varepsilon} = \varepsilon \Delta \boldsymbol{u}.$$

Recall that the approximate solution $\boldsymbol{u}^{\text{app}}$ to the original equations was expressed as,

$$\boldsymbol{u}^{\text{app}} = \boldsymbol{u}^{\text{int}}(t, \boldsymbol{y}) + \boldsymbol{u}^{b,0}\left(t, \boldsymbol{y}, \frac{z}{\varepsilon}\right) + \boldsymbol{u}^{b,1}\left(t, \boldsymbol{y}, \frac{1-z}{\varepsilon}\right) + ...$$

Here we make a simplification that the interior solution is given by a constant $\boldsymbol{q}$ (the solution of the limit system) so $\boldsymbol{u}^{\text{app}} = \boldsymbol{q} + \boldsymbol{V}(\boldsymbol{q}, z/\varepsilon)$. We only consider one of the two boundary layers so this means we can study the vertical domain $z > 0$, instead of $z \in [0, 1]$, and $\boldsymbol{y} \in \mathbb{T}^2$ or $\mathbb{R}^2$. This simplification gives the equations,

$$\partial_t \boldsymbol{u} + \left[\boldsymbol{q} + \boldsymbol{V}\left(\boldsymbol{q}, \frac{z}{\varepsilon}\right)\right] \cdot \nabla_{\boldsymbol{y}} \boldsymbol{u} + \frac{1}{\varepsilon} u_3 \partial_Z \boldsymbol{V}\left(\boldsymbol{q}, \frac{z}{\varepsilon}\right) + \frac{\boldsymbol{e} \times \boldsymbol{u}}{\varepsilon} + \frac{\nabla p}{\varepsilon} = \varepsilon \Delta \boldsymbol{u}.$$

If we now perform the change of scale, $\boldsymbol{u}(t, \boldsymbol{y}, z) = \boldsymbol{v}(\tau = t/\varepsilon, \boldsymbol{Y} = \boldsymbol{y}/\varepsilon, Z = z/\varepsilon)$ then we obtain an equation for $\boldsymbol{v}$, for $Z > 0$ and $\boldsymbol{Y} \in \mathbb{R}^2$,

$$\partial_\tau \boldsymbol{v} + [\boldsymbol{q} + \boldsymbol{V}(\boldsymbol{q}, Z)] \cdot \nabla_{\boldsymbol{Y}} \boldsymbol{v} + v_3 \partial_Z \boldsymbol{V}(\boldsymbol{q}, Z) + \boldsymbol{e} \times \boldsymbol{v} + \nabla_{\boldsymbol{X}} P = \Delta_{\boldsymbol{X}} \boldsymbol{v},$$

which is coupled with the continuity equation, $\nabla_{\boldsymbol{X}} \cdot \boldsymbol{v} = 0$. In the above $P = p/\varepsilon$ is the scaled pressure. This new rescaled problem can be written as,

$$\partial_\tau \boldsymbol{v} = L\boldsymbol{v}, \qquad L\boldsymbol{v} = \mathbb{P}[\Delta_{\boldsymbol{X}} \boldsymbol{v} - \boldsymbol{V} \cdot \nabla_{\boldsymbol{Y}} \boldsymbol{v} - v_3 \partial_Z \boldsymbol{V} - \boldsymbol{e} \times \boldsymbol{v}],$$

where $\mathbb{P}$ is the Leray projector. If there is an unstable eigenvalue λ for L, or in other words we can find $\boldsymbol{v}(\tau) = e^{\lambda \tau} \boldsymbol{W}$ with $\text{Re}\lambda > 0$, then we will have that $\|\boldsymbol{v}(\tau)\|_{L^2} \sim e^{\text{Re}\lambda \tau}$.

Once we then go back to the original scaling we have that $\|\boldsymbol{u}(t)\|_{L^2} \sim \varepsilon^{3/2} e^{\text{Re}\lambda t/\varepsilon}$, which is large for $t \gg \varepsilon$. In fact we can find $T_\varepsilon \to 0$ (e.g. $T_\varepsilon = \sqrt{\varepsilon}$) such that,

$$\sup_{[0, T_\varepsilon]} \|\boldsymbol{u}(t)\|_{L^2} \to \infty.$$

In this case we don't expect that $\boldsymbol{u}^\varepsilon \sim \boldsymbol{u}^{\text{app}}$. It is here that the condition on R_0 is important, as this being less than 1 is a condition for the spectrum of the linear operator L being stable. As in the statement of the theorem of Grenier-Masmoudi, R_0 in the case of this simplification is written as,

$$R_0 = \int_0^\infty Z |\partial_Z \boldsymbol{V}(\boldsymbol{q}, Z)| \, \mathrm{d}Z =: F(\boldsymbol{q}),$$

so the stability of the system will be dependent on the parameter $|\boldsymbol{q}|$, which will take a similar place to the Reynolds number here. One can study this numerically, to increase the size of $\boldsymbol{q}$ and investigate when instabilities start to appear in the system. This was done [Lilly (?)], and it was demonstrated that instabilities appear when $|q| \sim 55$, which is significantly larger than that which is obtained from energy estimates, $|\boldsymbol{q}| \sim 5$. In the range $5 < |\boldsymbol{q}| < 55$ we can observe behaviour where the norm $\|\boldsymbol{v}\|_{L^2}$ initially grows in time before an eventual decay to 0 over longer times. There is still no linear instability but the decay in energy is not monotone.

[more stuff]

4.4.1 Nonlinear instability

Here we will study the spectrum of the operator L, taking a partial Fourier transform in space owing to the finite vertical domain. The spectrum of interest is the union

$$\sigma(L) = \bigcup_{\boldsymbol{\xi}} \sigma(L_{\boldsymbol{\xi}}), \qquad L_{\boldsymbol{\xi}} = \mathbb{P}(\boldsymbol{\xi})[\Delta_{\boldsymbol{\xi}} \boldsymbol{v} - i\boldsymbol{\xi} \cdot \boldsymbol{V}\boldsymbol{v} - \boldsymbol{v}_3 \partial_Z \boldsymbol{V} - \boldsymbol{e} \times \boldsymbol{v}],$$

where $\Delta_{\boldsymbol{\xi}} = \partial_Z^2 - |\boldsymbol{\xi}|^2$. The $L_{\boldsymbol{\xi}}$ are the partial Fourier transforms of L. Aside, this kind of wave solution/transform is also known as a normal modes solution. Here this Leray projector $\mathbb{P}(\xi)$ operating on a field $\boldsymbol{u}$ gives its nondivergent part $\boldsymbol{v}$ with respect to the operator $\nabla_{\boldsymbol{\xi}}$.

$$\boldsymbol{u} = \nabla_{\boldsymbol{\xi}} w + \boldsymbol{v}, \qquad \text{with } \nabla_{\boldsymbol{\xi}} \cdot \boldsymbol{v} = 0,\ \nabla_{\boldsymbol{\xi}} = \begin{pmatrix} i\boldsymbol{\xi} \\ \partial_Z \end{pmatrix}.$$

Proposition 4.4.1. *For $\lambda \in \sigma(L_{\boldsymbol{\xi}})$ we have that,*

(i) For $|\boldsymbol{\xi}|$ sufficiently large, $\lambda - L_{\boldsymbol{\xi}}$ is invertible for $\mathrm{Re}\lambda \geq 0$,

(ii) For $|\boldsymbol{\xi}|$ sufficiently small, $\lambda - L_{\boldsymbol{\xi}}$ is invertible for $\mathrm{Re}\lambda \geq 0$ if $\boldsymbol{\xi} \neq 0$,

(iii) $(\lambda - L_{\boldsymbol{\xi}})$ is invertible for $|\mathrm{Im}\lambda|$ sufficiently large.

Remark 25. *We only need to study $\sigma(L_{\boldsymbol{\xi}})$ for $0 < r \leq |\boldsymbol{\xi}| \leq R$.*

Proof. (i) For looking at the energy estimate we reintroduce the pressure P and look at the full equations,

$$\begin{aligned} \lambda \boldsymbol{v} + i\boldsymbol{\xi} \cdot (\boldsymbol{q} + \boldsymbol{V})_{\boldsymbol{y}} \boldsymbol{v} + v_3 \partial_Z \boldsymbol{V} + \boldsymbol{e} \times \boldsymbol{v} + \nabla_{\boldsymbol{\xi}} P &= \partial_{ZZ} \boldsymbol{v} - |\boldsymbol{\xi}|^2 \boldsymbol{v} + \boldsymbol{F}, \\ \partial_Z v_3 + i\boldsymbol{\xi} \cdot \boldsymbol{v}_{\boldsymbol{y}} &= 0, \\ \boldsymbol{v}|_{Z=0} &= 0 \end{aligned}$$

where $\boldsymbol{F}$ is a forcing term and $\lambda = \gamma + i\tau$. This is a Fourier transform in the horizontal direction and a Laplace transform in time. Following this the variables $\boldsymbol{v}$ are complex so to find the energy estimate we multiply by $\bar{\boldsymbol{v}}$ before before taking the real part and integrating. The subsequent equation is then,

$$\gamma \|\boldsymbol{v}\|_{L^2}^2 + \mathrm{Re} \int v_3 \partial_Z \boldsymbol{V} \cdot \bar{\boldsymbol{v}} \, \mathrm{d}Z + \|\partial_Z \boldsymbol{v}\|_{L^2}^2 + |\boldsymbol{\xi}|^2 \|\boldsymbol{v}\|_{L^2}^2 \leq \|\boldsymbol{F}\|_{L^2} \|\boldsymbol{v}\|_{L^2}, \qquad (4.32)$$

eqn:energy

where we have used Cauchy-Schwarz. The L^2 norm here is in the Z variable as this is the only variable remaining. The integral term can be bounded by noting that the derivative $\partial_Z \boldsymbol{V}$ is bounded in L^∞ by a constant, and using Cauchy-Schwarz again. So this gives

$$(\gamma + |\boldsymbol{\xi}|^2) \|\boldsymbol{v}\|_{L^2}^2 + \|\partial_Z \boldsymbol{v}\|_{L^2}^2 \leq C \|\boldsymbol{v}\|_{L^2}^2 + \|\boldsymbol{F}\|_{L^2}^2.$$

If $\gamma + |\boldsymbol{\xi}|^2 > C$ then we can invert. [...]

(ii) Here we again use equation (4.32) but instead deal with the integral term in a slightly different way. We write

$$\begin{aligned} v_3 &= \int_0^Z \partial_Z v_3 \, \mathrm{d}Z = -i\boldsymbol{\xi} \cdot \int_0^Z \boldsymbol{v}_{\boldsymbol{y}} \, \mathrm{d}Z' \\ &= -i\boldsymbol{\xi} \cdot \int_0^Z \int_0^{Z'} \partial_Z \boldsymbol{v}_{\boldsymbol{y}} \, \mathrm{d}Z'' \, \mathrm{d}Z' \end{aligned}$$

where we have written a function as an intergal over Z of it's Z-derivative twice. Then using Cauchy-Schwarz the inner integral gives

$$\left| \int_0^{Z'} \partial_Z \boldsymbol{v_y} \, \mathrm{d}Z'' \right| \leq Z'^{1/2} \left\| \partial_Z \boldsymbol{v_y} \right\|_{L^2} ,$$

so

$$|v_3| \leq |\boldsymbol{\xi}| Z^{3/2} \left\| \partial_Z \boldsymbol{v_y} \right\|_{L^2} .$$

Similarly we have

$$|\boldsymbol{v_y}| \leq |Z|^{1/2} \left\| \partial_Z \boldsymbol{v_y} \right\|_{L^2} ,$$

so putting this all together gives the following bound for the integral term in (4.32),

$$\begin{aligned} \left| \mathrm{Re} \int v_3 \partial_Z \boldsymbol{V} \cdot \bar{\boldsymbol{v}} \, \mathrm{d}Z \right| &\leq |\boldsymbol{\xi}| \left(\int Z^2 |\partial_Z \boldsymbol{V}| \, \mathrm{d}Z \right) \left\| \partial_Z \boldsymbol{v} \right\|_{L^2}^2 \\ &\leq C|\boldsymbol{\xi}| \left\| \partial_Z \boldsymbol{v} \right\|_{L^2}^2 . \end{aligned}$$

The integral above can be made less than a constant C because the boundary layer is exponentially decaying, so the second moment is finite. Now if $|\boldsymbol{\xi}|$ is small enough then it can be absorbed in the energy dissipation term. So if $1 - C|\boldsymbol{\xi}| > 0$ we can invert. If $\boldsymbol{\xi} \neq 0$ we can invert as long as $\gamma + |\boldsymbol{\xi}|^2 > 0$, so if $\boldsymbol{\xi} \neq 0$, even if $\gamma = 0$ we can still invert.

(iii) So far we have only used information from the real part of the equation, but for this part we will look at the imaginary part after multiplying by $\bar{\boldsymbol{v}}$ and take the absolute value. The equation we obtain is

$$|\tau| \left\| \boldsymbol{v} \right\|_{L^2}^2 \leq C|\boldsymbol{\xi}| \left\| \boldsymbol{v} \right\|_{L^2}^2 + C \left\| \boldsymbol{v} \right\|_{L^2}^2 + \left\| \boldsymbol{F} \right\|_{L^2} \left\| \boldsymbol{v} \right\|_{L^2}$$

Now we combine with the inequality from the first part of the proof. For a positive constant A we have

$$\begin{aligned} \left[A(\gamma + |\boldsymbol{\xi}|^2) + |\tau| \right] \left\| \boldsymbol{v} \right\|_{L^2}^2 + A \left\| \partial_Z \boldsymbol{v} \right\|_{L^2}^2 \leq & (A+1) \left\| \boldsymbol{F} \right\|_{L^2} \left\| \boldsymbol{v} \right\|_{L^2} \\ & + (A+1)C \left\| \boldsymbol{v} \right\|_{L^2}^2 + C|\boldsymbol{\xi}|^2 \left\| \boldsymbol{v} \right\|_{L^2}^2 , \end{aligned}$$

which after moving things around says that $\lambda - L_{\boldsymbol{\xi}}$ is invertible if

$$\left[A(\gamma + |\boldsymbol{\xi}|^2) + |\tau| \right] - (A+1)C - C|\boldsymbol{\xi}|^2 > 0.$$

This is true for $|\tau|$ sufficiently large.

□

[...]

Proposition 4.4.2. *For $\gamma > 0, \boldsymbol{\xi} \neq 0$, the spectrum of $L_{\boldsymbol{\xi}}$ is made of eigenvalues which are the zeros of an analytic function $D(\lambda, \boldsymbol{\xi})$. Moreover, if D does not vanish on a compact set we get a resolvant estimate.*

Proof. Here we will provide only a sketch of the ODE proof. We want to study $L_{\boldsymbol{\xi}}\boldsymbol{v} = \lambda\boldsymbol{v} + \boldsymbol{F}$. Denoting

$$\boldsymbol{W} = \begin{pmatrix} v_1 \\ v_2 \\ v_3 \\ p \\ \partial_Z v_1 \\ \partial_Z v_2 \end{pmatrix},$$

the equivalent system of equations (with Dirichlet boundary conditions) is

$$\left\{ \begin{array}{rcl} \partial_Z \boldsymbol{W} & = & G(\lambda, \boldsymbol{\xi}, Z)\boldsymbol{W} + \mathbb{F} \\ \Gamma \boldsymbol{W}(0) & = & 0, \end{array} \right. \tag{4.33}$$

eq:lecture4p

where G is a matrix. We note 2 properties that the matrix G has.

1. $|G(\lambda, \boldsymbol{\xi}, z) - G_\infty(\lambda, \boldsymbol{\xi})| \leq C\mathrm{e}^{-Z/\sqrt{2}} \quad \forall Z > 0.$
2. $G_\infty(\lambda, \boldsymbol{\xi})$ has no eigenvalues on the imaginary axis for $\mathrm{Re}\lambda \geq 0$ and $\boldsymbol{\xi} \neq 0$. There are three of positive real part and three of negative real part.

The first of these uses the fact that as we take $Z \to \infty$ the matrix G converges to a constant matrix $G_\infty(\lambda, \boldsymbol{\xi})$. These two facts above together tell us that (4.33) has an exponential dichotomy. That is to say we can find projections $\Pi_+(\lambda, \boldsymbol{\xi}, Z), \Pi_-(\lambda, \boldsymbol{\xi}, Z)$ which are of rank 3, such that they commute with the resolvent of the system. I.e.

$$T(\lambda, \boldsymbol{\xi}, Z, Z')\Pi_\pm(\lambda, \boldsymbol{\xi}, Z') = \Pi_\pm T(\lambda, \boldsymbol{\xi}, Z, Z'),$$

where T here is such that if we apply the operator to a vector, we will get the solution to the homogeneous ODE with Cauchy data taken at Z'. Now we can solve the ODE (4.33) in the same way as was done in section 4.2 where there was a separation of the spectrum. We have

$$\begin{array}{rcl} \boldsymbol{W}_+ & = & -\int_Z^\infty T(Z, y)\Pi_+(y)\mathbb{F}(y)\,\mathrm{d}y \\ \boldsymbol{W}_- & = & T(Z, 0)\Pi_-(0)W(0) + \int_0^\infty T(Z, y)\Pi_-(y)\mathbb{F}(y)\,\mathrm{d}y. \end{array}$$

For $F = 0$, there is a non-trivial bounded solution if and only if $\Gamma|_{\mathrm{Im}\,\Pi_-(\lambda,\boldsymbol{\xi},0)}$ is not injective. Then $D(\lambda, \boldsymbol{\xi}) = \det\left(\Gamma|_{\mathrm{Im}\,\Pi_-(\lambda,\boldsymbol{\xi},0)}\right)$. [...] □

Now we state 2 further results regarding nonlinear instability. The first says that we can find initial data as close as we want to our basic stationary solution such that we will deviate from it a given distance.

theorem:D-G **Theorem 4.4.1** (Desjardins-Grenier)**.** *If*

$$\sigma_0 = \sup\{\mathrm{Re}\lambda(\boldsymbol{\xi}) \text{ s.t. } \lambda(\boldsymbol{\xi}) \text{ is an eigenvalue of } L(\boldsymbol{\xi}) \text{ with } \mathrm{Re}\lambda \geq 0, \boldsymbol{\xi} \neq 0\} > 0,$$

(so we have a nonlinear instability somewhere) with $\sigma_0 = \mathrm{Re}\lambda(\boldsymbol{\xi}_0)$ *and* $D^2\mathrm{Re}\lambda(\boldsymbol{\xi})|_{\boldsymbol{\xi}=\boldsymbol{\xi}_0}$ *not degenerate (where* D^2 *is the Hessian), then there exists initial data* $\boldsymbol{v}_0^\varepsilon$ *and* $C > 0$ *independent of* ε *such that* $\|\boldsymbol{v}_0^\varepsilon - \boldsymbol{V}(\boldsymbol{q}, Z)\|_{H^s} \leq \varepsilon^N$*, and the solution of*

$$\left\{ \begin{array}{rcl} \partial_t \boldsymbol{v} + \boldsymbol{v}\cdot\nabla\boldsymbol{v} + \boldsymbol{e}\times\boldsymbol{v} + \nabla p & = & \Delta\boldsymbol{v} \quad Z > 0 \\ \boldsymbol{v}|_{Z=0} & = & 0 \\ \boldsymbol{v}|_{t=0} & = & \boldsymbol{v}_0^\varepsilon \end{array} \right. \tag{4.34}$$

satisfies $\sup_{[0,T^\varepsilon]}\|\boldsymbol{v}^\varepsilon - \boldsymbol{V}(\boldsymbol{q})\|_{L^2} \geq C$ *where* $T^\varepsilon \sim |\log\varepsilon|$*. We could equivalently take the* L_∞ *norm here.* ε *is small and both* N *and* s *are as large as we want.*

Also, we state the result in the original coordinates (i.e. using z/ε etc.).

Theorem 4.4.2 (Desjardins-Grenier in original coordinates)**.** *Making the same assumption as in Theorem 4.4.1, there exists initial data* $\boldsymbol{u}_0^\varepsilon$ *and* $C > 0$ *such that* $\|\boldsymbol{u}_0^\varepsilon - \boldsymbol{V}(\boldsymbol{q}, z/\varepsilon)\|_{H^s} \leq \varepsilon^N$ *and* $\sup_{[0,\theta^\varepsilon]} \|\boldsymbol{u}^\varepsilon(\theta^\varepsilon) - \boldsymbol{V}\|_{L^\infty} \geq C$*, where* $\theta^\varepsilon \sim \varepsilon|\log\varepsilon| \to 0$ *as* $\varepsilon \to 0$*. Furthermore,* $\boldsymbol{u}^\varepsilon$ *solves*

$$\left\{ \begin{array}{rcl} \partial_t \boldsymbol{u}^\varepsilon + \boldsymbol{u}^\varepsilon \cdot \nabla \boldsymbol{u}^\varepsilon + \frac{1}{\varepsilon}\boldsymbol{e} \times \boldsymbol{u}^\varepsilon + \frac{1}{\varepsilon}\nabla p &=& \varepsilon \Delta \boldsymbol{u}^\varepsilon \\ \nabla \cdot \boldsymbol{u}^\varepsilon &=& 0 \end{array} \right. \tag{4.35}$$

If we use the L^2 *norm then the lower bound is* $C\varepsilon^{3/2}$*. This additional power of* ε *comes from the rescaling.*

Finally we state a positive result:

Theorem 4.4.3. *Take* $\boldsymbol{u}^{\text{app}} = \boldsymbol{u}^{0,\text{int}} + \dots$ *and assume that*

$$D(\boldsymbol{u}^{0,\text{int}}|_{t=0}(\boldsymbol{y}), \lambda, \boldsymbol{\xi}) \neq 0 \ \forall \lambda \ s.t \ \text{Re}\lambda \geq 0, \forall \boldsymbol{\xi} \neq 0, \forall \boldsymbol{y} \in \mathbb{T}^2 \ \text{or} \ \boldsymbol{y} \in \mathbb{R}^2. \tag{4.36}$$

Then $\exists T > 0$ *such that* $\sup_{[0,T]} \|\boldsymbol{u}^\varepsilon(t) - \boldsymbol{u}^{\text{app}}(t)\|_{L^\infty} \to 0$ *as* $\varepsilon \to 0$.

Bibliography

ratospheric [1] M. T Boehm and J. Verlinde, *Stratospheric influence on upper tropospheric tropical cirrus*, Geophysical research letters **27** (2000), no. 19, 3209–3212.

tta2012two [2] G. Boffetta and R. E Ecke, *Two-dimensional turbulence*, Annual review of fluid mechanics **44** (2012), 427–451.

r2021onset [3] T. Buckmaster, P. Germain, Z. Hani, and J. Shatah, *Onset of the wave turbulence description of the longtime behavior of the nonlinear schrödinger equation*, Inventiones mathematicae (2021), 1–69.

2010meddy [4] X. Carton, N. Daniault, J. Alves, L. Cherubin, and I. Ambar, *Meddy dynamics and interaction with neighboring eddies southwest of portugal: Observations and modeling*, Journal of Geophysical Research: Oceans **115** (2010), no. C6.

1996global [5] D. B Chelton and M. G Schlax, *Global observations of oceanic rossby waves*, Science (1996), 234–238.

0derivation [6] C. Collot and P. Germain, *Derivation of the homogeneous kinetic wave equation: longer time scales*, arXiv preprint arXiv:2007.03508 (2020).

9numerical [7] C. Connaughton, *Numerical solutions of the isotropic 3-wave kinetic equation*, Physica D: Nonlinear Phenomena **238** (2009), no. 23-24, 2282–2297.

4emergence [8] N. C Constantinou, B. F Farrell, and P. J Ioannou, *Emergence and equilibration of jets in beta-plane turbulence: applications of stochastic structural stability theory*, Journal of the Atmospheric Sciences **71** (2014), no. 5, 1818–1842.

copethesis [9] L. Cope, *The dynamics of grophysical and astrophysical turbulence*, Ph.D. Thesis, 2021.

3coarsening [10] G. Craig and J. Mack, *A coarsening model for self-organization of tropical convection*, Journal of Geophysical Research: Atmospheres **118** (2013), no. 16, 8761–8769.

hermocline [11] S. Cravatte, E. Kestenare, F. Marin, P. Dutrieux, and E. Firing, *Subthermocline and intermediate zonal currents in the tropical pacific ocean: Paths and vertical structure*, Journal of Physical Oceanography **47** (2017), no. 9, 2305–2324.

2004scaling [12] S. Danilov and D. Gurarie, *Scaling, spectra and zonal jets in beta-plane turbulence*, Physics of fluids **16** (2004), no. 7, 2592–2603.

pontaneous [13] E. Danioux, J Vanneste, P. Klein, and H Sasaki, *Spontaneous inertia-gravity-wave generation by surface-intensified turbulence*, Journal of fluid mechanics **699** (2012), 153–173.

t2015large [14] T. Dauhut, J.-P. Chaboureau, J. Escobar, and P. Mascart, *Large-eddy simulations of hector the convector making the stratosphere wetter*, Atmospheric Science Letters **16** (2015), no. 2, 135–140.

topological [15] P. Delplace, J. Marston, and A. Venaille, *Topological origin of equatorial waves*, Science **358** (2017), no. 6366, 1075–1077.

eng2021full [16] Y. Deng and Z. Hani, *Full derivation of the wave kinetic equation*, arXiv preprint arXiv:2104.11204 (2021).

008multiple [17] D. Dritschel and M. McIntyre, *Multiple jets as pv staircases: The phillips effect and the resilience of eddy-transport barriers*, Journal of the Atmospheric Sciences **65** (2008), no. 3, 855–874.

2018 [18] G. Düring and G. Krstulovic, *Exact result in strong wave turbulence of thin elastic plates*, Physical Review E **97** (2018Feb), no. 2.

2009 [19] C. Falcón, E. Falcon, U. Bortolozzo, and S. Fauve, *Capillary wave turbulence on a spherical fluid surface in low gravity*, EPL (Europhysics Letters) **86** (2009Apr), no. 1, 14002.

farrell2007structure [20] B. F Farrell and P. J Ioannou, *Structure and spacing of jets in barotropic turbulence*, Journal of the atmospheric sciences **64** (2007), no. 10, 3652–3665.

fjortoft1953changes [21] R. Fjørtoft, *On the changes in the spectral distribution of kinetic energy for twodimensional, nondivergent flow*, Tellus **5** (1953), no. 3, 225–230.

frisch1995turbulence [22] U. Frisch and A. N. Kolmogorov, *Turbulence: the legacy of an kolmogorov*, Cambridge university press, 1995.

gill2016atmosphere [23] A. E Gill, *Atmosphere—ocean dynamics*, Elsevier, 2016.

held1995surface [24] I. M Held, R. T Pierrehumbert, S. T Garner, and K. L Swanson, *Surface quasi-geostrophic dynamics*, Journal of Fluid Mechanics **282** (1995), 1–20.

hoskins1982mathematical [25] B. J Hoskins, *The mathematical theory of frontogenesis*, Annual review of fluid mechanics **14** (1982), no. 1, 131–151.

jiang2020fifty [26] X. Jiang, Á. F Adames, D. Kim, E. D Maloney, H. Lin, H. Kim, C. Zhang, C. A DeMott, and N. P Klingaman, *Fifty years of research on the madden-julian oscillation: Recent progress, challenges, and perspectives*, Journal of Geophysical Research: Atmospheres **125** (2020), no. 17, e2019JD030911.

khaykin20202019 [27] S. Khaykin, B. Legras, S. Bucci, P. Sellitto, L. Isaksen, F. Tence, S. Bekki, A. Bourassa, L. Rieger, D. Zawada, et al., *The 2019/20 australian wildfires generated a persistent smoke-charged vortex rising up to 35 km altitude*, Communications Earth & Environment **1** (2020), no. 1, 1–12.

kiladis2009convectively [28] G. N Kiladis, M. C Wheeler, P. T Haertel, K. H Straub, and P. E Roundy, *Convectively coupled equatorial waves*, Reviews of Geophysics **47** (2009), no. 2.

lapeyre2017surface [29] G. Lapeyre, *Surface quasi-geostrophy*, Fluids **2** (2017), no. 1, 7.

lynch2006emergence [30] P. Lynch, *The emergence of numerical weather prediction: Richardson's dream*, Cambridge University Press, 2006.

mcintyre1990dissipative [31] M. McIntyre and W. Norton, *Dissipative wave-mean interactions and the transport of vorticity or potential vorticity*, Journal of Fluid Mechanics **212** (1990), 403–435.

muller2012detailed [32] C. J Muller and I. M Held, *Detailed investigation of the self-aggregation of convection in cloud-resolving simulations*, Journal of the Atmospheric Sciences **69** (2012), no. 8, 2551–2565.

nazarenko2011wave [33] S. Nazarenko, *Wave turbulence*, Vol. 825, Springer Science & Business Media, 2011.

Newell [34] Alan C. Newell, S. Nazarenko, and L. Biven, *Wave turbulence and intermittency*, Physica D: Nonlinear Phenomena **152-153** (May 2001), 520–550 (English (US)). Funding Information: The authors thank Oleg Zaboronski for numerous helpful discussions. We are also grateful for support from EC Contract FMRX-CT98-0175 and from NSF Grant DMS 0072803.

north2014encyclopedia [35] G. R North, J. A Pyle, and F. Zhang, *Encyclopedia of atmospheric sciences*, Vol. 1, Elsevier, 2014.

pathak2018model [36] J. Pathak, B. Hunt, M. Girvan, Z. Lu, and E. Ott, *Model-free prediction of large spatiotemporally chaotic systems from data: A reservoir computing approach*, Physical review letters **120** (2018), no. 2, 024102.

plumb1977interaction [37] R. Plumb, *The interaction of two internal waves with the mean flow: Implications for the theory of the quasi-biennial oscillation*, Journal of Atmospheric Sciences **34** (1977), no. 12, 1847–1858.

raymond2009moisture [38] D. J Raymond and Ž. Fuchs, *Moisture modes and the madden–julian oscillation*, Journal of Climate **22** (2009), no. 11, 3031–3046.

reynolds1883xxix [39] O. Reynolds, *XXIX. An experimental investigation of the circumstances which determine whether the motion of water shall be direct or sinuous, and of the law of resistance in parallel channels*, Philosophical Transactions of the Royal society of London **174** (1883), 935–982.

s1975waves [40] P. B Rhines, *Waves and turbulence on a beta-plane*, Journal of Fluid Mechanics **69** (1975), no. 3, 417–443.

2generation [41] R. Scott and A-S Tissier, *The generation of zonal jets by large-scale mixing*, Physics of Fluids **24** (2012), no. 12, 126601.

Numerics [42] T. Y. Sheffield and B. Rumpf, *Ensemble dynamics and the emergence of correlations in one- and two-dimensional wave turbulence*, Phys. Rev. E **95** (2017Jun), 062225.

hokarthesis [43] I. Shokar, *Data-driven exploration of mid-latitude weather*, 2021.

n2012ocean [44] W. D Smyth and J. N Moum, *Ocean mixing by kelvin-helmholtz instability*, Oceanography **25** (2012), no. 2, 140–149.

1993frontal [45] C. Snyder, W. C Skamarock, and R. Rotunno, *Frontal dynamics near and following frontal collapse*, Journal of Atmospheric Sciences **50** (1993), no. 18, 3194–3212.

2006simple [46] R. Srinivasan, *Simple models with cascade of energy and anomalous dissipation*, oc6 0310) q Course Lectures (2006), 192.

ni2021wave [47] G. Staffilani and M.-B. Tran, *On the wave turbulence theory for stochastic and random multidimensional kdv type equations*, arXiv preprint arXiv:2106.09819 (2021).

xperiments [48] S. Thorpe, *Experiments on the instability of stratified shear flows: miscible fluids*, Journal of Fluid Mechanics **46** (1971), no. 2, 299–319.

010charney [49] A. Vallgren and E. Lindborg, *Charney isotropy and equipartition in quasi-geostrophic turbulence*, Journal of fluid mechanics **656** (2010), 448–457.

tmospheric [50] G. K Vallis, *Atmospheric and oceanic fluid dynamics*, Cambridge University Press, 2017.

2020trouble [51] G. K Vallis, *The trouble with water: Condensation, circulation and climate*, The European Physical Journal Plus **135** (2020), no. 6, 1–26.

ponentially [52] J Vanneste and I Yavneh, *Exponentially small inertia–gravity waves and the breakdown of quasi-geostrophic balance*, Journal of the atmospheric sciences **61** (2004), no. 2, 211–223.

013balance [53] J. Vanneste, *Balance and spontaneous wave generation in geophysical flows*, Annual Review of Fluid Mechanics **45** (2013), 147–172.

ds1968wave [54] J. Woods, *Wave-induced shear instability in the summer thermocline*, Journal of Fluid Mechanics **32** (1968), no. 4, 791–800.

ZLF [55] V. Zakharov, V. L'vov, and G. Falkovich, *Kolmogorov spectra of turbulence wave turbulence chapter 3 stationary spectra of weak wave turbulence*, 2003.

ng2020four [56] C Zhang, Á. Adames, B Khouider, B Wang, and D Yang, *Four theories of the madden-julian oscillation*, Reviews of Geophysics **58** (2020), no. 3, e2019RG000685.